ANNUAL REVIEW

INSTITUTE FOR MOLECULAR SCIENCE

1984

ANNUAL REVIEW

INSTITUTE FOR MOLECULAR SCIENCE

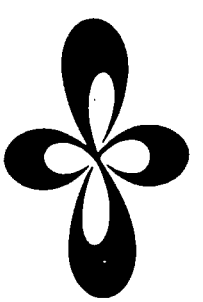

1984

Published by
Okazaki National Research Institutes
Institute for Molecular Science
Myodaiji, Okazaki 444, Japan
Phone 0564-54-1111
Telex 4537-475 KOKKEN J
December 27, 1984

IMS 1984

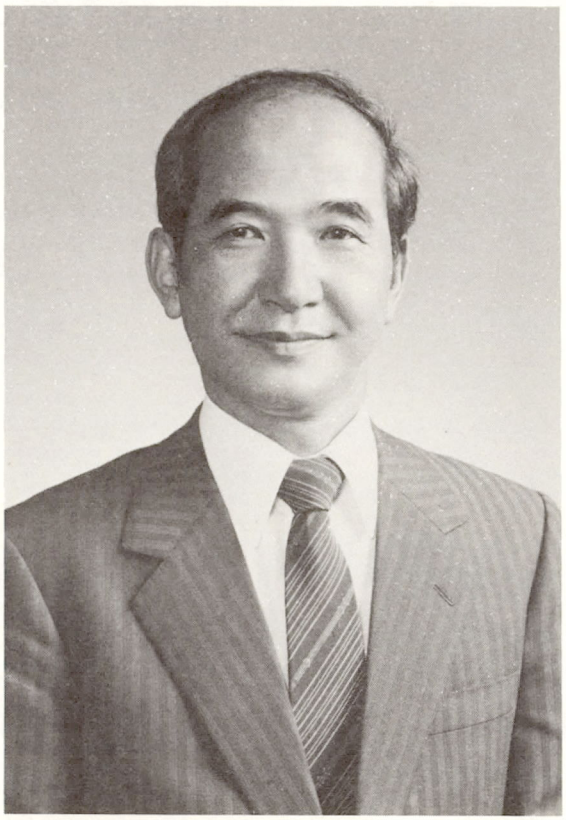

The institute for Molecular Science (IMS) which was established in April 1975 is now in its tenth year and is going to have the tenth Anniversary next May. I hope that IMS will be able to celebrate it by achieving the results anticipated from our Japanese molecular scientists in research activities at IMS itself and also in joint and exchange programs with outside scientists.

In the past year, the Ultraviolet Synchrotron Orbital Radiation (UVSOR) Project has continued to make progress by increasing the radiation intensity, improving measurement systems, and so on. I expect that UVSOR joint research programs with outside scientists will officially start in April 1985.

I am pleased to report that a new facility, "the Coordination Chemistry Laboratories" started this year with two laboratories, "Synthetic Coordination Chemistry" and "Complex Catalysis". The former laboratory has been transferred from the Research Institute for Iron, Steel and Other Metals, Tohoku Univesity for a period of two years. I would like to take this opportunity to thank the Institute and Tohoku University for their generous cooperation.

During the past year, IMS has had a number of new scientists as the staff members. Among them senior members were Dr. Y. Maruyama as Professor of Molecular Assemblies Dynamics Laboratory, Dr. F. Takei and Dr. S. Tero as Professor and Associate Professor of Synthetic Coordination Chemistry Laboratory, respectively, and Dr. K. Saito as Professor of Complex Catalysis Laboratory and Director of the Coordination Chemistry Laboratories. I strongly hope that these three new Laboratories will largely develop in future under the able leadership of the senior staff members.

Finally I am glad to announce that Professor Y. Morino has been appointed a Distinguished Research Consultant to join Professor M. Kotani and Professor K. Fukui.

November 1984

Saburo Nagakura
Director-General

CONTENTS

ORGANIZATION AND STAFF

Organization

The Institute for Molecular Science comprises seventeen research laboratories – each staffed by a professor, an associate professor, two research associates and a few technical associates –, two research laboratories with foreign visiting professors, and six research facilities. The laboratories are grouped into five departments and one facility for coordination chemistry:

Department of Theoretical Studies	Theoretical Studies I
	Theoretical Studies II
	Theoretical Studies III
Department of Molecular Structure	Molecular Structure I
	Molecular Structure II[2]
	Molecular Dynamics
Department of Electronic Structure	Excited State Chemistry
	Excited State Dynamics
	Electronic Structure[2]
	Molecular Energy Conversion[3]
Department of Molecular Assemblies	Solid State Chemistry
	Photochemistry
	Molecular Assemblies Dynamics[1]
	Molecular Assemblies[2]
	Synchrotron Radiation Research[3]
Department of Applied Molecular Science	Applied Molecular Science I
	Applied Molecular Science II[2]
Coordination Chemistry Laboratories[1]	Synthetic Coordination Chemistry
	Complex Catalysis

Research Facilities are:	Computer Center
	Low-Temperature Center
	Instrument Center
	Chemical Materials Center
	Equipment Development Center
	Ultraviolet Synchrotron Orbital Radiation (UVSOR) Facility.

1) Established in April, 1984.

2) Professors and associate professors are adjunct professors from universities.

3) Research Laboratories with foreign visiting professors.

Scientific Staff

Saburo NAGAKURA	**Professor, Director-General**

Department of Theoretical Studies

Theoretical Studies I

Keiji MOROKUMA	Professor
Iwao OHMINE	Associate Professor
Shigeki KATO	Research Associate (–March '84)[1]
Chikatoshi SATOKO	Research Associate
Koichi YAMASHITA	Research Associate (October '84–)
Nobuaki KOGA	Technical Assistant (–March '84) Technical Associate (April '84–)
Hideki TANAKA	Research Fellow (April '84–)
Kenshu KAMIYA	Graduate Student from Univ. of Tokyo* (April '83–)
Susumu MIZUUCHI	Visiting Research Fellow from Nippon Soda Co. (April '84–)

Theoretical Studies II

Hiroki NAKAMURA	Professor
Keiichiro NASU	Associate Professor
Kazuo TAKATSUKA	Research Associate
Hidemitsu HAYASHI	Research Associate
Akihiko OHSAKI	Technical Associate (April '84–)

Theoretical Studies III

Kimio OHNO	Adjunct Professor from Hokkaido Univ. (April '83–)
Masaru TSUKADA	Adjunct Associate Professor from Univ. of Tokyo (–March '83)
Isao SHIMAMURA	Adjunct Associate Professor from Inst. of Phys. and Chem. Res. (April '84–)
Katsuhisa OHTA	Research Associate

Department of Molecular Structure

Molecular Structure I

Eizi HIROTA	Professor
Shuji SAITO	Associate Professor
Chikashi YAMADA	Research Associate
Yasuki ENDO	Research Associate
Tetsuo SUZUKI	Technical Associate
Hideto KANAMORI	Technical Associate
Tatsuya MINOWA	Research Fellow (April '84–)

Molecular Structure II

Soji TSUCHIYA	Adjunct Professor from Univ. of Tokyo (April '83–)
Hiroyasu NOMURA	Adjunct Associate Professor from Nagoya Univ. (–March '84)
Hiroo HAMAGUCHI	Adjunct Associate Professor from Univ. of Tokyo (April '84–)
Kentarou KAWAGUCHI	Research Associate

Molecular Dynamics

Teizo KITAGAWA	Professor
Yasuo UDAGAWA	Associate Professor
Tadashi KATO	Research Associate (–March '84)[2]
Keiji KAMOGAWA	Research Associate
Kazuyuki TOHJI	Technical Associate
Hideji TANABE	Graduate Student from Toyohashi Univ. of Technology* (October '82–March '84)
Takashi OGURA	Graduate Student from Osaka Univ.* (April '83–)
Shinji HASHIMOTO	Graduate Student from Osaka Univ.* (April '83–)
Shoji KAMINAKA	Graduate Student from Hiroshima Univ.* (April '84–)
Takashi IDA	Graduate Student from Toyohashi Univ. of Technology* (April '84–)
Takanori MIZUSHIMA	Graduate Student from Toyohashi Univ. of Technology* (April '84–)

Department of Electronic Structure

Excited State Chemistry

Keitaro YOSHIHARA	Professor
Tadayoshi SAKATA	Associate Professor
Nobuaki NAKASHIMA	Research Associate
Kazuhito HASHIMOTO	Technical Associate (–February '84) Research Associate (March '84–)
Minoru SUMITANI	Technical Associate
Nobuo SHIMO	Visiting Research Fellow from Idemitsu Kosan Co., Ltd. (June '81–March '84)
Noriaki IKEDA	Research Fellow (April '82–March '84) IMS Fellow (April '84–)

Excited State Dynamics

Ichiro HANAZAKI	Professor
Nobuyuki NISHI	Associate Professor
Iwao NISHIYAMA	Research Associate
Hisanori SHINOHARA	Research Associate
Masaaki BABA	Technical Associate
Tohru OKUYAMA	Technical Associate
Kanekazu SEKI	Graduate Student from Univ. of Tokyo* (October '83–)

Electronic Structure

Noboru HIROTA	Adjunct Professor from Kyoto Univ. (April '82–March '84)
Hisaharu HAYASHI	Adjunct Professor from Inst. of Phys. and Chem. Res. (April '84–)
Yoshifumi TANIMOTO	Adjunct Associate Professor from Kanazawa Univ. (April '83–)
Ryoichi NAKAGAKI	Research Associate
Takeshi WATANABE	Technical Assistant
Mitsuo HIRAMATSU	Visiting Research Fellow from Hamamatsu Photonics K.K. (April '83–)
Yoshio FUKUDA	Visiting Research Fellow from Inst. of Phys. and Chem. Res. (April '84–)

Molecular Energy Conversion

Ernest R. Davidson	Visiting Professor from Univ. of Washington, U.S.A. (December '83–June '84)

Jon T. Hougen	Visiting Professor from NBS, U.S.A. (July '84–December '84)

Department of Molecular Assemblies

Solid State Chemistry

Hiroo INOKUCHI	Professor
Inosuke KOYANO	Associate Professor
Kenichiro TANAKA	Research Associate
Kazuhiko SEKI	Research Associate
Naoki SATO	Technical Associate (–March '84)[3]
Tatsuhisa KATO	Technical Associate
Kenichi IMAEDA	Technical Associate (September '84–)
Mototada KOBAYASHI	IMS Fellow (February '83–)
Akiharu HIOKI	Graduate Student from Nagoya Univ.* (October '81–March '84)
Eisuke NISHITANI	Graduate Student from Tokyo Inst. of Tech.* (October '81–September '83)
Hiromichi YAMAMOTO	Graduate Student from Nagoya Univ.* (April '83–)
Hiroaki KUMAGAI	Graduate Student from Nagoya Univ.* (April '82–March '84)
Masaie FUJINO	Graduate Student from Osaka Univ.* (October '83–March '84)
Takae TAKEUCHI	Graduate Student from Nara Women's Univ.* (April '84–)
Hitoshi HAYASHI	Visiting Research Fellow from Nippondenso Co., Ltd. (April '83–March 84)
Naohisa OHYAMA	Visiting Research Fellow from Nippondenso Co., Ltd. (April '84–)
Munehisa MITSUYA	Visiting Research Fellow from Hitachi Ltd. (April '84–)
Yoshio SUGIYAMA	Visiting Research Fellow from Nippon Sheet Glass Co., Ltd. (October '83–March '84)
Toshifumi NISHII	Visiting Research Fellow from Mitsubishi Petrochemical Co., Ltd. (June '84)

Photochemistry

Katsumi KIMURA	Professor
Kosuke SHOBATAKE	Associate Professor
Yohji ACHIBA	Research Associate
Kiyohiko TABAYASHI	Research Associate
Kenji SATO	Technical Associate
Shigeru OHSHIMA	Technical Associate (April '83–September '84)
Yatsuhisa NAGANO	Graduate Student from Osaka Univ.* (April '82–March '84, October '84–)
Atsunari HIRAYA	Graduate Student from Tohoku Univ.* (April '83–September '84) Technical Associate (October '84–)

Molecular Assemblies Dynamics

Yusei MARUYAMA	Professor (February '84–)
Tamotsu INABE	Research Associate (August '84–)
Rumiko HORIGUCHI	Graduate Student from Ochanomizu Univ.* (April '84–)
Hatsumi URAYAMA	Graduate Student from Ochanomizu Univ.* (April '84–)

Molecular Assemblies

Yusei MARUYAMA	Adjunct Professor from Ochanomizu Univ. (April

	'83–January '84)
Masahiro KOTANI	Adjunct Professor from Gakushuin Univ. (May '84–)
Naohiko MIKAMI	Adjunct Associate Professor from Tohoku Univ. (April '83–)
Gunzi SAITO	Research Associate (–January '84)[4]
Takehiko MORI	Research Associate (September '84–)

Synchrotron Radiation Research

Godfrey SAXON	Visiting Professor from Daresbury Laboratory, SERC, U.K. (October '83–March '84)
Willis B. PERSON	Visiting Professor from Florida Univ., U.S.A. (August '84–)

Department of Applied Molecular Science

Applied Molecular Science I

Hiizu IWAMURA	Professor
Tasuku ITO	Associate Professor
Tadashi SUGAWARA	Research Associate
Koshiro TORIUMI	Research Associate
Masako KATO	Technical Associate
Shigeru MURATA	Technical Associate
Hideyuki TUKADA	IMS Fellow (March '82–March '84)
Akira IZUOKA	Research Fellow (April '83–)
Masamichi ATO	Graduate Student from Nagoya Univ.* (October '81–March '84)
Tohru NAKANISHI	Graduate Student from Tokyo Metropolitan Univ.* (October '82–September '84)
Toshiaki KANAO	Graduate Student from Kumamoto Univ.* (April '83–March '84)
Yuji UMETSU	Graduate Student from Kumamoto Univ.* (April '84–)

Applied Molecular Science II

Akio YAMAMOTO	Adjunct Professor from Tokyo Inst. of Tech. (April '83–)
Kiyoshi MUTAI	Adjunct Associate Professor from Univ. of Tokyo (April '82–March '84)
Renji OKAZAKI	Adjunct Associate Professor from Univ. of Tokyo (April '84–)
Noboru KOGA	Research Associate

Coordination Chemistry Laboratories

Kazuo SAITO	Director

Synthetic Coordination Chemistry

Humihiko TAKEI	Professor
Shozo TERO	Associate Professor
Shin TSUNEKAWA	Research Associate
Syoichi HOSOYA	Research Associate
Masahiro EBIHARA	Graduate Student from Tohoku Univ.* (April '84–)

Complex Catalysis

Kazuo SAITO	Professor
Akira NAKAMURA	Adjunct Professor from Osaka Univ. (April '84–)
Kazuo KASHIWABARA	Adjunct Associate Professor from Nagoya Univ. (April '84–)
Kiyohiko NAKAJIMA	Graduate Student from Nagoya Univ.* (April '84–)

Research Facilities

Computer Center

Keiji MOROKUMA	Director
Hiroshi KASHIWAGI	Associate Professor
Unpei NAGASHIMA	Research Associate
Shigeyoshi YAMAMOTO	Technical Associate
Minoru SAITO	Graduate Student from Nagoya Univ.*

Low-Temperature Center

Hiroo INOKUCHI	Director
Toshiaki ENOKI	Research Associate

Instrument Center

Keitaro YOSHIHARA	Director
Iwao YAMAZAKI	Associate Professor
Keisaku KIMURA	Research Associate
Naoto TAMAI	Research Associate

Chemical Materials Center

Hiizu IWAMURA	Director
Hidemasa TAKAYA	Associate Professor
Kazushi MASHIMA	Research Associate
Masashi YAMAKAWA	Technical Associate (–March '84)
Tetsuo OHTA	Technical Associate (April '84–)

Equipment Development Center

Eizi HIROTA	Director
Tadaoki MITANI	Associate Professor
Yoshihiro TAKAGI	Research Associate
Yoshiki WADA	Graduate Student from Univ. of Tokyo* (April '84–)

Ultraviolet Synchrotron Orbital Radiation Facility

Hiroo INOKUCHI	Director
Makoto WATANABE	Associate Professor
Toshio KASUGA	Associate Professor
Takatoshi MURATA	Adjunct Associate Professor from Kyoto Univ. of Education (–March '84)
Hideo NAKAGAWA	Adjunct Associate Professor from Fukui Univ. (April '84–)
Hiroto YONEHARA	Research Associate

Technical Staff

Akira UCHIDA	Technical Division Head
Keiichi HAYASAKA	Technical Section Chief
Kusuo SAKAI	Technical Section Chief
Satoshi INA	Computer Center (Unit Chief)
Fumio NISHIMOTO	Computer Center
Takaya YAMANAKA	Instrument Center
Shunji BANDOW	Instrument Center
Kenichi IMAEDA	Low-Temperature Center (–September '84)
Kazuo HAYAKAWA	Equipment Development Center (Unit Subchief)

Hisashi YOSHIDA	Equipment Development Center
Masaaki NAGATA	Equipment Development Center
Toshio HORIGOME	Equipment Development Center (Unit Subchief)
Norio OKADA	Equipment Development Center
Mitsukazu SUZUI	Equipment Development Center
Nobuo MIZUTANI	Equipment Development Center
Shinji KATO	Equipment Development Center
Osamu MATSUDO	UVSOR Facility (Unit Chief)
Toshio KINOSHITA	UVSOR Facility
Masami HASUMOTO	UVSOR Facility
Jun-ichiro YAMAZAKI	UVSOR Facility (April '84–)
Eiken NAKAMURA	UVSOR Facility (April '84–)

* Carries out graduate research at IMS on the Cooperative Education Programs of IMS with graduate schools.
1) Present address: Dept. of Chemistry, Faculty of General Education, Nagoya Univ., Chikusa, Nagoya 464.
2) Present address: Dept. of Chemistry, Faculty of Science, Tokyo Metropolitan Univ., Setagaya, Tokyo 159.
3) Present address: Dept. of Chemistry, Faculty of Science, Kumamoto Univ., Kurogami, Kumamoto 860.
4) Present address: Institute for Solid State Physics, Univ. of Tokyo, Roppongi, Tokyo 106.

Foreign Visiting Staff

Terry A. Miller	Bell Lab. U.S.A.	June 28–Sept. 24, 1983
Robert J. Donovan	Univ. of Edinburgh U.K.	July 4–Sept. 23, 1983
James R. McNesby	Univ. of Maryland U.S.A.	Sept. 1–Dec. 15, 1983
Simon H. Bauer	Cornell Univ. U.S.A.	Sept. 16–Dec. 10, 1983
L. Vo Ky	Observatoire de Paris France	Nov. 6–Dec. 5, 1983
Edward C. Lim	Wayne State Univ. U.S.A.	Jan. 9–May 11, 1984
Pei Ji Wu	Institute of Chemistry Beijing, China	Jan. 17, 1984–Jan. 16, 1985
David Philips	Royal Institution U.K.	March 23–April 23, 1984
Virgil L. Goedken	Florida State Univ. U.S.A.	May 1–Aug. 15, 1984
Byoung J. Yoon	Kangreung Natl. Univ. Korea	June 12–Sept. 10, 1984
Kyu H. Chae	Chonnam Natl. Univ. Korea	June 16–Sept. 10, 1984
Klaus Kemnitz	Univ. Erlangen-Nuernberg West Germany	April 19, 1982–April 19, 1984
Tong Bor Tang	Cambridge Univ. U.K.	March 1, 1984–Feb. 28, 1986
Zdzislaw Latajka	Wroclaw Univ. Poland	March 5, 1984–March 4, 1985
John N. Moore	Royal Institution U.K.	March 21–July 22, 1984
Bee Tuan Lim	Wayne State Univ. U.S.A.	March 25–April 25, 1984
K. Szczepaniak	Polish Academy of Science Poland	Aug. 1–Sept. 30, 1984

COUNCIL

Saburo NAGAKURA, Director-General

Councillors

Chairman	Yasutada UEMURA	Professor, The Science University of Tokyo
Vice-Chairman	Kenichi FUKUI	President, Kyoto University of Industrial Arts and Textile Fibers
	Hideo AKAMATU	Professor Emeritus, The University of Tokyo and IMS
	Soichi IIJIMA	President, Nagoya University
	Masao KAKUDO	President, Himeji Institute of Technology
	Tetsuji KAMETANI	President, Hoshi University
	Noboru KOMATSU	President, Toyota Central Research & Development Laboratories, INC.
	Namio HONDA	President, Toyohashi University of Technology
	Osamu SHIMAMURA	Director, Sagami Chemical Research Center
	Ikuzo TANAKA	Professor, Tokyo Institute of Technology
	Sadao NAKAJIMA	Professor, Tokai University
	Hiroaki BABA	Professor, The Research Institute of Applied Electricity, Hokkaido University
	Masao FUJIMAKI	President, Ochanomizu University
	Minoru ODA	Director-General, The Institute of Space and Astronautical Science
	Michael KASHA	Professor, Florida State University
	Per-Olov LÖWDIN	Professor, University of Florida and Professor Emeritus, Uppsala University

The Council is the advisory board for the Director-General. Two of the councillors are selected among distinguished foreign scientists.

Professor Emeritus

Professor Hideo AKAMATU, *ex*-Director-General of IMS, was named the first Professor Emeritus of this Institute in September, 1982.

Distinguished Research Consultants

Kenichi FUKUI	President, Kyoto University of Industrial Arts and Textile Fibers; Professor Emeritus, Kyoto University
Masao KOTANI	Professor Emeritus, The University of Tokyo
Yonezo MORINO	Professor Emeritus, The University of Tokyo; Director and Supreme Consultant, Sagami Chemical Research Center

Administration Bureau

Akira MUROYA	Director-General, Administration Bureau
Minoru OKAMOTO	Director, General Affairs Department
Seigo MIURA	Director, Finance and Facilities Department
Haruhiko IWASA	Head, General Affairs Division
Shigeyoshi ONO	Head, Personnel Division
Takeru YAMAKAWA	Head, Research Cooperation and International Affairs Division
Shunsuke YAMAKI	Head, Budget Division
Wataru KOUCHI	Head, Accounts Division
Takashi YOKOYAMA	Head, Construction Division
Shoichi SATO	Head, Equipment Division

BUILDINGS AND CAMPUS

The IMS campus covering 62,561 m^2 is located on a low hill in the middle of Okazaki City. The inequality in the surface of the hill and growing trees are preserved as much as possible, and low-storied buildings are adopted for conservation of the environment. The buildings of IMS are separated according to their functions as shown in the map. The Research Office Building and all Research Facilities except for the Computer Center are linked organically to the Main Laboratory Building by corridors. Computer Center, Library, and Administration Buildings are situated between IMS and the neighboring National Institute for Basic Biology and National Institute for Physiological Sciences, because the latter two facilities are common to these three institutes.

The lodging facility of IMS called Yamate Lodge, located within 10 min. walk, has sleeping accommodations for 20 guests. Since June 1, 1981 a new lodging facility called Mishima Lodge has been opened. Mishima Lodge, located within four minutes' walk east of IMS can accommodate 30 guests and ten families. Scientists who visit IMS as well as the two other institutes can make use of these facilities. Foreign visiting scientists can also live at these lodgings with their families during their stay.

The Institute for Molecular Science

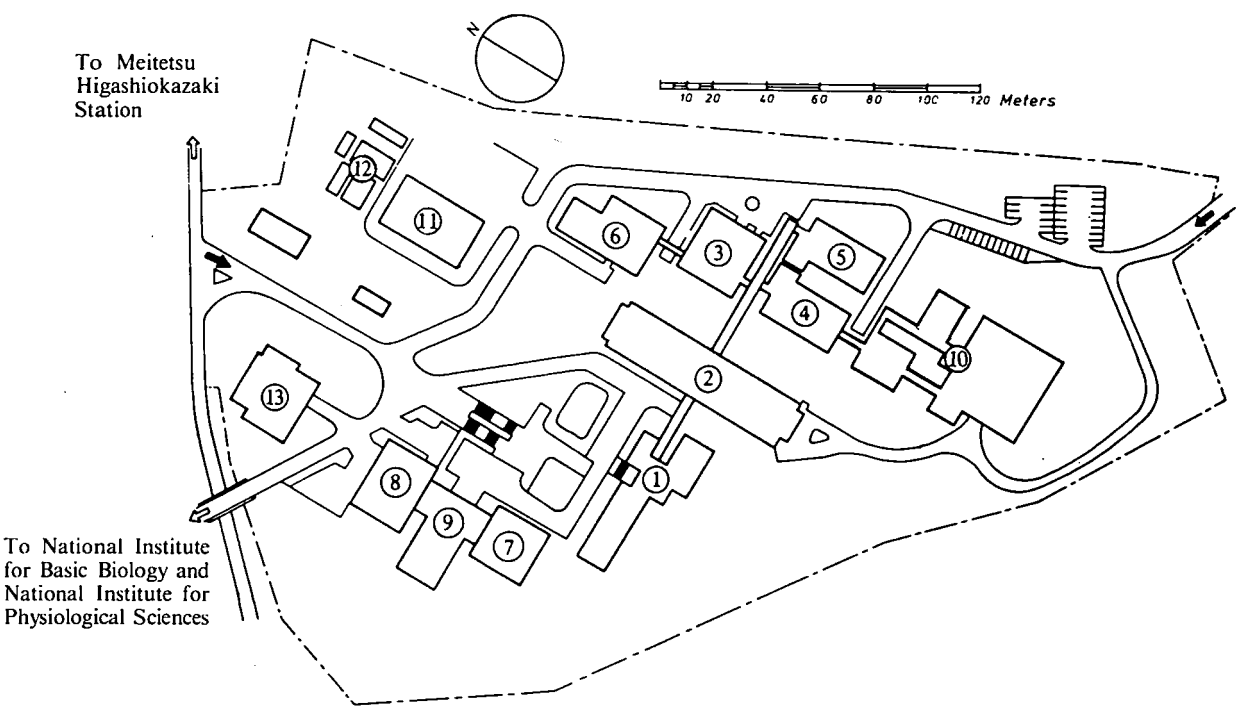

1. Research Office Building
2. Main Laboratory Building
3. Equipment Development Center
4. Instrument Center
5. Chemical Materials Center
6. Low-Temperature Center
7. Computer Center
8. Library
9. Central Administration
10. UVSOR Facility
11. Power Station
12. Waste-Water Disposition Facilities
13. Faculty Club

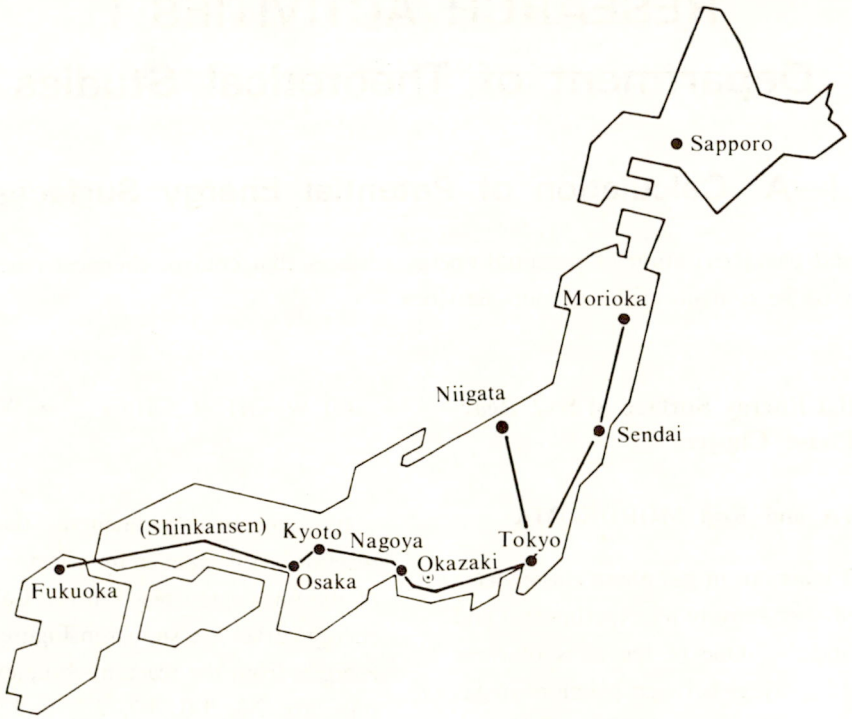

Okazaki (population 280,000) is 260 km southwest of Tokyo, and can be reached by train in about 3 hours from Tokyo via New Tokaido Line (Shinkansen) and Meitetsu Line.
The nearest large city is Nagoya, about 40 km west of Okazaki.

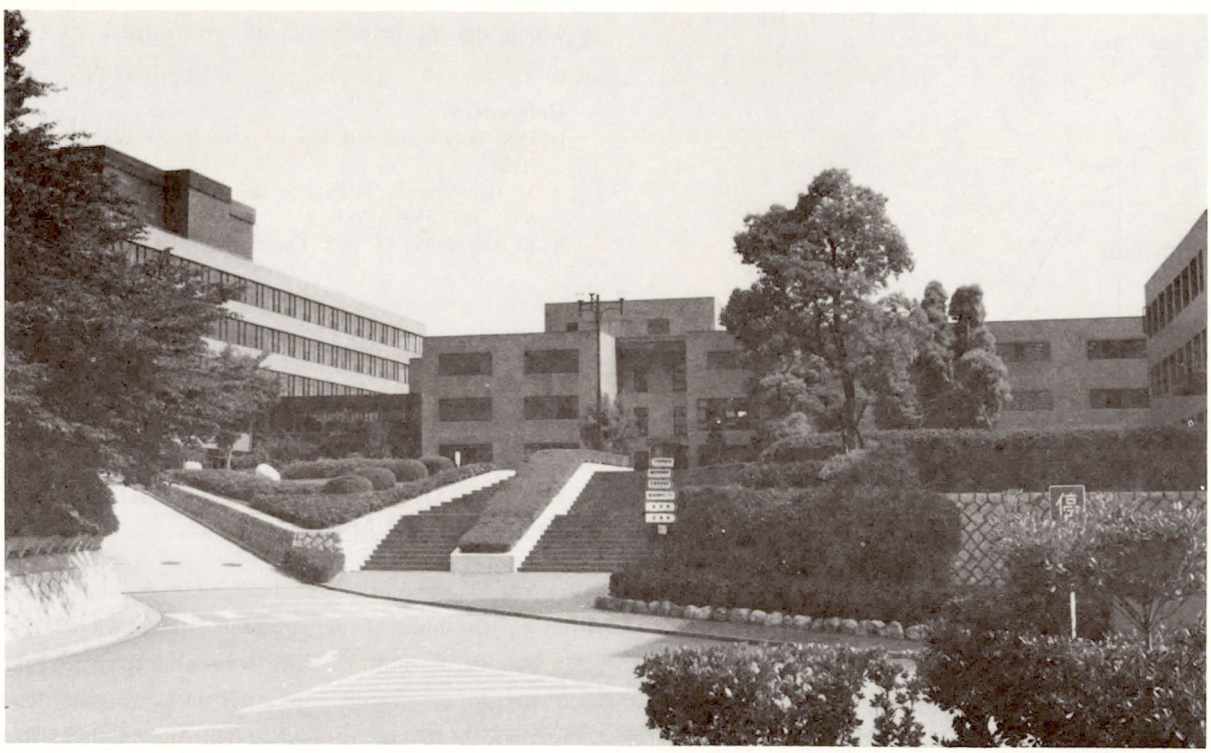

IMS, 1984

RESEARCH ACTIVITIES I
Department of Theoretical Studies

I—A Calculation of Potential Energy Surfaces

Calculation and characterization of potential energy surfaces that control chemical reactions and energy transfer remain to be a major field of our activities.

I-A-1 Potential Energy Surface of SN2 Reaction in Gas Phase Cluster

Katsuhisa OHTA and Keiji MOROKUMA

Recently, SN2 reactions in gas phase cluster have been investigated very actively by experimental and theoretical methods.[1,2,3] One of the aims of these studies is to make a bridge between reactions in gas phase and in solvent. Here we studied the following SN2 reactions with the ab initio method.

(1) $OH^- + CH_3Cl \longrightarrow CH_3OH + Cl^-$
(2) $OH^- + CH_3Cl\text{-}W \longrightarrow CH_3OH + Cl^-\text{-}W$
(3) $W\text{-}OH^- + CH_3Cl \longrightarrow W\text{-}CH_3OH + Cl^-$
(4) $W\text{-}OH^- + CH_3Cl\text{-}W \longrightarrow W\text{-}CH_3OH + Cl^-\text{-}W$

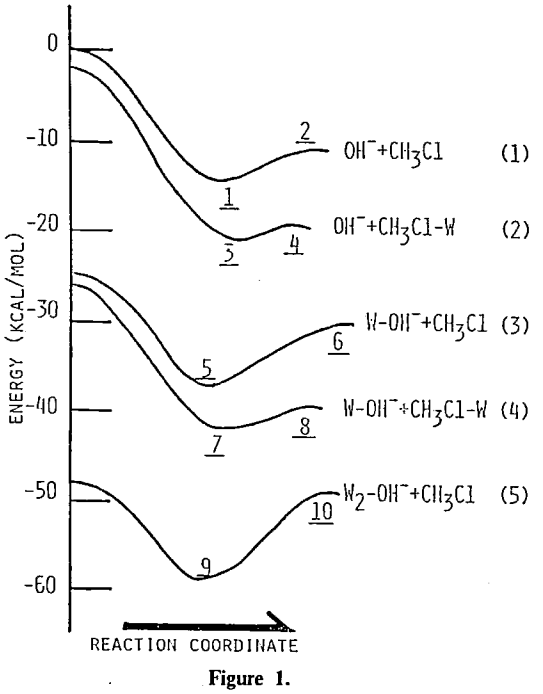

Figure 1.

(5) $W_2\text{-}OH^- + CH_3Cl \longrightarrow W_2\text{-}CH_3OH + Cl^-$. (W = H_2O)

It is known experimentally that the rate of the reaction (5) is smaller by a factor of 10^{-3} than that of the unsolvated reaction (1). Calculated potential energy curves are shown in Figure 1. The activation energies from the reactant complex to the transition state are 2.8, 1.0, 4.7, 2.3, and 9.5 kcal/mol for reactions (1)–(5), respectively. The reaction (5) has a large activation energy and the energy of the transition state is nearly equal to that of the reactants. The transition state of the reaction (4) is less stable than that of the reaction (5). Therefore the rate determing step of the reaction solvated by two water molecules is the methyl inversion process which occurs before the solvent transfer process.

References

1) D.K. Bohme and A.B. Raksit, *J. Am. Chem. Soc.*, **106**, 3447 (1984).
2) M. Henchman, J. F. Paulson, and P.M. Hierl, *J. Am. Chem. Soc.*, **105**, 5509 (1983).
3) K. Morokuma, *J. Am. Chem. Soc.*, **104**, 3732 (1982).

I-A-2 A Theoretical Study on Dimerization of Methylene and Silene in Ground and Excited States

Katsuhisa OHTA, Ernest R. DAVIDSON, and Keiji MOROKUMA

About 14 years ago, Hoffmann et al. showed within the limit of the extended Hückel theory that a non-least motion path was preferred for the formation of ground state ethylene from two singlet methylenes.[1] The ground state of methylene is a triplet, however, and it has been found by ab initio

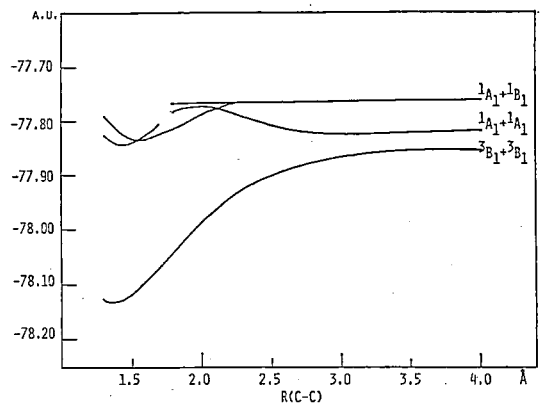

Figure 1. Potential curves for ground and excited ethylene along the Hoffmann's non-least motion path by MR-CI with MCSCF orbitals as functions of R(C-C).

MCSCF studies that two triplet methylenes can approach with each other along the least motion (planar) path and form ethylene in the ground state with no barrier. We have investigated the non-least motion dimerization of two triplet methylenes described by an MCSCF wavefunction. The first excited state (singlet dimerization) along the non-least motion path is also studied. Is there any barrier along the Hoffmann's path for the ground state (triplet methylene) dimerization? What is the actual state formed in the singlet dimerization? An isoelectronic system, SiH_2 has a singlet ($^1A_1$) as the ground state and a triplet ($^3B_1$) as the first excited state. The least and the non-least motion dimerization paths of SiH_2 fragments to disilene have been studied in comparison with those of CH_2. The coupling between of CH_2 and SiH_2 to form CH_2SiH_2 has also been investigated for the least and the non-least motion paths. The potential curves of CH_2 dimerization along the non-least motion path are shown in Figure 1, as an example of our results.

Reference

1) R. Hoffmann, R. Gleiter, and F.B. Mallory, *J. Am. Chem. Soc.*, **92**, 1460 (1970).

I-A-3 Controlling Barrier Heights for Dimerization of Silaethylenes

Keiji MOROKUMA

[*"Organosilicon Chemistry"* (ed. H. Sakurai), in press]

Silaethylene dimerizes very easily to give 1,3-disilacyclobutane. Silaethylenes that have been isolated so far have rather bulky substituents to prevent dimerization. The effect of substituents X and Y of SiHX = CHY on the dimerization barrier has been calculated for X or Y = H, CH_3, NH_2, OH, SH, F, CN, CHO, SiH_3 and NO_2. Among the singly substituted silaethylenes the barrier is the highest for Y = NH_2, followed by Y = OH, Y = F, Y = CH_3 and X = SiH_3. A π donating resonance substituent on the carbon atom and a σ donating inductive substituent on the silicon increase the barrier and therefore would prevent dimerization. The theoretical origin of the substituent effects has been discussed in detail.

I-A-4 Conjugation Between Si-Siσ Bonds and C≡Cπ Bonds in 3,4,7,8-Tetrasilacycloocta-1,5-diyne(1), and 3,6,7-Trisilacyclohepta-1,4-diyne(2)

Keiji MOROKUMA

[*"Organosilicon Chemistry"* (ed. H. Sakurai), in press]

Sakurai et al. (*J. Am. Chem. Soc.*, **105**, 3359 (1983)) have recently prepared **1** and **2**, and proposed from NMR and other evidences that the HOMO is raised substantially by extensive mixing of Si-Siσ bonds and C≡Cπ bonds. We have carried out geometry optimization of **1** and **2**. The calculated structure of **1** agrees well with the x-ray results, and the predicted structure of **2** has very distorted C≡C bonds. The HOMO of **1** as well as **2** is found to be a thorough mixture of Si-Siσ and C≡Cπ bonds. The origin of such an interaction as well as spectroscopic properties reflecting the mixing has been discussed.

I-A-5 Ab Initio Calculation of the Transition State for the Cope Rearrangement

Yoshihiro OSAMURA, Shigeki KATO, Keiji MOROKUMA, D. FELLER*, E.R. DAVID-

SON*, and W.T. BORDEN* *(*Univ. of Washington)*

[*J. Am. Chem. Soc.*, **106**, 3362 (1984)]

We reported findings of ab initio studies on the Cope rearrangement. In contrast to the MINDO results, we find the lowest energy chair (C_{2h} symmetry) species is the transition state for a concerted pericyclic process. However, this ab initio result is obtained only when a flexible basis set is used and when electron correlation is properly treated.

I-A-6 Potential Energy Surfaces of Photodissociation Reaction of SO_2

Kenshu KAMIYA *(Univ. of Tokyo and IMS)*, **Ernest R. DAVIDSON, and Keiji MOROKUMA**

Potential energy surfaces of photodissociation processes of SO_2 have been calculated with MRDCI method, in order to clarify the relationships between the characteristics of surfaces and dynamical aspects of the reaction. The SO_2 molecules initially excited to $C^1B_2(2^1A')$ state predissociates to give the products (SO + O) in their electronically ground states. In the present calculation, there have been found potential surface crossings between $2^1A'$ and $2^3A'$, and between $2^1A'$ and $3^3A''$ states in the region where the dissociative SO bond length is shorter than that of the avoided crossing region between $2^1A'$ and $3^1A'$. This suggests that a repulsive triplet state or states rather than a singlet state is responsible to predissociation process. Reaction dynamics can also be discussed qualitatively in terms of the shape of crossing seam between relevant electronic states.

I-A-7 Ab Initio Study on the Low-Lying Triplet States of Chlorobenzene

Nobuaki KOGA, Shin-ichi NAGAOKA*, Takeshi TAKEMURA*, Hiroaki BABA*, *(*Hokkaido Univ.)*, **and Keiji MOROKUMA**

Potential surfaces have been calculated by the ab initio UHF method with the 3-21G basis set for low-lying triplet states of chlorobenzene including all singly excited states from the highest occupied $\sigma_S(a_1)$, $\sigma_A(b_2)$, and $\pi_A(a_2)$ orbitals and higher two occupied $\pi_S(b_1)$ orbitals to the lowest vacant $\sigma_S^*(a_1)$, $\pi_S^*(b_1)$ and $\pi_A^*(a_2)$ orbitals. The geometries of the $^3(\pi_A,\pi_A^*)(^3A_1)$ and the $^3(\pi_S,\sigma_S^*)(^3B_1)$ states have been optimized with the energy gradient method. The C-Cl bond length of the $^3(\pi_S,\sigma_S^*)$ state is much longer (2.385Å) than that of the $^3(\pi_A,\pi_A^*)$ state (1.828Å) or that of the ground state (1.820Å). The minimum of the $^3(\pi_A,\pi_A^*)$ is lower than that of the $^3(\pi_S,\sigma_S^*)$ state by 20 kcal/mol. The point where the energy is the lowest on the seam of crossing between the two surfaces has also been obtained with a method of optimization with constraint using the energy gradient. The potential barrier thus obtained on the way from the $^3(\pi_A,\pi_A^*)$ state to the $^3(\pi_S,\sigma_S^*)$ state is 28 kcal/mol. The dissociation energy of the C-Cl bond in the $^3(\pi_S,\sigma_S^*)$ state is calculated to be 21 kcal/mol. The qualitative features of these calculatd results are consistent with those suggested on the basis of phosphorescence properties of halogenated benzenes in rigid-glass solution at 77K.

I—B Theoretical Studies of Molecular Interaction

This year we are fortunate to be able to work heavily on problems of molecular interaction, mainly in collaboration with three foreign visiting scientists: Prof. Ernest Davidson (Visiting Professor), Dr. Zdzislaw Latajka (JSPS Postdoctoral Fellow from Wroclaw) and Prof. Byoung Jip Yoon (IMS Japan-Korea Cooperative Program Participant).

I-B-1 Theoretical Studies of the Intermolecular Interactions. New Energy Decomposition Scheme at Electron Correlation Level

Zdzislaw LATAJKA and Keiji MOROKUMA

In this work we present a new energy decomposi-

tion procedure which is similar in spirit to the energy decomposition scheme proposed by Morokuma et al. at the HF level[1] but is extended to inclusion of the electron correlation. The simplest size-consistent post-Hartree-Fock procedure is Møller-Plesset (MP) perturbation theory and this method has been used to handling the electron correlation effects.

In the proposed method the correlation contribution to interaction energy (CINT) is written as the sum of the following terms:

$$CINT = CES + CEX + CPL + CCT + CMIX.$$

The correlation contribution to the electrostatic energy, CES, can be split into two contributions: CES = CES1 + CES2, where CES1 is equivalent to the well-known dispersion energy (DISP) and CES2 is a correction due to change of orbital energies but not orbitals upon the field of the second molecule. CEX, CPL, and CCT are the electron correlation contribution to the exchange, the polarization, and the charge transfer energy, respectively. CMIX is the coupling term among various interaction components and electron correlation.

The above described method is being used to analysis of interaction in broad range of molecular complexes from weak van der Waals systems to strong hydrogen bonded complexes. Full geometry optimization has been carried out at the 6-31G* Hartree-Fock level and the electron correlation has been studied using the TZP basis set. A general discussion about the origin or the nature of various interaction is presented.

Reference

1) K. Morokuma, *J. Chem. Phys.*, **55**, 1236 (1971); K. Kitaura and K. Morokuma, *Int. J. Quantum Chem.*, **10**, 325 (1976).

I-B-2 Possible Gas Phase Ion Pairs in Amine-HCl Complexes. An Ab Initio Theoretical Study

Zdzislaw LATAJKA, Shogo SAKAI, Keiji MOROKUMA, and Henryk RATAJCZAK *(Univ. of Wroclaw)*

[*Chem. Phys. Lett.*, **110**, 464 (1984)]

The very strong hydrogen bond in complexes between HCl and NH_3, CH_3NH_2, $(CH_3)_2NH$ and $(CH_3)_3N$ have been studied using the ab initio method with the DZP basis set. The main point of interest was the shape of hypersurface for proton transfer process. SCF full geometry optimization gives double minimum potential surfaces for amine-HCl complexes. Inclusion of the electron correlation at the second and third order of Møller-Plesset (MP) theory changes the qualitative feature of surfaces to a single minimum. For the CH_3NH_2-HCl complex we find a single flat-bottomed potential energy minimum corresponding to the molecular hydrogen bond with a substantially stretched H-Cl bond. For the $(CH_3)_2NH$-HCl complex there is a similar flat single minimum where the proton is shared between nitrogen an chlorine atoms. For the $(CH_3)_3N$-HCl complex a single minimum with the proton transferred to the nitrogen atom is found, suggesting the ion pair structure in the gas phase. Our results are consistent with the experimental observations from the IR matrix isolation experiments for these complexes[1] that each complex has single equilibrium structure, which increases the extent of proton transfer gradually with the number of methyl groups.

Reference

1) A.J. Barnes, T.R. Beech, and Z. Mielke, *J. Chem. Soc., Faraday Trans. 2*, **80**, 455 (1984); A.J. Barnes, J.N.S. Kuzniarski, and Z. Mielke, *ibid.*, **80**, 465 (1984).

I-B-3 On the Proton Field Gradient of Ice

Ernest R. DAVIDSON and Keiji MOROKUMA

[*Chem. Phys. Lett.*, **111**, 7 (1984)]

Ab initio calculations of the field gradient at the proton in ice are discussed. The major factor causing the observed reduction from the gas phase is the lengthening of the OH bond in ice. A secondary factor is the electrostatic and through-bond effect of the hydrogen bond.

I-B-4 A Proposed Antiferroelectric Structure for Proton Ordered Ice Ih

Ernest R. DAVIDSON and Keiji MOROKUMA

[*J. Chem. Phys.*, **81**, 3741 (1984)]

A new antiferroelectric structure for proton ordered ice Ih is proposed which has lower energy than the currently popular ferroelectric model. This new structure has 8 molecules per unit cell and $Pna2_1$ space group symmetry. The nearest neighbor interactions are optimum consistent with the oxygen $P6_3/mmc$ lattice.

I-B-5 Structure of Ice. Ab Initio Two- and Three-Body Water-Water Potentials and Geometry Optimization

Byoung Jip YOON* *(*Kangreung National Univ., Korea and IMS)*, **Keiji MOROKUMA, and Ernest R. DAVIDSON** *(IMS and Indiana Univ.)*

The OO distance in ice (2.76Å) is much shorter than in water dimer (2.98Å). No first principle potential function has successfully described the observed OO shrinkage. We have calculated a water-water two-body interaction potentials with ab initio MO method by varying not only the OO distance but also the OH distance. New analytical fits of two-body potential functions have been obtained. The nearest neighbor three-body potential has been also evaluated for proton-ordered ice-Ih structures. With ab initio one, two and nearest neighbor three-body potentials, <HOH fixed at the monomer value, we have been able to obtaine R_{OO} = 2.79Å, R_{OH} = 0.977Å with the binding energy of −15.8 kcal/mole per H_2O molecule for proton ordered antiferroelectric ice Ih. The three-body interaction, aided by the two-body interaction, contributes to the OO shrinkage. Factors that would favor larger R_{OH} stretch and R_{OO} shrinkage have been discussed.

I-B-6 Ab Initio MO Calculation of Force Constants and Dipole Derivatives for the Formamide Dimer. An Estimation of Hydrogen-Bond Froce Constants

Marek J. WOJCIK*, Akiko Y. HIRAKAWA*, Masamichi TSUBOI* *(*Univ. of Tokyo)*, **Shigeki KATO, and Keiji MOROKUMA**

[*Chem. Phys. Lett.*, **100**, 523 (1983)]

Ab Initio SCF MO calculations (with the 4-31G basis set) have been carried out to determine the equilibrium geometry, vibrational frequencies, dipole-moment derivatives, and force constants for intermolecular modes of the formamide dimer and its d_4 and d_6 derivatives. The results are correlated with monomer calculations and experimental data for crystalline formamide.

I—C Structure, Bonding and Reactivity of Transition Metal Complexes

We have continued to study chemistry of transition metal complexes, with a particular emphasis on the C-H activation in such complexes.

I-C-1 Intramolecular CH···M Interaction: A Theoretical Study of the Structure of Six-coordinate $Ti(C_2H_5)(PH_3)_2(X)_2(Y)$

Nobuaki KOGA, Shigeru OBARA, and Keiji MOROKUMA

[*J. Am. Chem. Soc.*, **106** 4625 (1984)]

We report the first ab initio molecular orbital result in which the intramolecular CH···M interaction is found between an inert alkyl group and a transition metal. The optimized geometry for $Ti(C_2H_5)(PH_3)_2(Cl)_2(H)$ has a distorted ethyl group with a short ethyl H^{β}···Ti distance. We also discuss the effect of ligands on the distortion of alkyl group.

I-C-2 Intramolecular CH···M Interaction: Ab Initio MO Study of the Structure of $Ti(CH_3)(PH_3)_2(X)_2Y$

Shigeru OBARA *(IMS and Kyoto Univ.)*, **Nobuaki KOGA, and Keiji MOROKUMA**

[*J. Organomet. Chem.*, **270**, C33 (1984)]

Ab initio MO calculations indicate that the nature of ligands X and Y and the PTiP angle affect the distortion of the methyl group of $Ti(CH_3)(PH_3)_2(X)_2Y$. With X = Cl, Y = Cl and PTiP = 75°, the TiCH angle is found to be 100° with the H···Ti distance of 2.51Å; the methyl group is distorted, suggesting an interaction between methyl CH bond and the metal atom. The origin of this distortion is attributed to the direct interaction between the CH σ bond and an unoccupied Ti d orbital.

I-C-3 A Theoretical Study on β-Elimination Reaction of Agostic Ethyl Complex $Pd(C_2H_5)(PH_3)(H)$

Nobuaki KOGA, Shigeru OBARA *(Kyoto Univ.)*, **Kazuo KITAURA** *(Osaka City Univ.)*, **and Keiji MOROKUMA**

The β-elimination reaction of coordinatively unsaturated 3-coordinate $Pd(C_2H_5)(PH_3)(H)$, which has an agostic interaction, i.e., intramolecular CH···M interaction, is studied by RHF method with energy gradient technique and second order Møller-Plesset perturbation(MP2) method. We fully optimized the geometry of transition state as well as equilibrium geometries at RHF level. The distance between the Pd atom and hydrogen at the transition state is 1.645Å, showing the PdH bond has nearly formed. The transition state is located late. The energy barriers of β-elimination reaction and the reverse insertion reaction are 11.0 kcal/mol and 8.0 kcal/mol, respectively, by RHF method. The corresponding values by MP2 method are 2.1 kcal/mol and 5.1 kcal/mol, respectively. Low activation barrier of β-elimination is ascribed to an agostic interaction found in $Pd(C_2H_5)(PH_3)(H)$. The effect of substituent in ethyl group is also discussed. Though such unsaturated intermediates may not be easily detectable experimentally, it is suggested that intramolecular CH···M interaction may be taking place more commonly than has been established.

I-C-4 Reaction Mechanisms of Oxidative Addition: $H_2 + Pt(0)(PH_3)_2 \rightarrow Pt(II)(H)_2(PH_3)_2$ and Reductive Elimination: $Pt(II)(H)(CH_3)(PH_3)_2 \rightarrow CH_4 + Pt(0)(PH_3)_2$: Ab Initio MO Study

Shigeru OBARA *(IMS and Kyoto Univ.)*, **Kazuo KITAURA, and Keiji MOROKUMA**

[*J. Am. Chem. Soc.*, in press]

Potential energy hypersurfaces of the reactions $H_2 + Pt(PH_3)_2 \rightarrow Pt(H)_2(PH_3)_2$ and $CH_4 + Pt(PH_3)_2 \rightarrow Pt(H)(CH_3)(PH_3)_2$ are investigated theoretically by fully optimizing the transition state as well as equilibrium geometries. These two hypersurfaces show the following contrasts. The H_2 addition reaction is exothermic, while the corresponding CH_4 addition reaction is almost thermoneutral. The transition state of the former reaction is in an early stage with the PPtP angle of 148°, whereas that of the latter is in the midpoint with the angle of 119°. The activation barrier is only 8 kcal/mole in the former, while it is 28 kcal/mole in the latter. The reaction coordinate vectors consist mainly of the H_2 translational mode in the former and of the HPtC bending mode in the latter. The large hydrogen isotope effect observed for the CH_4 reductive elimination is consistent with the calculated transition state. These differences in the potential energy hypersurfaces can be explained by the differences between the PtH and PtC bond strengths which are estimated to be 61–70 and 34–41 kcal/mole, respectively. The larger PtH bond strength results in a larger exothermicity, an early transition state, and hence a lower activation barrier.

I-C-5 An Ab Initio MO Study of the Coordination Modes and Bonding Nature of Rh(I)-N_2 Complexes

Shigeyoshi SAKAKI*, Keiji MOROKUMA, and

Katsutoshi OHKUBO* *(*Kumamoto Univ.)*

[*J. Am. Chem. Soc.*, in press]

An ab initio MO study of $RhCl(PH_3)_2L$ (L = η^1-end-on N_2, η^2-side-on N_2, C_2H_4, CO, HCN, HNC, and NH_3) is presented. First, two coordination modes of N_2, η^1-end-on and η^2-side-on, are compared, and it becomes clear that the η^2-side-on mode is less stable relative to the η^1-end-on mode, mainly due to the less electrostatic stabilization and secondarily due to the weaker σ-donation of the η^2-side-on mode. The bonding nature and electronic structure of the η^1-end-on N_2 complex are also examined. The π-back donative interaction contribute to the N_2 coordination more strongly than the σ-donation, and the relative importance of the π-back donation to the σ-donation is larger in the N_2 coordination than in the coordination of similar ligands, such as CO, HCN, and HNC. Finally, the coordinate bond of Rh(I) complexes are compared with that of Ni(0) complexes, and the versatile ability of $RhCl(PH_3)_2$ for complex formation is discussed.

I—D Development and Application of the LCAO-Xα Direct Force Calculation Method

An energy gradient method is developed for the LCAO-Xα scheme, which is quite convenient for the numerical calculations of forces acting on each ions in the cluster. This method is applied for various problems including chemisorption systems.

I-D-1 Force and Virial Formula in the Liner Combination of Atomic Orbitals Xα Method and its Application to Oxygen Chemisorption on the Al(111) ad Mg(0001) Surface

Chikatoshi SATOKO

[*Phys. Rev.* **B30**, 1754 (1984)]

An expression for the gradient (with respect to nuclear coordinates) of the electronic total energy is given using the linear combination of atomic orbitals Xα(LCAO-Xα) and related to the virial. The formulas are extended to the linear combination of plane-waves(LCPW) method. Our method is applied to the chemisorption of oxygen on Al(111) and Mg(0001) surfaces. The calculations are performed using O/Al_4 and O/Mg_4 model clustes with the metal-metal distance equal to the bulk. The calculated forces explain the experiments which report that oxygen is not absorbed below the Al surface but is absorbed below the Mg surface. The difference in the chemisorption processes is due to differences in the strength of the metal-metal bond interaction.

I-D-2 Chemisorption of Transition-metal Atoms on Silicon Surface

Shuhei OHNISHI *(NEC Corporation Fundamental Research Labs)* **and Chikatoshi SATOKO**

Chemisorption of transition-metal atoms on the silicon surface is of considerable importance in the silicide formation. We analyze forces acting on each atom using the self-consistent LCAO-Xα cluster method. The reaction path of the metal atom approaching to the on-top Si(1) is investigated by the model cluster, $Metal/Si(1)Si(2)_3H_9$. We found the following results: (1) The metal dz^2 orbital makes the σ-type bond with the dangling bond orbital of Si(1). Charge transfer from the metal to this dangling bond occurs in Ti and Cr but less in Ni cases. The forces acting on Si(1) from the second layer $Si(2)_3$ are 0.12, 0.28, and −0.13 in atomic unit in Ti, Cr, and Ni cases, respectively. It shows that chemisorptions along this reaction path make the Si(1)−Si(2) bond weak in Ti an Cr, and strong in Ni cases. This fact is strongly correlated with the charge transfer. It is consistent with the result of the force-analysis of the clean surface with one excess electron in the dangling bond. (2) There exists the

non-bonding metal 3d state below and above the Fermi level in Ni and Cr, Ti systems, respectively.

I-D-3 Slater-type Basis Sets in the LCAO-Xα Methods

Atsushi ETANI*, Shouichi TERAMAE*, Chikatoshi SATOKO, and Masaki SHINADA*
*(*University of Electro-Communications)*

Several approximations have been proposed to solve the local density or X-α equations which are usuful to include the correlation effects of solids and metal clusters. For an example, one can replace the real potential by a spherical potential such as the muffin-tin. However, the muffin-tin approximation is not good for molecules and surfaces. Another approximation is to limit the variational parameters in the coefficients of the linear combination of atomic orbitals. Accuracy of the calculated results is dependent on the choice of the atomic basis sets. The basis sets in the ab-initio Hartree-Fock method have been determined by many chemists, but the basis sets in the LDF method have not been published in papers. The reason is because the LDF equation has been solved by using the numerical basis sets. We are determing the optimized STO basis sets in the LDF method.

The basis set are given by the linear combination of the Slater-type orbital. The coefficient and exponents of the Slater orbital are determined from the minimization of the total energy. Figure 1 shows the dependence of the exponents of the single-zeta STO basis sets on the atomic number Z. The exponents of the double-zeta basis sets will be published elsewhere.

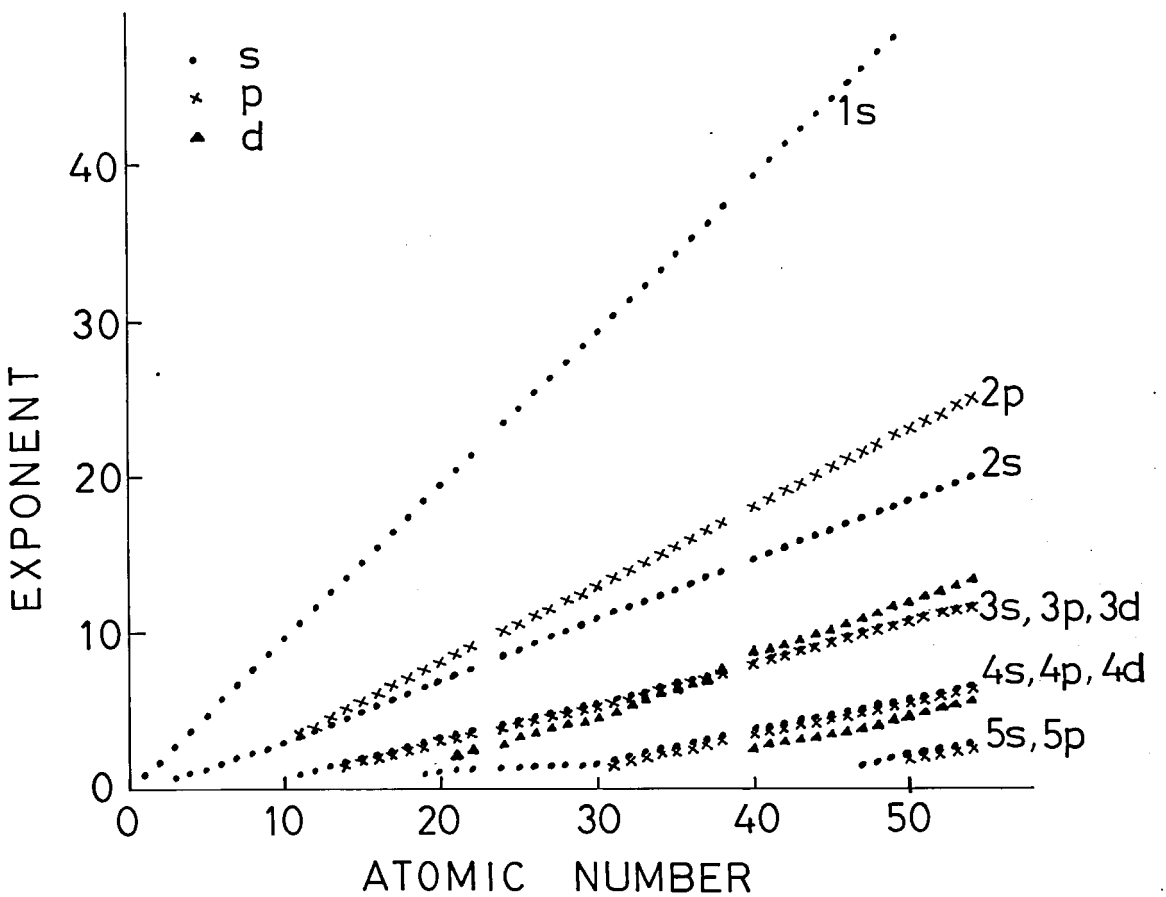

Figure 1. The dependence of the exponents of the minimal STO basis sets on the atomic number.

I—E Dynamics of Photochemical Processes in Gas and Liquid Phases

I-E-1 Nonadiabatic Couplings in Photochemical Processes of Polyenes

Iwao OHMINE

Mechanism of nonadiabatic transitions in the C = C torsional photoisomerization processes of polyenes is investigated by using the ab-initio configurational interaction method, calculating the low lying state potential energy surfaces and their nonadiabatic couplings. A multidimensional search for molecular conformations yielding strong nonadiabatic couplings is performed to find the origin of very fast photoisomerization kinetics, experimentally observed to be typically in the order of a few or few tens picoseconds. The shape of the potential surface crossing is found to be not in a simple conical form but multidimensional in nature and so that almost all the internal molecular motions in the crossing region cause the strong nonadiabatic couplings.

I-E-2 Energy Dissipation of Optically Excited Molecules in Liquid Phase

Iwao OHMINE

We are continuing to investigate on the energy dissipation mechanism of the highly excited molecules in the liquid phase. We choose an ethylene in Argon or water solvent as a model system, and performed the full three-dimensional molecular dynamics calculations. It is found that the rate of the intermolecular energy transfer from the excited ethylene to the solvent molecules depends strongly on the interaction strength among solvent molecules. We observed a kind of phase transitions in the decay rate for the change of Ar-Ar interactions from the weak limit (gas) to the strong limit (solid). The solvent acts as a solid in the short time scale, but as a liquid in the long time scale. This behavior of the solvent as the energy acceptor can be characterized by the modified general hydrodynamic equations.

I-F Dynamic Processes of Electronically Highly Excited States of Atoms and Molecules

An ultimate purpose of these studies is to understand the mechanisms of various dynamic processes of higher-(super-) excited states of molecules.

I-F-1 Dissociative Recombination in the Low Energy e + H_2^+ Collisions

Hidekazu TAKAGI *(Kitasato Univ.)* **and Hiroki NAKAMURA**

We have previously carried out the calculations of elastic scattering of electrons from H_2^+.[1] Using the information on the adiabatic quantum defect and electronic coupling deduced from these calculations, we are now investigating a variety of dynamic processes involving highly excited states of H_2. Dissociative recombination is one of the examples. We have employed the multi-channel quantum defect theory. Our results agree better with the experiment than the results obtained by Giusti et al.[2] The disagreement between the two theoretical results is attributed mainly to the difference of the adiabatic quantum defects used in the calculations. We think that the quantum defect used in Ref. 2) is not the proper one.

References

1) H. Takagi and H. Nakamura, *Phys. Rev.*, **A27**, 691 (1983).
2) A. Giusti-Suzor, J.N. Bardsley, and C. Derkits, *Phys. Rev.*, **A28**, 682 (1983).

I-F-2 Ionization Collisions between Two Excited Atoms: Application of the Glauber Amplitude in the Framework of the Impulse Approximation

Toshizo SHIRAI, Yohta NAKAI *(Japan Atomic Energy Research Institute)*, **and Hiroki NAKAMURA**

[*Phys. Rev.* **A30**, 1672 (1984)]

The cross section formula in the semiquantal approximation for the processes referred to in the title is rewritten so as to make it more useful in practice. The formula is shown to be further simplified by taking an average over the azimuthal quantum number of a highly excited hydrogenic atom to be ionized. Numerical applications with use of the Glauber amplitude for the electron-atom inelastic scattering are made to the ionization collisions between two excited hydrogen atoms with simultaneous excitation and deexcitation of one of the atoms. The results are compared with those obtained by using the Born amplitude and are analyzed in terms of the Glauber generalized oscillator strengths. One of the results is shown in Figure 1.

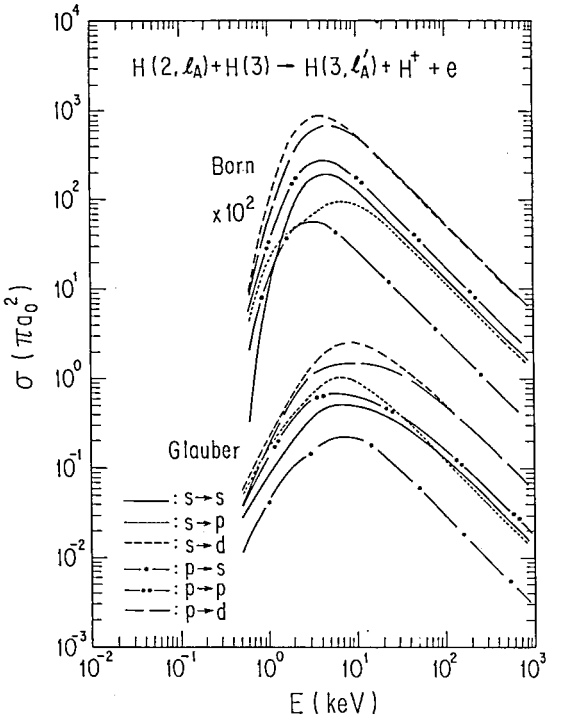

Figure 1. Ionization cross sections for $H(n_A = 2, l_A) + H(n_B = 3) \rightarrow H_A(n_A' = 3, l_A') + H^+ + e$. E is the collision energy in the center-of-mass system. The curves marked as "Born" and "Glauber" are obtained with use of the Born and Glauber approximations to e + H scattering amplitude, respectively.

I-G Semiclassical Theories for Nonadiabatic Transitions

We have proposed a general analytical procedure, a semiclassical theory in the dynamical-state representation, which makes a unified treatment of nonadiabatic transitions in atomic collisions possible. An application of the theory to a practical example has proved its usefulness. The work in this area is now continued to develop an analytical expression for the transition amplitude matrix for the nonadiabatic barrier penetration at energies lower than the maximum of the barrier caused by nonadiabatic coupling.

I-G-1 Semiclassical Scattering Theory Based on the Dynamical-state Representation: Application to the $Li^+ + Na$ and $Li + Na^+$ Collisions

Reiko SUZUKI *(Ochanomizu Univ.)*, **Hiroki NAKAMURA, and Eiichi ISHIGURO** *(Ochanomizu Univ.)*

[*Phys. Rev.* **A29**, 3060 (1984)]

A purely theoretical semiclassical method without any ambiguity is presented for the calculation of differential cross sections for atomic collision processes involving both radial and rotational (Coriolis) nonadiabatic couplings. The method is based on the recently proposed dynamical-state representation. This theory is applied to the asymmetric charge transfer and excitation in the $Li^+ + Na$ and $Li + Na^+$ collisions. The calculated differential cross sections are in good agreement with experimental results. Figure 1 shows one of the examples.

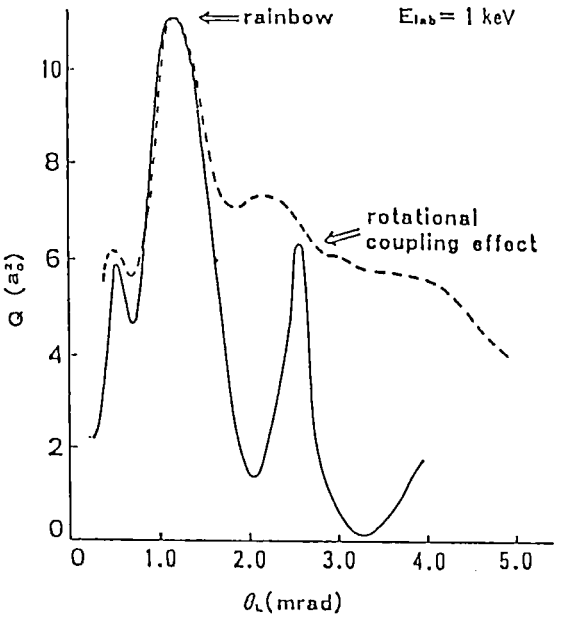

Figure 1. Differential cross sections for the $1\Sigma \rightarrow 2\Sigma$ transition at E_{lab} = 1 keV. Solid line: present theory. Dashed line: experiment.

I-H Studies of Chemical Reaction Dynamics

Our research activity in this area is pursued in two directions. One is a development of a new semiclassical theory in phase space. The other is the hyperspherical coordinate approach to atom transfer reactions.

I-H-1 A Semiclassical Theory in Phase Space for Molecular Processes

Kazuo TAKATSUKA and Hiroki NAKAMURA

[*J. Chem. Phys.*, in press]

In order to describe chemical processes including chemical reactions, we have devised a new quantum mechanical distribution function (Dynamical Characteristic Function, DCF) in phase space. The semiclassical equation of motion for DCF is composed of the classical Liouvillian and Lagrangian which operate linearly on DCF. This indicates that our distribution function can be propagated along the classical trajectories, with which the phase integral is associated. Thus our theory provides a new kind of phase-space-path-integrals. We have discussed the relationship of DCF with the Wigner function and the other semiclassical theories. Detailed analyses on our phase space function have been made.

One theoretical application of our theory is a bound state problem such as the vibrational spectra of molecules. Since DCF is defined in phase space, a canonical transformation suitable for the description of this sort of problem can be carried out in a simple manner. The periodic orbit theory of Gutzwiller,[1] Berry, and Tabor[2] has been proved to be reproduced in the case of regular spectrum. The extension to the irregular spectrum is now being studied. The numerical studies of our phase-space-path-integrals are also under way.

References

1) M.C. Gutzwiller, *J. Math. Phys.*, **11**, 1791 (1970), **12**, 343 (1971).
2) M.V. Berry and M. Tabor, *J. Phys.*, **A10**, 371 (1977).

I-I Electron-Correlation and Electron-Phonon Coupling in One-Dimensional Many-Electron System

In order to predict, optical, magnetic and electric properties of various newly synthesized one-dimensional materials from unified theoretical point of view, we study the phase diagram, optical and magnetic excitations of a one-dimensional many-electron system with the electron-electron repulsion and the electron-phonon coupling. We are especially interested to clarify how the quantum effect of phonon changes the phase diagram previously obtained within the adiabatic approximation.

I-I-1 Many-Polaron Theory for CDW, SDW and Superconducting Phases in One-Dimensional Peierls-Hubbard System

Keiichiro NASU

A one-dimensional many-electron system with the intra-site electron-electron(e-e) repulsion and the site-diagonal electron-phonon coupling is studied in the context of many-polaron theory, so as to clarify how the quantum effect of phonon changes the phase diagram previously obtained within the adiabatic approximation. The dynamical lattice distortion that follows the motion of an electron as its dress, as well as the frozen distortion one are taken into account by a variational method combined with a mean field theory for the many-polaron system. The resultant phase diagram is given in a tetrahedral coordinate space spanned by basic four parameters characterizing this system: the transfer energy of an electron between neighbouring two sites T, the e-e repulsive energy U, the e-p coupling energy S and the energy of site-localized phonon ω. This "T-U-S-ω tetrahedron" is proved to be divided into two regions: the CDW region and the SDW region, by the boundary interface S = U. In both regions, the *polaron self-shrinks* in its radius from a *large polaron* to a *small one* as the quantum nature of the phonon ($\equiv\omega/T$) increases, and this shrinkage comes from the decrease of the retardation effect of the phonon. In the CDW region, the small polaron superconducting state is almost degenerate with the CDW, while the large polaron superconducting state is almost same as the Pauli paramagnetic metal, being far unstable than the CDW. The transition from the large polaron to the small one is abrupt in the case of strong coupling ($T/S \ll 1$), while it is rather gradual in the weak coupling case ($T/S \gg 1$), indicating the importance of the *polaron radius* as the index of the retardation effect.

I—J Unified Theory for Resonant Raman, Hot Luminescence and Ordinary Luminescence with Nonradiative Process

To study the dynamics of lattice relaxation of optical excitations in solids and molecules, we derive an unified theory that covers all components of the resonant secondary radiation: resonant Raman scattering, the hot luminescence and the ordinary luminescence. We are especially interested to clarify how the nonradiative transition around the crossing point of two potential surfaces appears in each component of the resonant secondary radiation.

I-J-1 Resonant Raman, Hot Luminescence and Ordinary Luminescence of F Center in Alkali-Halides

Shinji MURAMATSU *(Utsunomiya Univ.)* **and Keiichiro NASU**

A theory for the resonant secondary radiation from F center in alkali halides is formulated so as to clarify how the non-radiative transition between

2p and 2s states manifestes itself in each component of the secondary radiation: the resonant Raman scattering, the hot luminescence and the ordinary luminescence. The 2p and 2s levels of the F electron are assumed to couple to the localized phonon modes with t_{1u} and a_{1g} symmetries in the O_h crystal field, and these localized phonon modes are also assumed to bi-linearly couple with wave-like phonon modes extending over the crystal. The spectral shape of the secondary radiation is calculated by solving the time evolution of the density matrix of $(2p \oplus 2s) \otimes (t_{1u} \oplus a_{1g})$ system, eliminating the wave-like phonon modes by the Markov approximation. The resultant spectrum can well explain the observed depolarization of the hot luminescence which comes from the 2p ↔ 2s nonradiative transition.

I-K Some Applications of Ab Initio Computation

I-K-1 Molecular Structure and Electronic Spectra of C_4

Akinori MURAKAMI *(Hokkaido Univ.)* **and Kimio OHNO** *(Hokkaido Univ. and IMS)*

The C_4 molecule is of great astronomical interest. Its analogues C_n(n = 5,7,···15) are suggested by Douglas[2] as a possible origin of the diffuse bands observed in the interstellar space.

An optically allowed transition of C_4 has been observed under laboratory conditions. The excitation energy is 2.43 eV (19564 cm^{-1}) and the upper state is presumably either $^3\Pi_u$ or $^3\Sigma_u^-$. The purpose of this calculation is to test the quality of our approximation against experiment findings and to propose a probable assignment.

The geometry of C_4 is determined both at the SCF level and at the limited CI level (single reference). A split-valence type basis set[3] is used. The optimised internuclear distances (Å) are shown in Table 1. The configuration state functions are generated under the following constraints:

1) The ls orbitals are always doubly occupied.
2) Single and double excitations from the reference configuration(s) are considered.

Individual configuration selection of CSF's is made.

At the optimised geometry of our SCF calculation, CI calculations (multi-reference) are carried out. The $^3\Sigma_g^- \rightarrow {}^3\Sigma_u^-$ and $^3\Sigma_g^- \rightarrow {}^3\Pi_u^-$ energy separations are calculated to be 3.1 eV and 1.2 eV, respectively. The observed transition is tentatively assigned as $^3\Sigma_g^- \rightarrow {}^3\Sigma_u^-$.

We are planning to use a more extended basis set by including polarization functions.

Table 1. Geometry of C_4

	Present		Whiteside[4]	Ewing[5]
Method	SCF	CI	SCF	SCF
R_{outer}	1.303	1.332	1.300	1.31
R_{inter}	1.273	1.296	1.276	1.28

References

1) IMS Adjunct Professor for 1983–1985.
2) A.E. Douglas, *Nature*, **265**, 130 (1977).
3) H. Tatewaki and S. Huzinaga, *J. Comp. Chem.*, **1**, 205 (1980).
4) R.A. Whiteside at al., *Chem. Phys. Letts.*, **78**, 539 (1981).
5) D.W. Ewing and G.V. Pfeifer, *Chem. Phys. Letts.*, **86**, 365 (1982).

I-K-2 Electronic Structure of Low-Lying Excited States of 2,4-Pentadienal

Takayuki SHODA *(Hokkaido Univ.)*, **Takeshi NORO** *(Hokkaido Univ.)*, **Tsutomu NOMURA** *(Hokkaido Univ.)*, **and Kimio OHNO**[1] *(Hokkaido Univ. and IMS)*

2,4-pentadienal is studied in this work as a simple model system of retinal. The aims of this calculation are

1) to compare three levels of configuration interaction (CI), i.e. singly excited σ,π CI (σ,π S-CI), singly and doubly excited π CI (π S,D-CI), and singly and doubly excited σ,π CI (σ,π S,D-DI).
2) to investigate the effect of the substitution of functional groups (C=O → NH) and its protonation. The substitution makes Shiff base (SB) from aldehyde and further protonation produces Protonated Shiff base (PSB).

The basis set of split-valence type[2] is used throughout the calculation.

The results of three kinds of CI on 2,4-pentadienal

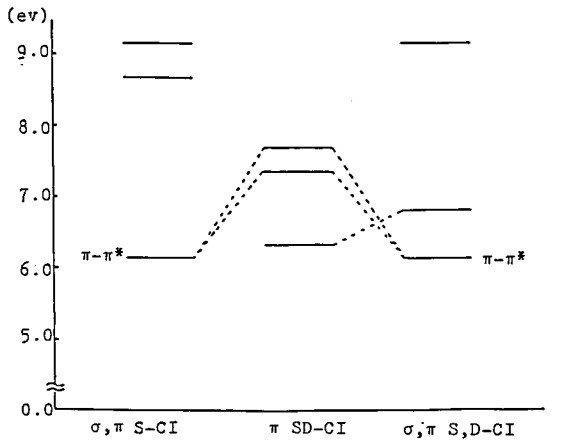

Figure 1. Comparison of excitation energies of aldehyde obtained by three kinds of CI.

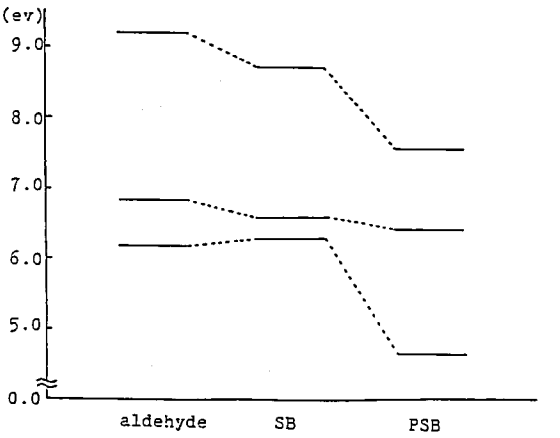

Figure 2. Comparison of excitation energies of the three systems.

are illustrated in Figure 1. States with a similar character are connected by dotted lines. From the figure, it is clear that π S,D-CI does not give reliable results and the correlation between σ and π electrons plays an important role in describing the lower excited states of the polyene. The second excited state in σ,π S,D-CI is a two-electron excitation state.

The excitation energies of the three systems obtained by σ,π S,D-CI are illustrated in Figure 2.

A big energy lowering of the first transition energy is seen in Figure 2 when the Shiff base is protonated. This had been noted by Suzuki et al.[3], based on their semi-empirical calculations.

After these pilot calculations, we plan to perform a series of calculations for longer polyenes and their protonated Shiff bases using either σ,π S-CI or σ,π S,D-CI.

References

1) IMS Adjunct Professor for 1983–1985.
2) H. Tatewaki and S. Huzinaga, *J. Comp. Chem.*, **1**, 205 (1980).
3) H. Suzuki et al., *J. Phys. Soc. Japan.*, **31**, 895 (1971); ibid., **34**, 156 (1973).

I-L Angular Momentum Transfer in Molecular Transition

I-L-1 Coupling of Large Angular Momentum with Small Angular Momentum

Isao SHIMAMURA *(Institute of Physical and Chemical Research and IMS)* **and A.C. ROY** *(Kalyani Univ., India)*

Coupling of angular momenta plays an important part in the analysis of and in the calculations for many physical and chemical systems. The basic quantity for coupling two angular momenta $\mathbf{j}_1\hbar$ and $\mathbf{j}_2\hbar$ to form $\mathbf{j}\hbar$ is the Clebsch-Gordan (CG) coefficient $C(j_1j_2j;\ m_1m_2m)$; $m_1\hbar$, $m_2\hbar$, and $m\hbar = (m_1 + m_2)\hbar$ are the projections of the three angular momenta onto a qunatization axis. Formulas for numerical calculation of the CG coefficients are known. Their analytic complexity, however, often hinders derivation of general angular-momentum-related properties of physical and chemical systems. The present work shows a great simplification that follows when j_1 is much larger than j_2.

One of the formulas that we have proved is

$$\{C(j_1,\ j_2,\ j_1 \pm \Delta j;\ m_1,\ m_2,\ m)\}^2 = \alpha(j_2,\ m_2,\ \Delta j)\{1 \pm (\Delta j/2)j_1^{-1} + O(j_1^{-2})\} \quad (1)$$

for $|m| = |m_1|$, α being calculable from a recurrence formula. Important features of this expression are (a) that it is independent of m_1, (b) that it shows a simple high-j_1 behavior depending only on Δj, and (c) that the terms of order j_1^{-1} for $j = j_1 + \Delta j$ are opposite in sign, all of which being valid to within

the first two terms in the inverse-power expansion. The high-j_1 formula (1) is also useful for numerical evaluation of the CG coefficients.

The present work is an extension of that reported in Ref. 1 for the case $m_1 = m_2 = m = 0$.

Reference

1) I. Shimamura, *Chem. Phys. Lett.*, **73**, 328 (1980).

I-L-2 Rotational Transitions of Symmetric-Top Molecules in Collisions or by External Perturbations

Isao SHIMAMURA *(Institute of Physical and Chemical Research and IMS)* **and A.C. ROY** *(Kalyani Univ., Inida)*

Spacings between molecular rotational levels are small. This makes it difficult to measure the cross sections for rotational transitions $\boldsymbol{J} \rightarrow \boldsymbol{J'}$ of molecules in collisions with other particles. Reliable theoretical calculations are too cumbersome to carry out for many different $\boldsymbol{J}$ and $\boldsymbol{J'}$; molecules in gas are usually distributed among many rotational states. One of us, however, has noted that most molecules occupy high rotational states, and has derived simple general formulas for transitions of *linear rotators* from high-J to high-J' states.[1,2] The present work is a generalization for symmetric-top molecules, for which the projection K of $\boldsymbol{J}$ onto the symmetry axis is a good quantum number.

Only on the assumption of long rotational period as compared with the collision time the following formulas, for example, are applicable to any collision system involving a symmetric-top molecule. $d\sigma(JK \rightarrow J \pm \Delta J,K')/d\omega = A(\Delta J,K' - K)[1 \pm (\Delta J/2)J^{-1} + O(J^{-2})]$ (for $|K| = |K'|$), $d\sigma(JK \rightarrow J \pm \Delta J,K')/d\omega = A(\Delta J,K' - K)[1 \pm \{(\Delta J/2) + B(\Delta J,K' - K)\}J^{-1} + O(J^{-2})]$ (in general). The A and B depend on the collision system. In fact these formulas apply also to transitions induced by any external perturbation.

In conclusion, cross sections for many different J and K are expressible in terms of only one or two parameters. The two cross sections $d\sigma(JK \rightarrow J \pm \Delta J,K')/\mathrm{d}\omega$ approach a common limit as J becomes large, one from above and the other from below in a nearly symmetric manner.

References

1) I. Shimamura, *Phys. Rev.*, **A28**, 1357 (1983).
2) I. Shimamura, *Electron-Molecule Collisions*, I. Shimamura and K. Takayanagi, eds. (Plenum, New York, 1984) p.89.

RESEARCH ACTIVITIES II
Department of Molecular Structure

II—A High Resolution Spectroscopy of Transient Molecules

During the course of chemical reactions many transient molecules appear as intermediates. Because of their high reactivities, i.e. their short lifetimes, these transients have remained to be relatively unknown and some of them have even escaped detection. Many of these molecules have open-shell electronic structures, which characterize them as free radicals; unpaired electrons cause splittings in high resolution spectra of such species through fine and hyperfine interactions. When properly analyzed, these splittings provide us with information on the electronic properties of molecules which is not obtainable for molecules without unpaired electrons. High resolution spectroscopy not only provides molecular constants of transient molecules at very high precision, but also allows us to unambiguously identify chemical species occurring in reaction systems and to unravel the details of reaction mechanisms. The present project will also be of some significance in related fields such as astrophysics and environmental sciences, and even in semiconductor fabrication.

II-A-1 Infrared Diode Laser Spectroscopy of the $^{15}NO_3$ Radical

Takashi ISHIWATA *(Tokyo Inst. Tech.)*, **Ikuzo TANAKA** *(Tokyo Inst. Tech.)*, **Kentarou KAWAGUCHI, and Eizi HIROTA**

In order to obtain further information on the anomalies observed for the diode laser spectrum of the NO_3 ν_3 N-O degenerate stretching band,[1] we have investigated the ν_3 band of $^{15}NO_3$ in a similar way. We have noticed two types of differences between the spectra of the two isotopic species. For $^{15}NO_3$, ^rR branches were found to be easier than ^PP branches to assign, in contrast with the case of $^{14}NO_3$ for which the reverse is true. The convergence of higher order terms seems to be faster in $^{15}NO_3$ than in $^{14}NO_3$; no N^6 terms were needed in analyzing the observed spectrum of $^{15}NO_3$ consisting of 10 ^PP, 38 ^rQ, and 43 ^rR branch transitions. Table I lists molecular parameters obtained from the least-squares analysis of the observed transition frequencies. The results on $^{14}NO_3$ are also given for comparison.

Reference

1) E. Hirota, K. Kawaguchi, T. Ishiwata, and T. Tanaka, *IMS Ann. Rev.*, 27 (1983).

Table I. Molecular Parameters of the NO_3 ν_3 Band (cm^{-1})[a]

Parameter	$^{14}NO_3$		$^{15}NO_3$	
	ν_3 state	Ground state	ν_3 State	Ground State
ν_0	1492.3929(9)		1472.8331(13)	
B	0.45522(11)	0.45746(12)	0.45580(18)	0.45851(19)
C	0.22713(6)	$B_0/2$	0.22785(9)	$B_0/2$
D_N	0.0000014(3)	0.0000016(3)	0.0000030(9)	0.0000042(10)
D_{NK}	−0.0000968(39)	−0.0000839(38)	−0.0000633(18)	−0.0000660(20)
$C\zeta$	0.04479(11)		0.03557(12)	
q_3	0.001624(33)		0.00141(69)	
l_3	0.0000004580(43)		0.0000004580[b]	
ε_{bb}	0.0280(27)	0.0277(28)	0.0212(46)	0.0251(45)
ε_{cc}	0.1197(36)	0.1117(34)	0.1432(26)	0.1428(27)

a. Values in parentheses denote one standard deviation and apply to the last digits of the constants.
b. Fixed to the $^{14}NO_3$ value.

II-A-2 The Microwave Spectrum of the PO_2 Radical

Kentarou KAWAGUCHI, Shuji SAITO, and Eizi HIROTA

We have previously observed far infrared laser magnetic resonance (FIR LMR) signals on 17 laser lines for a system of red phosphorus reacting with discharge products of a H_2/O_2 mixture and have ascribed these signals to the pure rotational transitions of PO_2.[1] Verma and McCarthy[2] have recently reported absorption spectra in the region of 3115 to 2680 Å observed for a PCl_3, O_2, and He mixture flash photolyzed and have ascribed them to the $2^2B_2 \leftarrow \tilde{X}^2A_1$ of PO_2. They have evaluated the ground-state ν_2 frequency to be 505 ± 4 cm^{-1}.

We have succeeded in observing the microwave spectrum of PO_2. The spectrum was about 50% stronger when red phosphorus was replaced by PH_3. The least-squares analysis of the observed spectral lines, about 100 in total, led to molecular parameters shown in Table I. The Fermi term of P is exceptionally large, and its correction term in K^2, σ_K, needs to be included in the fit. The present result allows us to make assignments for FIR LMR spectra; three of them are assigned to $\nu_2 = 1$. The observed centrifugal distortion constants lead to the following estimates for the three vibrational frequencies: $\nu_1 = 1089$, $\nu_2 = 377$, and $\nu_3 = 1269$ cm^{-1}, which suggest the assignment of Verma and McCarthy to be revised. The structure parameters are calculated from A_0, B_0, and C_0 to be r_0 (P − O) = 1.4665 Å and θ_0(O − P − O) = 135.3°.

Table I. Molecular Constants of the PO_2 Radical (MHz)[a]

Constant	Value	Constant	Value
A	104 506.961(36)	ε_{aa}	1636.45(35)
B	8 598.2802(51)	ε_{bb}	21.486(30)
C	7 921.4148(39)	ε_{cc}	−44.425(33)
		Δ_K^S	−0.691(60)
Δ_N	0.004 624(17)		
Δ_{NK}	−0.389 35(39)	σ_0	1669.7(20)
Δ_K	28.586 6(78)	σ_K	−0.258(48)
δ_N	0.000 9868(12)	T_{aa}	−141.0(12)
δ_K	0.046 11(81)	T_{bb}	216.63(57)

a. Values in parentheses denote three standard deviations and apply to the last digits of the constants.

References

1) K. Kawaguchi, N. Ohashi, and E. Hirota, *IMS Ann. Rev.*, 30 (1983)
2) R.D. Verma and C.F. McCarthy, *Can. J. Phys.*, **61**, 1149 (1983).

II-A-3 Infrared Diode Laser and Microwave Spectroscopy of the NCl Radical: Break-down of Born-Oppenheimer Separation

Chikashi YAMADA, Yasuki ENDO, and Eizi HIROTA

The NCl radical is an interesting species from both astronomical and environmental points of view. Our diode laser observation of its vibration-rotation spectrum has prompted us to detect the microwave spectrum, which was already reported.[1] In order to get more precise and detailed information, we have extended the measurement both in the infrared and microwave regions. Figure 1 shows a part of the observed diode laser spectrum.

The diode laser spectrum has been assigned to the $v = 1 \leftarrow 0$ up to $4 \leftarrow 3$ transitions for $N^{35}Cl$ and to the $v = 1 \leftarrow 0$ up to $3 \leftarrow 2$ for $N^{37}Cl$, while the pure rotational spectrum has been observed for $v = 1$, 2, and 3 and $v = 0$ and 1 for the two isotopic species, respectively. All these data were included in a least-squares analysis to derive Dunham coefficients. The isotope dependence was necessary to be included for ω_e (Y_{10}), B_e (Y_{01}), λ_e, and γ_e. The change of the spin-spin interaction constant with the vibrational excitation was discussed in terms of the second-order spin-orbit interaction through the $b^1\Sigma^+$ state.

Reference

1) C. Yamada, Y. Endo, and E. Hirota, *J. Chem. Phys.*, **79**, 4159 (1983).

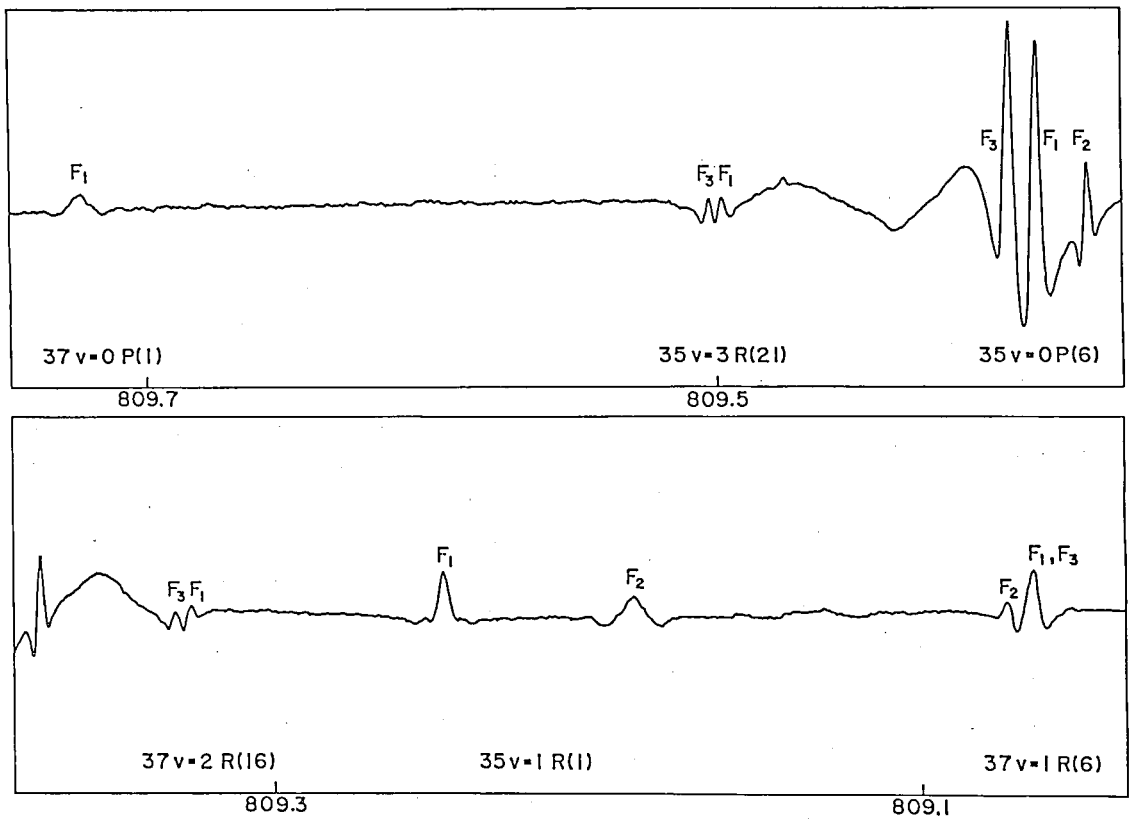

Figure 1. A part of the diode laser spectrum of NCl.

II-A-4 The ν_1 Band of the DO_2 Radical by Difference Frequency Laser and Diode Laser Spectroscopy: the Equilibrium Structure of the Hydroperoxyl Radical

Karen G. LUBIC *(NRC)*, **Takayoshi AMANO** *(NRC)*, **Hiromichi UEHARA** *(Josai Univ.)*, **Kentarou KAWAGUCHI, and Eizi HIROTA**

The hydroperoxyl radical is an important intermediate in chemical reactions involving both hydrogen and oxygen, and high resolution spectroscopic studies have already been extended to the pure rotation and fundamental vibration-rotation bands of the two isotopic species HO_2 and DO_2 with an exception of the ν_1 band of DO_2. Two types of spectroscopy have been applied to this band, and the observed lines, 181 in total, have been assigned to six subbands with $K_a = 2 \leftarrow 3$, $1 \leftarrow 2$, $0 \leftarrow 1$, $1 \leftarrow 0$, $2 \leftarrow 1$, and $3 \leftarrow 2$ and have been included in a least-squares analysis to determine molecular parameters for the upper state: A = 326 929.3(92), B = 31 683.68(36), C = 28 779.96(46), ε_{aa} = −26 039(38), ε_{bb} = −381.7(29), and ε_{cc} = 4.3(22), in MHz, and the band origin ν_0 = 2549.224 65(36) cm^{-1}, with one standard errors in parentheses. By combining these data with those for the ν_2/ν_3 bands of DO_2[1] and those for HO_2 already available in the literatures, the equilibrium structure of the hydroperoxyl radical was calculated with estimated uncertainties as follows: r_e(O − H) = 0.9707 ± 0.0020 Å, r_e(O − O) = 1.33054 ± 0.00085 Å, and θ_e(HOO) = 104.29 ± 0.31°.

Reference

1) H. Uehara, K. Kawaguchi, and E. Hirota, *IMS Ann. Rev.*, 37 (1983).

II-A-5 The Microwave Spectrum of the Chloromethyl Radical, CH_2Cl

Yasuki ENDO, Shuji SAITO, and Eizi HIROTA

The characteristic difference in the structures of the methyl (planar)[1] and trifluoromethyl (pyra-

midal)[2] radicals has now been fairly well understood by examining to what extent electrons are delocalized from the central carbon atom toward more electronegative fluorine atoms. In order to examine this explanation in more detail, we have investigated CH_2F by microwave spectroscopy,[3] and the present report describes a similar study on CH_2Cl.

The radical was generated by the reaction of CH_3Cl with 2450 MHz microwave discharge products of CF_4. The a-type R-branch transitions have been observed with resolved fine and hyperfine components for both the ^{35}Cl and ^{37}Cl isotopic species in the ground state. The small positive inertial defect, $\Delta_0 = 0.0333$ amuÅ^2, calculated from the observed rotational constants indicates that the radical is planar in the ground vibronic state. The observed fine and hyperfine interaction constants are consistent with $^2B_1$ symmetry, i.e. with the unpaired electron occupying a p_π orbital extending perpendicular to the molecular plane. The spin density on the Cl atom is calculated from T_{cc} to be 15.7%. Table I summarizes some of the main molecular parameters derived.

References

1) C. Yamada, E. Hirota, and K. Kawaguchi, *J. Chem. Phys.*, **75**, 5256 (1981).
2) Y. Endo, C. Yamada, S. Saito, and E. Hirota, *J. Chem. Phys.*, **77**, 3376 (1982); C. Yamada and E. Hirota, *J. Chem. Phys.*, **78**, 1703 (1983).
3) Y. Endo, C. Yamada, S. Saito, and E. Hirota, *J. Chem. Phys.*, **79**, 1605 (1983).

Table I. Molecular Parameters of the $CH_2{}^{35}Cl$ Radical[a]

Constant	Value	Constant	Value
A	274 380(78)	a_F(Cl)	8.64(29)
B	15 948.0282(126)	T_{aa}(Cl)	−32.285(85)
C	15 057.0443(123)	T_{bb}(Cl)	−22.74(128)
ε_{aa}	−3 149.45(36)	χ_{aa}(Cl)	−66.09(22)
ε_{bb}	−237.623(114)	χ_{bb}(Cl)	42.6(26)
ε_{cc}	11.814(100)		

a. In MHz. Values in parentheses denote 2.5 standard deviations and apply to the last digits of the constants.

II-A-6 High Resolution, cw Laser Induced Fluorescence Study of the $A^2\Pi_u - X^2\Sigma_g^+$ System of N_2^+

Terry A. Miller *(Bell Lab. and IMS)*, **Tetsuo SUZUKI, and Eizi HIROTA**

[*J. Chem. Phys.*, **80**, 4671 (1984)]

In spite of the importance of N_2^+ in many fields, the A-X transition has been rather sparingly studied and the A state is not particularly well characterized. In the present study the N_2^+ ion was produced by Penning ionization of N_2 by He metastables formed upstream in a DC discharge and was detected by laser induced fluorescence using a single mode, cw dye laser, thereby demonstrating the feasibility of continuous ion monitoring and measurement of ion Doppler profiles. A detailed spectral analysis has been performed for 173 transitions of the 4-0 A-X Meinel band system of N_2^+. Molecular constants for both the X and A states are obtained. By combining the present results with earlier optical emission work on other vibrational transitions of the Meinel system, equilibrium molecular constants are obtained.

II-A-7 Dipole Moment of HNO in the $\tilde{A}^1A''(100)$ State

Kojiro TAKAGI *(Toyama Univ.)*, **Tetsuo SUZUKI, Shuji SAITO, and Eizi HIROTA**

The Stark effect of HNO in the $\tilde{A}^1A''(100)$ state has been measured using an MODR technique. The observed rotational transitions and the dipole moment calculated from the measured Stark effect are as follows: $3_{21} - 3_{22}$, $M_J = 3$ and $5_{23} - 5_{24}$, $M_J = 5$ yielding $\mu_a = 1.057(6)$ D, $4_{31} - 4_{32}$, $M_J = 4$ and $5_{32} - 5_{33}$, $M_J = 5$ $\mu_a = 1.089(6)$ D, and $6_{16} - 7_{07}$, $M_J = 4,5,6$ $\mu_b = 1.311(7)$ D. The present μ_a values may be compared with 1.083(10) D and 1.079(25) D which Dixon and Noble[1] derived from an OODR experiment for $K_a = 3$ and 4, respectively. The Stark components of the last transition is displayed in Figure 1. The electrode spacing was calibrated by measuring the Stark effects of the HNO ground-state transition, $2_{20} - 2_{21}$, with the dipole moment reported by Johns and McKellar,[2] $\mu_a = 0.996(6)$ D and $\mu_b = 1.28(2)$ D. The dipole moment is thus little changed upon A ← X excitation, as other molecular constants such as structural parameters.

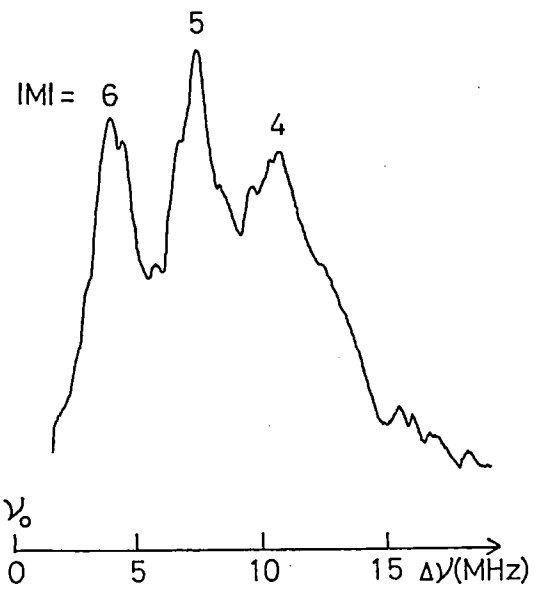

Figure 1. The $6_{16} - 7_{07}$ transition of HNO in $\tilde{A}^1A''(100)$ observed by MODR with a Stark field of 1600 V/cm. The pumped optical transition was $^rQ_0(6)$ at 16 023.52 cm^{-1}.

References

1) R.N. Dixon and M. Noble, *Chem. Phys.*, **50**, 331 (1980).
2) J.W.C. Johns and A.R.W. McKellar, *J. Chem. Phys.*, **66**, 1217 (1977).

II-A-8 The Microwave Spectrum of the PCl Radical

Tatsuya MINOWA, Shuji SAITO, and Eizi HIROTA

Little has been known about the molecular structure of the PCl radical; Huber and Herzberg[1] have included only three electronic states with the T_e, ω_e, and $\omega_e x_e$ values in their compilation.

We have recently observed the microwave spectrum of $P^{35}Cl$, which was generated by an internal discharge in PCl_3 contained in a 3.5 m long absorption cell. The discharge current was about 30 mA. One hundred and six lines were observed, which were assigned to the transitions of $N = 5 \leftarrow 4$ up to $11 \leftarrow 10$.

A least-squares analysis using Hund's case (b) wavefunctions as bases was performed to determine molecular parameters shown in Table I. When the magnetic hyperfine coupling constants of both the P and Cl nuclei are compared with the corresponding atomic values of Morton and Preston,[2] the s character and the spin density are calculated to be (0.86%, 87.2%) and (0.12%, 13.9%) for P and Cl, respectively.

References

1) K.P. Huber and G. Herzberg, "Molecular Spectra and Molecular Structure IV. Constants of Diatomic Molecules", Van Nostrand Reinhold, New York, 1979.
2) J.R. Morton and K.F. Preston, *J. Magn. Reson.*, **30**, 577 (1978).

Table I. Molecular Constants of the PCl Radical[a]

Constant	Value	Constant	Value
B	7558.3446(15)	b(Cl)	18.87(12)
D	0.006 3646(81)	c(Cl)	−36.64(36)
		eQq(Cl)	−45.5(15)
λ	127 542.87(81)		
λ_D	−0.13640(66)	b(P)	274.15(21)
		c(P)	−479.82(63)
γ	−91.511(33)		

a. In MHz. Values in parentheses denote three standard deviations and apply to the last digits of the constants.

II-A-9 The Microwave Spectrum of the Vinoxy Radical, CH_2CHO

Yasuki ENDO, Shuji SAITO, and Eizi HIROTA

The vinoxy radical has attracted attention, presumably because of its role in many organic reactions and also of its characteristic structure. A large number of spectroscopic studies have already been performed using various kinds of techniques. The present study employed microwave spectroscopy to obtain detailed information on the molecular structure, in particular on the planarity and the electronic structure of the molecule through the rotational constants and the fine/hyperfine structures.

The vinoxy radical was generated by either $CH_3CHO + F$ or $C_2H_4 + O$. The former is much more efficient than the latter in generating the radical, while the latter gives cleaner spectrum than the former. About 150 lines were observed, which were assigned to a-type R branch transitions with $N = 4 \leftarrow 3$ up to $8 \leftarrow 7$, but no b-type transitions have been identified. Two of the three protons were found to produce hyperfine structures, and, because the off-diagonal dipolar term T_{ab} was determined

together with ε_{ab} for both the protons, the principal values of **T** with the transformation angle were obtained and were unambiguously assigned to the two protons in the CH_2 group. This result implies that the resonance form in the ground electronic state is $\cdot CH_2 - CH = O$ rather than $CH_2 = CH - O\cdot$. The rotational constants which listed in Table I with other parameters lead to the inertial defect of 0.058 amuÅ^2, indicating the molecule to be planar.

Table I. Molecular Constants of the Vinoxy Radical[a]

Constant	Value	Constant	Value
A	66 676.70(47)	$a_F(1)$	−56.48(23)
B	11 447.0478(63)	$T_{aa}(1)$	12.17(15)
C	9 758.9165(60)	$T_{bb}(1)$	−14.52(39)
		$T_{ab}(1)$	∓23.93(29)[b]
ε_{aa}	−898.91(14)		
ε_{bb}	−66.078(32)	$a_F(2)$	−54.57(21)
ε_{cc}	−0.667(26)	$T_{aa}(2)$	−28.26(14)
$(\varepsilon_{ab} + \varepsilon_{ba})/2$	±84.165(61)[b]	$T_{bb}(2)$	28.07(33)
		$T_{ab}(2)$	∓5.28(29)[b]

a. In MHz. Values in parentheses denote 2.5 standard deviations and apply to the last digits of the constants.
b. The three signs are correlated and must be taken in the same order.

II-A-10 Infrared Diode Laser Spectroscopy of the PCl Radical in the $X^3\Sigma^-$ State

Hideto KANAMORI, Chikashi YAMADA, Kentarou KAWAGUCHI, James E. BUTLER *(NRL and IMS)*, **and Eizi HIROTA**

In concurrence with a microwave study (II-A-8), we have investigated the PCl radical also by infrared diode laser spectroscopy. The radical was generated by a discharge in a PCl_3/H_2 mixture with the partial pressures of 300/100 mTorr. The region of 560 to 575 cm^{-1} was scanned, and 60 and 30 lines were assigned to the $v = 1 \leftarrow 0$ and $2 \leftarrow 1$ bands of $P^{35}Cl$ and 21 lines to $v = 1 \leftarrow 0$ of $P^{37}Cl$. Assuming isotope relations between constants of the two species, all the observed lines were included in a least-squares analysis. Molecular constants thus derived are summarized in Table I. The centrifugal distortion constant is calculated from the formula $D_e = 4B_e^3/\omega_e^2$ to be 2.12749 10^{-7} cm^{-1}, which agrees well with the observed value 2.12432 10^{-7} cm^{-1}. The equilibrium rotational constant B_e gives r_e to be 2.0146 Å which may be compared with the r_e values of Cl_2 (1.9879 Å) and P_2 (1.8934 Å).

Table I. Molecular Constants of the PCl Radical[a]

Constant	Value	Constant	Value
ω_e	551.384 90(42)	λ_e	4.260 443(72)
$\omega_e x_e$	2.226 01(14)	α^λ	0.020 223(112)
B_e	0.252 874 98(17)	λ_D	0.455 24(93)10^{-5}
α^B	0.001 512 29(27)		
γ^B	0.000 001 617(62)	γ_e	0.303 049(382)10^{-2}
		α^γ	−0.004 076(637)10^{-2}
D_e	0.212 431(94)10^{-6}		
β^D	0.000 056(34)10^{-6}	γ_D	0.212(367)10^{-7}

a. In cm^{-1}. Values in parentheses denote one standard error and apply to the last digits of the constants.

II-A-11 Excimer Laser Photolysis of SO_2: Spin Polarization in SO Generated

Hideto KANAMORI, Kentarou KAWAGUCHI, James E. BUTLER *(NRL and IMS)*, **Chikashi YAMADA, and Eizi HIROTA**

The photochemical processes induced in sulfur dioxide by the 193 nm excimer laser line have been

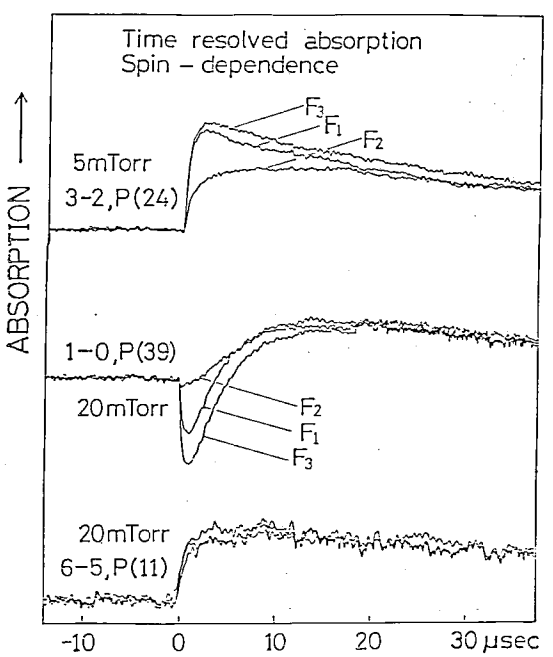

Figure 1. Time profiles of vibration-rotation signals of SO generated by photolyzing SO_2 with the 193 nm excimer laser line. The difference between the F_1/F_3 and F_2 components is clearly seen for the upper two transitions, whereas the last transition does not show such difference.

investigated by examining vibration-rotation transitions of the reaction product SO by the use of tunable infrared diode laser spectroscopy. Only $X^3\Sigma^-$ ground-state SO molecules were detected. About 70% of the nascent SO molecules were found to be in the v =2 state, about 20% in v = 1, and some in v = 5, and in each vibrational state the rotational distribution differed significantly from the thermal distribution, and was shifted towards higher rotational levels in lower vibrational states. A more interesting observation is that the electron spin is polarized in the v = 1 and 2 states, i.e. the F_1 and F_3 spin sublevels are more populated than the F_2 level in these states. Figure 1 shows the time profiles of the signals for the $v = 3 - 2$ P(24), $v = 1 - 0$ P(39), and $v = 6 - 5$ P(11) transitions; for the former two the F_1 and F_3 components are clearly stronger than the F_2 component by a factor of 3 or more. It is suspected that the spin polarization is ascribed to spin-orbit mixing of the SO_2 $\tilde{C}$ state to which SO_2 is initially pumped by the excimer laser with a repulsive triplet state.

II-A-12 Infrared Absorption Spectrum of SO

Hideto KANAMORI, Kentarou KAWAGUCHI, Chikashi YAMADA, and Eizi HIROTA

The vibrational and rotational levels of the SO molecule in the $X^3\Sigma^-$ state have been extensively investigated by microwave,[1] infrared laser magnetic resonance (IR LMR),[2] and difference-frequency laser[3] spectroscopy. We have recently detected SO molecules by diode laser spectroscopy which were generated by photolyzing SO_2 by a 193 nm excimer laser (II-A-11) and have observed the vibration-rotation transitions of up to $v = 6 - 5$; about 100 lines have been recorded. Combining this result with the previous microwave result of Bogey et al.,[1] the vibrational parameters are revised as follows:

$$\omega_e = 1150.791\ 05(51)\ \mathrm{cm}^{-1},$$
$$\omega_e x_e = 6.409\ 41(14)\ \mathrm{cm}^{-1},$$
$$\omega_e y_e = 0.013\ 017(11)\ \mathrm{cm}^{-1},$$

where the values in parentheses denote one standard error and apply to the last digits of the constants. The accuracy has been improved by a factor of 8 to 40.

References

1) M. Bogey, C. Demuynck, and J.L. Destombes, *Chem. Phys.*, **66**, 99 (1982).
2) K. Kawaguchi, C. Yamada, and E. Hirota, *J. Chem. Phys.*, **71**, 3338 (1979).
3) M. Wong, T. Amano, and P. Bernath, *J. Chem. Phys.*, **77**, 2211 (1982).

II-A-13 Microwave-Optical Double Resonance Spectroscopy of the NCO Radical in the $\tilde{A}^2\Sigma^+$ State

Tetsuo SUZUKI, Shuji SAITO, and Eizi HIROTA

As described previously,[1] we have extended the wavelength region of our cw dye laser to the region of 430 to 480 nm using Exciton dyes S420 and C460. As an application of the dye laser in this region, the microwave-optical double resonance (MODR) spectrum of the NCO radical in the $\tilde{A}^2\Sigma^+$ state was observed. Bolman et al.[2] have reinvestigated the $\tilde{A}$-$\tilde{X}$ band system of NCO in detail, and their data were readily used to predict the frequencies of the three lowest rotational transitions, $N = 1 - 0$, $2 - 1$, and $3 - 2$, in the $\tilde{A}$ state.

The dye laser delivered the output power of 30 to 40 mW. The NCO radical was generated by the reaction of HNCO of 1 mTorr with microwave discharge products of CF_4 of 40 to 50 mTorr. Two lines were observed for $N = 1 - 0$; the higher component is about 2.5 times more intense than the lower component, and the two lines have, respectively, about 32 MHz and 10 MHz separations between the maxima and minima of the first derivative lineshape. Three and two lines were also observed for the $N = 2 - 1$ and $3 - 1$ transitions, respectively.

References

1) T. Suzuki, S. Saito, and E. Hirota, *IMS Ann. Rev.*, 40 (1983).
2) P.S.H. Bolman, J.M. Brown, A. Carrington, I. Kopp, and D.A. Ramsay, *Proc. R. Soc. London*, Ser. **A343**, 17 (1975).

II-A-14 The $A^2\Pi \leftarrow X^2\Sigma^+$ System of the SiN Radical by Infrared Diode Laser Spectroscopy

Chikashi YAMADA and Eizi HIROTA

In contrast with an isovalent radical CN, the B-A and A-X transitions of SiN have not been observed, leaving the location of the A state and a few other excited states relative to the ground state rather uncertain. Bredohl et al.[1] estimated the term value of the A state to be about 8000 cm^{-1} from perturbations observed for the $X^2\Sigma^+$ $v = 8$ state. Linton[2] interpreted perturbations in the $D^2\Pi$ $v = 3$ state to be caused by the $B^2\Sigma^+$ $v = 9$ to 11 states and presumed the A state to be located between 2500 and 4000 cm^{-1} above the ground state.

In the course of studying discharge plasma of SiH_4 diluted with N_2 using infrared diode laser spectroscopy, we have observed a number of strong, Zeeman-sensitive absorption lines in the 5 μm region. Figure 1 shows a part of the observed spectrum, which is assigned to the $A^2\Pi_{1/2} - X^2\Sigma^+$ transition. When least-squares analyzed, the observed spectrum leads to the upper-state B rotational constant that agrees with the B value of the A $v = 1$ state reported by Bredohl et al.,[1] and is thus assigned to the 1,0 band. We have, in fact, observed some lines in the 10 μm region.

References

1) H. Bredohl, I. Dubois, Y. Houbrechts, and M. Singh, *Can. J. Phys.*, **54**, 680 (1976).
2) C. Linton, *J. Mol. Spectrosc.*, **55**, 108 (1975).

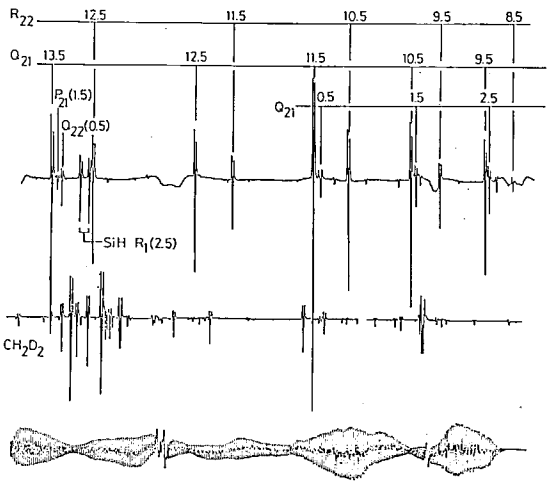

Figure 1. A part of the $A^2\Pi_{1/2} - X^2\Sigma^+$ v = 1 − 0 band of SiN.

II-A-15 The Microwave Spectrum of the CH_3S Radical

Yasuki ENDO, Shuji SAITO, and Eizi HIROTA

The thiomethoxy radical CH_3S is an analogue of the methoxy radical which has a ^2E ground electronic state, and these two will exhibit the effect of Jahn-Teller interaction even in their ground

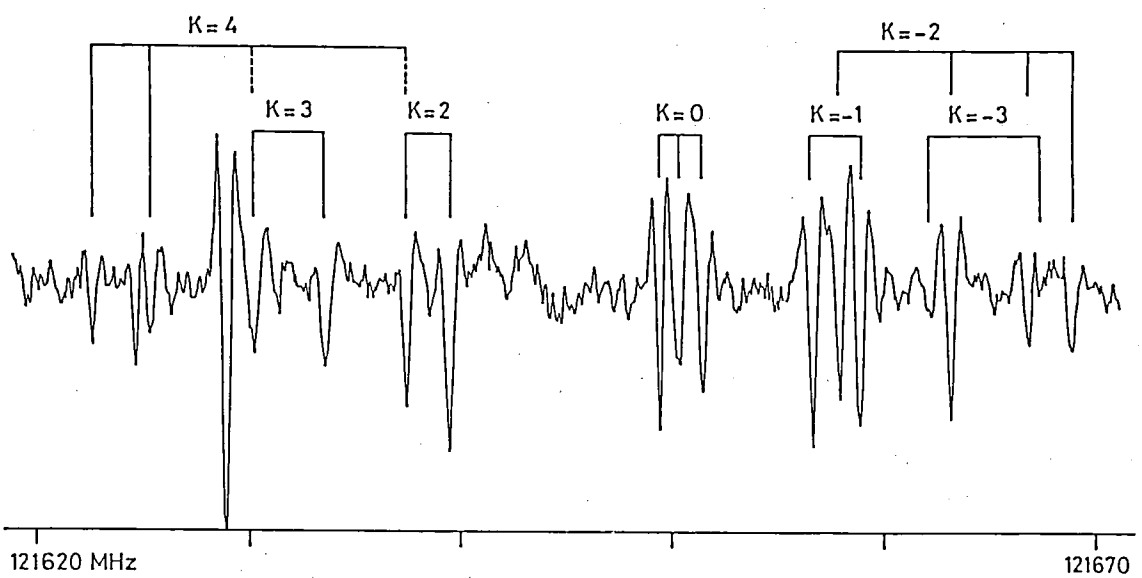

Figure 1. The $J = 4.5 \leftarrow 3.5$ transition of CH_3S in the $^2E_{1/2}$ state.

states when investigated by high resolution spectroscopic tools such as microwave spectroscopy. We have already reported the result on CH_3O,[1] and a similar study on CH_3S is described here.

The CH_3S radical was generated by the reaction of CH_3SH with F. The reaction mixture was pumped through a cell by a turbo pump with a speed of 50 to 60 *l*/s. The total pressure was maintained less than 5 mTorr. Figure 1 shows the $J = 4.5 \leftarrow 3.5$ transition of CH_3S in the $^2E_{1/2}$ state; the *K* structure characteristic of a ^2E molecule is easily discernible, and is further split by the proton hyperfine interaction. The $J = 5.5 \leftarrow 4.5$, $4.5 \leftarrow 3.5$, and $2.5 \leftarrow 1.5$ transitions have been observed for $^2E_{3/2}$, and the former two for $^2E_{1/2}$, and all the observed spectra are being analyzied.

Reference

1) Y. Endo, S. Saito, and E. Hirota, *J. Chem. Phys.*, **81**, 122 (1984).

II-A-16 The Dye Laser Excitation Spectrum of the C_2 $d^3\Pi_g$ — $a^3\Pi_u$ Transition (the Swan Band)

Tetsuo SUZUKI, Shuji SAITO, and Eizi HIROTA

Hakuta[1] has recently pointed out that there is an inconsistency between molecular constants of C_2, in particular the spin-orbit coupling constants *A*, of the a state obtained from the $b^3\Sigma_g^+ - a^2\Pi_u$ (Ballik-Ramsay) and $d^3\Pi_g - a^3\Pi_u$ bands. This is primarily due to the fact that $\Delta\Omega = 0$ transitions normally observed for the Swan band are insufficient to determine the *A* constants of the d and a states separately.

We have recently succeeded in observing $\Delta\Omega = \pm 1$ as well as $\Delta\Omega = 0$ components of the d-a $v = 1 - 0$ transition by laser excitation spectroscopy with Doppler-limited resolution. The C_2 molecule was obtained by the reaction of CH_4 (1 mTorr) with microwave discharge products of CF_4 (80 mTorr). About 240 lines were assigned in the region of 21100 to 21270 cm^{-1}, of which about 50 lines were due to $\Delta\Omega = \pm 1$. A least-squares analysis of the observed spectrum leads to molecular constants listed in Table I; the $a^3\Pi_u$ $v = 0$ constants thus obtained agree well with those Amiot et al.[2] derived from the Ballik-Ramsay band.

References

1) K. Hakuta, *Laser Kenkyu*, **11**, 568 (1983).
2) C. Amiot, J. Chauville, and J.-P. Maillard, *J. Mol. Spectrosc.*, **75**, 19 (1979).

Table I. Molecular Constants of C_2 in the $a^3\Pi_u$ $v = 0$ and $d^3\Pi_g$ $v = 1$ States[a]

Constant	$a^3\Pi_u$ $v = 0$		$d^3\Pi_g$ $v = 1$
	present	Amiot et al.[2]	present
A_v	−15.2690(19)	−15.2629(45)	−13.8742(20)
λ_v	−0.1540(14)	−0.1574(38)	0.0160(15)
$\lambda_{\perp v}$	−0.6763(15)	−0.6760(20)	−0.6208(15)
B_v	1.623 964(55)	1.623 990(18)	1.725 332(55)
D_v	6.360(78) 10^{-6}	6.4405(38) 10^{-6}	6.940(78) 10^{-6}
p_v	5.19(38) 10^{-3}	4.55(20) 10^{-3}	8.24(38) 10^{-3}
q_v	−1.081(50) 10^{-3}	−1.0559(48) 10^{-3}	−1.637(48) 10^{-3}
A_{Dv}	2.26(35) 10^{-4}	3.78(11) 10^{-4}	5.31(38) 10^{-4}
T_{10}(d-a)	21 132.24006(90)		

a. In cm^{-1}. Values in parentheses denote 2.5 standard errors and apply to the last digits of the constants.

II-A-17 The Microwave Spectrum of the PF_2 Radical

Shuji SAITO, Yasuki ENDO, and Eizi HIROTA

During the course of studying the PF radical[1] generated by the discharge in a PH_3/CF_4 mixture, we observed a number of paramagnetic lines, which we assigned to the PF_2 radical. No previous studies have been reported on spectroscopy of PF_2 in the gas phase.

The ground state of PF_2 belongs to $^2B_1$ of C_{2v} symmetry, and the K_aK_c = ee and oo levels are split into 12 components by the spin-rotation and P and F hyperfine interactions, wherease the F hyperfine interaction is absent in the K_aK_c = eo and oe levels. Seven rotational transitions with $I_F = 0$ were first analyzed to determine 13 molecular constants, which were then fixed in analyzing two $I_F = 1$ transitions. The rotational constants thus obtained lead to the r_0 structure: r(P − F) = 1.5792Å and θ(F − P − F) = 98.493°. It is interesting to note that the ε_{aa} spin-rotation interaction constant is very small (−32 MHz). This may imply that excited electronic states contributing to ε_{aa} are highly located and/or their contributions are cancelled. The T_{cc} dipolar hyperfine constants give the spin densities of 92.4% and 8.1% for P and F, respectively, while the Fermi

terms lead to the s characters of 1.65% and 0.18% for the two atoms.

Reference

1) S. Saito, Y. Endo, and E. Hirota, *IMS Ann. Rev.*, 36 (1983).

II-A-18 The Microwave Spectrum of the H_2D^+ Ion: the $2_{20} - 2_{21}$ Transition

Shuji SAITO, Kentarou KAWAGUCHI, and Eizi HIROTA

Molecular ions have recently attracted considerable interest presumably because of their important roles in interstellar space. The H_3^+ ion is the most fundamental one among others, and Oka[1] has observed its ν_2 vibration-rotation band by difference-frequency laser spectroscopy. However, because of lack of a permanent dipole moment, H_3^+ is difficult to detect in the microwave region. The singly deuterated species H_2D^+ is more promising, because its dipole moment has been estimated to be as large as 0.6 D.[2] As shown in the upper trace of Figure 1, we have observed the $2_{20} \leftarrow 2_{21}$ transition of H_2D^+ using a DC discharge in a mixture of H_2 and D_2 with a hollow cathode cooled to liquid nitrogen temperature. We have made the assignment, based upon the chemistry for production of the ion, the observed linewidth which is about 0.7 MHz FWHM, in good agreement with the Doppler width of 0.79 MHz calculated for H_2D^+, and the spectral intensity which decreases to 1/5 by a magnetic field of 50 G, as shown in the lower trace of Figure 1. The transition frequency was measured to be 155 987.185 ± 0.037 MHz.

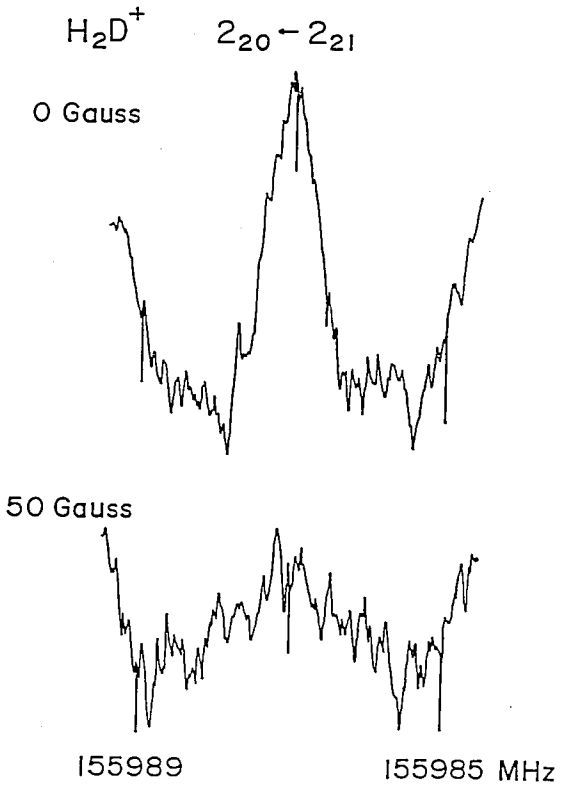

Figure 1. The $2_{20} \leftarrow 2_{21}$ transition of H_2D^+. The lower trace shows the ion production to be sensitive to the external magnetic field; the line almost disappeared by a 50 G magnetic field applied to the hollow cathode.

References

1) T. Oka, *Phys. Rev. Lett.*, **45**, 531 (1980).
2) A. Dalgarno, E. Herbst, S. Novick, and W. Klemperer, *Astrophys. J.*, **183**, L131 (1973).

II-A-19 Spin Density and Ionization Potential of Diatomic Free Radical

Eizi HIROTA

The magnetic hyperfine interaction constants a, b, c, and d determined for diatomic free radicals allow us to estimate the s character and spin density of the unpaired electron orbital. The free radicals so far examined are listed in Table I, where the spin density α^2 or β^2 is also included. For a Π radical it may be calculated by either $d + c/3$ or $-(5/3)c$, the former being preferred. For a $^3\Sigma^-$ radical the latter is employed. It is remarkable that the spin densities α^2 and β^2 of the three $^3\Sigma^-$ molecules satisfy the normalization condition $\alpha^2 + \beta^2 = 1$. In two $^2\Sigma^+$ molecules the unparied electron orbital is a σ orbital, so that $(5/6)c$ is used to calculate β^2.

The spin density is related to the orbital energies, which may be estimated from the ionization potentials (IP) of the atoms and the molecule involved. Namely, Δ denotes the difference between the IP's of the two atoms and δ the difference between the IP's of the less electronegative atom and of the molecule, then $\beta^2 = \delta/(\Delta + 2\delta)$ is derived using a simple LCAO model. Table I shows that, when both Δ and δ are available, β^2 calculated from them agree quite well with that derived from the magnetic hyperfine constants, provided that the

Table I. Spin Densities in Diatomic Free Radicals

Groups (elect. conf.)	Free Radical	β^2(F,Cl) $d + c/3$	$-(5/3)c$	Δ (eV)	δ (eV)	β^2 (Δ,δ)
IV – VII	CF	0.153	0.134	6.16	2.06	0.200
$^2\Pi_r$	SiF	0.068	0.066	9.27	0.87	0.079
$\sigma^2\pi^4\pi^*$	GeF	~0.05		9.54	0.42	0.040
	CCl	0.157	0.150	(2.7~3.7)		
	SiCl	0.090	0.080	(5.9~6.9)		
		α^2(N, P)				β^2
V – VI	NO	0.669	0.709	(3.6~2.6)	(0.7~1.7)	
$^2\Pi_r$	PO	0.668	0.755	2.61	2.61	0.333
$\sigma^2\pi^4\pi^*$	NS	0.514	0.561	(0)		
		β^2(F, Cl)				
VI – VII	SF	0.110	0.120	7.06		
$^2\Pi_i$	OCl	0.324	0.351	(0.39~1.39)	2.61	
$\sigma^2\pi^4\pi^{*3}$						
		α^2(N,P) $-(5/3)c$	β^2(F,Cl) $-(5/3)c$			
V – VII	PF	0.913	0.091	6.42		
$^3\Sigma^-$	NCl	0.758	0.219	(3~5)		
$\sigma^2\pi^4\pi^{*2}$	PCl	0.869	0.136	(3~4)		
		β^2 or α^2(N) $(5/6)c$				
IV – V	CN	0.363				
$^2\Sigma^+$	SiN	0.567		(1.9~2.9)		
$\pi^4\sigma$						

IP's of N and Cl are revised to 10 ~ 11 and 14 ~ 15 eV, respectively.

II-A-20 Harmonic and Anharmonic Potentials of the H_3^+ Ion

Eizi HIROTA

In view of great importance of the H_3^+ ion, as mentioned in II-A-18, harmonic and anharmonic potential constants have been calculated from the existing data.

The internal coordinate is chosen to be the change in the H-H distance. When the ν_2 band origin 2521.564 cm^{-1} reported by Oka[1] is taken to be the harmonic frequency together with an assumed value 3200 cm^{-1} for ν_1, the two harmonic potential constants are calculated to be $F_{11} = 2.353$ md/Å and $F_{12} = -0.163$ md/Å.

The third-order anharmonic constants may be estimated from the vibration-rotation constants α_2^B and α_2^C and the *l*-type doubling constant q_2, which Oka reported in Ref. 1. There are three third-order constants F_{111}, F_{112}, and F_{123}, whereas both α_2^B and α_2^C are linear functions of $F_{111} - F_{123}$ and q_2 of $F_{111} - 3F_{112} + 2F_{123}$, i.e. $(F_{111} - F_{123}) - 3(F_{112} - F_{123})$. The observed α_2^B, α_2^C, and q_2 constants lead to $F_{111} - F_{123}$ and $F_{112} - F_{123}$ to be -13.663 and -0.672 md/Å^2, respectively. Recently Amano and Watson[2] observed the ν_1 band of H_2D^+. Although it is not possible to reproduce their α_1 values within experimental errors, their results suggest $F_{111} = -13.16 \sim -12.56$, $F_{112} = -0.17 \sim +0.23$, and $F_{123} = 0.5 \sim 0.9$ md/Å^2. Table I compares the r_e, F_{11}, and F_{111} of H_3^+ with those of the H_2 molecule.

References

1) T. Oka, *Phys. Rev. Lett.*, **45**, 531 (1980).
2) T. Amano and J.K.G. Watson, *J. Chem. Phys.*, in press.

Table I. Comparison of Molecular Constants of H_3^+ and H_2

Constant	H_3^+	H_2
r_e(Å)	0.873	0.74144
F_{II}(md/Å)	2.353	5.750
F_{III}(md/Å^2)	−13.16 ~ −12.56	−37.387

II-A-21 Infrared Diode Laser Spectroscopy of the CCO Radical Generated by Excimer Laser Photolysis of C_3O_2

Chikashi YAMADA, Hideto KANAMORI, Hiroyuki HORIGUCHI *(Univ. of Tokyo)*, **and Eizi HIROTA**

An excimer laser photolysis technique combined with infrared diode laser spectroscopy as described in II-B-1 has been applied to the CCO radical. The radical was generated by photolyzing carbon suboxide with either the 248 nm or the 193 nm laser line; the 193 nm line is preferred, because emission accompanying the photolysis is weaker than in the case of using the 248 nm line.

We have succeeded in observing the ν_1 band of the CCO radical in the 1970 cm^{-1} region; 34 lines were recorded and assigned to the transitions P(8) to R(26). The least-squares analysis gave molecular constants shown in Table I; the band origin agrees with the value obtained in an Ar matrix (1969 cm^{-1})[1] and that from laser induced fluorescence (1967 cm^{-1}).[2] The photolysis may involve many steps, because it takes about 100 μsec for the signal to grow and about 500 μsec to disappear.

References

1) M.E. Jacox, D.E. Milligan, N.G. Moll, and W.E. Thompson, *J. Chem. Phys.*, **43**, 3734 (1965).
2) W.M. Pitts, V.M. Donnelly, A.P. Baronavski, and J.R. McDonald, *Chem. Phys.*, **61**, 451 (1981).

Table I. Molecular Constants of the CCO Radical[a]

Constant	$v = 0$	$v = 1$
B	[0.385 119 652]	0.382 044 2(86)
D	[0.000 000 194 03]	0.000 000 188(12)
λ	[0.386 4]	0.394 7(12)
λ_D	[−0.000 000 177]	[−0.000 000 177]
γ	[−0.000 594 301]	−0.000 555(40)
ν_0		1970.864 34(95)

a. In cm^{-1}. Values in parentheses denote 2.5 standard errors and apply to the last digits of the constants. Those in square brackets are assumed (the ground-state parameters are taken from the microwave results, II-A-22).

II-A-22 The Microwave Spectrum of the CCO Radical

Chikashi YAMADA, Hideto KANAMORI, Shuji SAITO, and Eizi HIROTA

Because of radioastronomical interest, we have observed the microwave spectrum of the CCO radical in the $\tilde{X}^3\Sigma^-$ state. The radical was generated by a 30 mA DC glow discharge in a flow of carbon suboxide C_3O_2 with a pressure of 30 mTorr. Our previous result using diode laser kinetic spectroscopy (II-A-21) made narrow the frequency region to be scanned. Seven rotational transitions of $N = 2 \leftarrow 1$ up to $8 \leftarrow 7$ were observed, each consisting of three spin components, except for the F_3 component of the $N = 2 \leftarrow 1$ transition which was too weak to measure. Table I lists molecular constants derived from a least-squares analysis of the observed spectrum, together with those obtained by Devillers and Ramsay[1] from the optical spectrum. The accuracy has been considerably improved, especially for B_0 and r_0.

Reference

1) C. Devillers and D.A. Ramsay, *Can. J. Phys.*, **49**, 2839 (1971).

Table I. Molecular Constants of the CCO in $\tilde{X}^3\Sigma^-$[a]

Constant	present[b]	Ref. 1)
B_0	11 545.5967(20)	11 545(6)
D_0	0.005 817(20)	0.006[c]
λ_0	11 583(115)	11 572(150)
λ_D	−0.005 3(15)	–
γ_0	−17.817(14)	−21(9)

a. In MHz.
b. Values in parentheses denote 2.5 standard errors and apply to the last digits of the constants.
c. Calculated from $D = 4B^3/\omega^2$ with ω = 1074 cm^{-1}.

II-A-23 Magnetic Field Modulated Laser Spectroscopy of Molecular Ions: The ν_2 Band of HCO^+

Kentarou KAWAGUCHI, Chikashi YAMADA, Shuji SAITO, and Eizi HIROTA

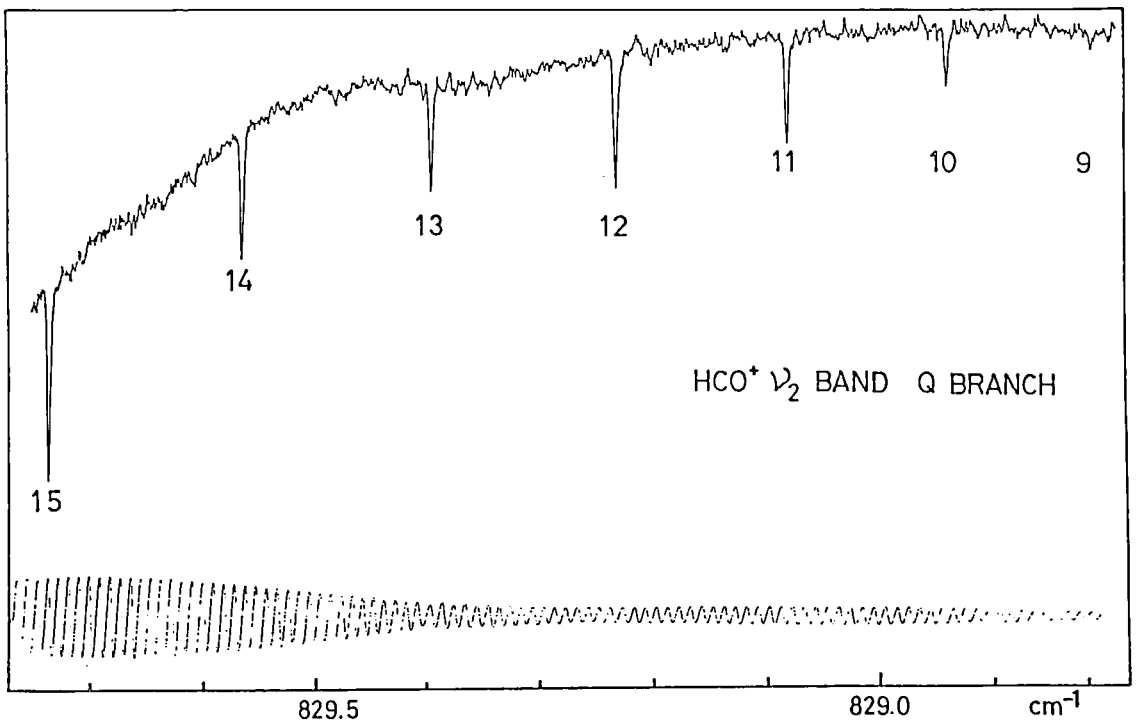

Figure 1. A part of the HCO^+ ν_2 band.

Because of its importance in many fields the molecular ion is one of the central themes for molecular spectroscopy. A remarkable progress has recently been made on infrared spectroscopy using color center, difference-frequency, and diode lasers as sources, and several protonated ions have been detected. Since these species are diamagnetic, velocity modulation developed by Gudeman et al.[1] has been successfully employed in discriminating their absorption lines from those of neutrals.

We have observed that, when an external magnetic field is applied to a hollow cathode, the ion production efficiency is considerably reduced. Because neutrals are much less affected than ions, we have developed a modulation method for selectively detecting ions, and have successfully applied it to the HCO^+ ν_2 band. Figure 1 shows a part of the observed spectrum. The ion was generated by a DC discharge in an H_2(115 mTorr) and CO(115 mTorr) mixture, and the AC and DC magnetic fields were 176 Gauss peak-to-peak at 1.74 kHz and 88 Gauss, respectively. The rotational and *l*-type doubling constans in the $\nu_2 = 1$ state and the band origin were determined to be 1.490 274(14), 0.007 0510(44), and 828.2305(9) cm^{-1} with three standard errors in parentheses.

Reference

1) C.S. Gudeman, M.H. Begemann, J. Pfaff, and R.J. Saykally, *Phys. Rev. Lett.*, **50**, 727 (1983).

II-A-24 Diode Laser Spectroscopy of the CO_2^+ ν_3 Band Using Magnetic Field Moldulation of the Discharge Plasma

Kentarou KAWAGUCHI, Chikashi YAMADA and Eizi HIROTA

The CO_2^+ molecular ion has been expected to bear a similarity with the BO_2 radical in that the ν_3 antisymmetric stretching band has an anomalously low frequency (1423 and 1278 cm^{-1} for CO_2^+ and BO_2, respectively, as compared with 2349 cm^{-1} of CO_2) with a large, negative anharmonicity. We have previously explained the similar behavior of the BO_2 ν_3 mode in terms of a vibronic interaction between $\tilde{X}^2\Pi_g$ and $\tilde{A}^2\Pi_u$ through the ν_3 mode.[1]

We have successfully applied the magnetic field modulation method of discharge plasma (II-A-23) in detecting the ν_3 band of CO_2^+. A DC discharge of

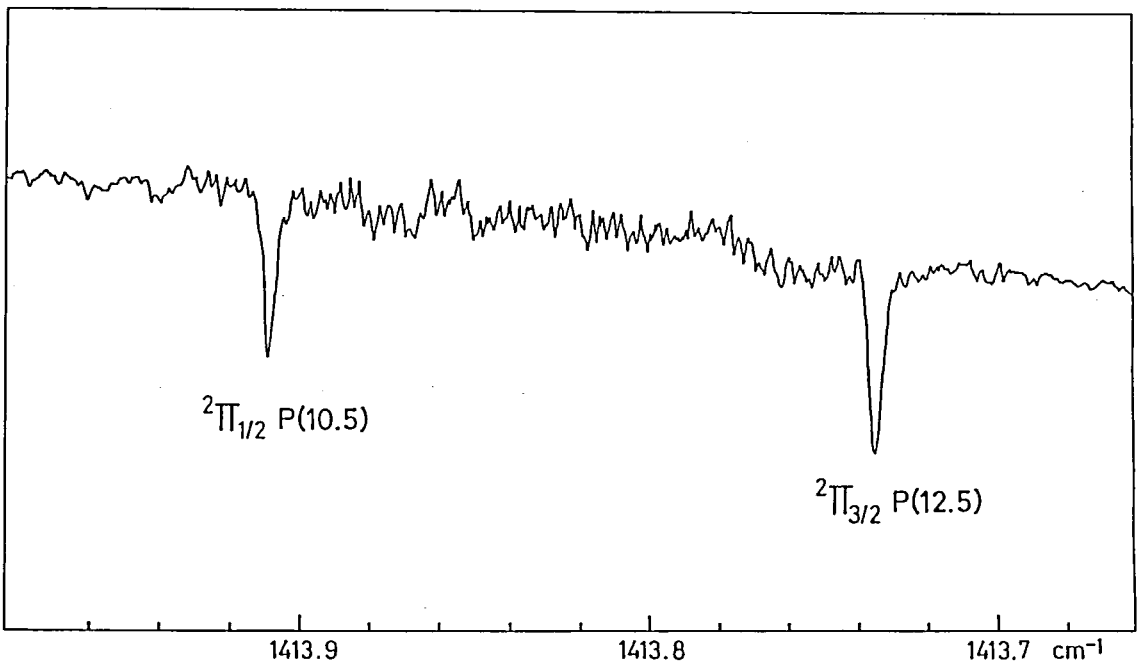

Figure 1. Two lines of the CO_2^+ ν_3 band observed by diode laser spectroscopy with magnetic field modulation of the discharge plasma.

200mA in pure CO_2 generated the ion, the abundance of which was modulated by an AC magnetic field 76 G peak-to-peak at 6.5 kHz superimposed on a 37 G DC field. Figure 1 shows two lines thus observed. Both $^2\Pi_{3/2}$ and $^2\Pi_{1/2}$ were identified, and a least squares analysis of the observed spectrum led to the following constants: B_0 = 0.380 523(48), B_2 = 0.376 298(54), and ω_0 = 1423. 0821(8) cm^{-1} with three standard errors in parentheses. The band origin, combined with Johns' ($2\nu_3$)value[2] of 2938 cm^{-1}, gives the $2\nu_3 - \nu_3$ hot band origin to be 1515 cm^{-1}, which is much larger than the ν_3 value. The vibronic interaction model of Ref. 1 has been successfully applied to $CO_2^+\nu_3$. It has also explained the discrepancy between the observed intensity and the transition dipole moments calculated by Chin and Person.[3]

References

1) K. Kawaguchi, E. Hirota, and C. Yamada, *Mol. Phys.*, **44**, 509 (1981).
2) J.W.C. Johns, *Can. J. Phys.*, **42**, 1004 (1964).
3) S. Chin and W.B. Person, *J. Phys. Chem.*, **88**, 553 (1984).

II—B Development of New Instruments and New Experimental Methods for High Resolution Spectroscopy

The scope of a research is limited by the techniques and the capabilities of instruments available to a researcher. This is particularly true for spectroscopic investigations of simple molecules, radicals, and ions, which are one of the main research themes this Department is interested in. The high precision with which we determine molecular parameters often unravels new features of molecular structure which have previously escaped experimental observation. The diversity of molecular systems which we can detect and analyze is often limited by the sensitivity of the spectrometer employed. Thus it is imperative for us to steadily improve our research facilities and to develop equipments of radically new conceptual designs. The rewards of these efforts will include not only the detailed knowledge of the molecules under investigation, but also

contributions to related fields. Various technical problems need to be sovled to attain these goals. In this respect the collaboration of the Equipment Development Center on joint research programs will be indispensable. New instruments developed in this program promise to open new research areas in the field of molecular science.

II-B-1 Infrared Diode Laser Spectroscopic System for Transient Molecules Generated by an Excimer Laser

Hideto KANAMORI, Kentarou KAWAGUCHI, James E. BUTLER *(NRL and IMS)*, Chikashi YAMADA, and Eizi HIROTA

A spectroscopic system in which transient molecules are ganerated by an excimer laser and are monitored by a diode laser has previously been described briefly.[1] Since then it has been greatly improved. Figure 1 illustrates the system. The diode laser system is essentially identical to that reported in Ref. 2, except that the detector and the accompanying amplifier are slightly modified to improve the time response. The excimer laser employed delivers an output of 100 mJ/pulse at 193 nm with the repetition rate of up to 100 Hz, which is introduced into an absorption cell through a window placed just above a mirror for multiple reflection of the infrared laser beam, which is reflected by the upper part of the mirrors so that the IR and UV beams overlap with each other as closely as possible. The observed signal is processed by a transient digitizer, which consists of 1024 8-bit channels with the maximum speed of 50 nsec/channel and is triggered by a separate pulse, synchronized with the excimer laser triggering pulse. The output of the digitizer is accumulated by a microcomputer and is then transferred to a minicomputer for further processing. This data acquisition system acts as a double gated integrator and also as a signal avarager; the former is chosen when the spectrum is recorded by scanning the diode laser, while the latter is suitable in recording the transient behavior of a line. The system has been applied to a few cases, as described in II-A-11 and II-A-21.

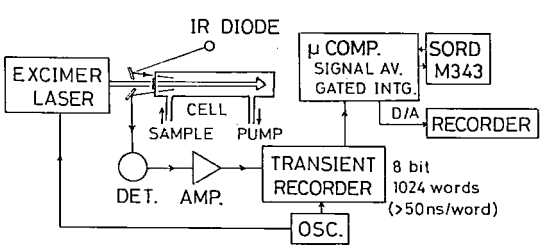

Figure 1. IR diode laser system with an excimer laser for photolysis.

References

1) J.E. Butler, K. Kawaguchi, H. Kanamori, C. Yamada, and Eizi Hirota, *IMS Ann. Rev.*, 41 (1983).
2) C. Yamada, K. Nagai, and E. Hirota, *J. Mol. Spectrosc.*, **85**, 416 (1981).

II-B-2 Infrared Diode Laser Spectroscopic System with Multiphoton Ionization

Tatsuya MINOWA, Kentarou KAWAGUCHI, Hideto KANAMORI, Chikashi YAMADA, and Eizi HIROTA

Multiphoton ionization (MPI) provides us with a means of high sensitivity and high selectivity for detecting a small amount of molecular species. A spectroscopic system is being constructed which incorporates an infrared diode laser with an MPI facility; it will allow us to observe extremely weak infrard spectra of short lived molecules without losing high resolution.

The pumping for MPI is accomplished by an excimer-laser-pumped dye laser, and a timing circuitory has been constructed which allows us to record the difference between the signals just after and before each dye laser pulse and to repeat the same process with the diode laser switched off and subtract this from the earlier signal. Transient molecule is prepared in a beam using another excimer laser for photolysis. The MPI signal has been observed for NO using the timing device.

II—C High Resolution Spectroscopy of Molecules of Fundamental Importance

The need for high quality spectroscopic data has recently been increasing, especially for molecules of fundamental importance. Perhaps such spectroscopic data have been accumulated in the past because of interest in precise molecular structure determination. However, research activities in other related fields such as reaction kinetics, environmental sciences, plasma chemistry and physics, astronomy, and semiconductor technology have recently been advanced such that precise spectroscopic data are indispensable as a means of monitoring molecules. Spectroscopic data which are available at present are not necessarily good enough and must often be replaced by new data that meet necessary requirements. Such spectroscopic data on chemically stable molecules of fundamental importance will be presented in this section.

II-C-1 The Microwave Spectra of Deuterated Silanes: SiH_3D, SiH_2D_2, and $SiHD_3$

Keiichi OHNO *(Hiroshima Univ.)*, **Hiroatsu MATSUURA** *(Hiroshima Univ.)*, **Yasuki ENDO, and Eizi HIROTA**

A previous measurement[1] on SiH_2D_2 has been extended and a least-squares analysis of the observed spectrum has yielded the rotational constants, as shown in Table I. A force field of Duncan and Mills[2] was employed to calculate the centrifugal distortion constants, which are compared with the observed values in Table II. By using only one third-order anharmonic potential constant F_{iii} for the Si-H stretching of -12.54 md/Å^2, the equilibrium Si-H distance was calculated to be 1.4741 Å from the rotational constants of SiH_2D_2.

In the course of measuring the SiH_2D_2 spectrum, we noticed that high K_a transitions are much weaker than low K_a transitions. We have explained this observation by the centrifugal distortion effect on the dipole moment; the dipole moment thus induced can be about one third as large as the isotope-induced dipole moment for $J = 5$ levels.

Table I. Rotational Constants of SiH_2D_2 (MHz)[a]

Constant	$^{28}SiH_2D_2$	$^{29}SiH_2D_2$	$^{30}SiH_2D_2$
A	69 585.436(46)	69 562.548(32)	69 541.000(33)
B	57 305.308(49)	57 305.785(39)	57 306.241(41)
C	49 487.485(44)	49 475.819(32)	49 464.838(33)

a. Values in parentheses denote 2.5 standard errors and apply to the last digits of the constants.

Table II. Observed and Calculated Centrifugal Distortion Constants of Deuterated Silanes (MHz)

Species	Constant	obs	calc
$^{28}SiH_2D_2$	Δ_J		0.478 99
	Δ_{JK}	−0.300 87	−0.289 17
	Δ_K	0.931 5	0.911 17
	δ_J	0.109 81	0.107 66
	δ_K	−0.183 22	−0.179 78
$^{28}SiH_3D$	D_J	0.469 0[a]	0.490 84
$^{28}SiHD_3$	D_J	0.489 3[b]	0.493 34
		0.476 5[c]	

a. R.W. Lovejoy and W.B. Olson, *J. Chem. Phys.*, **57**, 2224 (1972).
b. C. Frommer, R.W. Lovejoy, R.L. Sams, and W.B. Olson, *J. Mol. Spectrosc.*, **89**, 261 (1981).
c. K. Ohno, H. Matsuura, and H. Murata, *Chem. Lett.*, 27 (1982).

References
1) K. Ohnao, H. Matsuura, Y. Endo, S. Saito, and E. Hirota, *IMS Ann. Rev.*, 43 (1983).
2) J.L. Duncan and I.M. Mills. *Spectrochim. Acta*, **20**, 523 (1964).

II-C-2 Infrared Diode Laser Spectroscopy of the ν_{11} Band of Triacetylene

Keiji MATSUMURA *(Seinan Gakuin Univ.)*, **Hideto KANAMORI, Kentarou KAWAGUCHI, Eizi HIROTA, and Takehiko TANAKA** *(Kyushu Univ.)*

We have previously shown on diacetylene that Stark modulation infrared diode laser spectroscopy is useful in observing not only infrared active bands but also infrared inactive bands.[1] The present study has extended a similar measurement to the $\nu_8(\Pi_g)$ and $\nu_{11}(\Pi_u)$ CCH bending bands of triacetylene.

The observation of the ν_{11} band is straightforward; five P branch and 35 R branch transitions were observed and analyzed to give $B'' = 0.044\ 1726(26)$, $B' - q'/2 = 0.044\ 1796(27)$, $D'' = D' = 1.233(373)\ 10^{-9}$, and $\nu_0 = 621.34038(24)\ cm^{-1}$ with one σ in parentheses. When Stark modulation was used, a strong signal was observed near the band origin, i.e. among a dense spectrum of Q branch transitions. Its phase shows that the ν_8 state lies above the ν_{11} state.

Reference
1) K. Matsumura, K. Kawaguchi, E. Hirota, and T. Tanaka, *IMS Ann. Rev.*, 44 (1983).

II-C-3 High Resolution Infrared Spectrum of Methane-d_2 in the 2000 ~ 2400 cm^{-1} Region

Mitsuru AKIYAMA *(Tokai Univ. and IMS)* **and Eizi HIROTA**

A previous study[1] which analyzed the ν_2, ν_8, and $\nu_4 + \nu_9$ bands (and also a part of $2\nu_4$, the lowest band) has been extended so as to include $2\nu_7$ and $\nu_4 + \nu_7$. In view of an extremely large Coriolis interaction between the ν_4 and ν_7 fundamental bands ($|\xi_{47}^a|$ is as large as 4 cm^{-1}), these two new states have been expected to exert large perturbations to ν_2, ν_8, and other states.

A first clue to the $2\nu_7$ spectrum was obtained from strong lines around 2100 cm^{-1}, which were assigned to ^PP branch transitions. This band is strongly perturbed near the band origin, and the ^rR branch is much stronger than ^PP, while Q branch transitions are widely spread. Elimination of the $2\nu_7$ lines thus assigned and of the $2\nu_4$ spectrum previously analyzed has disclosed the $\nu_4 + \nu_7$ band. Then a least-squares analysis was carried out including the ν_2, $2\nu_7$, $\nu_4 + \nu_7$, and $2\nu_4$ states, and led to a surprising conclusion that ν_2 and $2\nu_7$ must be interchanged. As shown in Table I, molecular constants thus obtained are much more reasonable than those previously reported,[2] which are essentially those of the $2\nu_7$ state.

References
1) M. Akiyama and E. Hirota, *IMS Ann. Rev.*, 43 (1983).
2) M. Akiyama, T. Nakagawa, and K. Kuchitsu, *J. Mol. Spectrosc.*, **64**, 109 (1977).

Table I. Molecular Constants of CH_2D_2 (cm^{-1})

Constant	$\nu_2 = 1$ present	$\nu_2 = 1$ Ref. 2)	ground state[a]
ν_0	2146.4	2203.222	
A	4.198	4.539	4.30278
B	3.404	3.4234	3.50588
C	3.012	3.0083	3.05006
$\Delta_J\ 10^4$	0.6	−0.10	0.4642
$\Delta_{JK}\ 10^4$	−2.7	5.4	−0.158
$\Delta_K\ 10^4$	−0.6	−26	0.730
$\delta_J\ 10^4$	−0.7	−0.13	0.0884
$\delta_K\ 10^4$	1.6	1.2	−0.419

a. J.C. Deroche and G. Guelachvili, *J. Mol. Spectrosc.*, **56** 76 (1975).

II-C-4 The Microwave Spectra of Deuterated Germanes: GeH_3D, GeH_2D_2, and $GeHD_3$

Keiichi OHNO *(Hiroshima Univ.)*, **Hiroatsu MATSUURA** *(Hiroshima Univ.)*, **Yasuki ENDO, and Eizi HIROTA**

As an extension of microwave investigations on deuterated MH_4 type molecules (II-C-1 and Ref. 1), the three deuterated germanes were studied. The three species were prepared by the reduction of GeH_3Cl, GeH_2Br_2, and $GeHCl_3$ with $LiAlD_4$. A source frequency modulation microwave spectrometer was used with a 350 cm long absorption cell

cooled to −160°C. The sample pressure was 20 to 40 mTorr.

The $J = 1 \leftarrow 0$ transition was observed for five Ge isotopic species of GeH_3D (^{70}Ge, ^{72}Ge, ^{73}Ge, ^{74}Ge, and ^{76}Ge) and three of $GeHD_3$(^{70}Ge, ^{72}Ge, and ^{74}Ge). A similar observation was carried out also for GeH_2D_2; several Q branch transitions were recorded with one R branch transition $1_{11} - 0_{00}$, and are being least-squares analyzed.

Reference

1) E. Hirota and M. Imachi, *Can. J. Phys.*, **53**, 2023 (1975).

II-C-5 The Microwave Spectra of Deuterated Stannanes

Keiichi OHNO *(Hiroshima Univ.)*, **Hiroatsu MATSUURA** *(Hiroshima Univ.)*, **Yasuki ENDO, and Eizi HIROTA**

Two deuterated species SnH_2D_2 and $SnHD_3$ of another MH_4 type molecule, stannane, were investigated by microwave spectroscopy. As the weight of the central atom M increases, the isotope-induced dipole moment seems to be decreased; it has been rather difficult to observe microwave spectra of deuterated stannanes. Two R branch transitions $J = 1 \leftarrow 0$ and $2 \leftarrow 1$ were observed for $SnHD_3$ and three R branch (including $1_{11} \leftarrow 0_{00}$) and a few Q branch transitions were detected for SnH_2D_2, each consisting of three major Sn isotopic species, ^{116}Sn, ^{118}Sn, and ^{120}Sn. The observed spectra are being analyzed.

II—D Raman Spectroscopy and Its Application

Raman scattering reveals a vibrational spectrum which is sensitive to a molecular structure and an interatomic potential. We apply this technique to investigate the following three problems; 1) Structure-function relationship of biological pigments and their model compounds, 2) Structure of reaction intermediates, 3) Liquid structure. The first project utilizes the resonance enhancement of Raman intensity, which enables us to observe the vibrational spectra of chromophores selectively for a small amount of a dilute solution. Various kinds of hemeproteins, flavoproteins, and retinoid proteins are currently investigated. The second project aims to determine resonance Raman spectra of transient molecules, that is, photointermediates and excited molecules, by using two-color delayed laser pulses and optical multichannel detection system. The third project intends to evaluate a relative size of solute/solvent and solvent/solvent interactions for a binary mixtures of liquids. For this purpose a system to measure Raman difference spectra with high sensitivity was constructed.

II-D-1 Correlation between The Iron-Histidine Stretching Frequencies and Oxygen Affinity of Hemoglobins; A Continuous Strain Model

Shigeru MATSUKAWA *(Kanazawa Univ.)*, **Kazuhiro MAWATARI** *(Kanazawa Univ.)*, **Yoshimasa YONEYAMA** *(Kanazawa Univ.)*, **and Teizo KITAGAWA**

The iron-histidine (F8) stretching Raman lines of various mutant hemoglobins (Hb) with various levels of oxygen affinity were observed. The oxygen binding equilibrium curves were obtained from the same preparations used for the Raman measurements and three MWC parameters as well as K_1, the dissociation constant for oxygen which leaves Hb lastly, were determined. The high affinity deoxyHb gave the Fe-histidine stretching Raman line at 220–222 cm^{-1} similar to the isolated chains and deoxyMb, while the low affinity one gave the stretching mode at 214–216 cm^{-1}, in agreement with the previous observations. However, deoxyHb's with intermediate levels of oxygen affinity unexpectedly exhibited the Fe-histidine stretching mode at intermediate frequencies, but not at two frequencies corresponding to high- and low-affinity deoxyHb's. Therefore, this could not be interpreted as a mixture of the high- and low-affinity species as postulated by the simple two state model. The variation of the Fe-histidine stretching frequencies

was interpreted, in the present study, in terms of the strain imposed on the Fe-histidine bond by the globin and was correlated with the dissociation constants, K_I. The plots of the observed Fe-histidine stretching frequencies versus log K_I were found to fit the expected function of log K_I surprisingly well.

II-D-2 Resonance Raman Study on Binding of Chloride to the Chromophore of Halorhodopsin

Akio MAEDA *(Kyoto Univ.)*, **Tarou OGURUSU** *(Kyoto Univ.)*, **Toru YOSHIZAWA** *(Kyoto Univ.)*, **and Teizo KITAGAWA**

The resonance Raman spectra of halorhodopsin was investigated to elucidate the chloride-chromophore interaction. A frequency of the in-phase C = C stretching mode was shifted from 1530 to 1528 cm^{-1} upon replacement of nitrate with chloride, in accordance with what was expected from the shift of the absorption maximum from 567 to 576 nm. The chloride effect was also found with the protonated Schiff base C=NH stretching modes, which were located at 1635 cm^{-1} and 1642 cm^{-1} in the presence and absence of chloride, respectively. However, the corresponding frequencies of the deuterated Schiff base linkage exhibited little dependence on chloride. The N-H bending mode of the protonated Schiff base at 1352 cm^{-1}, which was apparently replaced by a Raman line at 977 cm^{-1} in D_2O, did not undergo the chloride effect. The Raman spectrum in the 1150–1250 cm^{-1} region was unaffected by the chloride. These observations and simple vibrational calculations suggest that chloride is not hydrogen bonded to the Schiff base proton but its binding affects a limited set of force constants of the C=NH moiety presumably through a direct interaction with a π-orbital of nitrogen.

II-D-3 Resonance Raman Study of Heme Structural Characteristics and Heme Linked Ionization of Cytocrome *c* Peroxidase

Shinji HASHIMOTO, Junji TERAOKA, Toshio INUBUSHI *(Univ. of Pennsylvania)*, **Takashi YONETANI** *(Univ. of Pennsylvania)*, **and Teizo KITAGAWA**

Resonance Raman spectra of ferrous and ferric cytochrome *c* peroxidase and its ES complex were investigated. The Fe(II)-histidine stretching Raman line was assigned on the basis of the frequency shift upon ^{54}Fe isotopic substitution. This lead us to a general conclusion that the strong hydrogen bonding of proximal histidine and thus partial anionic character of the coordinated imidazole is common characteristics of all peroxidases. The pK_a of the heme linked ionization was determined to be 7.3 from the intensity analysis of the Fe(II)-histidine stretching Raman line. The Raman spectrum of ferriCcP strongly suggested that the heme is placed under equilibrium between the five- and six-coordinate structures. At neutral pH it is biased to the five coordinate structure but at acidic pH the six coordiante heme becomes dominant. However, acidification by HNO_3, H_2SO_4, CH_3COOH, HBr, or HI resulted in somewhat different populations of the two forms at an identical pH. Cl^- was bound to the heme iron at only acidic pH, but F^- was bound even at pH 6.0. Accordingly, it is inferred that a water molecule is hydrogen bonded to distal histidine near the sixth coordination position of the heme iron but is not coordinated to the heme iron. Protonation of distal histidine allows the coordination of the water molecule to the heme iron in one hand, and causes a conformation change of a whole molecule, resulting in a frequency shift of Fe-histidine stretching mode on the other. Then the discrepancy between the Raman and x-ray crystallographic studies is interpreted satisfactorily.

II-D-4 Resonance Raman Study on Photoreduction of Cytochrome Oxidase

Takashi OGURA, Shinya YOSHIKAWA *(Konan Univ.)*, **and Teizo KITAGAWA**

Resting cytochrome oxidase under anaerobic conditions gave the resonance Raman (RR) spectrum identical with that of dithionite-reduced enzyme when it was excited at 441.6 nm, indicating occurrence of photoreduction. Under aerobic conditions, however, the Fe-histidine stretching (214 cm^{-1}) and the formyl CH = O stretching (1665 cm^{-1})

lines of ferrous cytochrome a_3 were absent despite that other parts were similar to the spectrum of reduced enzyme upon excitation at 441.6 nm. The aerobic sample gave the RR spectrum of ferric enzyme upon excitation at 406.7 nm. Under the aerobic conditions identical with Raman experiments, oxygen consumption synchronized with laser irradiation was observed. This indicated that the aerobic laser irradiation brought about photosteady state of oxygen reduction. Therefore, it was inferred that the enzyme in the photosteady state contained ferrous cytochrome *a* and ferric cytochrome a_3, and excitations at 441.6 and 406.7 nm emphasized the RR spectrum of ferrous cytochrome *a* and ferric cytochrome a_3, respectively. This kind of valency hybrid cytochrome oxidase was also produced for cyanide complex and their RR spectra were also determined.

II-D-5 Resonance Raman Studies on an Analogue of Bacteriorhodopsin L_{543} Intermediate

Akio MAEDA *(Kyoto Univ.)*, **Keiji KAMOGAWA, and Teizo KITAGAWA**

Resonance Raman (RR) spectra of bacteriorhodopsin (bR) at weakly alkaline pH were measured with time delayed two pulse laser technique as well as with the combination of a CW laser and a spinning cell. The N-H bending mode at 1349 cm^{-1} disappeared upon alkalization while the C = NH stretching mode of the protonated Schiff base remained unaltered. The C(14)–C(15) stretching mode at 1200 cm^{-1} was shifted to 1189 cm^{-1} at pH 10.5 and a few other lines in the 1300–1500 cm^{-1} region also appreciably changed. With the N-deuterated sample the N-D in-plane bending mode at 976 cm^{-1} was upshifted upon the alkalization. These spectral changes are closely similar to those upon the formation of the L_{543} intermediate at neutral pH. The RR spectra of bR at pH 10.5 did not change in the 1–50 μs range of delay time, where the RR spectra of the L_{543} intermediate was observed at neutral pH. These results suggest that the L_{543} intermediate corresponds to a deprotonated form of a neighboring amino acid residue with pK_a = 10. This means that translocation of a proton in the protein moiety precedes the proton release of the protonated Schiff base.

II-D-6 Time-Resolved Resonance Raman Spectra of Bacteriorhodopsin and Halorhodopsin

Keiji KAMOGAWA, Akio MAEDA *(Kyoto Univ.)*, **and Teizo KITAGAWA**

A system to measure transient Raman spectra was constructed with two pulsed lasers and optical multichannel analyzers, and applied to bacteriorhodopsin (bR) and halorhodopsin (hR). The light adapted bR or hR kept at 4°C was irradiated at 590 nm with YAG-pumped dye laser at 20 mW (15 Hz) and was probed at 510 nm by flash lamp-pumped dye laser, which was fired with variable time delay from the YAG pulse. The scattered light was dispersed with a single monochromator (f = 50 cm) and detected with a gated optical multichannel analyzer. The transient resonance Raman (RR) spectra of a bR photointermediate named bL_{550} was observed at 2 and 100 μs after the YAG pulse. The C = C and C = NH stretching modes were shifted to higher frequency but the Raman line at 1200 cm^{-1} was shifted to lower frequency, in good agreement with the reported spectra. It is emphasized, however, that there is no shoulder or an extra RR line at higher frequency side of the C = C stretching RR line which was noted in the spectra of the CW-laser excitation. Therefore, the present method can probe a more pure preparation of an intermediate. The RR spectra of hR in the presence and absence of chloride were different when YAG pulse was not fired, but both gave the RR spectra similar to that of bL_{550} when the probe pulse was ignited 100 μs after the YAG pulse.

II-D-7 Solute/Solvent and Solvent/Solvent Interactions in Methanol Solutions: Quantitative Separation by Raman Difference Spectroscopy

Keiji KAMOGAWA and Teizo KITAGAWA

Solute/methanol and methanol/methanol interactions were investigated by Raman difference

spectroscopy. Small frequency shifts of the CH_3 symmetric stretching vibration of CH_3OH upon mixing with polar liquids such as H_2O and CF_3COOH, nonpolar liquids such as CCl_4 and C_6D_6, and methanol isotope were observed with the optical multichannel detection system constructed in this laboratory. Molar frequency shifts, $\Delta\nu_{Sol}$ and $\Delta\nu_{MeOH}$, which are indicative of strength of solute/methanol and methanol/methanol interactions, respectively, were derived from the concentration dependence of the frequency shifts. These quantities reflected structural features of CH_3OH specific to mixing with each liquid.

II—E Structure of Noncrystalline Solid and Liquid

The structures of liquid and noncrystalline solids still largely remain to be determined. Since the majority of chemical reactions takes place in the liquid state and amorphous solids exhibit interesting and important properties such as conductivity and catalytic activity, it is necessary to determine their structure from molecular viewpoint in order to understand their functions.

EXAFS (Extended X-Ray Absorption Fine Structure) is best suited for the determination of local structures around a central metal atom in disordered system such as liquid and amorphous materials. Among amorphous solids supported catalysts have been chosen as an object because of the importance in chemistry and of scarce knowledge about their structure. The local structure changes during the catalyst synthesis procedures have been pursued about Ni/SiO_2, Fe/SiO_2, and Co/TiO_2 systems. Now the structure changes of catalyst during the reactions are being studied by the use of an *in-situ* cell.

The study of solution structure also has made a progress by the use of light scattering, Raman and ir spectroscopy as well as theoretical approach. Especially an application of high pressure to Raman spectroscopy has made it possibe to determine ΔV as well as ΔH by the conformational change. A study along this line has an wide application for the systems composed of several conformers.

II-E-1 Catalyst Preparation Procedure Probed by EXAFS Spectroscopy. II. Cobalt on Titania

Kazuyuki TOHJI, Yasuo UDAGAWA, Shuji TANABE*, Tadashi IDA*, and Akifumi UENO**
*(*Graduate Student from Toyohashi Univ. of Technology, **Toyohashi Univ. of Technology)*

[*J. Am. Chem. Soc.* in press]

EXAFS was used, in combination with electron microscopy, NMR, and x-ray diffraction, to probe environments of Co atoms at every elementary step of the preparation procedure for TiO_2 supported Co catalyst. Special emphasis was placed on the relationship between the particle size and the methods, and conditions, of the catalyst preparation.

The species which are formed during the course of the preparation were clearly identified, and it was found that a cluster size as small as about 8 A can be estimated from the analysis of EXAFS spectra, Fourier transform of which is shown in Figure 1.

It was also found that bulklike Co_3O_4, very tiny Co_3O_4 clusters, and complex oxide $CoTiO_3$ are formed by the calcination, depending upon the preparation method and temperature. It is concluded that the precedent species of oxide and their sizes before reduction have strong effects on the size of metal particles in the resultant catalyst.

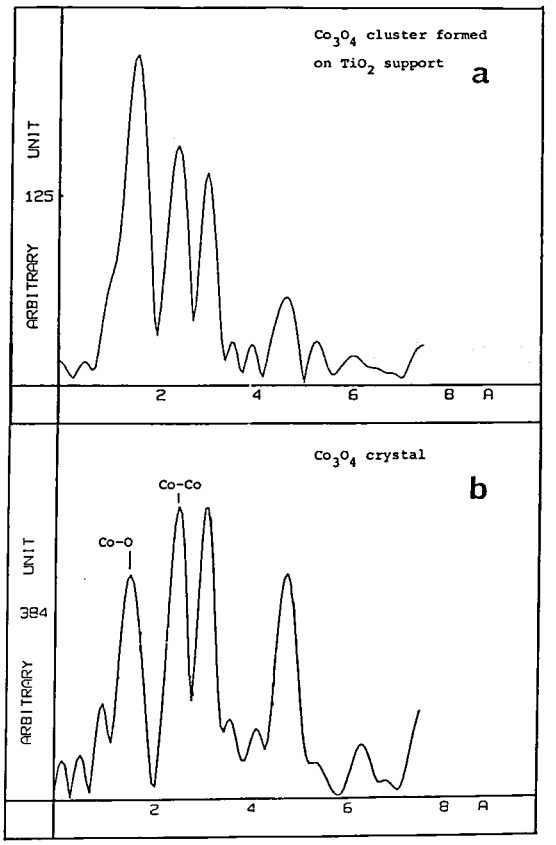

Figure 1. Fourier transforms of the sample calcined at 723 K (a) and of Co_3O_4 powder (b). Notice that the peak positions are the same although the relative intensities decrease with distance in (a).

II-E-2 Size Control of Iron Particles on SiO_2 Support

Syuji TANABE*, Takashi IDA*, Akifumi UENO, Yoshihide KOTERA**, Kazuyuki TOHJI, and Yasuo UDAGAWA** *(*Graduate Student from Toyohashi Univ. of Technology, **Toyohashi Univ. of Technology)*

[*Chem. Lett.* in press]

A new method to control the size of iron particles in Fe/SiO_2 catalyst was studied. The catalyst was prepared by drying and then calcining a gel obtained by hydrolysis of the mixed solution of ethyl silicate and iron(III) nitrate dissolved in ethylene glycol. Iron particles were deposited in an even size level by reducing the calcined catalyst in hydrogen stream. EXAFS, ir and magnetic measurements were employed to reveal the reason why the size of iron particles was controlled evenly in the catalyst thus prepared.

II-E-3 Pressure Effect on Conformational Equilibria of 1,2-Dichloroethane and 1,2-Dibromoethane by Means of Raman Spectroscopy

Hiroyasu NOMURA*, Kenji MURASAWA*, Nobuyuki ITO, Fumisato IIDA**, and Yasuo UDAGAWA** *(*Nagoya Univ. and IMS, **Graduate Student from Tokyo Metropolitan Univ.)*

[*Bull. Chem. Soc. Jpn.* in press]

The conformational equilibria of 1,2-dichloroethane and 1,2-dibromoethane have been investigated through a study of the pressure and temperature dependences of these materials in pure liquid states. The volume changes estimated here under a trans-gauche transformation of 1,2-dichloroethane and 1,2-dibromoethane are $-2.7 + 0.4$ and $-5.2 + 0.5$ cm^3/mol, respectively.

II-E-4 Pressure and Temperature Effects on the Conformational Equilibria between the Rotational Isomers of sec- and iso-Butyl Halides

Hiroyasu NOMURA*, Yasuo UDAGAWA and Kenji MURASAWA* *(*Nagoya Univ. and IMS)*

[submitted to *J. Mol. Structure*]

The conformational changes of iso-butyl halides and sec-butyl halides in pure liquid state have been analyzed by Raman spectroscopy as a function of temperature and pressure. The enthalpy and volume differences of these halgenoalkanes have been measured. According to the thermodynamical consideration, the relation between ΔH and ΔV is discussed and also the configurational entropy difference of each rotational isomers in liquid state was estimated from the spectroscopic data, combining the ultrasonic relaxation data reported in literatures.

II-E-5 Estimation of the Parameters in the Kirkwood-Buff Theory of Solution using Percus-Yevick Fluid Mixtures

Kazuyuki KOJIMA *(Nagoya Univ.)*, **Tadashi KATO, and Hiroyasu NOMURA** *(Nagoya Univ. and IMS)*

[*J. Solution Chem.* **13**, 1271 (1984)]

Parameters G_{11} in the Kirkwood-Buff theory of solution were calculated for binary mixtures of Lennard-Jones 6–12 molecules by using the Percus-Yevick theory. Calculation were carried out for various parameters in the LJ potential. Under the Lorentz-Berthelot rules, G_{11} and/or G_{22}-composition curves do not show a maximum for any parameters in the LJ potential. When the intermolecular interaction between different species becomes much weaker than that expected from the Berthelot rule, G_{11} and G_{22} show a maximum and G_{12} a minimum. The pressure effect on G_{ij} was examined and calculations at constant pressure were also carried out. G_{ij} is almost independent of the pressure when the ratio of the molecular volume of two components is in the range 1.0 to 2.5. Comparison was made between experimental and calculated G_{ij} for cyclohexane-2,3-dimethylbutane and acetonitrile-toluene systems. For the latter system, the quantitative agreement between the calculated and experimental could not be obtained but showed that the characteristics of G_{ij} composition curves can be explained qualitatively by using PY theory.

RESEARCH ACTIVITIES III
Department of Electronic Structure

III—A Unimolecular Reactions Initiated by UV and VUV Laser Irradiation

Irradiation of molecules with UV or VUV light often induces photodissociation. Besides direct photodissociation and predissociation, we have recently been investigating another type of photodissociation, which consecutively involves excitation of electronically excited state, efficient internal conversion to the ground electronic state, and dissociation. The ground electronic state thus produced has a very high vibrational energy, in other words, it is vibrationally very hot. Since the internal energy of this state is determined by photon energy and is unique, we can directly obtain the specific rate constants of unimolecular dissociation. We firstly describe photodissociation of olefines to allylic radicals and of toluene to benzyl radical. We secondly describe a mechanism of collisional cooling of hot molecules. Finally we discuss transient absorption spectra observed by ArF laser flash photolysis of several silicon compounds.

III-A-1 Photodissociation Mechanism of Olefines: Hot Olefines and Hot Radicals

Nobuaki NAKASHIMA, Nobuo SHIMO, Noriaki IKEDA, and Keitaro YOSHIHARA

Formation rates of allylic radicals have been measured directly at low pressures, for example, 4×10^7 s^{-1} for 2,3,3-trimethyl-1-butene (TMB).[1] We have proposed a mechanism that C-C bonds at the β position to a double bond dissociate after internal conversion to "hot" olefines (vibrationally highly excited states in the ground electronic state).[1,2] With an ArF laser (193 nm) as an exciting source, nanosecond time-resolved absorption spectra of TMB have been measured in the presence of foreign gases. In Figure 1, spectra at "t = 0" (immediately after excitation) and 60–260 ns are shown in the presence of 250 Torr of nitrogen. The spectrum at "t = 0" includes hot TMB, hot methyl radical (~216 nm), and hot allylic radical (~240 nm). A monotonical spectrum shorter than 230 nm can be assigned to hot TMB and can be explained in terms of a red-shifted tail of the N-V transition.

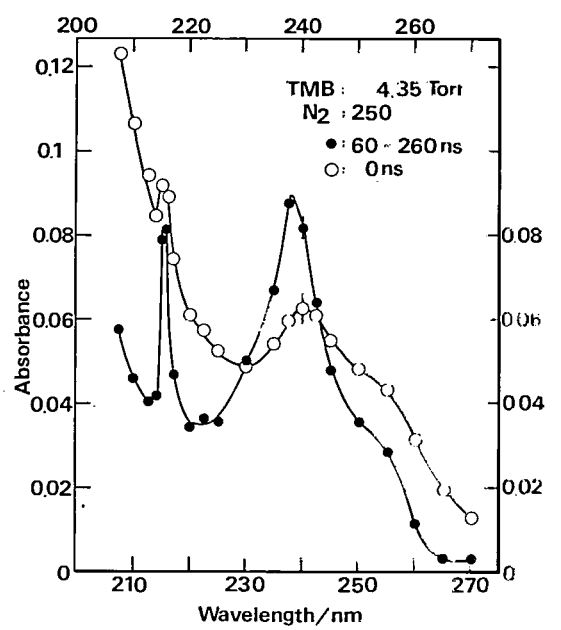

Figure 1. Time-resolved absorption spectra of 2,3,3-trimethyl-1-butene at 4.35 Torr in the presence of 250 Torr of nitrogen.

References

1) N. Nakashima, N. Shimo, N. Ikeda, and K. Yoshihara, *J. Chem. Phys.*, **81**, 3738 (1984).
2) N. Shimo, N. Nakashima, N. Ikeda, and K. Yoshihara, *IMS Ann. Rev.*, 53 (1983).

III-A-2 Direct Measurement of Unimolecular Dissociation Rate of Toluene to Benzyl Radical with 193 nm Photo-excitation

Noriaki IKEDA, Nobuaki NAKASHIMA, and Keitaro YOSHIHARA

ArF laser flash photolysis of toluene in the gas

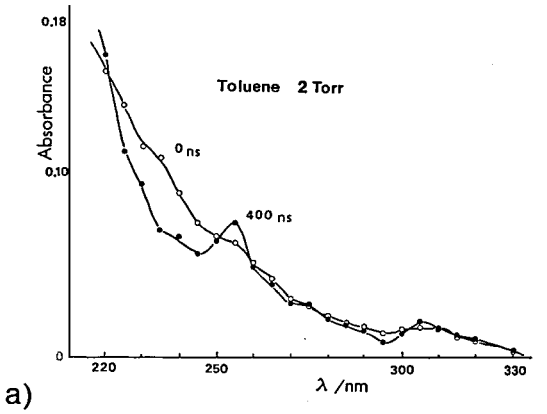

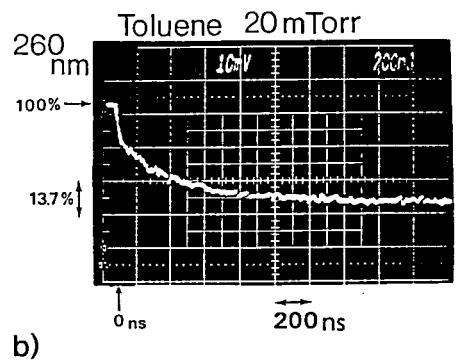

Figure 1. a) Time-resolved absorption spectra of toluene at a pressure of 2 Torr. b) A rise curve of absorption due to benzyl radical formation from hot toluene under collision free conditions.

phase has been studied. Time-resolved absorption spectra show that hot toluene (S_0^{**}) is formed after rapid internal conversion from the S_3 state, and then dissociates to benzyl radical as shown in Figure 1a. The formation rate of benzyl radical from hot toluene has been measured to be $2.4 \pm 0.2 \times 10^6$ s^{-1} under collision free conditions as shown in Figure 1b. The unimolecular reaction is found to be explained in terms of thermal reaction, namely, dissociation from vibrationally excited states with a confined internal energy. This is the first observation of such processes in aromatic hydrocarbons. Another dissociation path to benzyl radical formation has also been revealed, since the radical is formed even under high pressure conditions. The results are important to photochemistry of benzene derivatives in the gas phase with excitation of VUV light.

III-A-3 Theory of Time-Resolved Photon Absorption by Molecules after Radiationless Transition: Application to Benzene after $S_2 \rightsquigarrow S_0$.

Yuichi FUJIMURA *(Tohoku Univ.)*, **Minoru ARAI** *(Tohoku Univ.)*, **Nobuaki NAKASHIMA, and Keitaro YOSHIHARA**

[*Bull. Chem. Soc. Jpn.*, **57** 2947 (1984)]

Expressions for the intensity of the time-resolved absorption (TPA) by molecules after radiationless transition have been derived. It is assumed that a non-equilibrium vibronic distribution is realized after the radiationless transition and relaxes to the equilibrium one. Two types of non-equilibrium distributions, Poisson distribution and canonical distribution with temperature higher than that of the heat bath are taken into account. The theory developed is applied to the TPA spectra ($S_3 \leftarrow S_0$) of benzene after the internal conversion $S_2 \rightsquigarrow S_0$ (N. Nakashima and K. Yoshihara, *J. Chem. Phys.*, **79**, 2727, 1983). It is shown that the expression for the absorbance in the Sulzer-Wieland model is involved in the expression derived using the canonical distribution.

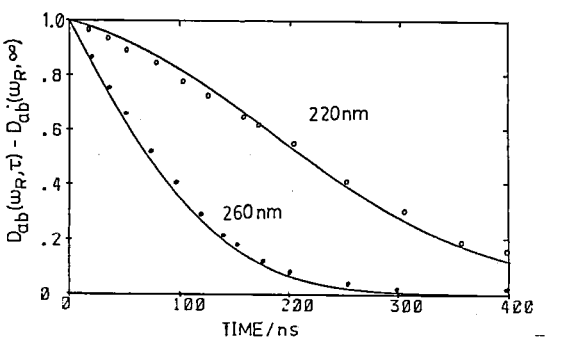

Figure 1. The calculated decay curves, $D_{ab}(W_R, \tau) - D_{ab}(W_R, \infty)$ at 220 and 260 nm. The measured values of the absorbances of the 2 Torr benzene and 10 Torr propane are denoted at 220 nm (O) and 260 nm (●).

III-A-4 Laser Flash Photolysis of Silicone Compounds

Nobuo SHIMO *(Idemitsu Kosan)*, **Nobuaki NAKASHIMA, and Keitaro YOSHIHARA**

Some silicone compounds were photolyzed with an ArF excimer laser. Hexamethyl-disilane (Me_3-$SiSiMe_3$, HMDS) and allyltrimethylsilane ($CH_2 = CHCH_2SiMe_3$, ATMS) gave the same transient absorption spectra having a peak at 256 nm. This absorption was quenched by NO added as a monoradical scavenger. This absorption is assigned to trimethylsilyl radical. Photolysis of disilane gave two transient absorption spectra. The one that has a maximum peak a 252 nm can be assigned to silyl radical, and the other is a monotonic spectrum between 210–280 nm.

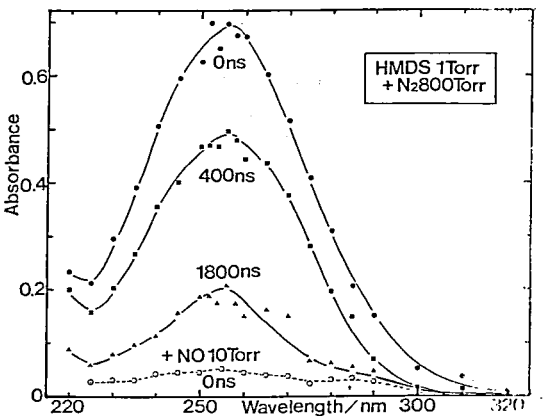

Figure 1. Transient absorption spectra of hexamethyldisilane after excitation with ArF laser in the gas phase.

III—B Radiationless Processes in Large Molecules — Channel Three in Benzene

We are interested in the photochemical and photophysical properties of benzene, a prototype of aromatic hydrocarbons. Upon exciting the S_1 manifold, photochemical valence-isomerization takes place and benzvalene is confirmed. The nonradiative pathways are strongly depending on exciting wavelengths and suddenly opens a new pathway, called channel three, by which vibrational energy in excess of about 2800 cm^{-1} is lost at an anomalously rapid rate. Excitation was made above the channel three threshold with a recently developed high power, picosecond, narrow bandwidth laser continuously tunable from 214 to 252 nm. The dramatic channel three effect was indeed observed in both quantum yields and lifetimes and three orders of magnitude change was found upon excitation at all vibrational levels. Single vibronic level fluorescences were observed and a pronounced line broadning and non-exponential fluorescence decay were found above the channel three threshold. The principal cause of the channel three was discussed in relation to intramolecular vibrational redistribution.

III-B-1 Single Vibrational Level Dependence of Picosecond Fluorescence in the Channel 3 Region of Benzene

Keitaro YOSHIHARA, Desmond V. O'CONNOR, Minoru SUMITANI, Yoshihiro TAKAGI, and Nobuaki NAKASHIMA

[*Appl. Picosecond Spectry. to Chemistry*, K.B. Eisenthal Ed., Reidel, NATO ASI Series, 261 (1984)]

An investigation of fluorescence spectra, quantum yields and decay times in collision-free benzene vapour excited to high excess energies in S_1 has been carried out. At longer wavelengths quantum yields and spectra are normal and lifetimes are single-exponential as shown in Figure 1(a). In the next region, corresponding to *ca.* 2800–3800 cm^{-1} excess energy, the quantum yields decrease sharply and decay curves are non-exponential as shown in Figure 1(b). Most of the structure in fluorescence spectra is washed out, only the strong progressions in ν_1 being visible. In the third region, above 4000 cm^{-1}, the quantum yields decrease but at a slower rate while the observed decay is again exponential.

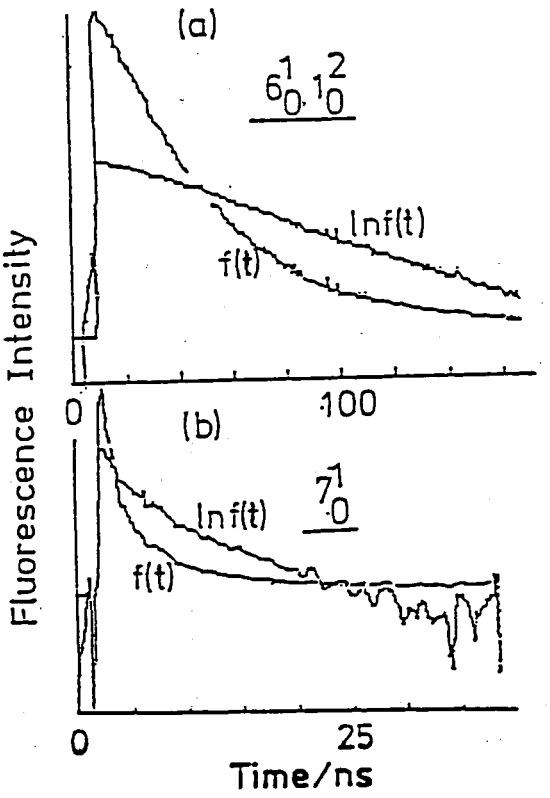

Figure 1. Fluorescence decay of benzene. (a) Excitation at 247.1 nm ($6_0^1 1_0^3$), excess energy (ΔE): 2367 cm^{-1}. Single exponential decay of 47 ns. (b) Excitation at 242.8 nm (7_0^1), ΔE = 3080 cm^{-1}. Non-exponential decay. Simulation with two exponents gives 4.0 and 18 ns.

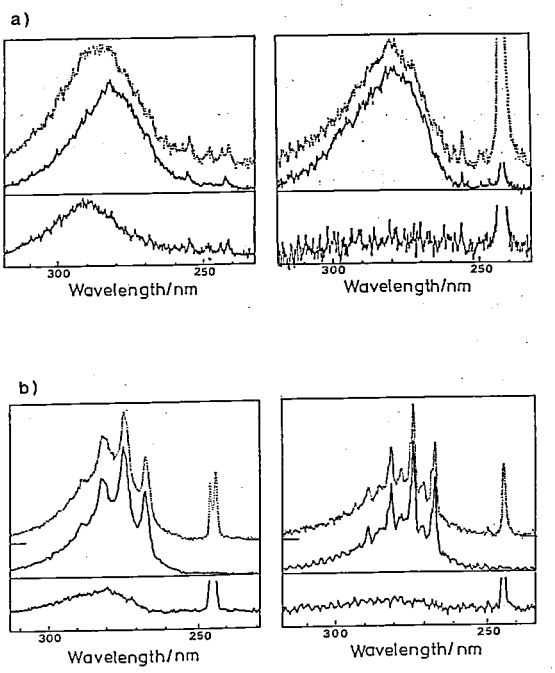

Figure 1. (a) Time-resolved fluorescence spectra of $6^1 1^3$ in S_1 benzene under bulb and cold beam conditions. Left; observed in the bulb condition. Upper figures: Points, early gated spectrum obtained with 5 ns gate centered 1.5 ns after laser pulse; line, late gated spectrum obtained with 5 ns gate centered 6.5 ns after laser pulse. Lower figure: early-minus-late gated difference spectrum. Right; observed under the cold beam condition. Other conditions are same as in the bulb condition.
(b) Time-resolved fluorescence spectra of 7^1. Left; observed in the bulb condition. Upper figures: Points, early gated spectrum; line, late gated spectrum. Lower figure; early-minus-late gated difference spectrum. Right; observed under the cold beam condition.

III-B-2 The Importance of the ν_7 Vibration in the Study of Channel Three Decay in S_1 Benzene

Minoru SUMITANI, Desmond V. O'CONNOR, Yoshihiro TAKAGI, and Keitaro YOSHIHARA

[*Chem. Phys. Lett.*, **108**, 11 (1984)]

Time-resolved fluorescence spectra and decay times of the $7^1 1^n$ vibronic bands were observed under bulb and cold beam conditions. The unique properties of these bands compared with other vibronic bands are shown in Figure 1, taking the fluorescence from the $6^1 1^3$ and 7^1 levels as examples. In the bulb experiment there is an enhanced contribution of the broad background emission in the early gated spectrum (left bottom figures), which is assigned to hot band effect. This enhancement disappears completely in the beam experiments where early and late gated spectra are virtually identical (right bottom figures). The broad fluorescence under cold beam conditions is assigned to emission from background vibronic levels that are populated through intramolecular vibrational redistribution (IVR), while the structured component is emission from the optically prepared state. It is evident, therefore, IVR is very inefficient in the levels 7^1 and $7^1 1^1$. Nontheless their fluorescence shows the channel 3 behaviour as $6^1 1^n$ etc. do, which are considerably affected by IVR. Therefore channel three and IVR are separate and independent processes.

III-B-3 Channel Three Decay in C_6D_6

Desmond V. O'CONNOR, Minoru SUMITANI, Yoshihiro TAKAGI, Nobuaki NAKASHIMA, Keiji KAMOGAWA, Yasuo UDAGAWA, and Keitaro YOSHIHARA

[*Chem. Phys.*, in press]

Fluorescence decay has been detected in C_6D_6 for excitation wavelengths down to 231 nm, corresponding to 5000 cm^{-1} excess energy in S_1. As the excitation energy passes the channel three threshold the sharp decrease in quantum yield and lifetime, characteristic of C_6H_6 decay, is again observed as shown in Figure 1. This threshold is at about the same excess energy, 2800 cm^{-1} as in C_6H_6. In contrast to C_6H_6, spectra following excitation above the threshold are broad and featureless. Hot band transition from S_0 and anharmonic interactions between vibrational levels in S_1 render population of individual pure levels impossible. These interactions are invoked to account for the difference between the non-exponential decay in C_6H_6 and the exponential decay in C_6D_6. The dynamical behaviour at higher excess vibrational energy is explained with a mechanism involving complete randomisation of vibrational energy as well as a coupling of S_1 with an isomeric form.

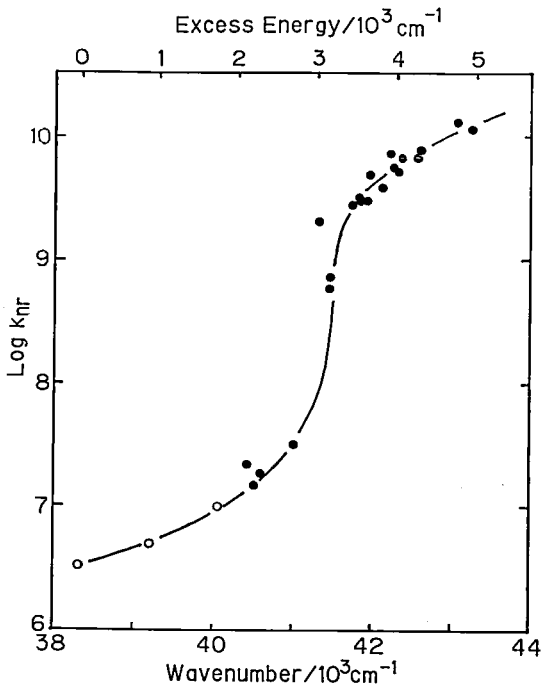

Figure 1. Plot of log k_{nr} (non-radiative rate constant) vs excitation energy for C_6D_6. The three open symbols, which correspond to the transitions 6_0^0, $6_0^0 1_6^1$, and $6_0^0 1_6^2$, were taken from the following reference.
A.S. Abramson, K.Y. Spears, and S.A. Rice, *J. Chem. Phys.*, 56, 2291 (1972).

III-B-4 Intramolecular Electronic and Vibrational Redistribution and Chemical Transformation in Isolated Large Molecules — S_1 Benzene

Keitaro YOSHIHARA, Minoru SUMITANI, Desmond V. O'CONNOR, Yoshihiro TAKAGI, and Nobuaki NAKASHIMA

[*Ultrafast Phenomena*, A.H. Auston and K.B. Eisenthal Ed., Springer, 345, (1984)]

Fluorescence quantum yields, decay times and spectra have been measured following excitation of benzene vapour above the channel three threshold. Channel three decay was observed for all vibrational levels, even these not excited via line-broadened transitions. In addition it was observed that fluorescence decay curves resulting from excitation just above the channel three threshold were non-exponential. It is proposed that the cause of absorption line broadening — intramolecular vibrational redistribution (IVR) — is not directly

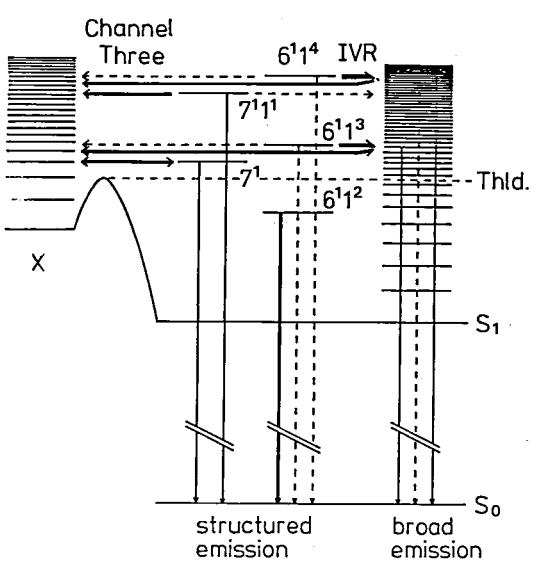

Figure 1. Schematic diagram of energy flow in the channel three region of benzene.

related to channel three. It is postulated to be coupling to a state X, which could be an isomeric form of benzene or a hidden singlet electronic state, as illustrated in Figure 1. In this way the rapid decrease in lifetime observed for these levels can be explained. Non-exponential decays are the result of a "communication" between state X and the precurser level or levels.

III—C Dynamic Behavior of Excited States

Optical excitation of molecules to electronic excited states causes a variety of dynamical behavior, depending on electronic structures and environments, such as energy transfer, proton transfer, chemical reaction, radiationless transition, ionization and others. Most of these processes fall into the picosecond time scale. Energy transfer in submonolayer dye on organic single crystals and electron transfer through surfaces were studied with a time-correlated single photon counting/synchronously pumped mode-locked dye laser system. Time-resolved energy transfer among micellized sites of dyes were studied with sodium dodecyl sulfate micelles. Picosecond laser fluorometry is a powerful technique to study dynamics of various components in biological materials. A system of enzyme-inhibitor system was investigated. Transient absorption spectroscopy was applied to the dynamics of intramolecular motion of polymers. High power picosecond and subpicosecond UV laser system was constructed based upon a combination of a colliding pulse passive mode-locking ring dye laser, three-state dye amplifier pumped by a YAG laser, and a XeCl excimer laser (see Special Research Projects).

III-C-1 A Novel System for the Study of Electron Transfer: Dye Molecules Adsorbed on Organic Single Crystals at a Very Low Coverage

Klaus KEMNITZ, Toshiro MURAO, Naoto TAMAI, Iwao YAMAZAKI, Nobuaki NAKASHIMA, and Keitaro YOSHIHARA

The system of dye molecules adsorbed on single crystals allows the separate measurement of energy and electron transfer. From the coverage dependent fluorescence decay of dye molecules adsorbed on naphthalene and phenanthrene single crystals, the nature of two-dimensional energy transfer among adsorbed dye molecules was deduced and the fluorescence lifetime of adsorbed monomer could be obtained. Uninfluenced by energy transfer at a coverage of 1/100, electron transfer was studied with anthracene and pyrene systems, where the rate constant for electron transfer and the free energy difference ΔG_0 could be determined simultaneously. The results obtained from the measurements of both energy and electron transfer led to the development of a detailed picture of the surface of organic crystals and of a modified crystal growth technique.

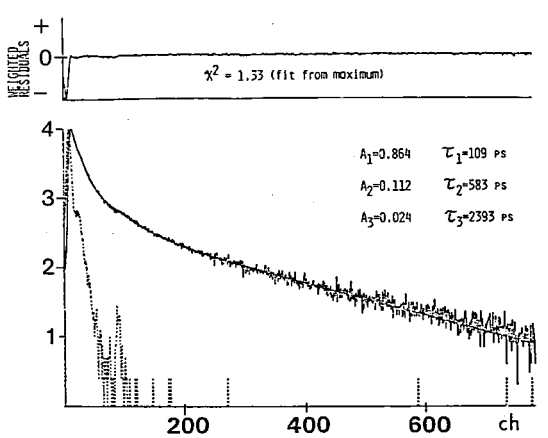

Figure 1. Fluorescence decay and its simulation of a system of rhodamine B on a single crystal of anthracene. The decay was fitted with three exponents with weighted residuals χ^2 = 1.3. 100 ch = 1.28 ns.

III-C-2 Micellized Sites of Dyes in Sodium Dodecylsulfate Micelles as Revealed by Time-resolved Energy Transfer Studies

Kazuo KASATANI *(Mi'e Univ.)*, **Masahiro KAWASAKI** *(Mi'e Univ.)*, **Hiroyasu SATO** *(Mi'e Univ.)*, **and Nobuaki NAKASHIMA**

[*J. Phys. Chem.*, in press]

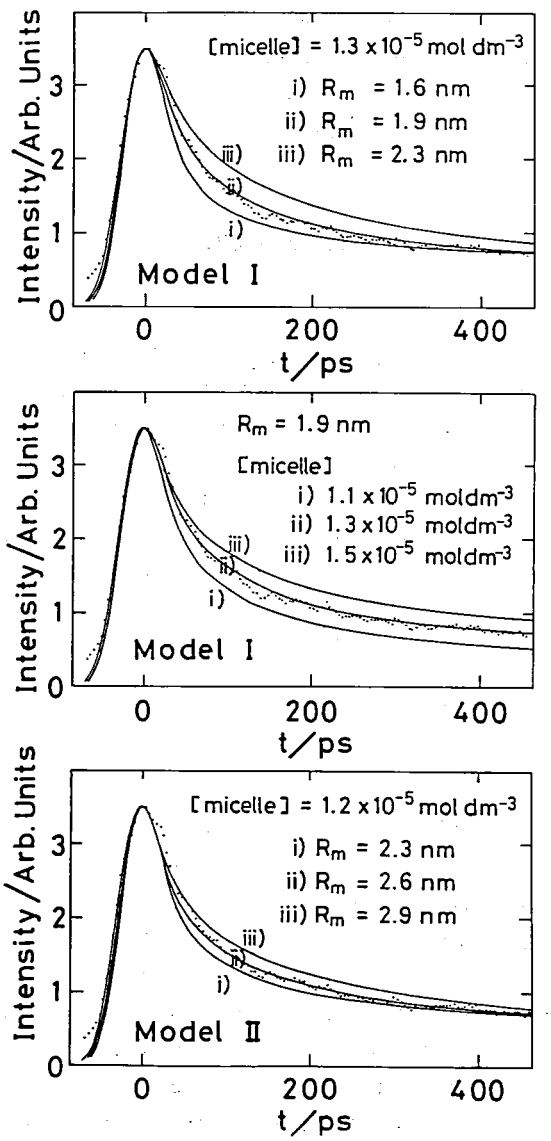

Figure 1. Dots are experimental data points. [Rh-6G] = 4.0 × 10^{-6} mol dm^{-3}, [HITC] = 4.0 × 10^{-5} mol dm^{-3}, [SDS] = 8.0 × 10^{-3} mol dm^{-3}. The best-fit value of two adjustable parameters are R_m = 1.9 nm, [micelle] = 1.3 × 10^{-5} mol dm^{-3} for model I, R_m = 2.6 nm, [micelle] = 1.2 × 10^{-5} mol dm^{-3} for model II, respectively. When the value of one parameter was changed, the value of the other parameter was fixed at the best-fit value.

The time-resolved energy transfer studies can reveal the location of organic molecules solubilized in micelles, along with the size and concentration of micelles. We studied the energy transfer from Rhodamine 6G (Rh-6G) to 1,3,3,1',3',3'-hexamethylindotricarbocyanine iodide (HITC) in sodium dodecyl sulfate (SDS) micelles. Two models, namely, (I) that the dyes are micellized in the surface layer of micelles and (II) that they are micellized in the micellar interior, were used in the simulation of fluorescence decay curves of Rh-6G in the presence of HITC. The former model gave the size and concentration of micelles in accordance with the other methods, while the latter did not. Based on these results, it was concluded that these dyes are micellized in the region near the surface of SDS micelles. Examples of the simulated fluorescence decay curves including the best-fit curves are shown in Figure 1.

III-C-3 Picosecond Laser Fluorometry of FAD of D-Amino Acid Oxidase-Benzoate Complex

Kunio YAGI *(Nagoya Univ.)*, **Fumio TANAKA** *(Mi'e Nursing College)*, **Nobuaki NAKASHIMA, and Keitaro YOSHIHARA**

[*J. Biol. Chem.*, **258**, 3799 (1983)]

Formation of a complex of D-amino acid oxidase (D-amino acid: O_2 oxidoreductase (deaminating), EC 1.4.3.3) and benzoate, an enzyme-substrate complex model, was studied by measuring the fluorescence lifetime of the coenzyme FAD of the complex by using a mode-locked Nd:YAG laser and a streak camera. The value of lifetime was 60 ± 10 ps in the monomer of the complex and it was extremely short (≪5 ps) in the dimer of the complex. Since the values of fluorescence lifetime of the coenzyme are 130 ps in the monomeric form of free enzyme and 40 ps in the dimeric form of free enzyme, the decrease in the lifetime upon complex formation with benzoate is slight in the monomer (reduced to one-half) whereas marked in the dimer (reduced to less than 1/10). By analyzing the fluorescene decay curve, a dissociation constant of the monomer-dimer equilibrium of the complex was evaluated to be 0.4 ± 0.3 μM, which is much smaller than that in free enzyme. Fluorescence analysis under steady state excitation revealed that the apparent dissociation constant (K) of FAD from the enzyme was decreased by 1:1000 upon the complex formation. Relative quantum yield of the fluorescence of FAD in the complex to that of free FAD exhibited appreciable dependence on the complex concentration: greater in the monomer and less in the dimer. These results suggest that a molecular interaction between FAD and amino acid residue(s) is strengthened by the complex

formation, which contributes to a remarkable conformational change in the protein moiety of the complex. Comparison of D-amino acid oxidase-benzoate complex with the haloenzyme is given in Table I.

Table I. Comparison of D-amino acid oxidase-benzoate complex with the holoenzyme free from benzodate.
Data were obtained at 20°C, pH 8.3, in 0.017 M pyrophosphate buffer.

	Benzoate complex	Holoenzyme
Fluorescence lifetime (ps)		
Dimer	$\ll 5$	40[a]
Monomer	60	130[a]
Relative quantum yield of FAD in the enzyme to free FAD[b]	0.0048–0.0077	0.08–0.13[a]
Apparent dissociation constant of FAD (nM)[b]	0.14–0.15	100–300
Dissociation constant of dimer into monomer (μM)	0.4±0.3	3.7

[a] N. Nakashima, K. Yoshihara, F. Tanaka, and K. Yagi, *J. Biol. Chem.*, **225**, 5261 (1980).
[b] The values in the range of concentration 10–50 μM.

III-C-4 Absorption Spectrum of the Triplet State and the Dynamics of Intramolecular Motion of Polystyrene

Seiichi TAGAWA *(Univ. of Tokyo)*, **Nobuaki NAKASHIMA, and Keitaro YOSHIHARA**

[*Macromelecules*, **17**, 1167 (1984)]

Transient absorption spectra in the wavelength range between 220 and 900 nm have been measured by KrF excimer laser (248 nm) photolysis of polystyrene in cyclohexane solutions as shown in Figure 1. Although the absorption spectrum with the shoulder around 300–350 nm and a small tail around 400 nm had been correlated to the triplet state of polystyrene, the $T_n \leftarrow T_1$ absorption spectrum of polystyrene with a single peak at 230 nm, two shoulders around 250–270 and 300–350 nm, and a small tail in the wavelength region longer than $\lambda = 400$ nm is identified clearly in the present work, in addition to the excimer absorption band at 520 nm with a lifetime of 20 ns, which had been reported previously by us. The lifetime of the triplet state of polystyrene is 110 ns and is a clue to the internal rotation of polystyrene, because the lifetime of the triplet state of polystyrene is determined by self-quenching on the basis of intramolecular interaction between triplet- and ground-state chromophores. Comparison of the present results with literature values for internal rotation, measured by other techniques, is also presented.

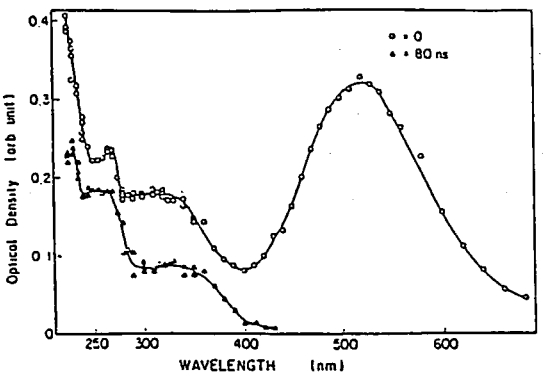

Figure 1. Transient absorption spectra observed in the 248 nm laser photolysis of 1 base mM deaerated solution of polystyrenen in cyclohexane immediately (O) and at 80 ns (Δ) after 15 ns pulses.

III—D Solar Energy Conversion by Using Photocatalytic Effects of Semiconductors and Dyes

— Decomposition of Water and Application to Organic Synthesis —

Essential roles are played by semiconductors and dyes in the photocatalytic effects to which a particular attention has been paid in connection to the direct conversion of solar energy to chemical energy. One of the most important applications is the water splitting reaction. Photocatalytic reactions of water with various organic compounds are also interesting not only from the view point of hydrogen production but also from that of the application to organic synthesis. In order to elucidate the mechanism of these photocatalytic reactions, we need detailed knowledges on the electronic structures of adsorbed molecules, the fundamental processes of photoinduced electron transfer at the semiconductor-liquid interface and catalysis on the surface.

Work on the following topics is in progress with the purpose of clarifying the photocatalytic effects of semiconductors and dyes from the view point of solar energy conversion.

III-D-1 Highly Efficient Photocatalytic Production of Amino Acids from Organic Acids-Ammonia-Water by Powdered Semiconductor

Tadayoshi SAKATA and Kazuhito HASHIMOTO

Amino acid production by irradiating a mixture of various organic compounds and ammonia with UV light has been investigated mainly from the view point of chemical evolution. In 1979, Reiche and Bard demonstrated that various amino acids were produced from methane-ammonia-water with Pt/TiO_2 under near UV irradiation. Here we report highly efficient photocatalytic synthesis of amino acids from organic acids in ammonia water by use of powdered semiconductors. The quantum yields of these reactions amount to 20–40% with visible light without metal catalyst such as Pt. Moreover the reactions are highly selective and depend strongly on the kind of semiconductors. Among various organic acids, keto-, hydroxy- and unsaturated carboxylic acids were found to produce efficiently the corresponding amino acids. The reactions are classified into three types whose typical examples are shown in Figure 1. High efficiency of these reactions also suggests an important role of photocatalytic processes in the chemical evolution, since various organic acids including lactic and glycol acids can be produced easily in the Miller's type experiments.

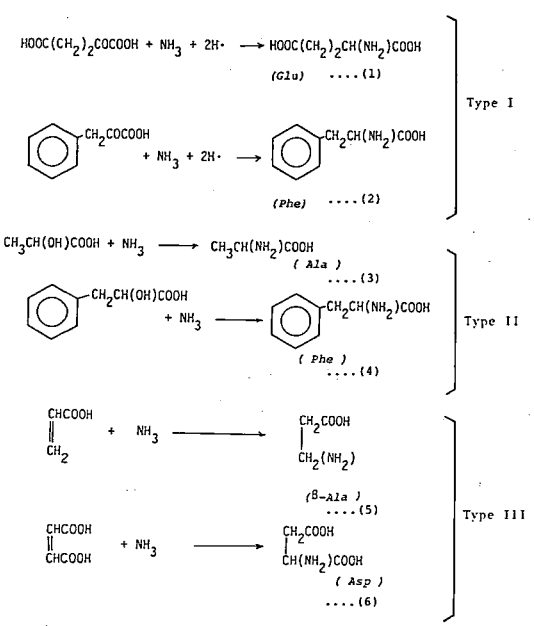

Figure 1. Some typical examples of photocatalytic amino acid synthesis from organic acid-ammonia-water by powdered semiconductor.

III-D-2 Photo-Knoop Reaction — Photosynthesis of Amino Acid from Keto-Carboxylic Acid and Ammonia by Use of Dyes

Tadayoshi SAKATA and Kazuhito HASHIMOTO

Not only the powdered semiconductors but also various dyes were found to function as excellent photocatalysts for amino acid synthesis from keto-carboxylic acid and ammonia in the aqueous solution. In these reactions a sacrificial agent such as triethanol-amine(TEOA) is used to reduce imino acid which is produced thermally from keto-carboxylic acid and ammonia. The assumed reaction scheme of this type is expressed as,

$$\begin{aligned} &RCOCOOH + NH_3 \\ &\longrightarrow RC(=NH)COOH + H_2O \\ &\xrightarrow{2H\cdot} RCH(NH_2)COOH + H_2O \end{aligned} \qquad (I)$$

This reaction resembles the Knoop reaction in which imino acid is reduced thermally by using hydrogen and Pt catalyst. However, in the present photocatalytic reaction, excited dye oxidizes a sacrificial agent like TEOA and the dye itself is reduced. For fluorescein derivatives and $Ru(bpy)_3^{2+}$, they are known to undergo one electron reduction under alkaline condition. These reduced dyes are thought to reduce the imino acid, since they have a strong reducing power. Unlike the Knoop reaction Pt is not necessary in the present reaction. In addition to the photo-Knoop reaction, we tried additive reactions of NH_3 to the unsaturated carboxylic acids such as maleic, cinnamic and acrylic acids. Several reactions were successful. For

Table I. Quantum yields of photocatalytic amino acid synthesis

Reaction	Photocat.	Q.Y.(%)	wavelength
2-ketoglutaric acid + NH_3 + 2H· $\xrightarrow{2h\nu}$ Glu	ZnTPPS[a]	30	436 nm
acrylic acid + NH_3 $\xrightarrow{h\nu}$ β-Ala	Acridine Yellow	42	450 nm
	ZnTPPS[a]	38	436 nm

a) Zn-p-sulfonatophenylporphyrin

instance, β-Ala was produced efficiently and selectively by the addition of NH_3 to acrylic acid by use of ZnTPP as a photocatalyst. Table I shows some examples of these reactions and the quantum yields(Q.Y.'s) of the reaction. As is shown in this table, the quantum yields of these reactions are very high with visible light. Because of the simplicity and high efficiency, this method might be one of the promising means for amino acid synthesis.

III-D-3 Effect of Semiconductor on Photocatalytic Decomposition of Lactic Acid

Hisashi HARADA *(Meisei Univ.)*, **Tadayoshi SAKATA, and Toyotoshi UEDA** *(Meisei Univ.)*

Photocatalytic reactions of particulate semiconductors have been investigated not only from the view point of solar energy conversion but also from that of organic synthesis. From this view point, the specificity of the photocatalyst to a given reaction is important to control the reaction. Here we report the dependence of the photocatalytic reaction of lactic acid on the kind of semiconductor. Platinized TiO_2 and CdS were found to decompose lactic acid very efficiently. The quantum yield of hydrogen production amounts to 70% for Pt/TiO_2 and 40% for Pt/CdS. Interestingly, a clear difference was observed in the reaction products, depending on the kind of semiconductor as shown in Table I. For Pt/TiO_2, the main products are H_2, CO_2 and acetaldehyde, whereas for Pt/CdS they are H_2 and pyruvic acid. This result suggests that the following reactions take place.

$$Pt/TiO_2: CH_3CH(OH)COOH \longrightarrow H_2 + CO_2 + CH_3CHO \quad (1)$$

$$Pt/CdS: CH_3CH(OH)COOH \longrightarrow H_2 + CH_3COCOOH \quad (2)$$

The difference in the reaction can be explained by the difference in oxidation power of the photogenerated holes in the valence band of each semiconductor. Photocorrosion of CdS was found to be suppressed during the reaction and the photocatalytic activity was maintained for more than 300 hours irradiation.

Table I. Photocatalytic reaction products from lactic acid-water (1:10 in volume) solution[a]

Catalyst[b]	Product /mmol					
	H_2	CO_2	CH_3CHO	C_2H_5OH	CH_3COOH	$CH_3COCOOH$
Pt/TiO_2	1.21	1.43	1.08	0.047	0.151	–
Pt/CdS	1.20	0.015	–	–	–	0.80

[a]Irradiated with 1 KW Xe lamp (under 500 W operation) for 4 hours. [b]300 mg catalyst was used.

III-D-4 Photocatalysis of Zinc Sulfide Microcrystals for Reductive Hydrogen Evolution in Water/Methanol System

Shozo YANAGIDA,* Hiroshi KAWAKAMI,* Kazuhito HASHIMOTO, Tadayoshi SAKATA, Chyongjin PAC,* and Hiroshi SAKURAI**
*(*Osaka Univ.) (**Nara Tech. College)*

[*Chem. Lett.*, 1149 (1984)]

In photocatalytic H_2 evolution, using an aqueous methanol system, high quality microcrystalline (cubic) ZnS powders have been found to be comparable in activity with freshly prepared ZnS suspensions when illuminated with an appropriate light intensity. Comparison of the photoactivities of some commercial ZnS with their surface properties has revealed that the surface purity of ZnS plays an important role in the photocatalysis. The time resolved photoluminescence of ZnS does not show a single exponential decay but instead can be divided roughly into two components, a fast ($\tau = 32$ ns) and a slow (610 ns) one, whose spectra differ from each other as shown in Figure 1. Neither diethyl-amine nor methylviologen quenched the luminescence in water from a 337 nm excitation. These results are inconsistent with a recent report on a colloidal ZnS system.[1] Since diethylamine is a good electron donor in the photocatalysis by ZnS, the electron-hole pairs, which give rise to photoluminescence, are indifferent to the interfacial reaction. Other sources of electron-hole pairs play a more important role in the electron transfer reactions.

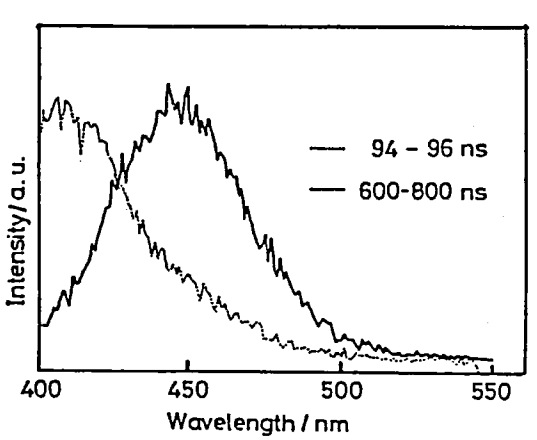

Figure 1. Time-resolved luminescence spectra of commercial ZnS powder (under vacuum) observed with a nsec photon counting system.

Reference
1) A. Henglein and M. Gutierrez, *Ber. Bunsenges. Phys. Chem.*, **87**, 852 (1983).

III-D-5 Photocurrent Transients of Semiconductor-Electrolyte Circuit to a Short Laser Pulse

Tadayoshi SAKATA and Kazuhito HASHIMOTO

The phototransient response of a circuit with semiconductor-electrolyte interface has been reported by many people. Although any clear explanation has not been established yet, the experimental results have suggested that such measurements can provide important information about the dynamical processes at the semiconductor-electrolyte interface. We and R.H. Wilson proposed a simple model to describe the transient behavior of the photocurrent. According to this model, a rise of photocurrent due to the charge transfer at the interface is expected to be observed for a highly doped semiconductor electrode with a large capacitance. Interestingly, for a highly doped TiO_2 single crystal electrode ($4 \times 10^{19}/cm^3$), we could observe a slow rise in the time domain of 100 −1000 ns. One of the examples of the oscilloscope traces is shown in Figure 1. Since this slow rise depends on the kind of redox agents, it is considered to reflect the charge transfer at the interface. A fast rise, which is observed just after the laser pulse, was found to have a rise time of 9 ns, independent of the varied load resistance and kind

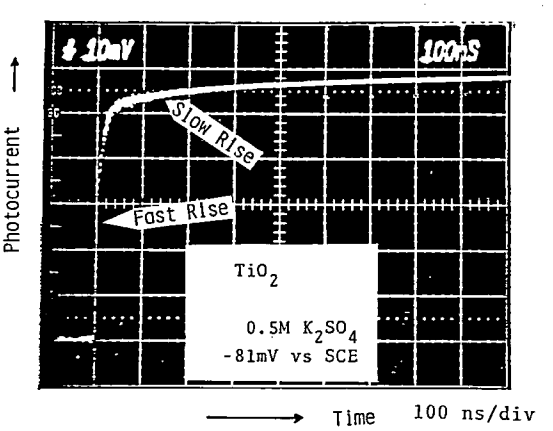

Figure 1. Transient photocurrent of a highly doped TiO_2 single crystal electrode ($4 \times 10^{19}/cm^3$).

of redox species. Since the response time of the electrochemical cell is shorter than 1 ns, this fast rise is not due to RC process but seems to be related with the charge separation process within the semiconductor.

III-D-6 Mechanism of Photocurrent Generation in a Dye Sensitized Semiconductor Electrode Photoelectrochemical Cell

Kazuhito HASHIMOTO and Tadayoshi SAKATA

The mechanism of current generation in a photoelectrochemical cell employing a dye sensitized semiconductor electrode was studied by measurement of the transient photocurrent with a pulsed laser and the fluorescence lifetime of the excited dyes. For the <ZnO | rose bengal, Na_2SO_4 | Pt> cell, the transient photocurrent rises with a time constant of 6.8 ns and decays non-exponentially in the time region of a hundred microseconds. For the band gap irradiation of ZnO electrode, the rise time is 3.1 ns and the decay profiles are the same as that for visible light irradiation. An analysis of these data suggests that the rise time corresponds to charge separation process and the decays were determined by the external RC constant. By measurement of the luminescence lifetimes of rose bengal and rhodamine B, which are adsorbed on semiconductor plates or quartz under air, it was found that for some cases fluorescence was quenched by the semiconductor, suggesting electron transfer occurs from the excited singlet states of these dyes. For the other cases, electron transfer might occur from triplet states. Because of heavy atom effect, intersystem crossing of rose bengal occurs earlier than the electron transfer. These are summarized in Figure 1.

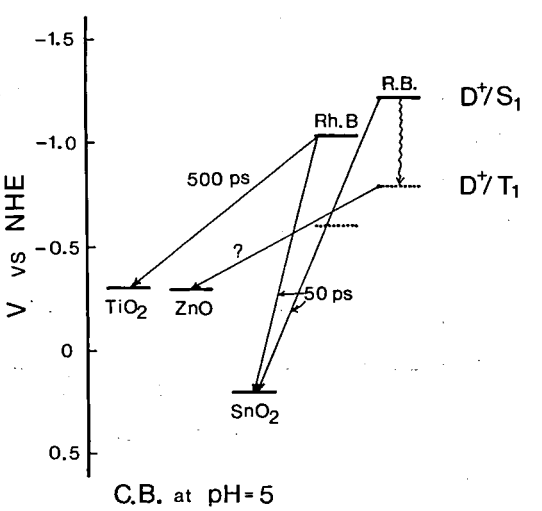

Figure 1. Electron transfer from excited dyes to the semiconductors.

III-D-7 Electron Transfer and Luminescence Lifetime of Excited $Ru(bpy)_3^{2+}$ Derivatives Adsorbed on Semiconductor Surface

Kazuhito HASHIMOTO, Hirofumi TAKEMURA,* Tadayoshi SAKATA, Tetsuo SAJI,* Masamichi FUJIHIRA,* and Shigeru AOYAGI*
*(*Tokyo Inst. Tech.)*

Decay curves and time resolved spectra of the luminescence from the excited states of $Ru(bpy)_3^{2+}$ derivatives, [(i) $Ru[(bpy)_2pby(COOC_{18}H_{37})_2]^{2+}$, (ii) $Ru[(bpy)_2bpy(COOH)_2]^{2+}$], which are physically adsorbed (i) and chemically attached by a carboxyl bond (ii-a) or aminopropyl bond (ii-b) on the

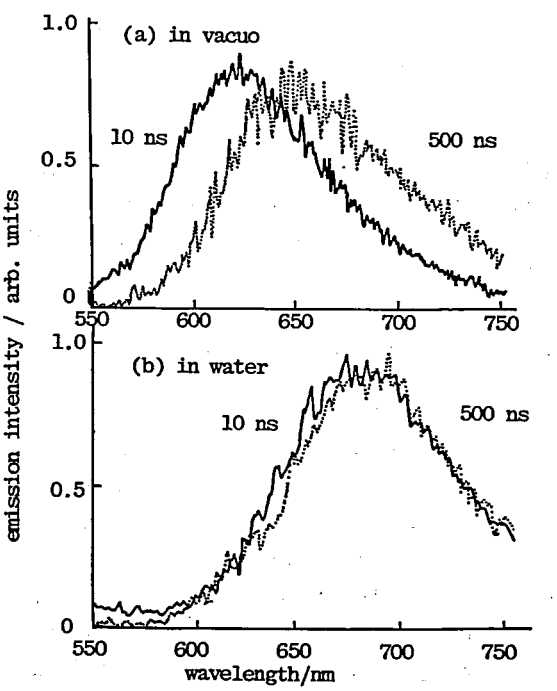

Figure 1. Time resolved spectra of $Ru(bpy)_3^{2+}$ derivative physically adsorbed on TiO_2.

surface of TiO_2 powder, were measured *in vacuo*, in water and in several organic solvents. In most cases the luminescence was quenched strongly. In such cases a fast decay component was observed besides the normal long decay component, which is observed in the absence of semiconductor. These results suggest an electron transfer from the excited state of the dye to the conduction band of TiO_2. *In vacuo* the emission spectrum of the fast component shifted to shorter wavelengths than that of the slow component. This may be explained as follows. The ground state dye molecules, which can participate in the electron transfer, are stabilized by the interaction with the semiconductor surface.[1] This blue shift becomes smaller in water as shown in Figure 1 for derivative (i), suggesting that the interaction of the dye with the surface becomes smaller in the presence of water. Acutually the lifetime of the fast component in water, 125 ns, is longer than that *in vacuo* (20 ns). For derivative (ii-a) no fast component was observed in water suggesting that the electron transfer efficiency is quite low in this case. Moreover, the lifetimes of the fast components for derivative (ii-a), and (ii-b) were found to depend strongly on the nature of the solvent.

Reference

1) T. Kajiwara, K. Hashimoto, T. Kawai and T. Sakata, *J. Chem. Phys.*, **86**, 4516 (1982).

III-D-8 Dynamic Processes of Photocatalytic Reactions on Semiconductor Surfaces with Pulsed Laser Illumination and Time Resolved Mass Spectroscopy

Kazuhito HASHIMOTO and Tadayoshi SAKATA

By the use of a nanosecond laser and a high-vacuum system equipped with a pulsed molecular beam source, time dependent release from the surface of the powdered semiconductor photocatalyst of the reactants, reaction intermediates and reaction products were detected using a quandrupole mass spectrometer. Species can be observed in the time region of several tens to several hundred microseconds. Figure 1-(a) and (b) show the mass spectra of the incident molecular beam and of the molecules desorbed from the surface of photocatalyst, TiO_2 by photo-irradiation, respectively. Besides the reactants, H_2 and formaldehyde are detected as products. An analysis of the time resolved curves of these mass signals gives information about how the light energy is distributed into translational energy of the molecules . The energy distributions of the reactants can be accurately fitted to the Boltzmann distribution, suggesting that the reactants are desorbed from the surface by a thermal process. However, the same curves of the reaction products cannot be analyzed in the same way. Under the assumption that the reaction products are released from the surface several tens of microseconds after irradiation, theoretical analysis accurately explains the observed data.

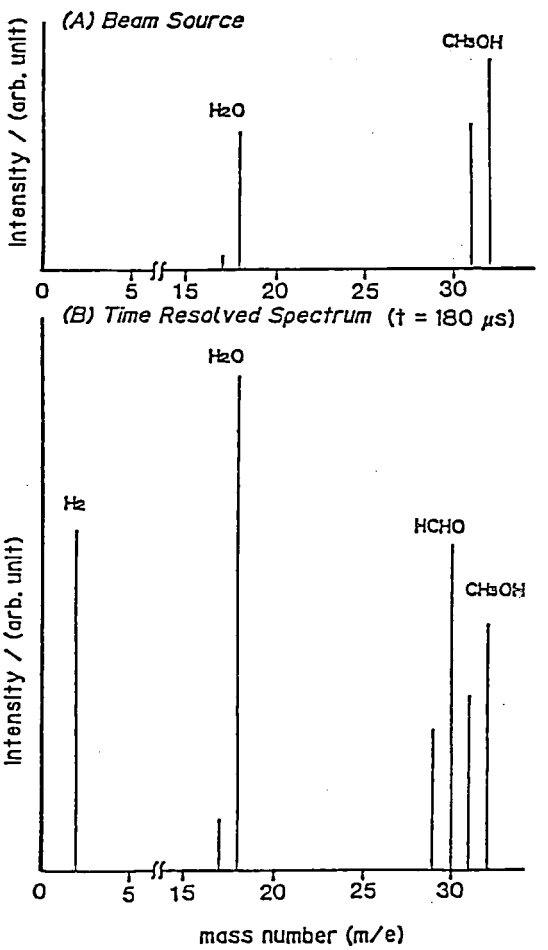

Figure 1. Time resolved mass spectra of the reaction of methanol and water on a TiO_2 photocatalyst.

III—E Dynamical Processes in Electronically and/or Vibrationally Excited Molecules

III-E-1 Infrared Photodissociation of Benzene Dimer; Translational Energy Distribution of Dissociation Fragment

Iwao NISHIYAMA and Ichiro HANAZAKI

The vibrational predissociation of benzene dimer has been investigated in our laboratory (IMS Annual Review 1983). The important conclusion is that the predissociation proceeds slowly after the rapid intramolecular vibrational redistribution. The dissociation mechanism should then be interpreted on the basis of a statistical theory. We have analysed the translational energy distribution of the dissociation fragments by the RRK equation,

$$f_R(E) = \frac{s-1}{E_{avl}}\left(1 - \frac{E}{E_{avl}}\right)^{s-2}$$

where E is the translational energy, E_{avl} is the available energy and s is the number of vibrational modes. Since E_{avl} is known to be 3.4 kJ/mol, s was taken as an only adjustable parameter. The best fit was obtained for $s = 6(\pm 2)$. The average translational energy was determined to be 0.6 kJ/mol. Although the experimental error was fairly large, the obtained number of modes agreed well with the number of low-frequency intermolecular vibrational modes of benzene dimer. The simple statistical model seems to work well in interpreting the vibrational predissociation mechanism.

III-E-2 Acoustically Oscillating Emission from NO_2^* Produced by Infrared Photosensitized Reaction in $SF_6 + NO_2$

Susumu KUWABARA, Keiji KUWATA, Iwao NISHIYAMA, and Ichiro HANAZAKI

[*Chem. Phys. Lett.*, **106**, 540 (1984)]

An oscillating time profile was observed in the visible emission of NO_2 in the $NO_2 + SF_6$ system irradiated by an intense CO_2 laser pulse. Emission spectra indicated the emitting species to be NO_2^*. Measurements of time intervals of the emission as well as the time profile of the optacoustic signal after the infrared irradiation (Figure 1) confirmed that the oscillation was caused by the modulation due to the shock wave produced in the radial direction of a cylindrical cell. Considerations on reaction kinetics have led us to conclude that the excitation of NO_2 into NO_2^* occurs through the collisional energy transfer from the vibrationally hot SF_6 which is first produced by the infrared multiphoton excitation and then repeatedly produced upon periodical concentration of shock wave at the cell center.

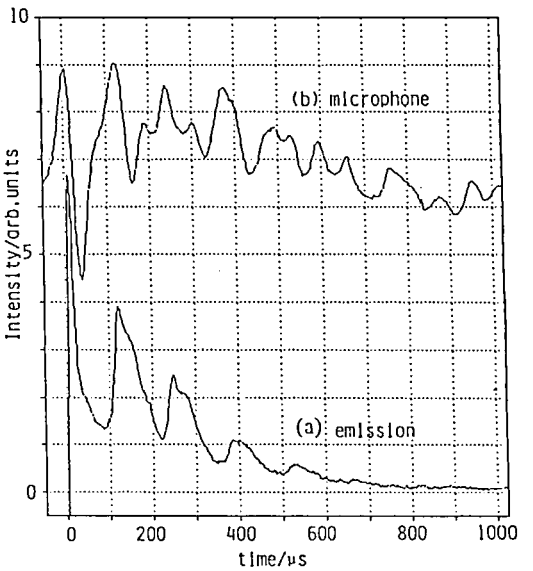

Figure 1. Time profile of emission intensity (a) and sound wave (b). Partial pressure: SF_6 10 Torr and NO_2 5 Torr. Laser fluence is 1.7 J cm^{-2}.

III-E-3 The $S_1(n,\pi^*)$ State of Cyclobutanone and Cyclopentanone in Supersonic Nozzle Beam

Masaaki BABA and Ichiro HANAZAKI

[*J. Chem. Phys.*, in press]

Fluorescence excitation spectra of cyclobutanone and cyclopentanone have been observed for their (n,π^*) transitions in a pulsed supersonic nozzle beam

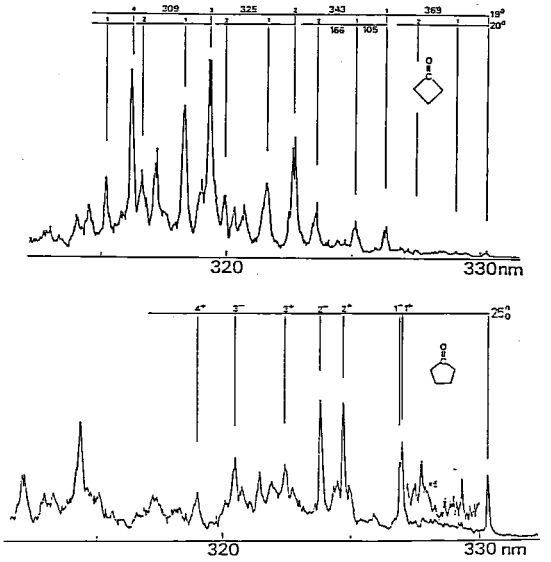

Figure 1. Fluorescence excitation spectra of cyclobutanone and cyclopentanone in Ar supersonic nozzle beam.

using a high power tunable laser (Figure 1). A drastic reduction of hot bands has been attained making it possible to discuss the vibronic assignments in more detail than the previous works of the vapour absorption spectra. It was found that the C=O out-of-plane wagging mode was active for both molecules and that the molecules were pyramidally distorted in the excited states as predicted by Walsh's rule. We have determined the barrier height to inversion (V) and the C=O out-of-plane bent angle at the potential minimum (θ_m) for the $S_1(n,\pi^*)$ state; V = 680 cm^{-1} and θ_m = 34° for cyclopentanone, and V = 1850 cm^{-1} and θ_m = 42° for cyclobutanone. The V values are much higher than formaldehyde presumably due to the ring tension. Also active were the ring twisting and flapping (pseudorotation) in cyclopentanone and the ring puckering in cyclobutanone. The latter was found to have a double minimum potential with V = 16.9 cm^{-1}.

III-E-4 Barrier Height to Inversion of Aliphatic Carbonyl Compounds in the $S_1(n,\pi^*)$ State; *ab initio* Study of Formaldehyde

Masaaki BABA, Umpei NAGASHIMA, and Ichiro HANAZAKI

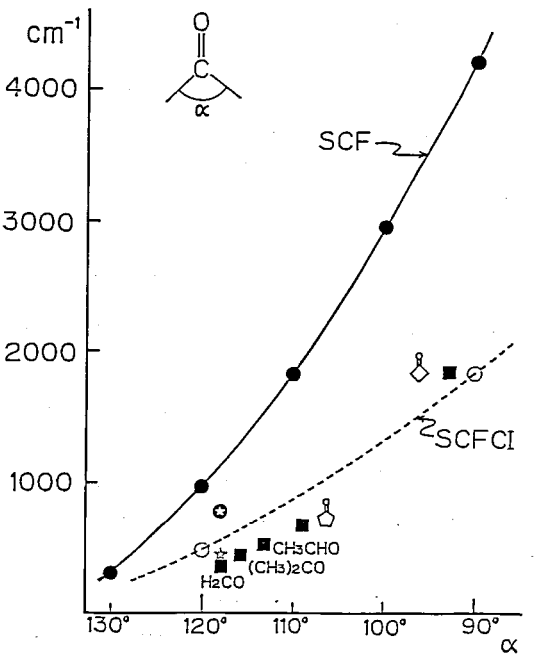

Figure 1. Barrier heights to inversion of aliphatic carbonyl compounds and the results of calculations for formaldehyde.

[*Chem. Phys.*, in press]

As predicted by Walsh for formaldehyde, aliphatic carbonyl compounds are pyramidally distorted in the $S_1(n,\pi^*)$ state. The double minimum potentials for this pyramidal distortion have recently been determined for acetaldehyde, acetone and cyclic ketones using the supersonic nozzle beam technique. We have found a good correlation between the barrier height to inversion and the angle between the two bonds adjacent to the carbonyl carbon atom. In order to elucidate the correlation in more detail, we performed *ab initio* calculations for the S_1 state of formaldehyde with changing HCH angle α. As can be seen from Figure 1, the results of the SCF and SCFCI calculations are in good agreement with the experimental results. It is shown that the barrier height to inversion of the aliphatic carbonyl compound is related to the degree of sp hybridization on the carbonyl carbon atom which, in turn, is predominantly determined by α. The barrier height increases as α decreases from 120° to 90°. Therefore, it is natural that the barrier height of cyclobutanone is much higher than that of formaldehyde.

III-E-5 The $S_1(n,\pi^*)$ States of Acetaldehyde and Acetone in Supersonic Nozzle Beam; CH_3 Internal Rotation and C=O Out-of-plane Wagging

Masaaki BABA, Ichiro HANAZAKI, and Umpei NAGASHIMA

[Submitted to *J. Chem. Phys.*]

Fluorescence excitation spectra of CH_3CHO, CH_3CDO, $(CH_3)_2CO$ and $(CD_3)_2CO$ have been observed in a pulsed supersonic nozzle beam using a high power tunable laser. The spectra of CH_3CHO and CH_3CDO and the vibronic assignments are shown in Figure 1. The excitation spectrum of CH_3CHO has been reported by Noble *et al.* for the low energy region[1] and is in good agreement with the present result. Active are the C=O out-of-plane wagging and the methyl internal rotation (torsion) in the acetaldehyde and acetone spectra. The barrier heights to inversion (V) and to methyl rotation (V_3) have been determined in the $S_1(n,\pi^*)$ states[2]; $V = 541$ cm^{-1} and $V_3 = 691$ cm^{-1} for CH_3CHO, $V = 578$ cm^{-1} and $V_3 = 645$ cm^{-1} for CH_3CDO, $V = 466$ cm^{-1} and $V_3 = 740$ cm^{-1} for $(CH_3)_2CO$, and $V = 480$ cm^{-1} and $V_3 = 720$ cm^{-1} for $(CD_3)_2CO$. The V values are not so different from the value of formaldehyde (356.2 cm^{-1}). The V_3 values are much higher than those in the ground states. It is considered to be due to the interaction between the π^*-orbital on the carbonyl carbon and the σ-orbital on the methyl hydrogen.

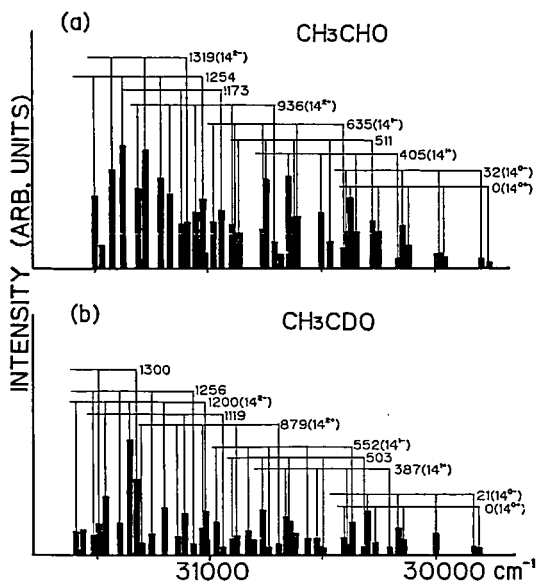

Figure 1. Fluorescence excitation spectra and assignments of CH_3CHO and CH_3CDO in Ar supersonic nozzle beam.

References

1) M. Noble, E.C. Apel and E.K.C. Lee, *J. Chem. Phys.*, **78**, 2219 (1983).
2) M. Baba and I. Hanazaki, *Chem. Phys. Lett.*, **103**, 93 (1983).

III-E-6 *Ab initio* Study of Methyl Internal Rotation of Acetaldehyde in the $S_1(n,\pi^*)$ State

Masaaki BABA, Umpei NAGASHIMA and Ichiro HANAZAKI

Using the supersonic nozzle beam technique, we have determined frequencies of the vibrational levels of the methyl rotation (torsion) mode in the $S_1(n,\pi^*)$ states of acetaldehyde and acetone. The barrier height to methyl rotation in the S_1 state was much higher than that in the ground state. In order to investigate the origin of this barrier, we performed *ab initio* SCF calculations for acetaldehyde. The geometrical parameters are shown in Figure 1 and the results are summarized in Table I. In the ground state, the H eclipsing O conformation is stable ($\varphi_m = 0°$) which is consistent with the calculations by Davidson and Allen[1] and the

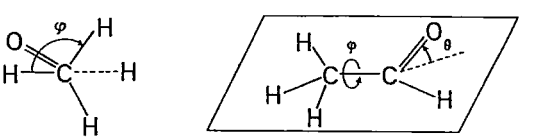

Figure 1. Geometrical parameters of acetaldehyde.

Table I. *Ab initio* calculation for the barrier height to CH_3 rotation of acetaldehyde (energies in units of hartree)

φ	S_0	S_1(planar)	$S_1(\theta = 32°)$
0°	−152.951430	−152.818537	−152.828701
20°	.950883	.819001	.826782
40°	.949790	.819872	.825609
60°	.949243	.820279	.826380
80°	.949790	.819871	.828292
100°	.950883	.819001	.829437
φ_m	0°	60°	103°
ΔE(cm^{-1})	480.0	382.3	860.9

experimental results. However, in the pyramidal S_1 state (θ=32°), the C-H bond is nearly perpendicular to the C=O bond at the energy minimum and the barrier height to methyl rotation is much higher than that in the ground state. A detailed analysis of the density matrix suggests that the π-type interaction between methyl and carbonyl carbons is dominant in determining the potential to internal rotation.

Reference

1) R.B. Davidson and L.C. Allen, *J. Chem. Phys.*, **54**, 2828 (1971).

III—F Study on Photochemical and Photophysical Processes Related to Interstellar and Planetary Space Chemistry

Photochemical and photophysical events happening in interstellar space or in outer planetary space are of great interest in relation to chemical evolution of simple molecules. VUV photons fill diffuse molecular clouds and penetrate into dense molecular clouds. Many problems exsist to be solved. Our effort is focused mainly on the surface phenomena on icy grains.

III-F-1 Photodetachment of Surface Molecules upon Electronical Excitation to Valence States

Nobuyuki NISHI and Tohru OKUYAMA

In a recent paper[1], we have reported a new phenomenon of photodetachment of surface molecules on molecular solids for the excitation to Rydberg excited states of NH_3 and H_2O. Molecules on molecular solids are bound through intermolecular interactions such as van der Waals forces or hydrogen bondings. Ground state molecular orientations are stabilized at the potential minimum formed by the electronic interactions between molecules. Excitation of an electron to a high quantum number orbitals (Rydberg state excitation) deformes the potential of molecular pair states resulting in the enlargement of the intermolecular distances.

Solid CO_2 and solid C_2H_2 were deposited with guest molecules (CH_3C_2H, CH_3Cl, CH_3OH, C_3H_8, C_4H_{10}, etc.) on a quartz surface at 100 K. A part of wide laser beams (193 nm or 248 nm) was irradiated on the surface in an ultra-high vacuum chamber. Typical beam intensities on the surface were 0.2–5 mJ/cm^2. The observed translational energy distributions were described by Maxwell-Boltzmann distribution functions, with mean translational energies $\bar{E}_t$ (= $\frac{3}{2}$ kT). The translational

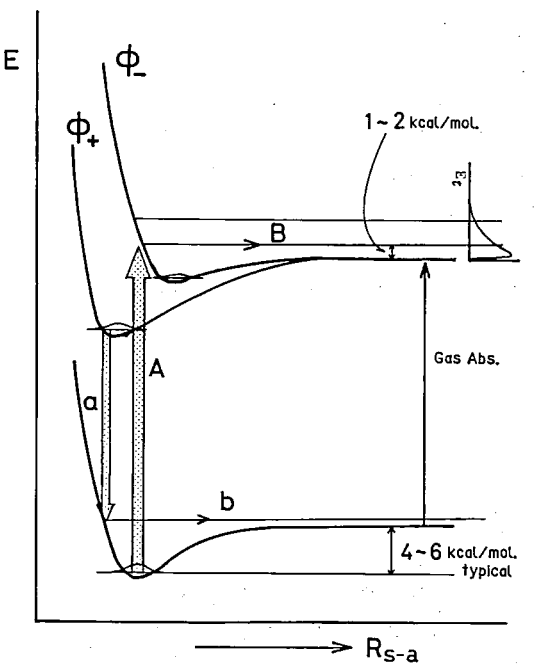

Figure 1. The surface-adsorbate potantials of the ground and excited valence states. Two types of the excited potentials are possible (ϕ_+ & ϕ_-). In ϕ_+ state, the adsorbate (an edge molecule or a sigle molecule sitting on the surface) is attracted by the surface. Electronical relaxation to the ground state pumps down the pair to the repulsive wall at a Franck-Condon state. The allow down to the ground state does not mean an optical transition but it means a radiationless transition to highly vibrationally excited levels of the ground state at the adsorbate-surface geometry equilibrium in the excited state. The ϕ_- state has a repulsive wall at the Franck-Condon state pumped optically from the ground state.

energies of the detached molecules were not affected by laser power in the range examined and showed differencies on the host-guest combination and the surface roughness. The observed mean energies are in the range of 1–2 kcal/mol in most cases. The intensity increased linearly proportionally to the increment of laser power in the low energy range. The signals of C_4H_{10} and C_3H_8, which have no absorption at the laser wavelengths, were observed when they were deposited with C_2H_2 or CH_3C_2H. Figure 1 explains the proposed mechanism of the photodetachment upon valence state excitation.

Reference

1) N. Nishi, H. Shinohara, and T. Okuyama, *J. Chem. Phys.*, **80**, 3898 (1984).

III-F-2 Photodissociation of CS_2 on CO_2 Ices

Nobuyuki NISHI, Masahiro KAWASAKI *(Mi'e Univ.)*, **and Tohru OKUYAMA**

Dynamics of surface photodissociation is one of the interesting subjects in the fields of chemical physics and astrochemistry. The technique of the photofragment spectroscopy has been applied to the analysis of the photodissociation of surface molecules. Figure 1 shows the time-of-flight spectra of atomic sulfur fragments dissociated upon the 193 nm laser excitation of CS_2 molecules in molecular beams (upper) and on the CO_2 surface (lower). Molecular beam CS_2 is known to dissociate rapidly producing sulfur atoms in the excited ^1D state as well as in the ground ^3P state. The time-of-flight spectrum in Figure 1 shows the two peaks corresponding to the respective electronic state. The fragment from the surface showed the TOF spectrum starting at a shorter time and peaking at the same time as that of the peak of the ground state sulfur from the molecular beam. The surface TOF signal shows a very broad low energy component ($\bar{E}_t$ = 2 kcal/mol). This component is attributed to the sulfur atoms scattered by the collision with surface molecules. Its intensity changed drastically depending on the roughness of the surface. The TOF spectrum suggests that the photodissociation of surface CS_2 occurs through the lowest triplet state which has a repulsive potential in nature. The intersystem crossing is enhanced by the coupling of the surface CS_2 with the phonon field of the CO_2 ice. The highest translational energy (the convergence limit of the distribution) coincides with the total available energy ($h\nu - D_0$) of the gas molecule. The average E_t of the high energy sulfur is 16 kcal/mol which is high enough to induce hot sulfur atom chemistry on low temperature surfaces.

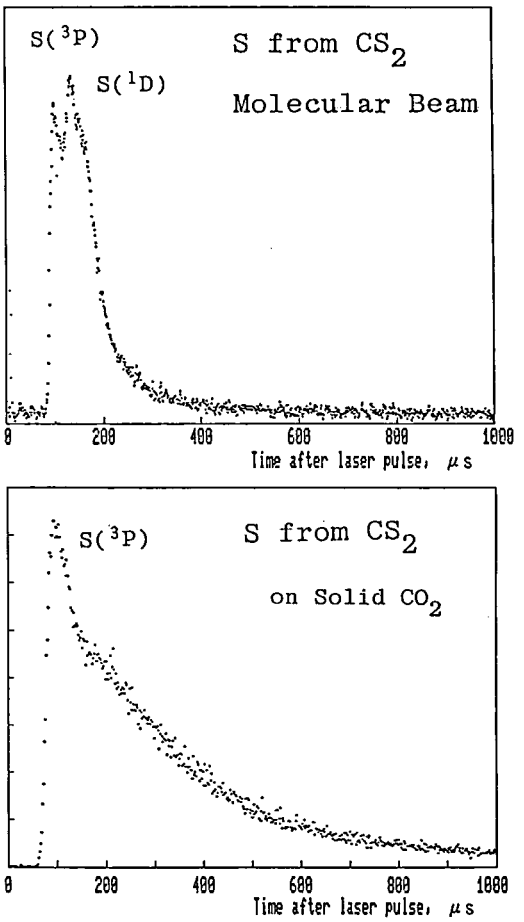

Figure 1. Time-of-flight spectra of recoiling sulfur atoms from molecular beam CS_2 (upper) and surface CS_2 on solid CO_2 (lower).

III-F-3 Photochemical Reactions in Molecular Solid Containing CH_3CN and NH_3 Studied by UV Laser Photodesorption of Surface Molecules

Tohru OKUYAMA and Nobuyuki NISHI

[*Nippon Kagaku Kaishi*, 1506, 1984]

UV light from an expanded laser at 193 nm or a

low pressure marcury lamp (254 nm + 185 nm) was irradiated on the solid composed of CH_3CN and NH_3 at 77 K ~ 130 K. Primary photochemical processes were studied by the photodesorption of product molecules on the solid surface. A pulsed laser at 248 nm (~20 mJ/cm^2) was used as a photodesorption light source and the mass numbers and translational energies of the photoproducts were measured by a quadrupole mass spectrometer. Figure 1 shows the time-of-flight (TOF) spectra of the photoproducts ejected from the solid surface. Formation of $C_2H_2N_2$ and C_2H_4 from CH_3CN has been ascribed to a disproportionation reaction of two acetonitrile molecules, which is the main reaction in a pure acetonitrile solid.

$$2CH_3CN \xrightarrow{h\nu} C_2H_2N_2 + C_2H_4 \quad (1)$$

Aminoacetonitrile (NH_2CH_2CN) and acetamidine ($CH_3C(NH_2)$=NH) were formed through a bimolecular condensation reaction of CH_3CN and NH_3 and the additioin reaction of the two parent molecules, respectively.

$$NH_3 + CH_3CN \xrightarrow{h\nu} NH_2CH_2CN + H \quad (2)$$

$$\xrightarrow{h\nu} CH_3C(NH_2)=NH \quad (3)$$

The product analysis of the $CH_3CN + NH_3$ solid irradiated with a low pressure marcury lamp at 77 K ~ 130 K was performed by the use of a liquid chromatography and a high resolution mass spectrometer. As well as the primary products, many large molecules such as DAMN (diaminamaleonitrile), AICN (5-amino-4-imidazolecarbonitrile) and other HCN origomers, were detected in secondary photoproducts, which are known as precursor molecules in the prebiotic synthesis of purines, amino acids and peptides.

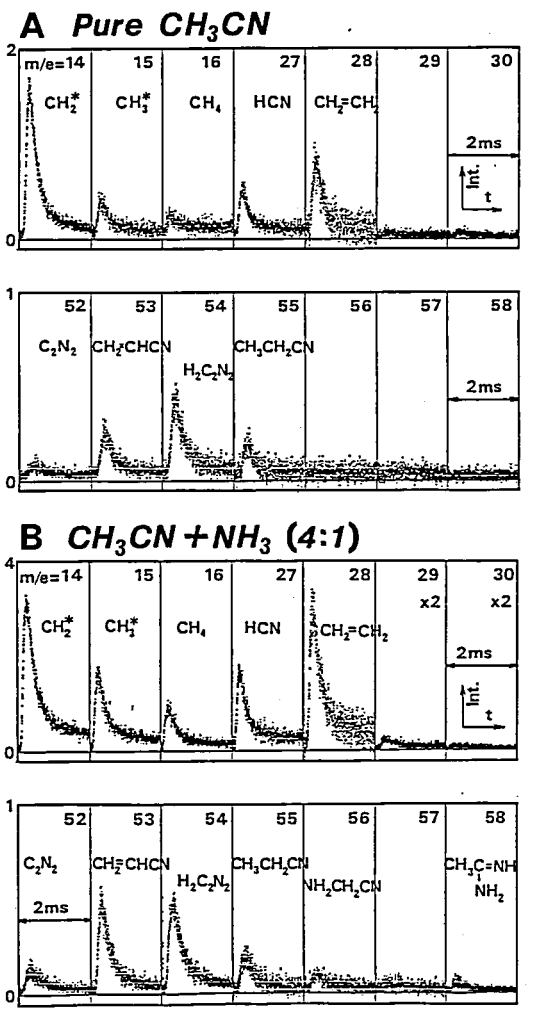

Figure 1. TOF spectra of photoproducts sputtered by 248 nm laser pulses (~20 mJ/cm^2) after irradiation with 5×10^4 shots at 193 nm (~5 mJ/cm^2) on the pure solid of CH_3CN (A) and on the mixed solid of NH_3 and CH_3CN (1:4) (B). CH_2* and CH_3* mean the secondary fragments generated from CH_3CN by electron impact (electron energy = 20 eV) in the ionizer.

III-F-4 Competition of Fluorescence and Reation Processes in the Low-lying Excited States of Cyanoacetylene

Kanekazu SEKI *(Univ. Tokyo and IMS)*, **Kwang Yul CHOO** *(Seoul National Univ.)*, **Nobuyuki NISHI, and Minoru KINOSHITA** *(Univ. Tokyo)*

Cyanoacetylene and its poly-yne derivatives HC_nN(n = 1,3,5,7,9,11) were identified as interstellar molecules by radioastronomy. Cyanoacetylene is believed to play an important role in the process of complex molecule formation. In order to understand photochemical reactions of cyanoacetylene from low-lying excited states, fluorescence and its excitation spectra have been observed by a conventional photon counting method. The fluorescence excitation spectra are shown in Figure 1. The assignment of the vibronic bands was made based on King's table.[1] In the $\tilde{B}$ state region, the structure of the excitation spectrum coincides with that of the absorption spectrum. The progressions of π-type

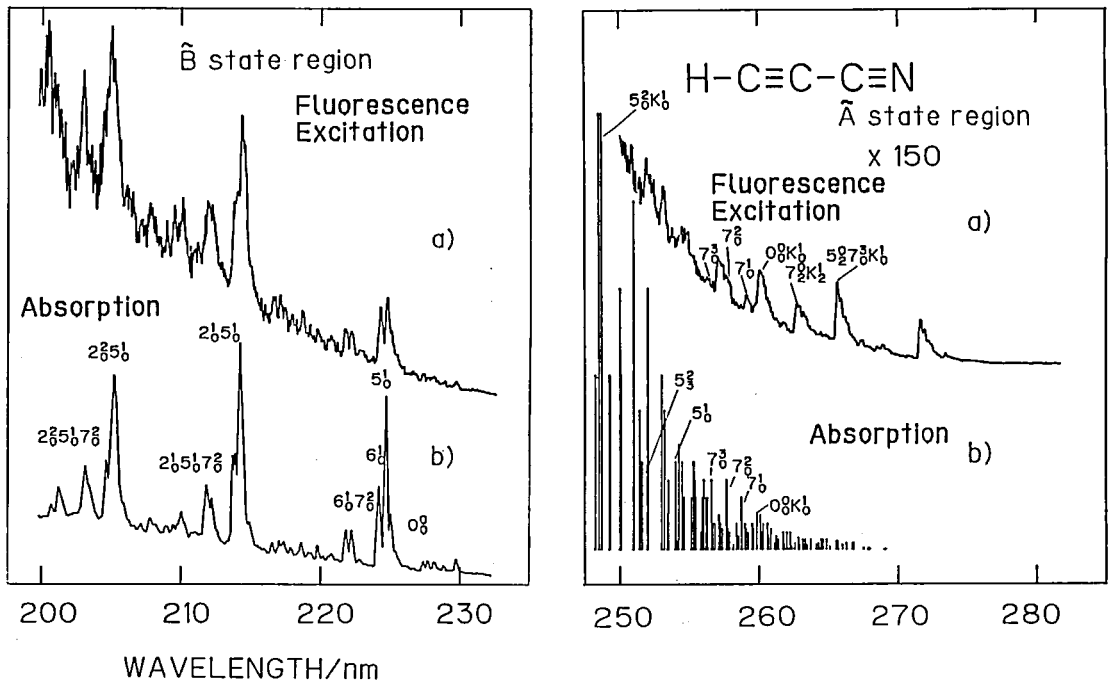

Figure 1. Fluorescence excitation spectra (a) and absorption spectra (b) of cyanoacetylene (HC_3N). The intensity of excitation spectra in the $\tilde{A}$ state region (right) is expanded 150 times as large as that in the $\tilde{B}$ state region (left).

bending vibrations(ν_5, ν_6, ν_7) appear strongly in these spectra. On the other hand, the $\tilde{A} \leftarrow \tilde{X}$ excitation spectrum is dissimilar to the absorption spectrum in the intensity of the vibronic bands. Especially the excitation to the C-C-H bending vibrational levels of ν_5 mode does not show any fluorescence. No structure appeared in the excitation spectrum from 230 nm to 250 nm. These facts suggest that some radiationless transitions (possibly reactions) occur from the vibrational excited states of the $\tilde{A}$ state. From the analogy of the photochemical reaction of acetylene it is suggested that the radiationless processes include an isomerization into a triplet carbene (:C = C(H)CN).

Reference

1) V.A. Job and G.W. King, *J. Mol. Spectrosc.*, **19**, 155 (1966).

III-F-5 Laser Photolysis of Acetylene at 193 nm: Two Pathways of Formation of Diacetylene

Kanekazu SEKI *(Univ. Tokyo and IMS),* **Nobuyuki NISHI, Tohru OKUYAMA, Hisanori SINOHARA, Nobuaki NAKASHIMA, Keitaro YOSHIHARA, and Minoru KINOSHITA** *(Univ. Tokyo)*

Nanosecond laser photolysis of acetylene at 193 nm has been studied to know the reaction dynamics of the formation of diacetylene in a pressure region of 30 ~ 500 Torr. The time-resolved absorption spectra after laser pulse irradiation are shown in Figure 1 together with the absorption spectra of diacetylene. As clearly seen in the figure, the peaks observed in the time-resolved spectra result from the formation of diacetylene. The time behavior of the peaks shows that there are two pathways of the diacetylene formation. The first one, which finished within the laser pulse width of 15 ns(FWHM), is attributed to the reaction of C_2H radicals:

$$C_2H_2 \xrightarrow{h\nu} C_2H + H,\ C_2H + C_2H_2 \longrightarrow C_4H_2 + H.$$

The second one is a slow process of diacetylene formation observed from 0 ns to 1500 ns. Here, we

define "$t = 0$" at the end of the laser pulse (~20 ns). The diacetylene formation rate becomes independent on the C_2H_2 pressure about 200 Torr. This fact is explained by introducing the following two reaction processes.

$$C_2H_2 \xrightarrow{h\nu} C_2H_2^* \longrightarrow C_2H_2^{\dagger} \xrightarrow{+C_2H_2} C_4H_2 + H_2 \quad (1)$$

$$C_2H_2^* \xrightarrow{+C_2H_2} C_4H_4^{\dagger} \xrightarrow{k_2} C_4H_2 + H_2 \quad (2)$$

Reaction sequence (1) is the main process below 100 Torr. The metastable species $C_2H_2^{\dagger}$ is considered to be a vinylidene radical or a triplet state acetylene. The rate determining step in process (2) is the final reaction. The formation rate k_2 is measured to be 2.0×10^6 s^{-1}.

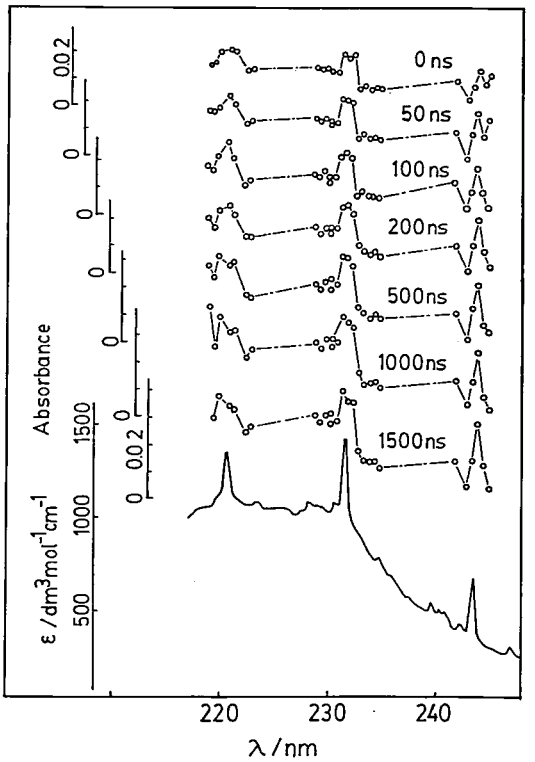

Figure 1. Time-resolved absorption spectra of the acetylene photolyzed by 193 nm laser pulses; concentration: 100 Torr. The lower is the absorption spectrum of diacetylene in gas phase.

III—G Photodissociation of Molecular Beams by UV Lasers

III-G-1 Photodissociation of Tetramethyltin at 193 nm in a Molecular Beam

Masahiro KAWASAKI*, Kazuo KASATANI*, Hiroyasu SATO* *(Mi'e Univ.*)*, **Hisanori SHINOHARA, and Nobuyuki NISHI**

Molecular beams of $Sn(CH_3)_4$ are photodissociated at 193 nm. Methyl photofragments were detected by a mass spectrometer providing a translational energy distribution. The energy peak at ~7 kcal/mol decreases gradually in the high energy side. The absorption of 193 nm light (148 kcal/mol) is expected to open the following three dissociation pathways based on the thermochemical data;

$$Sn(CH_3)_4 \longrightarrow Sn(CH_3)_3 + CH_3, \quad \Delta H^0 = 88 \text{ kcal/mol}, \quad (1)$$

$$\longrightarrow Sn(CH_3)_2 + 2CH_3, \quad \Delta H^0 = 129 \text{ kcal/mol}, \quad (2)$$

$$\longrightarrow SnCH_3 + 3CH_3, \quad \Delta H^0 = 146 \text{ kcal/mol}. \quad (3)$$

In the two-body dissociation (1), a spectator model predicts the average translational energy($\bar{E}_t$) of ~30 kcal/mol, while three-body dissociation (2) has $\bar{E}_t$ = 12 and 5 kcal/mol for sequential and simultaneous dissociation, respectively, on the equipartition model given by Baer et al.[1] The sequential three body dissociation explains the observed energy distribution satisfactorily.

Reference

1) T. Baer, A.E. Depriso, and J.J. Hermans, *J. Chem. Phys.*, **76**, 5917 (1982).

III-G-2 Photodissociation of Molecular Beams of Alkyl Sulfides

Masahiro KAWASAKI*, Kazuo KASATANI*, Hiroyasu SATO* *(Mie Univ.*)*, Hisanori SHINOHARA, and Nobuyuki NISHI

Photofragment spectroscopy has been applied to the photodissociation of CH_3SCH_3, CD_3SCD_3, CH_3SSCH_3 and C_2H_5SH at 193 nm. The primary processes observed are CS bond rupture for these molecules. The S-H bond breaking was not observed in C_2H_5SH photolysis. This result is consistent with the quantum chemical calculation by Bendazzoli et al.[1] According to them the transition at 5 eV is $1^1B_2 \leftarrow 1^1A_1$ or $9a_1 \leftarrow 3b_2$. This lowest virtual orbital($9a_1$) has a predominant 4s character. The 4s orbital is slightly mixed with the 2s orbital of carbon to give a molecular orbital with a moderate antibonding character with respect to the S-C bond. The energy distribution is well represented by a Possionian but not by the RRKM theory. It indicates that the dissociation is direct. The spectator and rigid rotor model predict that the fraction of translational energy (f_T) defined as E_t/E_{avl} is 0.9. The experimentally observed f_T is 0.7. It shows that the CD_3S radical is vibrationally excited. Laser-induced-fluorescence experiment suggested that the vibrationally excited mode is not CS stretching one but probably umbella inversion mode of a CH_3 group.

Reference

1) G.L. Bendazzoli, G. Gottarelli, and P. Palmieri, *J. Am. Chem. Soc.*, **96**, 11 (1974).

III—H Formation and Properties of Hydrogen-Bonded Molecular Clusters Both in Supersonic Nozzle Beams and Inert-Gas Matrices at Low Temperatures

III-H-1 Mass Spectroscopic Observation of an Enhanced Structural Stability of Water-Ammonia Binary Clusters at n = 20 in the Series $(H_2O)_n(NH_3)_mH^+$ ($0 \leqq n + m \leqq 32$)

Hisanori SHINOHARA, Umpei NAGASHIMA, and Nobuyuki NISHI

[*Chem. Phys. Lett.*, **111**, 511 (1984)]

An enhanced structural stability of water-ammonia mixed clusters has been observed via a molecular-beam-mass spectrometry. The mixed clusters exhibit distinct intensity maxima at $(H_2O)_{20}(NH_3)_{1-5}H^+$ and a less pronounced one at $(H_2O)_{27}NH_4^+$ in the mass spectra. The fact that the positions of these enhanced peaks are independent of the stagnation pressure and ionization conditions, strongly suggests that they stem primarily from an intrinsic structural stability of the binary clusters corresponding to the above "magic numbers". Figure 1 clearly illustrates that the mixed clusters, $(H_2O)_n(NH_3)_{1-3}H^+$, have distinct intensity maxima at n = 20.

The observed intensity maxima of the clusters $(H_2O)_nNH_4^+$ at n = 20 are consistently explained if

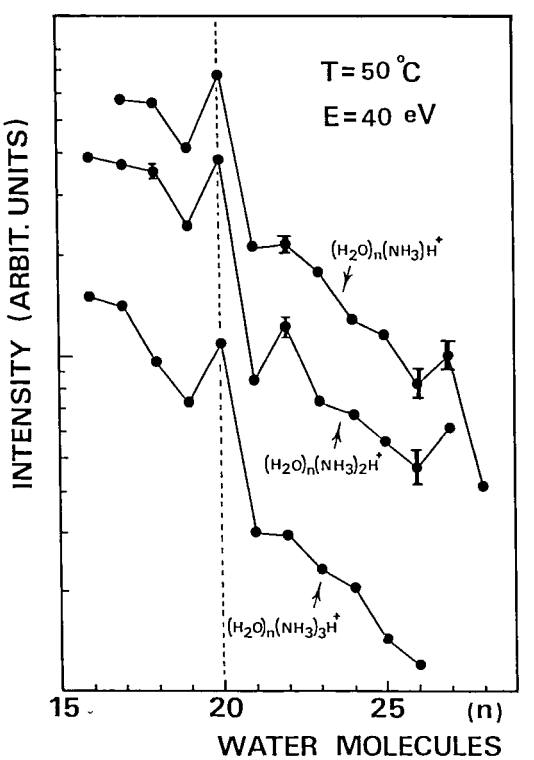

Figure 1. Semilogarithmic plot of mixed cluster intensity versus the number of H_2O molecules in the cluster. Three plottings are shown in the figure containing one, two, and three ammonia molecules in the mixed clusters. Uncertainties determined by experimental reproducibility are presented in the figure.

one assumes that the 20 water molecules jointly construct a deformed pentagonal dodecahedron cage structure with an NH_4^+ ion trapped in its center. The present "ion clathrate" model is based on a strong Coulombic interaction between the NH_4^+ ion and the surrounding 20 water molecules, where the number of hydrogen bonds is maximized and the condition of maximum symmetry is imposed. The present study suggests that an H_3O^+ ion plays an important role in the center of a pentagonal dodecahedron for the stability of the $(H_2O)_{21}H^+$ cluster.

III-H-2 Photoionization of Ammonia Clusters in a Pulsed Supersonic Nozzle Beam by Vacuum-UV Rare-Gas Resonance Lines

Hisanori SHINOHARA, Nobuyuki NISHI, and Nobuaki WASHIDA *(National Institute for Environmental Studies)*

[*Chem. Phys. Lett.*, **106**, 302 (1984)]

Unprotonated ammonia cluster ions, $(NH_3)_3^+$ and $(NH_3)_4^+$, were detected as well as $(NH_3)_2^+$ in addition to normally observed protonated clusters $H^+(NH_3)_{n-1}$ by VUV photoionization mass spectroscopy using rare-gas resonance lamps(Ar,Kr) and a pulsed molecular-beam-mass spectrometer system. Figure 1 compares mass spectral patterns at four different ionization energies: 11.83 and 11.62, 10.64 and 10.03, 10.03 and 8.44 eV. The relative intensities $(NH_3)_n^+/H^+(NH_3)_{n-1}$ are different among the spectra: much larger at lower excitation energies. The relative intensities $(NH_3)_n^+/H^+(NH_3)_{n-1}$ are determined by competition of the following two pathways:

$$(NH_3)_n + h\nu \rightarrow [(NH_3)_n^+]_{vip} + e^-$$

$$\longrightarrow (NH_3)_{n-2}NH_4^+ + NH_2 + e^-, \quad \text{(dissociated)}$$

$$\longrightarrow (NH_3)_{n-2}NH_4^+ \cdots NH_2 + e^-, \quad \text{(proton-transferred)}$$

where vip represents vertically ionized point. The results are discussed in terms of probable intracluster ion-molecule reaction.

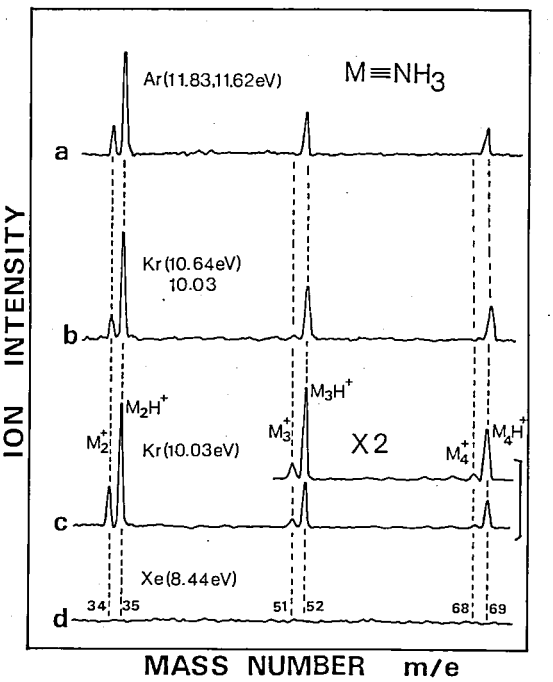

Figure 1. Comparison of the mass spectral pattern of ammonia clusters at four different excitation energies: (a) 11.83 and 11.62 eV (Ar lamp: LiF window), (b) 10.64 and 10.03 eV (Kr lamp: MgF_2 window), (c) 10.03 eV (Kr lamp: CaF_2 window), and (d) 8.44 eV (Xe lamp: sapphire window). The conditions: 760 Torr stagnation pressure; room temperature; 10 accumulation. Aside from the excitation energy, all experimental conditions are kept constant.

III-H-3 Identification of Ammonia Clusters in Low Temperature Matrices Using FTIR Short-Pulsed Matrix Isolation Technique

Teruhiko NISHIYA *(Kyoto Univ.)*, **Noboru HIROTA** *(Kyoto Univ.)*, **Hisanori SHINOHARA, and Nobuyuki NISH**

The clustering of ammonia in Ar matrices has been studied at matrix to absorber ratio(M/S) between 160 and 2000. Figures 1(a)–(d) present Fourier-transform infrared (FTIR) spectra for ammonia and its clusters in the ν_2 bending region. At M/S = 2000, the spectrum is dominated by the inversion mode of the monomer together with a band at 999 cm^{-1}. It is expected that the $(NH_3)_2$ band should be the first to appear (among various cluster absorptions) even at dilute M/S ratios, followed by $(NH_3)_3$ and higher clusters as the M/S ratio is raised. As can be seen from the figure, the 999 cm^{-1} absorption is the first to grow as the concentration is increased. This band has been

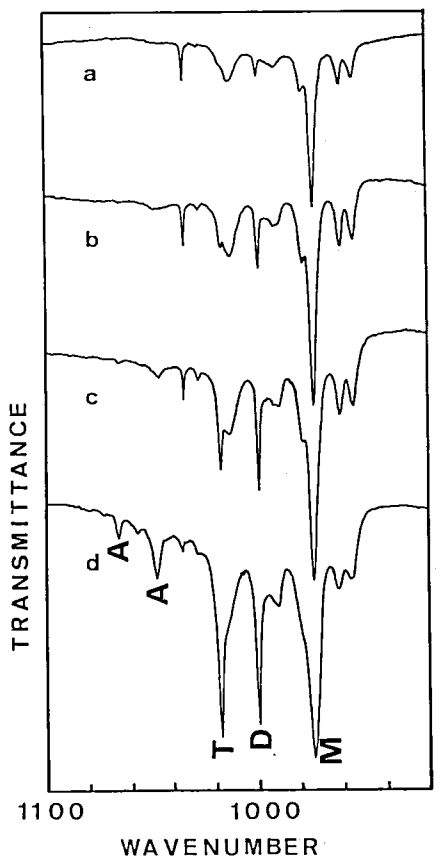

Figure 1. The inversion mode (ν_2) region of NH_3 in Ar matrices over a range of concentrations: (a) M/S = 2000, (b) M/S = 1000, (c) M/S = 500, and (d) M/S = 160; stagnation pressure 600 Torr. M, D, T, and A in the spectrum signify ammonia monomer, dimer, trimer, and clusters of unspecified size (but larger than the trimer), respectively.

attributed to $(NH_3)_2$ by Abouaf-Marguin et al.[1] and is assigned here also to the dimer. Another prominent feature at 1018 cm^{-1} grows rapidly relative to the dimer over a wide range of concentration from M/S = 160 to 2000. The small peaks appeared at 1028, 1047, and 1065 cm^{-1} also grow, though much less, relative to the dimer. It seems reasonable to assign the absorption at 1018 cm^{-1} to $(NH_3)_3$ and the rest of the weak lines to multimers of unspecified size, but larger than the trimer.

The aggregation of ammonia occurs in the bulk of the matrices; and the clustering processes are discussed in terms of a simple rate-equation treatment based on a stepwise self-association mechanism.

Reference

1) L. Abouaf-Marguin, M.E. Jacox, and D.E. Milligan, *J. Mol. Spectrosc.*, **67**, 34 (1977).

III—I Effects of External Magnetic Field upon Chemical Reactions

Magnetic field effects upon chemical reactions provide us with (1) method for studying reaction mechanisms and (2) technique for controlling reaction rates and product yields. At present, we study magnetic field effects on chemical reactions in solutions, especially photochemistry and electrochemistry in order to clarify reaction mechanisms. Since application of magnetic field effects to related areas, *e.g.* combustion is of some importance, an apparatus for gas phase reactions in the presence of an external magnetic field is under construction.

III-I-1 Reaction Mechanism of Photo-Fries Rearrangement as Revealed by Magnetic Field Effects. An Example of Magnetically Active Isotope Substitution

Ryoichi NAKAGAKI, Mitsuo HIRAMATSU *(Hamamatsu Photonics K.K. and IMS)*, **Takeshi WATANABE, Yoshifumi TANIMOTO** *(Kanazawa Univ. and IMS)*, **and Saburo NAGAKURA**

Reaction mechanism of photo-Fries rearrangement of 1-naphthyl acetate and 1-naphthyl 1-^{13}C-acetate in acetonitrile has been studied by means of steady state photolysis and laser flash photolysis. A radical pair consisting of 1-naphthoxyl and acetyl radicals is found to be reaction intermediate. The yield of an in-cage product, 2-acetyl-1-naphthol, from the ester labelled by magnetically active carbon ^{13}C exhibits a positive external magnetic field effect, while the yield of the same product from the normal ^{12}C ester is insensitive to the presence of an external high magnetic field (0.64T). The magnetic field effect upon photo-rearrangement of the labelled ester was found to be due to change in the intersystem crossing rate between

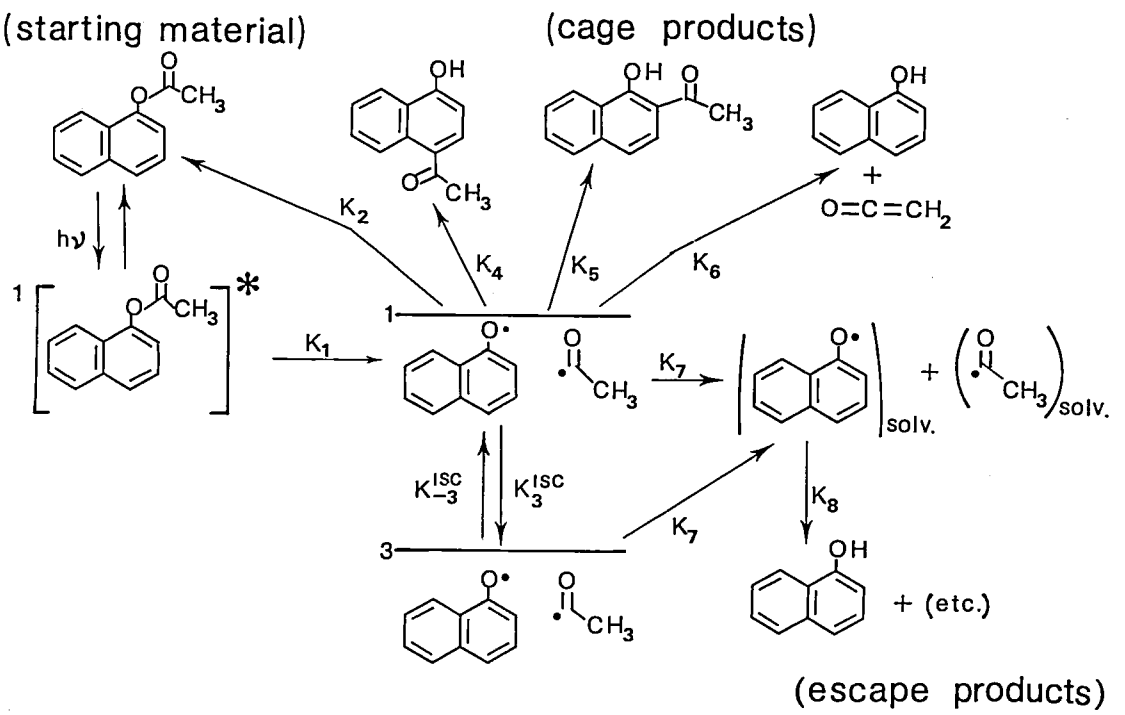

Figure 1. Reaction scheme for photo-Fries rearrangement of 1-naphthyl acetate. k_1 (bond dissociation), k_2 (recombination), k_3 and k_{-3} (intersystem crossing), k_4 and k_5 (in-cage rearrangement), k_6 (in-cage disproportionation), k_7 (escape process), and k_8 (radical quenching).

singlet and triplet radical pairs induced by hyperfine coupling between magnetically active nuclei (^{1}H and ^{13}C) and an unpaired electron in acetyl radical. It is concluded that in-cage products are formed through singlet radical pairs. A reaction scheme for photo-Fries rearrangement of the ester is summarized in Figure 1.

III-I-2 The Magnetic Field Effects on Electrolysis

Takeshi WATANABE, Yoshifumi TANIMOTO *(Kanazawa Univ. and IMS)*, **Tadayoshi SAKATA, Ryoichi NAKAGAKI, Mitsuo HIRAMATSU** *(Hamamatsu Photonics K.K. and IMS)*, **and Saburo NAGAKURA**

We have studied several electrochemical reactions by means of potentiometry in the presence of an external magnetic field. The magnetic field remarkably affects electrolytic reduction of Fe^{3+} and oxidation of Fe^{2+} in the region of current density where the reaction is diffusion-controlled. The magnetic field effect was observed even in the range of current density of $10^{-5} - 10^{-6}$ A/cm^2, where it is usually believed to be reaction-controlled. In addition, corrosion of Au electrode and generation of oxygen gas were also found to be influenced by the magnetic field. All results were interpreted in terms of the magnetohydrodynamic effect.

III-I-3 Magnetic Field Effects on the Photolysis of *p*-Benzoquinone Derivatives in Sodium Dodecyl Sulfate Micelles

Yoshifumi TANIMOTO *(Kanazawa Univ. and IMS)*, **Hiroko UDAGAWA** *(Kanazawa Univ.)*, **Yoshihide KATSUDA** *(Kanazawa Univ.)*, **and Michiya ITOH** *(Kanazawa Univ.)*

[*J. Phys. Chem.*, **87**, 3976 (1983)]

Magnetic field effects on the photochemical reactions of *p*-benzoquinone derivatives were studied in sodium dodecyl sulfate (SDS) micellar solutions by steady-state and nanosecond laser flash photolysis. The relative quantum yield of the disappearance of quinones by steady irradiation decreases with increasing magnetic field up to 250–350 G and then reaches a constant value. In the laser flash photolysis, the decay of a transient due to the semiquinone radicals in micellar solution consists of "fast" and "slow" decay components (~100 ns and 50–100 μs), the intensity ratio of which decreases by 20–40% with a magnetic field of 400–1000 G. The triplet-singlet intersystem crossing (isc) of a 2,5-dimethyl-*p*-benzosemiquinone-dodecyl sulfate ion radical pair is 2.6×10^6 and $1.0 \times 10^6 s^{-1}$ at 0 and 950 G, respectively. The results are discussed in terms of the radical-pair model in which the triplet-singlet intersystem crossing of radical pairs is influenced by the external magnetic field.

III-I-4 Magnetic Field Effect on the Hydrogen Abstraction of Xanthone from Xanthene in SDS Micelles

Yoshifumi TANIMOTO *(Kanazawa Univ. and IMS)*, **Masanobu TAKASHIMA** *(Kanazawa Univ.)*, **and Michiya ITOH** *(Kanazawa Univ.)*

[*Chem. Phys. Lett.*, **100** 442 (1983)]

The magnetic field effect (<800 G) on the hydrogen abstraction of xanthone from xanthene in SDS aqueous micellar solutions was studied using laser flash photolysis. The rate of triplet-singlet intersystem crossing of the radical pair of xanthone ketyl and 9-xanthenyl formed upon photolysis decreases from $1.4 \times 10^6 s^{-1}$ at 0 G to $0.4 \times 10^6 s^{-1}$ at 640 G.

RESEARCH ACTIVITIES IV
Department of Molecular Assemblies

IV—A Photoelectron Spectroscopy of Organic Solids in Vacuum Ultraviolet Region

Photoelectron spectra of organic solids, such as aromatic solid, aliphatic compounds, and polymers, were observed.

IV-A-1 Elimination of Sample Charging in UV Photoemission from Single Crystals of Several Polycyclic Hydrocarbons.

Bernhard M. SCHMID *(Univ. Stuttgart and IMS)*, **Naoki SATO, Hiroo INOKUCHI and Nobert KARL** *(Univ. Stuttgart)*

[*Chem. Lett.*, 1897 (1983)]

In observation of UV photoemission spectra of single crystals of polycyclic hydrocarbons, we applied the following two methods to eliminate sample charging; (1) covering a sample with a thin layer of gold and (2) inducing photoconduction in the sample with low-energy light. Their ionization thresholds obtained are all smaller than the values for corresponding polycrystalline thin films as listed in Table I.

Table I. Ionization thresholds of polycyclic hydrocarbons in the single crystalline (I_c^{th}) and polycrystalline states (I_s^{th}).

Compound	I_c^{th}/eV	I_s^{th}/eV	ΔI^{th}/eV
Anthracene	5.67	5.75	0.08
Pyrene	5.58	7.8	0.2_2
Perylene	5.12	5.2	0.0_8
Benzo[ghi]perylene	5.26	5.4	0.1_4

IV-A-2 Intramolecular Energy Band Dispersion of n-$C_{36}H_{74}$ Observed by Angle-Resolved Photoemission with Synchrotron Radiation

Kazuhiko SEKI *(HASYLAB at DESY, FRG and IMS)*, **U. Karlsson** *(HASYLAB and Linköping Univ., Sweden)*, **R. Engelhardt** *(Univ. Hamburg, FRG)* **and E. E. Koch** *(HASYLAB at DESY).*

[*Chem. Phys. Lett.*, **103**, 343 (1984)]

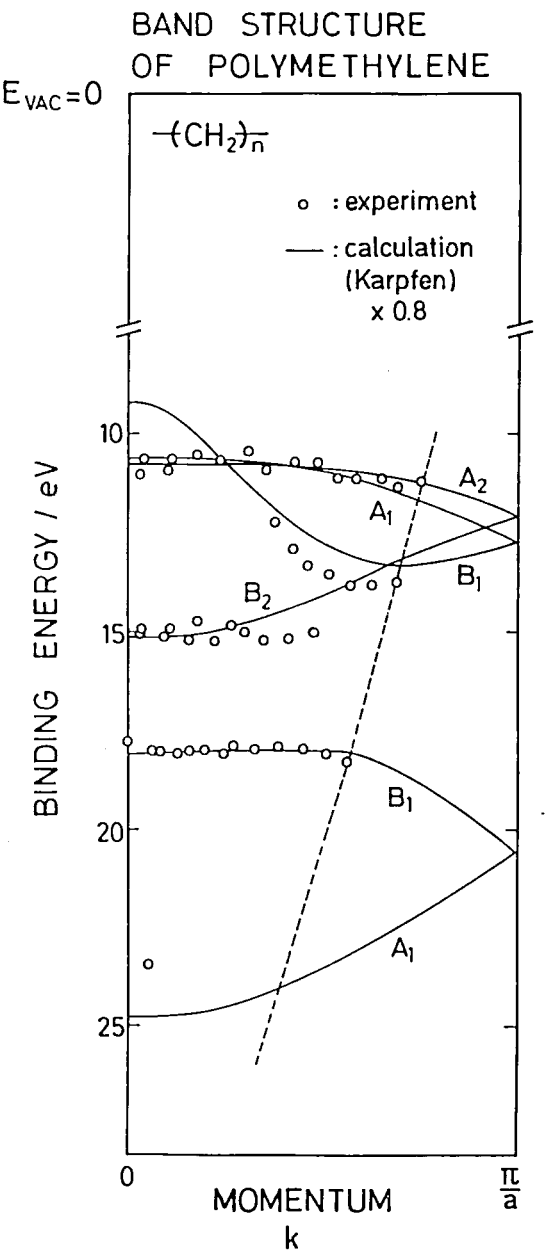

Figure 1. Experimentally determined electronic band structure for n-$C_{36}H_{74}$ (circles). The calculated band structure for polyethylene (solid lines) is the results by Karpfen[1] (0.8 times contracted and shifted for the best fit with experimental data).

The energy band dispersion $E=E(k)$ is determined for the valence bands in a long-chain alkane n-$C_{36}H_{74}$ by angle-resolved photoemission from an oriented polycrystalline sample using synchrotron radiation. Comparison with theoretical calculation[1] for a single chain in Figure 1 shows good qualitative agreement for the position, width, and dispersion of the valence band. This is the first observation of energy band dispersion in an organic molecular solid.

Reference

1) A. Karpfen, *J. Chem. Phys.*, 75, 238 (1981).

IV-A-3 Intramolecular Band Mapping of Poly (*p*-phenylene) by UV Photoelectron Spectroscopy of Finite Polyphenyls

K. SEKI *(HASYLAB at DESY, FRG and IMS)*, **U. O. KARLSSON** *(HASYLAB at DESY and Linköping Univ., Sweden)*, **R. Engelhardt** *(Hamburg Univ.)*, **E. E. Koch** *(HASYLAB at DESY)*, **and W. Schmidt** *(Biochem. Inst. fur Umweltcarcinogene, FRG).*

Ultraviolet photoelectron spectra were measured of solid sexiphenyl with synchrotron radiation and of geseous polyphenyls from biphenyl to sexiphenyl with a HeI light source. The similarity of the spectrum from the solid with the XPS spectrum of poly(*p*-phenylene) (PPP) shows the usefulness of sexiphenyl as a model compound of PPP. Examination of the fine structure observed in the low binding energy region (Figure 1) clearly shows how the electronic structure of the *p*-phenyls evolves from that of benzene, including the effects of deeper levels and of the nonplanarity of the molecular geometry. The experimental $E=E(k)$ energy band dispersion relation of a PPP can be deduced by giving each energy level of the oligomers an appropriate k value. An extrapolation for the total band width and the threshold photoemission energy of solid PPP yields 3.95 eV and 6.65 eV, respectively.

IV-A-4 Ultraviolet Photoelectron Spectroscopy of Some Fundamental Vinyl Polymers and the Evolution of Their Electronic Structures.

CHEN Shang Xian *(Inst. Chem., Academia Sinica, China and IMS)*, **Kazuhiko SEKI, Hiroo INOKUCHI, Shimpei HASHIMOTO** *(Japan Synthotic Rerbber Co.)*, **Nobuo UENO** *(Chiba Univ.)* **and Kazuyuki SUGITA** *(Chiba Univ.).*

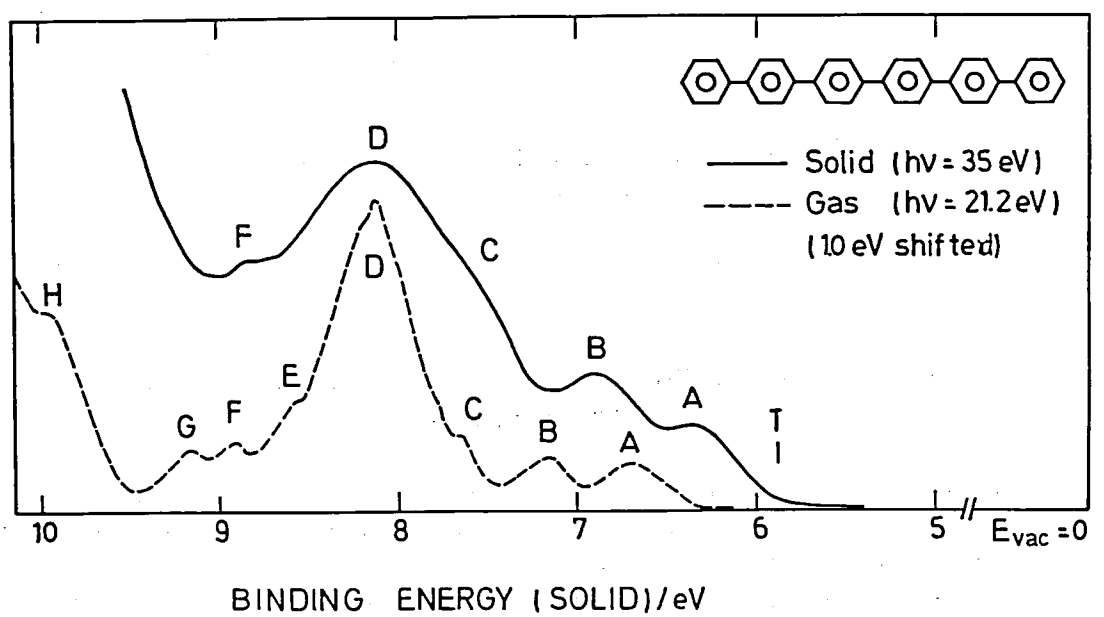

Figure 1. Low-binding-energy region of the photoelectron spectra for gas and solid sexiphenyl.

UV photoelectron spectra were measured for polypropylene (PP), poly(vinyl fluoride) (PVF), 1,2-polybutadiene (1,2-PBD), poly(vinyl chloride) (PVC), and poly(vinyl alcohol) (PVA). Their threshold ionization energies are listed in Table I with those of unit compounds CH_2CHX, where X is the pendant. The evolution of their electronic structures, together with those of previously measured polyethylene (PE) and polystyrene (PS) were clarified by analyzing the photoelectron spectra of small related compounds (including the new data of 1,3-propanediol). With these results, the polymers were classified into three groups with increasing order of localization of the positive hole in the cationic state: (1) PE, PP and PVF, (2) 1,2-PBD, PVC and PVA and (3) PS as a representative of aromatic-pendant polymers.

Table I. The threshold ionization energies of vinyl polymers (I_s^{th}) and the gas phase threshold ionization energies of their "unit" compounds (I_g^a).

Compound	I_s^{th}/eV	assignment	Unit compound	I_g^a(unit)/eV	ΔI/eV[c]
PE	8.5[a]	backbone	CH_3CH_3	11.7	3.2
PP	8.5	backbone	$CH_3CH_2CH_3$	11.1	2.6
PVF	9.2	backbone	CH_3CH_2F	11.7	2.5
1,2-PBD	7.5	pendant π	$CH_3CH_2CH{=}CH_2$	9.7	2.2
PVC	8.8	pendant n_{Cl}	CH_3CH_2Cl	11.0	2.2
PVA	8.0	pendant n_O	CH_3CH_2OH	10.3	2.3
PS	6.9[b]	pendant π	$CH_3CH_2C_6H_5$	8.6	1.7

a) M. Fujihira and H. Inokuchi, Chem. Phys. Lett., 17, 554 (1972).
b) M. Fujihira, T. Hirooka, and H. Inokuchi, Chem. Phys. Lett., 19, 584 (1973).
c) $\Delta I \equiv I_g^a(\text{unit}) - I_s^{th}$.

IV—B Electric and Photo-conduction of Organic Solids

Among many organic semiconductive materials, a few compounds, such as tetrabenzo [*de, hi, op, st*] pentacene (TBPA) and TTF-derivatives, show peculiar electrical character. Further, TBPA shows reversible photooxygenation in the solution and also in the condensed phase. The photoconduction of TBPA and tetrabenzo [*a, cd, j, lm*] perylene has been observed with ultra-high vacuum photoconduction apparatus.

IV—C Electron Transfer and Electron Transport in Cytochrome c_3

Magnetic resonance study of cytochrome c_3 and also hydrogenase has been studied. (See VII—G)

IV—D Physics and Chemistry of Graphite and its Intercalates

The analysis of hydrogen dissociation and chemisorption mechanism on graphite and alkali metal intercalation compounds (GIC) is one of the main subjects in this research field. The electron transfer and heat capacity measurement in GIC + H_2 ternary system, and also the superconduction of GIC are being studied. Further, we are observing the positron-annihilation of GIC and its hydrogen-chemisorbed compounds.

IV-D-1 Superconductivity in C_8Rb

Mototada KOBAYASHI, Akihiko SUMIYAMA,* Toshiaki ENOKI, Mizuka SANO, Hiroo INOKUCHI, Yasukage ODA* and Hiroshi NAGANO*** *(*I.S.S.P., Univ. of Tokyo, **Kumamoto Univ.)*

The superconductivity in C_8Rb was observed in AC magnetic susceptibility and magnetization measurements by use of a dilution refrigerator. Figure 1. shows the temperature dependences of χ' and χ'' for C_8Rb. χ' and χ'' are real and imaginary susceptibilities, respecitvely. Measuring field H_m was applied perpendicularly to the layers. The transition temperature T_c is 26 mK.

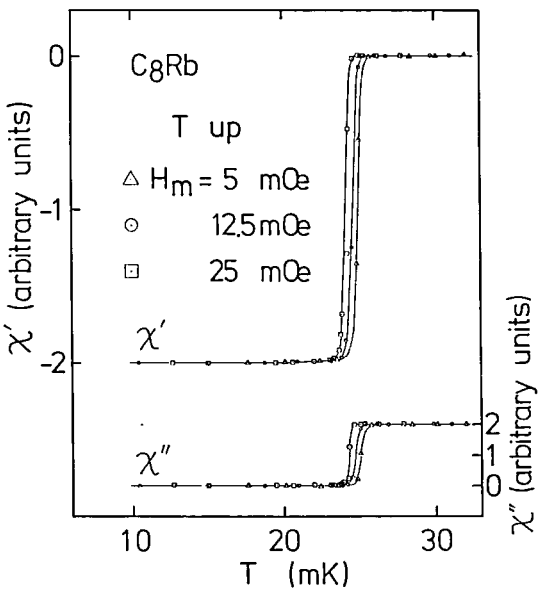

Figure 1. Temperature dependences of χ' and χ'' for C_8Rb. Values of measuring field H_m denote the amplitudes of the magnetic fields calculated from the alternating currents in a primary coil.

Reference

1) N. B. Hannay, T. H. Geballe, B. T. Matthias, K. Andres, P. Schmidt and D. MacNair: *Phys. Rev. Lett.*, **14** (1965) 225.

IV-D-2 Chemisorption of Hydrogen into a Graphite-Potassium Intercalation Compound C_8K Studied by Means of Positron-Annihilation

Hideki MURAKAMI,* Mizuka SANO *(Kumamoto Univ.)*, **Ikuzo KANAZAWA,* Toshiaki ENOKI, Toshikazu KURIHARA,* Yoshiharu SAKURAI* and Hiroo INOKUCHI** *(*Tokyo Gakugei Univ.)*

The Doppler-broadened positron-annihilation spectra for C_8K and $C_{24}K$ are composed of two Gaussian bands. Upon introduction of hydrogen to C_8K, the both bands sharpened, which indicates the conversion of hydrogen atoms to hydride ions through charge transfer from graphitic layers and the formation of positronium hydride.

IV—E Organic Metals

Since the discoveries of two-dimensional nature of $(BEDT\text{-}TTF)_2ClO_4$(1,1,2-trichloroethane (TCE))$_{0.5}$[1] and superconductivity of $(BEDT\text{-}TTF)_2ReO_4$[2], BEDT-TTF complexes become one of the well-known high-conductive organic compounds besides the TMTSF complexes. Our continued interest in the electric, magnetic, optical and structural properties of these complexes has been focused on a variety of new BEDT-TTF and its related complexes and also on $(TMTSF)_2ClO_4$.

References

1) G. Saito, T. Enoki, K. Toriumi and H. Inokuchi, Solid State Commun. **42**, 557 (1982).
2) S. S. Parkin, E. M. Engler, R. R. Schumaker, R. Lagier, J. C. Scott and R. L. Greene, *Phys. Rev. Lett.*, **50**, 270 (1983).

IV-E-1 Suppression of Peierls Transition by Chemical Modification

Gunzi SAITO, Toshiaki ENOKI, Hiroo INOKUCHI, and Hayao KOBAYASHI *(Toho Univ.)*

[*J. Phys. (Paris)*, **44**, 1195 (1983)]

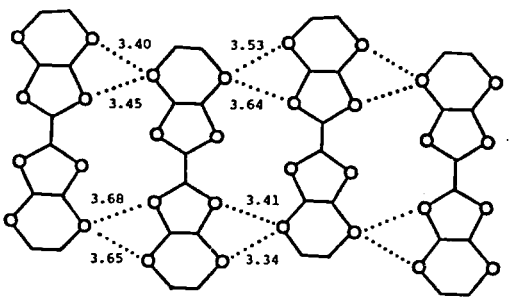

Figure 1. View along the a axis at room temperature showing 2D network composed of sulfur atoms in $(BEDT\text{-}TTF)_2ClO_4(TCE)_{0.5}$. Sulfur atoms are indicated by open circles. Shorter intermolecular distance (S····S) are illustrated.

There are mainly three phase transitions in the low-dimensional metals caused by the instability of metallic phase. The first one is the Peierls transition due to the electron-phonon interaction. The second one is the metal to insulator transition due to SDW originated from the spin-spin corelation. The last one is the transition to superconducting state. In organic metals, the Peierls transition is predominant and usual organic metals, become insulator by this mechanism at low temperature. Therefore, to synthesize an organic superconductor, suppression of the Peierls transition is the first inevitable requirement.

In an organic cation radical salt $(BEDT\text{-}TTF)_2ClO_4(TCE)_{0.5}$, a remarkable suppression of the metal-insulator transition is achieved and quasi metallic character is observed down to 1.4 K at ambient pressure. The electrical, optical, and structural (Figure 1) data show this salt is quite two-dimensional, and these data demonstrate that a chemical modification such as the extension of TTF skeleton by appropriate alkylchalcogenide substituents has substantial effect to increase the interchain interaction and therefore to suppress the Peierls instability. We propose practical molecular designing of organic metals with strong interchain interaction, which possibly become organic superconductors.

IV-E-2 The Intermolecular Interaction of Tetrathiafulvalene and Bis(ethylenadithio)-tetrathiafulvalene in Organic Metals

Takehiko MORI,* Akiko KOBAYASHI,* Yukiyoshi SASAKI,* Hayao KOBAYASHI *(Toho Univ.)*, **Gunzi SAITO, and Hiroo INOKUCHI.**

[*Bull. Chem. Soc. Jpn.*, **57**, 627 (1984)]

The relation between the anisotropy of the band structure and the arrangement of the organic molecules is investigated for two organic donors, TTF and BEDT-TTF by means of the extended Hückel molecular orbital calculation.

IV-E-3 The Crystal Structures and Electrical Resistivities of $(BEDT\text{-}TTF)_3(ClO_4)_2$ and $(BEDT\text{-}TTF)_2ClO_4(C_4H_8O_2)$

Hayao KOBAYASHI *(Toho Univ.)*, **Reizo KATO,* Takahiko MORI,* Akiko KOBAYASHI,* Yukiyoshi SASAKI,* Gunzi SAITO, Toshiaki ENOKI, and Hiroo INOKUCHI** *(*Tokyo Univ.)*

[*Chem. Lett.*, 179 (1984)]

The crystal structures of $(BEDT\text{-}TTF)_3(ClO_4)_2$ and $(BEDT\text{-}TTF)_2ClO_4(C_4H_8O_2)$ were determined. In both crystals, BEDT-TTF molecules are arranged side-by-side. The ClO_4-complex including $(C_4H_8O_2)$ is a semiconductor, and the 3:2 salt undergoes a sharp metal-insulator transition at 170 K.

IV-E-4 The Crystal Structures of $(BEDT\text{-}TTF)ReO_4(THF)_{0.5}$ and $(BEDT\text{-}TTF)IO_4(THF)_{0.5}$

Hayao KOBAYASHI *(Toho Univ.)*, **Akiko KOBAYASHI** *(Tokyo Univ.)*, **Yukiyoshi SASAKI** *(Tokyo Univ.)*, **Gunzi SAITO, and Hiroo INOKUCHI.**

[*Chem. Lett.*, 183 (1984)]

The crystal structures of $(BEDT\text{-}TTF)ReO_4(THF)_{0.5}$ and $(BEDT\text{-}TTF)IO_4(THF)_{0.5}$ are reported. These salts of BEDT-TTF cations are isomorphic. There are chains of BEDT-TTF dimers. The bond lengths of $BEDT\text{-}TTF^+$ differ systematically from those of the neutral BEDT-TTF molecule.

IV-E-5 Band Structures of Two Types of $(BEDT\text{-}TTF)_2I_3$

Takehiko MORI,* Akiko KOBAYASHI,* Yukiyoshi SASAKI,* Hayao KOBAYASHI *(Toho Univ.)*, **Gunzi SAITO, and Hiroo INOKUCHI** *(*Tokyo Univ.)*

[*Chem. Lett.*, 957 (1984)]

On the basis of the extended Hückel molecular orbital calculation, the intermolecular overlaps of the highest occupied molecular orbitals are calculated for α- and β-$(BEDT\text{-}TTF)_2I_3$.. α-Type is a two dimensional semimetal or a narrow gap semiconductor. β-Type is a two-dimensional metal which has an almost isotropic closed Fermi surface.

IV-E-6 The Polarized Reflectance Spectrum of a Novel Organic Conductors $(BEDT\text{-}TTF)_2ClO_4(C_2H_3Cl_3)_{0.5}$

Hiroyuki TAJIMA,* Kyuya YAKUSHI,* Haruo KURODA,* Gunzi SAITO, and Hiroo INOKUCHI *(*Tokyo Univ.)*

[*Solid State Commun.*, **49**, 769 (1984)]

The polarized reflectance spectrum of $(BEDT\text{-}TTF)_2ClO_4(C_2H_3Cl_3)_{0.5}$ was measured at room temperature over the spectral region from 340 cm^{-1} to 25,000 cm^{-1}. The spectrum provided an evidence for the anisotropic two-dimensional character for this complex. The optical conductivity spectrum exhibits the existence of an optical band gap of about 0.2 eV, suggesting that this material is a semimetal rather than a metal.

IV-E-7 The Crystal Structures of $(TMTTF)_2ReO_4$

Hayao KOBAYASHI *(Toho Univ.)*, **Akiko KOBAYASHI,* Yukiyoshi SASAKI,* Gunzi SAITO, and Hiroo INOKUCHI** *(*Tokyo Univ.)*

[*Bull. Chem. Soc. Jpn.*, **57**, 2025 (1984)]

In $(TMTTF)_2ReO_4$ crystal, TMTTF molecules are stacked face-to-face to form a zig-zag column. Although the structure of $(TMTTF)_2ReO_4$ closely resembles that of the analogous compound, $(TMTSF)_2ReO_4$, the loose intermolecular contacts in $(TMTTF)_2ReO_4$ suggest that the intermolecular interaction appears to be much weaker than that in $(TMTSF)_2ReO_4$.

IV-E-8 Superconductivity and Metal-Nonmetal Transitions in $(TMTSF)_2ClO_4$

Takehiko ISHIGURO,* Keizo MURATA,* Koji KAJIMURA,* Nobumori KINOSHITA,* Hiroshi TOKUMOTO,* Madoka TOKUMOTO,* Takashi UKACHI,* Hiroyuki ANZAI,* and Gunzi SAITO *(*Electrotechnical Lab.)*

[*J. Phys. (Paris)* **44**, 1195 (1983)]

$(TMTSF)_2ClO_4$ undergoes the metal-nonmetal (MN) transition above the superconductivity (SC) transition under a certain condition. The SC and MN transitions are influenced by resistance jumps and cooling speed across the order-disorder transition of ClO_4 anions. The interplay of the SC and SDW phases is discussed with regard to these influences.

IV-E-9 Magnetoresistance of $(TMTSF)_2ClO_4$

Koji KAJIMURA,* Hiroshi TOKUMOTO,* Madoka TOKUMOTO,* Keizo MURATA,* Takashi UKACHI,* Hiroyuki ANZAI,* and Gunzi SAITO *(*Electrotechnical Lab.)*

[*J. Phys. (Paris)* **44**, 1059 (1983)]

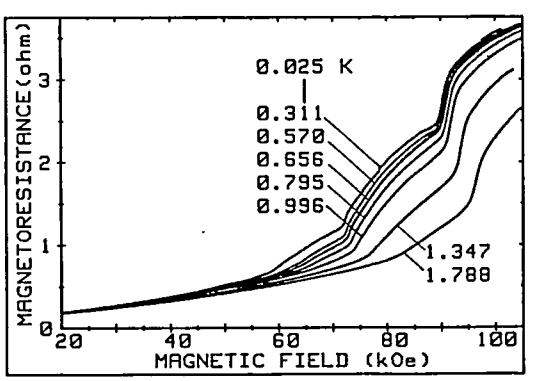

Figure 1. Quantum osillations of magnetoresistance of $(TMTSF)_2ClO_4$ in the R state at various temperature for downward sweep.

Transverse magnetoresistance of $(TMTSF)_2ClO_4$ was found to exhibit Shubnikov-de Haas-type oscillation whose fields were strongly temperature dependent (Figure 1). The oscillation had no periodicity in the inverse field and exhibited a clear hysteresis aroud 90kOe. These experimental facts suggest that there are closed orbits on the Fermi surface and energy band structures are altered by the magnetic field.

IV-E-10 Mechanical Twinning of $(TMTSF)_2ClO_4$ Single Crystal

Takehiko ISHIGURO,* Takashi UKACHI,* Madoka TOKUMOTO,* Keizo MURATA,* Koji KAJIMURA,* Hioryuki ANZAI,* Katsuo KATO *(Nat. Inst. Res. Inorg Materials)*, **and Gunzi SAITO** *(*Electrotechnical Lab.)*

[*J. Phys. (Paris)* **44**, 1063 (1983)]

Mechanical kinks are formed in a needle crystal of $(TMTSF)_2ClO_4$ by applying stresses perpendicular to the needle axis. By the x-ray precession photography, it was found that the kink is ascribed to the mechanical twinning with the boundary on the (210) plane.

IV-E-11 Effects of Solvents and Cell Design for Crystal Growth of Organic Metals

Hiroyuki ANZAI,* Tetsuo MORIYA,* Ken NOZAKI,* Takashi UKACHI,* and Gunzi SAITO *(*Electrotechnical Lab.)*

[*J. Phys. (Paris)* **44**, 1195 (1984)]

The crystals of TTF- and TMTTF-TCNQ have been obtained by the diffusion method. The amount of the used reagents and shape of the crystals. The crystals of $(TMTTF)_2BF_4$ and $(TMTSF)_2ClO_4$ have been synthesized by the electrochemical method. Several types of the growing cell have been tested, and spectroscopic and chemical analysis for the crystal-growth mechanism have been presented.

IV-E-12 ESR g Factors of Isolated $(TMTSF)^+$ and $(TMTSF)_2ClO_4$ single Crystals: Comparison with Molecular Orbital Calculation

Nobumori KINOSHITA,* Madoka TOKUMOTO,* Hiroyuki ANZAI,* Takehiko ISHIGURO,* Gunzi SAITO, Tokio YAMABE, and Hiroyuki TERAMAE**** *(*Electrotechnical Lab. **Kyoto Univ.)*

[*J. Phys. Soc. Jpn.*, **53**, 1504 (1984)]

Measurements and comparisons were performed at 4.2 K on the ESR g tensor both of a single crystal of $(TMTSF)_2ClO_4$, and its acetone solution in which cations exist in the form of $TMTSF^+$. The results showed that there was no wide difference between the g anisotropy of the single crystal and solution. The g factors, calculated from molecular orbitals (MO) of a TSF^+ cation which were computed using semi-empirical SCF method, were then fitted to those of the single crystal, and π-electron distribution was decided from the highest occupied MO.

IV—F Studies of Ion-Molecule Reactions by a Threshold Electron-Secondary Ion Coincidence (TESICO) Technique

The knowledge of the microscopic reaction cross sections for evolution of a system in a single reactant quantum state (translational, rotational, vibrational, and electronic) to a single product quantum state is essential for a complete understanding of a chemical reaction. Ion-Molecule reactions are particularly suited for studying such microscopic cross sections since ions can readily be prepared in various internal states in the initial ionization processes, such as photo-ionization, and the emitted photoelectrons provide information on the distribution among these states.

In this project, we study state-selected ion-molecule reactions by the use of a photoionization technique which utilizes the threshold photoelectron-secondary ion coincidence. The technique allows direct

determination of $\sigma(i, v)$, i.e. the reaction cross section as a function of the internal and collisional energies of reactants. The selection of electronic, vibrational, rotational, and fine-structure states are possible by this technique.

IV-F-1 A State Selected Study of Ion-Molecule Reactions in the $(D_2\text{-}N_2)^+$ System

Kenichiro TANAKA, Tatsuhisa KATO, and Inosuke KOYANO

In order to elucidate the reaction mechanism of ion-molecule reactions, we have applied the **TESICO** technique[1] to the internal state selection of the primaty ions in the reactions

$$D_2^+(v) + N_2 \rightarrow N_2^+ + D_2 \quad (1a)$$
$$\rightarrow N_2D^+ + D \quad (1b)$$
$$N_2^+(\epsilon,v) + D_2 \rightarrow D_2^+ + N_2 \quad (2a)$$
$$\rightarrow N_2D^+ + D. \quad (2b)$$

The results obtained for Reaction (1) are summarized in *Figure 1*, where the relative cross sections are plotted as a function of the vibrational quantum number of D_2^+. As can be seen from the figure, the cross section of Reaction (1a) shows an interesting variation as the vibrational quantum number changes at all collision energies studied (2.5, 6, and 9 eV). The cross section seems to vary regularly with the vibrational quantum number, increasing at odd quantum numbers and decreasing at even quantum numbers. In contrast, the cross section of Reaction (1b) has been found to be almost independent of vibrational quantum number, its value decreasing with increasing collision energy.

In case of Reaction (2), the relative reaction cross sections have been determined for vibrational states $v = 0 - 3$ of $N_2^+(X^2\Sigma_g^+)$ and $v = 0 - 3$ of $N_2^+(A^2\Pi_u)$ at two collision energies (0.5 and 1.3 eV). It has been found that while the cross sections for Reactions (2a) are almost independent of both the vibrational and electronic states of the primary ions, the cross sections for Reaction (2b) strongly depend on the electronic state of the primary ions, the $A^2\Pi_u$

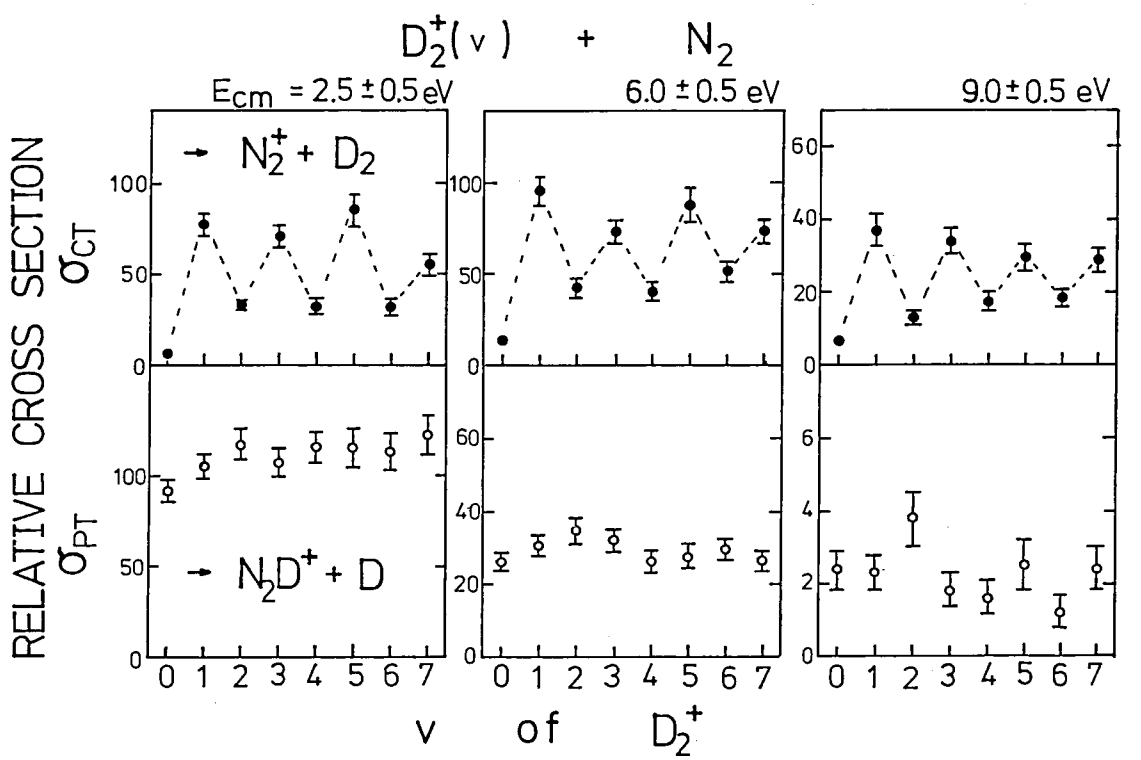

Figure 1. State selected relative cross section for Reaction (1) as a function of vibrational quantum number v of D_2^+.

excited state exhibiting lower reactivity than the $X^2\Sigma_g^+$ ground state.

These salient features of the experimental results can not simply be explained in terms of the energy resonance and Franck-Condon factors between the reactant and product states. These results, however, certainly bear valuable information on the dynamics of Reactions (1) and (2). Detailed analysis are in progress.

Reference

1) I. Koyano and K. Tanaka, *J. Chem. Phys.*, **72**, 4858 (1980).

IV-F-2 Vibrational State Dependence of the Cross Sections in the Reaction $C_2H_2^+$ (ν_2) + $D_2(H_2)$

Kenji HONMA *(Univ. of Tokyo)*, **Tatsuhisa KATO, Kenichiro TANAKA, and Inosuke KOYANO**

[*J. Chem. Phys.*, **81** in press]

Vibrational-state selected reaction cross sections have been measured for four product channels of the reaction $C_2H_2^+ + D_2$, by use of the threshold electron-secondary ion coincidence (**TESICO**) technique. The ν_2 vibrational states of the $C_2H_2^+$ ion were selected up to $v = 2$ and the collision energies were changed from 0.2 to 3.7 eV. At low collision energies close to 0.2 eV, considerable enhancement of the cross sections for the channels producing $C_2H_2D^+$ and $C_2HD_2^+$ was observed when the vibrational quantum number was increased successively. As the collision energy was increased, the extent of this enhancement diminished gradually and the cross sections finally became almost independent of v at about 2 eV. The cross section for the H/D exchange channel, on the other hand, was found to decrease with increasing vibrational quantum number at low collision energies. However, the $v = 0$ and $v = 1$ cross sections of this channel, especially the former, decayed very quickly as the collision energy was increased, reaching essentially zero at ~2eV, while the cross section for $v = 2$ remained substantial even at this and higher collision energies. These results have been discussed in terms of two concurrent reaction mechanisms, *i.e.*, a complex mechanism predominanting at low collision energies and a direct one predominating at high collision energies. The ν_2-state selected cross sections for the reaction $C_2H_2^+ + H_2 \rightarrow C_2H_3^+ + H$ have also been studied in a similar collision energy range for comparison.

IV-F-3 Mode Specificity in the Reaction $C_2H_4^+(\nu_2,\nu_4) + C_2H_4 \rightarrow C_3H_5^+ + CH_3$

Kenichiro TANAKA, Tatsuhisa KATO, and Inosuke KOYANO

The TESICO technique has been applied to the selection of vibrational states of poliatomic ions, such as $C_2H_4^+$, where more than one modes of vibration can be excited. Threshold electron spectrum of C_2H_4 shows several peaks corresponding to ν_2 and ν_4 vibrational progressions of the ground state $C_2H_4^+$ ions. Thus, the system involving $C_2H_4^+$ provides an opportunity to investigate mode specificity in chemical reactions.

Relative cross sections of the reaction $C_2H_4^+ + C_2H_4 \rightarrow C_3H_5^+ + CH_3$ (1) have been determined for four vibrational states $(\nu_2,\nu_4) = (0,0)$, (0,2), (1,0), and (1,2). The experimental results, given in **Figure 1**, showed that, at intermediate collision energies around 0.2 eV, the former two states have cross sections of essentially the same magnitude which is definitely larger than that for the last two states, the last two states again having the same cross sections. These results indicate that while ν_2 vibration has prohibiting effect on Reaction (1), ν_4 vibration has nothing to do with the reaction. At lower and higher collision energies, however, the cross sections behaved quite differently as the vibrational states were varied, as shown in **Figure 1**.

Reaction (1) is known to proceed via an intermediate complex at low collision energies.[1] Thus, the above results are considered as reflecting the mode specificity in the unimolecular decomposition of the intermediate complex. The mode specificity in such processes is expected to be observed only when the decomposition rate of the complex is faster than the intramolecular vibrational energy re-distribution (*IVR*) rate. For Reaction (1), we consider that the decomposition rate becomes comparable to the *IVR* rate at the intermediate collision energies around 0.2 eV. We interpret the

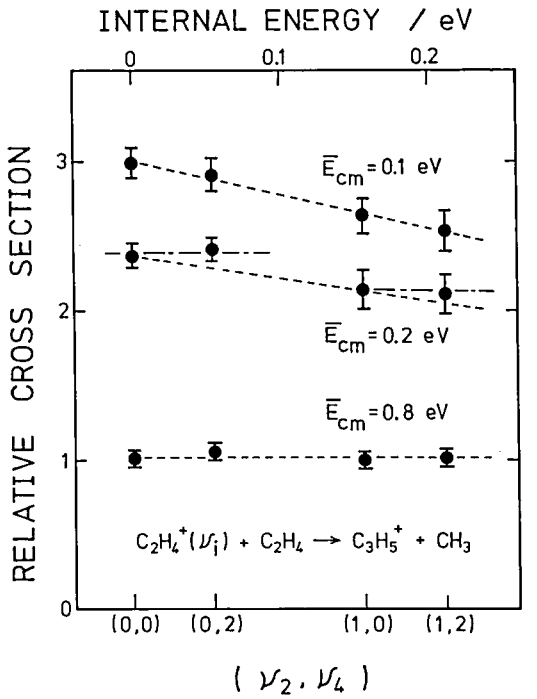

Figure 1. Vibrational state dependence of the cross sections of Reaction (1).

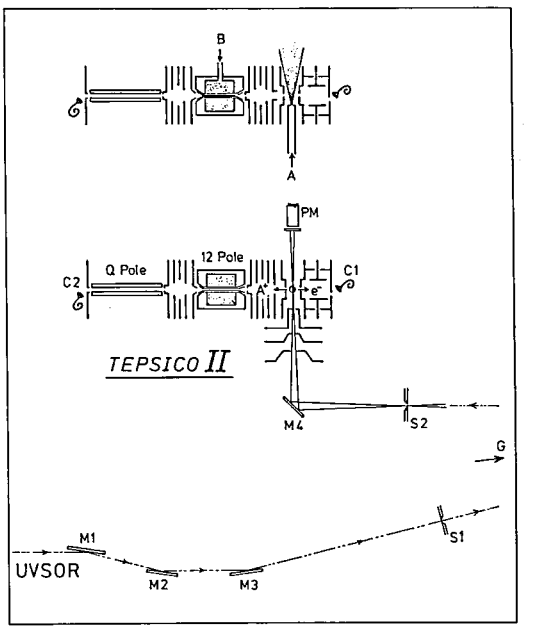

Figure 1. Schematic diagram of the **TEPSICO-II.** M1-M3 premirrors for monochromator; S1, S2 entrance and exit slit of monochromator; G Grating; M4 focusing mirror; C1, C2 channel multipliers for detection of electrons and ions; PM photomultiplier; B neutral reactant gas.

result at this energy as indicating that the ν_2 vibration of the original ion effectively enhances the decomposition of the complex back to the reactants, thus reducing the probability of the forward decomposition, whereas the ν_4 vibration does not effectively couple with either of these decomposition coordinates. The insensitivity of the cross sections to vibrational energy of either mode at higher collision energies is considered to be due to a mechanism change from complex to direct one.

Reference

1) Z. Herman, A. Lee, and R. Wolfgang, *J. Chem. Phys.*, **51**, 452 (1969).

IV-F-4 Design and Construction of the TESICO-II Apparatus for use with Synchrotron Radiation.

Kenichiro TANAKA, Tatsuhisa KATO, and Inosuke KOYANO

The helium Hopfield continuum light source, which is currently used in the **TEPSICO** apparatus,[1] has several limitations in terms of the intensity and the available wavelength range. An obvious solution to these problems is the use of synchrotron radiation (**SR**). We have designed and constructed a new apparatus, named **TEPSICO-II**, which is intended to use with the **UVSOR** storage ring.

The features of the new apparatus, as compared with the old one, are (i) installation of a 3m-normal incidence monochromator for higher resolution of the incident photons, (ii) use of a new type of steradiancy analyzer for more efficient collection of the threshold electrons, and (iii) use of a dodecapole ion guide in the reaction region to ensure the hundred percent collection of the secondary ions regardless of their initial momenta. With the first feature combined with the much higher intensity of **SR**, we aim at the rotational-state selection of some molecular ions in chemical reactions. The second feature allows us shorter data collecting time than before, and the third one enables us to determine absolute reaction cross sections over a wide range of collision energy and reaction exoergicity. A schematic of the apparatus is shown in **Figure 1**.

Reference

1) I. Koyano and K. Tanaka, *J. Chem. Phys.*, **72**, 4858 (1980).

IV—G Photoionization Processes in Small Molecules

Two techniques have generally used for the study of molecular photoionization processes, *i.e.*, measurements of photoionization efficiency curves (**PIEC**) and photoelectron spectra (**PES**). While **PIEC** yields a wealth of information on the ionization processes and energy levels of ions and neutral molecules, difficulty is often encountered with this technique when autoionization obscures the step structure of the curve. In such a situation, we often resort to **PES** which provides precise locations of ionic states and transition probabilities of these states. However, ionic states that can be studied by the ordinary (constant wavelength) **PES** are largely limited to the states which combine with the ground states of the parent molecule with favorable Franck-Condon factors. Another type of photoelectron spectroscopy is the threshold electron spectroscopy (**TES**) which uses a variable wavelength light source and detects only the zero kinetic energy photoelectrons (threshold electrons). In this method, ionic states which are not favored by direct ionization are often observed through resonance autoionization.

In this project, we study photoionization processes in small molecules by simultaneous measurements of photoionization efficiency curves and threshold electron spectra. Furthermore, we find that the analysis of autoionizing transitions is often possible utilizing charge-transfer processes of the product ions. This technique is also incorporated.

IV-G-1 New Vibrational Assignments for the Autoionization Bands of O_2 Based on Isotope Shifts

Eisuke NISHITANI *(Tokyo Inst. of Tech.)*, **Ikuzo TANAKA** *(Tokyo Inst. of Tech.)*, **Kenichiro TANAKA, Tatsuhisa KATO, and Inosuke KOYANO**

[*J. Chem. Phys.*, **81**, 3429 (1984)]

The relative photoionization efficiency curves of $^{16}O_2$, $^{16}O^{18}O$ and $^{18}O_2$ have been obtained in the 660-1035 Å region. Based on the detailed analysis of the observed isotope shifts, the autoionizing peaks in the 855-1010 Å region were newly assigned. The strong peaks in the 900-1010 Å region, which had been classified as belonging to four different (**H, H', M,** and **M'**) progressions, were assigned to a single progression of the $3s\sigma_g$ Rydberg state ($H^3\Pi_u$) converging to $O_2^+(a^4\Pi_u)$. Similarly, the peaks in the 855-925 Å region were assigned to a single progression of the $3s\sigma_g$ Rydberg state ($J^3\Pi_u$) converging to $O_2^+(A^2\Pi_u)$. Molecular constants of these two states have been determined as follows, all in the unit of cm^{-1} except δ and r_e.

$H^3\Pi_u$; $3s\sigma_g$	$J^3\Pi_u$; $3s\sigma_g$
$D_0 = 28249 \pm 26$	$D_0 = 21832 \pm 33$
$\omega_e = 1058.5 \pm 3.0$	$\omega_e = 1010.0 \pm 5.5$
$\omega_e x_e = 10.56 \pm 0.20$	$\omega_e x_e = 3.70 \pm 0.39$
$T_0 = 99639 \pm 10$	$T_0 = 106053 \pm 17$
$\delta = 1.096 \pm 0.001$	$\delta = 1.133 \pm 0.002$
$r_e = 1.37 \pm 0.01$ Å	

IV—H Spectroscopy and Chemical Dynamics Using Supersonic Nozzle Beams

The usefulness of supersonic nozzle beams has increasingly been recognized in both spectroscopy and chemical dynamics. The capability of cooling internal degrees of freedom of molecules and the possibility of producing various kinds of molecular clusters are important properties of the technique. In this project, we aim at high resolution absorption and Raman spectroscopy, dynamical studies of cluster reactions, and their combination, utilizing the above properties of supersonic nozzle beams.

IV-H-1 Velocity Distribution and Velocity Slip in Supersonic Rare Gas Beams. Atoms from Binary and Clusters from Pure Sources.

Kenichiro TANAKA, Tatsuhisa KATO, Inosuke KOYANO, Norio TAKAHASHI *(Kyoto Univ.)*, **Tomio MORIYA** *(Kyoto Univ.)*, **and Koji TESHIMA** *(Kyoto Univ.)*

[*Rarefied Gas Dynamics*, in press]

A systematic experimental study has been made of the velocity distribution of each species in molecular beams sampled from free-jet expansions of binary gas mixtures and pure gases, using a standard time-of-flight technique. In the case of pure gases, interest was centered on the clusters formed during the expansion. In binary mixtures, the parallel temperature of the heavier species was found to be higher than that of the lighter one and the mean mass velocity of the lighter species was found to be larger than that of the heavier one. An example of the experimental results is shown in **Figure 1**. These results agreed well with the gas kinetic calculations using the moment method.[1] For clusters from pure gases, however, the experimental results agreed only qualitatively with calculations.

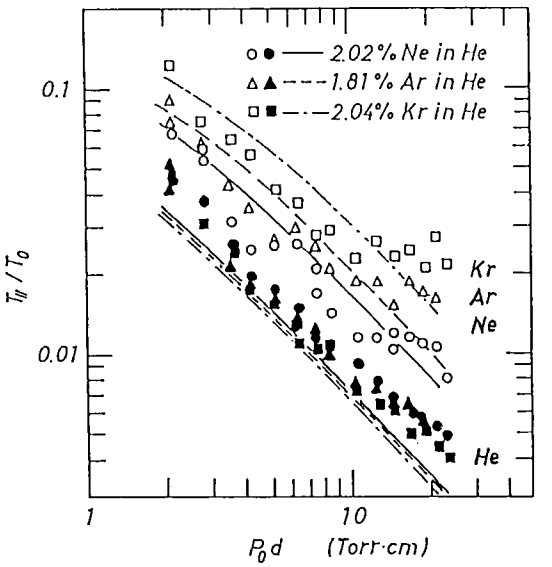

Figure 1. Parallel temperature of each component species in seeded molecular beams.

Reference

1) N. Takahashi and K. Teshima, *Memories of Faculty of Engineering, Kyoto Univ.* **45**, 79 (1983).

IV—I HeI Photoelectron Spectroscopic Studies of Gaseous Molecules

Molecular photoelectron spectroscopy of a HeI (584 Å) resonance radiation has been used for a long time to study ionization potentials of valence electrons for a number of organic and inorganic compounds in the gas phase [Kimura et al., Handbook of HeI Photoelectron Spectra (Halsted, 1981)]. There still seems to be many interesting subjects to be studied by this technique. In this project we have applied this technique to study correlations of ionization potentials with other chemical or physical properties for large molecules.

IV-I-1 Study on He(I) Photoelectron Spectroscopy and Voltammetry for Ferrocene Derivatives

Takeko MATSUMURA-INOUE *(Nara University of Education)* **and Kiyo KURODA** *(Kansai Medical College)*, **Yoshi UMEZAWA** *(Hokkaido Univ.)*, **Yohji ACHIBA and Katsumi KIMURA**

He(I) photoelectron spectra of sandwich compounds with different central metals have widely been studied because of their volatile properties. On the other hand, electrochemical studies have extensively been carried out on ferrocene derivatives with various substituents on the cyclopentadienyl rings.

In the present work, we have obtained gas-phase photoelectron spectra for several ferrocene derivatives at the temperature from 25°C to 80°C, in order to clarify the effect of substituents on the ionization potentials as well as to examine the correlation between the electrochemical oxidation potentials and the first ionization potentials. It has been found that the first four ionization potentials vary linearly with the value of the Hammet

Figure 1. Correlation between the oxidation potentials and the first ionization potentials of ferrocene derivatives.
Substituent: 1. H, 2. 1,1'-$(CH_3)_2$, 3. $CH_2N(CH_3)_2$, 4. CH_2OH, 5. $COCH_3$, 6. CHO, 7. $COOCH_3$, 8. $C(CH_3)_3$.

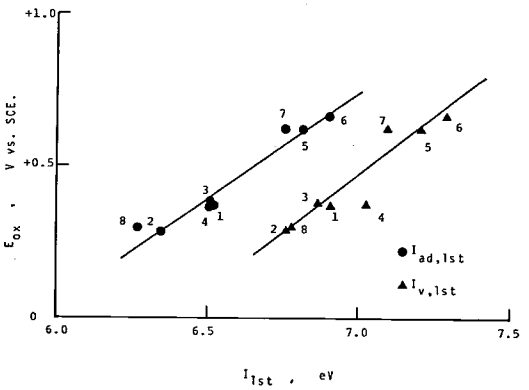

substitution constant of the substituents. Good linear correlation between the oxidation potential and the adiabatic and the vertical first ionization potential has been obtained as given in Figure 1.

IV—J Studies of Hydrogen-Bonded Dimers by Photoelectron Spectroscopy

Photoelectron spectra of hydrogen-bonded dimers produced in a supersonic expansion are interesting from a geometrical point of view as well as an electronic point of view. The first two ionization bands in a HeI photoelectron spectrum of the water dimer $(H_2O)_2$ have been found to be very broad [Tomoda, Achiba and Kimura, *Chem. Phys. Lett.* **87**, 197 (1982)], suggesting that the equilibrium geometry of the water dimer cation considerably differs from that of the neutral water dimer because of proton transfer. This phenomenon is probably common for many other hydrogen-bonded dimers. In this sense, the proton transfers of the water dimer cation in the ground state and the lowest excited state are prototype examples for many general linear hydrogen-bonded dimers. In this project we have been continueing to study the hydrogen-bonded dimer cations from both experimental and theoretical points of view.

IV-J-1 Proton-Transfer Potential-Energy Surfaces of the Water Dimer Cation $(H_2O)_2^+$ in the $1^2A''$ and $1^2A'$ States

Shinji TOMODA and Katsumi KIMURA

[*Chem. Phys.*, **82**, 215 (1983)]

Ab initio potential energy surface calculations have been carried out for the water dimer cation as well as the neutral dimer to clarify the essential features of ionization and the subsequent relaxation behavior. The potential energy surfaces of the dimer cation in a linear trans conformation have clearly indicated proton transfer with no activation energy barrier in both the ground ($1^2A''$) and the first excited ($1^2A'$) state. A potential-energy correlation scheme is shown in Figure 1 for the neutral and the ionic states.

The following conclusions have been obtained for the $1^2A''$ and the $1^2A'$ ionic state. (1) The potential surface has only one minimum at which the geometry is regarded as a complex between an oxonium ion (H_3O^+) and a hydroxyl radical (OH). This geometry differs quite largely from that of the neutral dimer. (2) Proton transferring relaxation from the vertically ionized point to the potential minimum may easily occur with no activation energy. (3) The potential minimum is still far from the wide Frank-Condon region expected from the shallow potential minimum of the neutral dimer. (4) There exist two dissociation channels to $H_3O^+ + OH$ and to $H_2O^+ + H_2O$. The former dissociation energy is much smaller than the latter. A semi-quantitative estimation is also given for the first photoelectron band width of the water dimer.

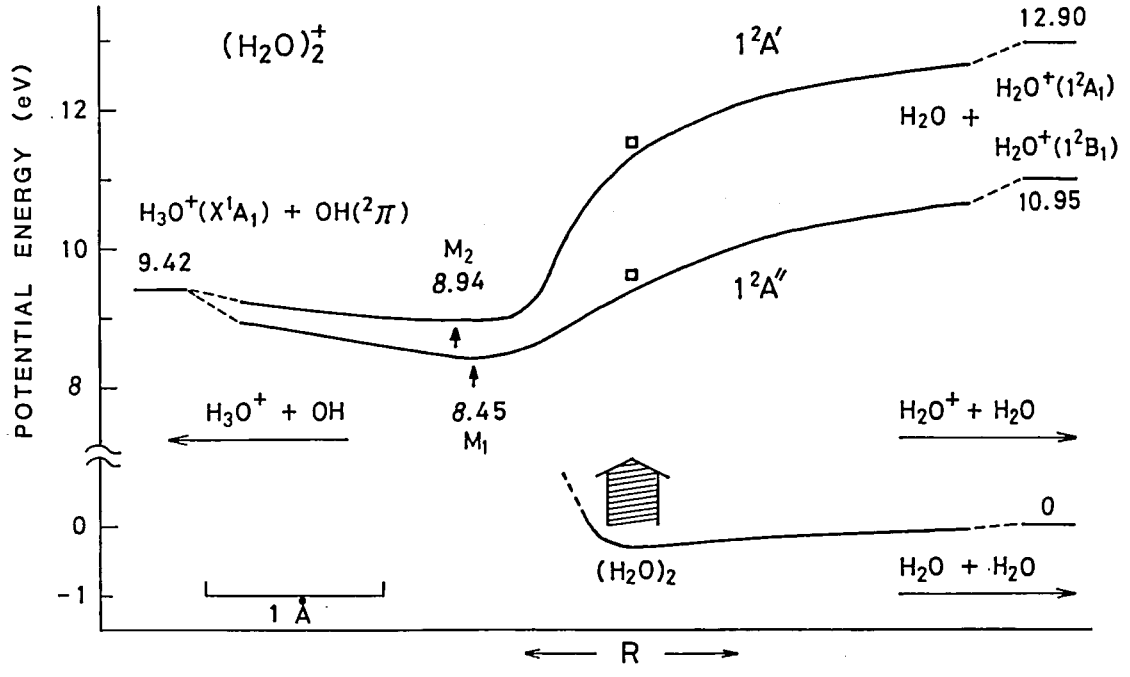

Figure 1. Potential energy correlation diagrams of the water dimer cation in the $1^2A''$ and the $1^2A'$ state along the vertual reaction coordinate (R) between the two kinds of dissociation limits, $H_2O^+ + H_2O$ and $H_3O^+ + OH$. The Franck-Condon transition from the initial neutral dimer potential curve is illustrated by a hatched big arrow. The vertically ionized points are indicated by squares. Values are in eV units.

IV-J-2 Do We Observe the "Adiabatic" Ionizations of the Water Dimer?—An Interpretation of the Threshold Ionization Energy and the Nature of the Ionic States—

Shinji TOMODA *(Osaka Univ.)* **and Katsumi KIMURA**

[*Chem. Phys. Lett.*, **111**, 434 (1984)]

Physical meaning of the experimentally observed threshold ionization energy (I_{th}) of the water dimer (11.1 eV,[1] 11.2 eV[2]) is discussed in terms of the proton-transfer potential energy surfaces of $(H_2O)_2^+$ in the $1^2A''$ and $1^2A'$ states within the framework of the Franck-Condon principle. The I_{th} is interpreted to indicate an appreciable lower bound of the first ionization band approximately limited by the Franck-Condon factor (Figure 1). A possibility that the real adiabatic ionization energies (I_a) are not observed in the photoionization experiments[1,2] is suggested. In this case the dissociation energy of $(H_2O)_2^+$ may be corrected to a larger value by an amount of several tenths of an electron volt.

The locations of the ionization sites and the mechanism of the relaxation in the ionic states are also discussed on the basis of the Mulliken population analysis.

References

1) S. Tomoda, Y. Achaba and K. Kimura, *Chem Phys. Lett.*, **87**, 197 (1982).
2) C. Y. Ng, D. J. Trevor, P. W. Tiedeman, S. T. Ceyer, P. L. Kronebusch, B. H. Mahan and Y. T. Lee, *J. Chem. Phys.*, **67**, 4235 (1977).

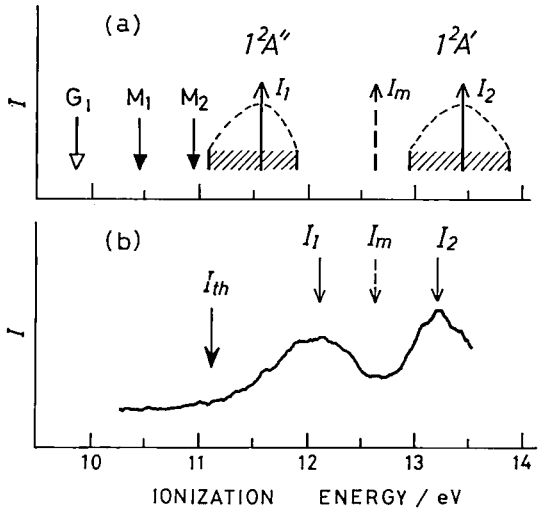

Figure 1. Comparison of the calculated ionization energies and the experimental photoelectron spectrum for the water dimer. (a) Ionization energies calculated for the $1^2A''$ and the $1^2A'$ ionic state of $(H_2O)_2^+$. Values are corrected in such a way that the first vertical IE of the monomer (I_m, a broken arrow) becomes equal to the experimental one (12.62 eV). The estimated photoelectron bands are shown schematically by the hatched regions. G_1, M_1 and M_2 indicate the IE's corresponding to the geometry-optimized $1^2A''$ cation, the $1^2A''$ potential minimum and the $1^2A'$ potential minimum, respectively. (b) The experimental photoelectron spectrum [Ref. 1]. I_{th}, I_1 and I_2 indicate the threshold, the first vertical and the second vertical ionization energy, respectively.

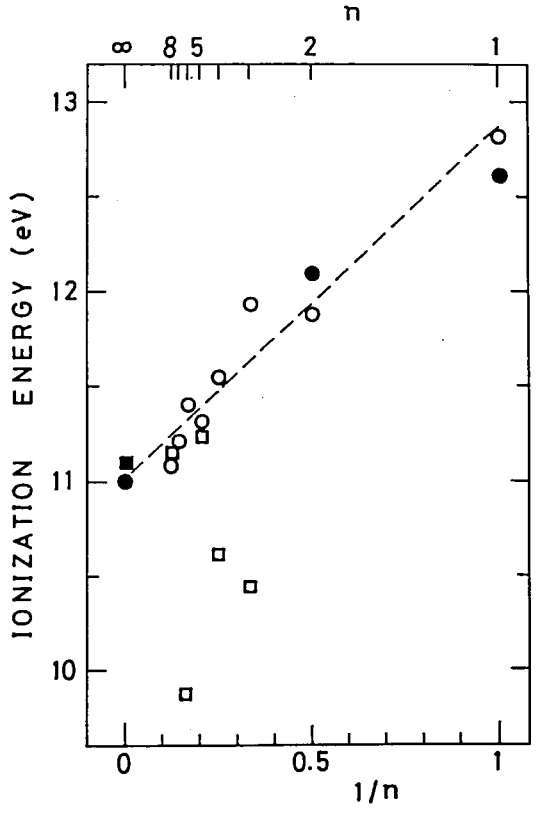

Figure 1. The first vertical ionization energies of $(H_2O)_n$: n = 1 – 8, plotted against $1/n$. The experimental values for the water molecule, the dimer and the ice are shown by solid symbols. Calculated values (I_{mk}) are shown by open circles and squares for the a- and b-type clusters, respectively. A straight line fitted to the a-type clusters is shown by a broken line (I_{mk} = 11.0 + 1.85($1/n$), in eV).

IV-J-3 Ionization Energies and Hydrogen-Bond Strength of the Water Clusters

Shinji TOMODA and Katsumi KIMURA

[*Chem. Phys. Lett.*, **102**, 560 (1983)]

The first vertical ionization energies (I_v's) of the water clusters $(H_2O)_n$ for n = 1 – 8 have been evaluated from *ab initio* SCF MO calculations based on the Koopmans' theorem. The model clusters have been restricted to those with C_s symmetry (except the heptamer), which may be regarded as parts of the ordinary hexagonal ice (ice I). The O-H bond length and the O···O distance are assumed to be 0.9572 Å and 2.75 Å, respectively. From the orbital energy of the HOMO (4-31G basis set) we have evaluated "modified Koopmans' theorem ionization energy" (I_{mk}) by an empirical equation which was obtained by a least squares fit to the experimental I_v's for the monomer.

The I_{mk} values are given in Figure 1 as a function of the reciprocal cluster size, $1/n$. Reasonable agreement between I_{mk} and the experimental values is seen for the monomer and the dimer. The smooth change and the saturation of I_{mk} values for the a-type model clusters as well as the agreements with the experimental values for ice suggest that the pentamer and/or the octamer may be regarded as reasonably good models for ice I in discussing the ionization properties. Relative stability of the various clusters has been also discussed in terms of "the hydrogen-bond strength per bond (B_h)" which is defined by the total electronic energies of the monomer and cluster.

IV—K Developement of Excited-State Photoelectron Spectroscopy with Resonant Multiphoton Ionization and Its Applications

Selective excitation/ionization of molecules by UV and visible tunable lasers by means of a multiphoton ionization photoelectron spectroscopic technique has been found to provide new information about dynamic behavior of excited states that cannot be obtained by other spectroscopic methods [IMS *Annual Review* (1980–83)]. In this sense, this technique will rapidly develope as a powerful tool for studying photochemical and photophysical behavior of excited states from a new spectroscopic point of view. The technique itself has almost been established, although further improvement is needed. In this project we have been extending our laser photoelectron spectroscopic studies to various molecular systems in supersonic jet.

IV-K-1 Multiphoton Ionization Photoelectron Spectroscopy on Dynamic Behavior of Excited Molecules

Yohji ACHIBA and Katsumi KIMURA *(Nippon Kagaku Kaishi*, in press)

Multiphoton Ionization (MPI) experiments with one- and two-color lasers were carried out mainly for NO molecule in the gas phase to study dynamic behavior of its highly excited states including super-excited states. The setup of two-color laser system is shown in Figure 1. Molecules of NO were excited to specific vibrational levels ($v' = 0$ or 4) of Rydberg A and C states as an intermediate resonant state. In the ionization experiments, we have initially measured ion-current spectra as a function of laser wavelength, and then obtained photoelectron spectra at several ion-current peaks which correspond to specific vibrational (and rotational) levels of the Rydberg states. In direct (1 + 1) and (2 + 1) resonant ionization of NO through the Rydberg A and C states, we have obtained single photoelectron peaks due to $\Delta v = 0$ ionization transitions. However, when NO is excited in such a way that the $\Delta v = 0$ ionization transition is energetically inhibited, we have obtained the pohtoelectron spectra corresponding to autoionization from super-excited states. It is emphasized that the present work presents several typical important examples for studying dynamic behavior of higher excited states of molecule in the gas phase.

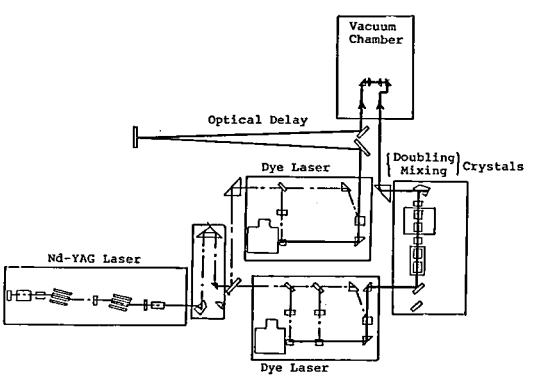

Figure 1. The setup of the laser system used for MPI ion-current and photoelectron energy measurements.

IV-K-2 Multiphoton Ionization Photoelectron Spectroscopic Study on NO: Autoionization Pathway through Dissociative Super-Excited Valence States

Yohji ACHIBA, Kenji SATO, and Katsumi KIMURA

We have carried out measurements of total ion-current and photoelectrons to study autoionization of NO molecule through the two-photon resonant, valence-excited $B^2\Pi$ state at the $v' = 9$ level (designated as B-9). The ion-current spectrum of the B-9 state shows several intensity-anomalous rotational lines as well as normal Q-branch rotational lines as shown in Figure 1. Each of the photoelectron spectra obtained at the normal rotational lines accompanys three energetically accessible vibrational bands with branching ratios of 0.65 ($v^+ = 2$), 0.30 ($v^+ = 1$) and 0.05 ($v^+ = 0$). On the other hand, each of the photoelectron spectra obtained at the intensity-anomalous rotational lines suggests a relatively high yield of the

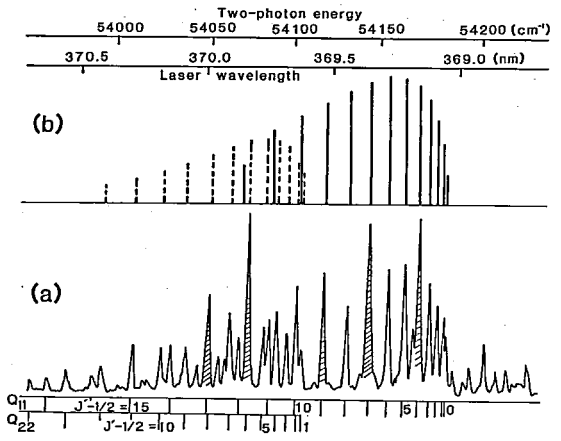

Figure 1. A (2 + 1) MPI ion-current spectrum of NO molecule through two-photon resonant $B^2\Pi$, $v' = 9$ state. (a) An MPI spectrum measured for NO with an effusive beam source. Intensity-anomalous peaks are shaded. (b) An intensity distribution calculated for the rotational line profile at 220 K. The Q_{11} and Q_{22} sequences are indicated by solids and broken lines, respectively.

$v^+ = 0$ ion, and there seems to be no photoelectron angular dependence for the $v^+ = 0$ band.

From these experimental results, we have deduced the following conclusions. 1) The overall process of producing the normal rotational lines is represented by $X \xrightarrow{2h\nu} B\text{-}9 \xrightarrow{h\nu} I^* \rightsquigarrow NO^+$, where I^* means the super-excited valence $I^2\Sigma^+$ state and $\rightsquigarrow$ indicates electronic autoionization forming the ground electronic state of ions. 2) The ionization scheme of producing the intensity-anomalous rotational lines is expressed by $X \xrightarrow{2h\nu} B\text{-}9 \xrightarrow{h\nu} N\text{-}6 \longrightarrow B'^* \rightsquigarrow NO^+$, involving an accidental double resonance, where N is the Rydberg $N(4d\delta)^2\Delta$ state, B'^* is the super-excited valence $B'^2\Delta$ state, and $\longrightarrow$ means an electronic coupling between the Rydberg and the valence states. 3) No photoelectron angular dependence occurs for the $v^+ = 0$ band, probably because of relatively long lifetime of the Rydberg N state.

IV-K-3 The Ar-NO van der Waals Complex Studied by Resonant Multiphoton Ionization Spectroscopy Involving Photoion and Photoelectron Measurements

Kenji SATO, Yohji ACHIBA, and Katsumi KIMURA

[*J. Chem. Phys.*, **81**, 57 (1984)]

Using a 5 % mixture of NO in Ar in a supersonic free jet, we have carried out measurements of the total ion current in the 380-385 nm laser wavelength region. We have also measured photoelectron kinetic energy spectra at individual ion current peaks. In the ion-current spectrum we have observed a new vibtrational progression which consists of four peaks in the wavelength region longer than the peak of the two-photon transition of free NO molecule: NO (X, $v'' = 0$) → NO (C, $v' = 0$) (Figure 1). It has been concluded that the new ion-current peaks are attributed to bound-to-bound transitions of the Ar-NO van der Waals complex from its ground state to the two-photon resonant state expressed by Ar-NO* ($C^2\Pi$, $v' = 0$), in which the NO component is in the 3pΠ Rydberg state. The whole resonant ionization process studied is expressed by Ar-NO (X, $v'' = 0$) → Ar-NO* (C, $v' = 0$) → Ar-NO^+ (X, $v^+ = 0$). Each ion-current peak separation is about 50 cm^{-1}, which may correspond to the frequency of the Ar-NO intermolecular stretching vibration, showing a strong anharmonicity. The dissociation energy (D_0) of the Ar-NO* ($C^2\Pi$) state has been found to be 0.058 ± 0.001 eV. From the photoelectron spectra, we also conclude that the adiabatic ionization energy of Ar-NO is $I_a = 9.148 \pm 0.005$ eV and the

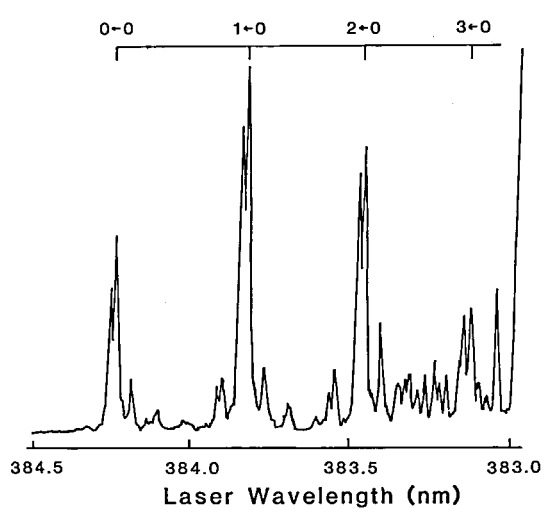

Figure 1. An MPI ion current spectrum obtained with a free jet of a mixture of 5% NO in Ar in the laser wavelength region 383–384.5 nm. The stagnation pressure was 1 atom.

dissociation energy of the Ar-NO^+ ($X^1\Sigma^+$) ion is D_0 = 0.132 + 0.005 eV.

IV-K-4 Multiphoton Ionization Photoelectron Spectroscopy and Two-Color Multiphoton Ionization Threshold Spectroscopy on the Hydrogen Bonded Phenol and 7-Azaindole in a Supersonic Jet

Kiyokazu FUKE *(Keio Univ.)*, **Hidetoshi YOSHIUCHI** *(Keio Univ.)*, **Koji KAYA** *(Keio Univ.)*, **Yohji ACHIBA, Kenji SATO and Katsumi KIMURA**

[*Chem. Phys. Lett.*, **108**, 179 (1984)]

The initial stateges of solvation and crystallization were studied for several hydrogen bonded complexs of phenol and 7-azaindole in a supersonic jet by the use of multiphoton ionization photoelectron spectroscopy (MPI-PES) and two-color multiphoton threshold spectroscopy. The observed reduction of the first adiabatic ionization potential due to complex formation has been ascribed to stabilization of the ionized cluster. Photoelectron spectra of phenol and its hydrogen bonded complexes with water are shown in Figure 1. The results are compared with the stabilization of the electronic S_1 state of the clusters.

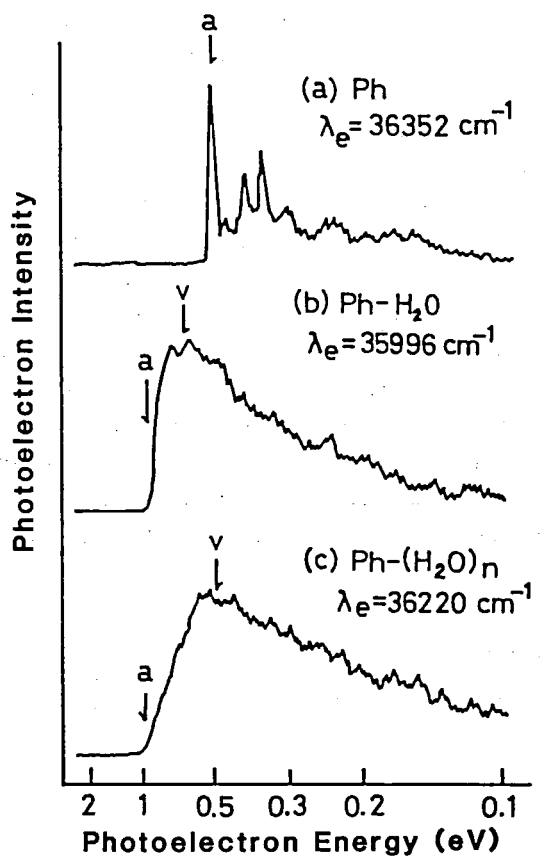

Figure 1. Photoelectron spectra of hydrogen-bonded complexes of phenol with water. The ionization transition takes place via a (1 + 1) resonant ionization through the S_1-state origins. Letters a and v indicate the positions of adiabatic and vertical ionization potentials, respectively.

IV-K-5 Multiphoton Ionization of Triethylamine: Determination of the Vibrationless S_2 Level by Laser Photoelectron Spectroscopy

Masahiro KAWASAKI *(Mie Univ.)*, **Kazuo KASATANI** *(Mie Univ.)*, **Hiroyasu SATO** *(Mie Univ)*, **Yohji ACHIBA, Kenji SATO, and Katsumi KIMURA**

Triethylamine was excited to a vibrational level of the S_2 (Rydberg) state and then ionized with a (2 + 1) resonance multiphoton ionization method. One of the important conclusions deduced from this study is that the vibrationless level of the S_2 state is obtainable from a photoelectron spectroscopic point of view. The vibrationless level thus determined is $E_0(S_2)$ = 41200 cm^{-1}. It should also be mentioned that only the ionization through the S_2* state is detectable under the present experimental conditions, although the occurence of fast intramolecular electronic relaxation $S_2^* \rightsquigarrow S_1^*$ has so far been reported in the previous fluorescence studies.

IV-K-6 New Aspects of the "Channel Three" Problem in Benzene, as revealed by Multiphoton Ionization Photoelectron Spectroscopy

Yohji ACHIBA, Atsunari HIRAYA *(Tohoku Univ., IMS)*, **and Katsumi KIMURA**

[*J. Chem. Phys.*, **80**, 6047 (1984)]

Combining a photoelectron spectroscopic technique with a (1 + 1) resonant ionization method, we have investigated intramolecular decay processes of benzene in its S_1 state under collision-free condi-

tions. Photoelectron spectra were obtained by selective excitation of benzene with a pulsed UV laser at several single vibronic levels of the S_1 state up to an internal energy (ΔE) of 5000 cm^{-1}.

These spectra strongly suggest that the excitation of benzene at the vibronic bands above the onset of the "channel three" is followed by intramolecular vibrational redistribution within the S_1 state. It is concluded that there are no decay channels faster than this redistribution process up to $\Delta E = 5000$ cm^{-1} at the first decay stage. The results of the integrated multiphoton ionization intensity distribution over the vibronic bands, as well as the internal-energy dependent spectral changes observed in the photoelectron spectra (Figure 1), also strongly suggest that the channel three is initiated by the redistributed vibrational modes, which lead to a fast internal conversion to the ground electronic state.

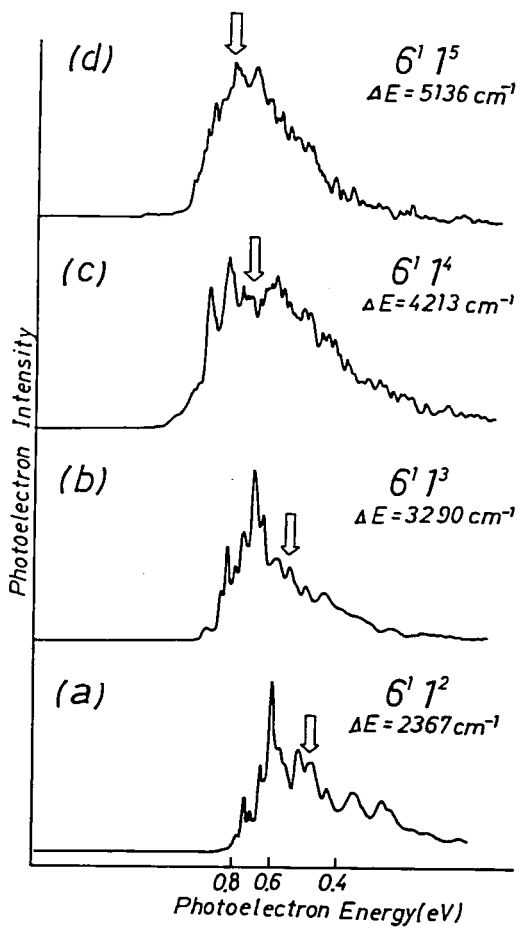

Figure 1. Photoelectron spectra obtained by excitation of the single vibronic levels of benzene; (a) $6^1 1^2$, (b) $6^1 1^3$, (c) $6^1 1^4$, and (d) $6^1 1^5$. The arrows indicate the positions of the expected $\Delta v = 0$ ionization transitions.

IV-K-7 Identification of the Lowest Energy $n\pi^*$ States in Polycyclic Monoazines: Quinoline and Isoquinoline

Atsunari HIRAYA *(Tohoku Univ. and IMS)*, **Yohji ACHIBA, Katsumi KIMURA, and Edward C. LIM** *(Wayne State Univ. and IMS)*

[*J. Chem. Phys.*, in press]

The location of the lowest energy $n\pi^*$ singlet state relative to that of the lowest energy $\pi\pi^*$ state is crucial for the interpretation of the photophysical properties of nitrogen-heterocyclic compounds. However the lowest energy $n \rightarrow \pi^*$ transitions in polycyclic monoazines are too weak to be detected in conventional absorption spectroscopy. As a consequence, $n\pi^*$ absorption in vapor phase has never been identified in any of these compounds. We obtained the resonance-enhanced two-color (tunable UV + 193 nm) ionization spectra of jet-cooled quinoline and isoquinoline as shown in Figure 1, which locate the electronic origins of the lowest energy $n\pi^*$ state in these molecules. Presently determined $S_2(\pi\pi^*)$–$S_1(n\pi^*)$ energy gap of ~1100 cm^{-1} for isoquinoline is in remarkable agreement with the value recently predicted on the basis of indirect evidence.[1] Consistent with the larger S_2–S_1 energy gap of ~1800 cm^{-1} for quinoline, the spectrum in the region of the S_2 is much more complex in this molecule as compared to isoquinoline. These results demonstrate the utility of the technique in detecting very weakly allowed electronic transitions and non-emitting excited states.

Reference

1) A. K. Jameson, B. E. Forch, K. T. Chen, S. Okajima, H. Saigusa and E. C. Lim, *J. Phys. Chem.*, in press.

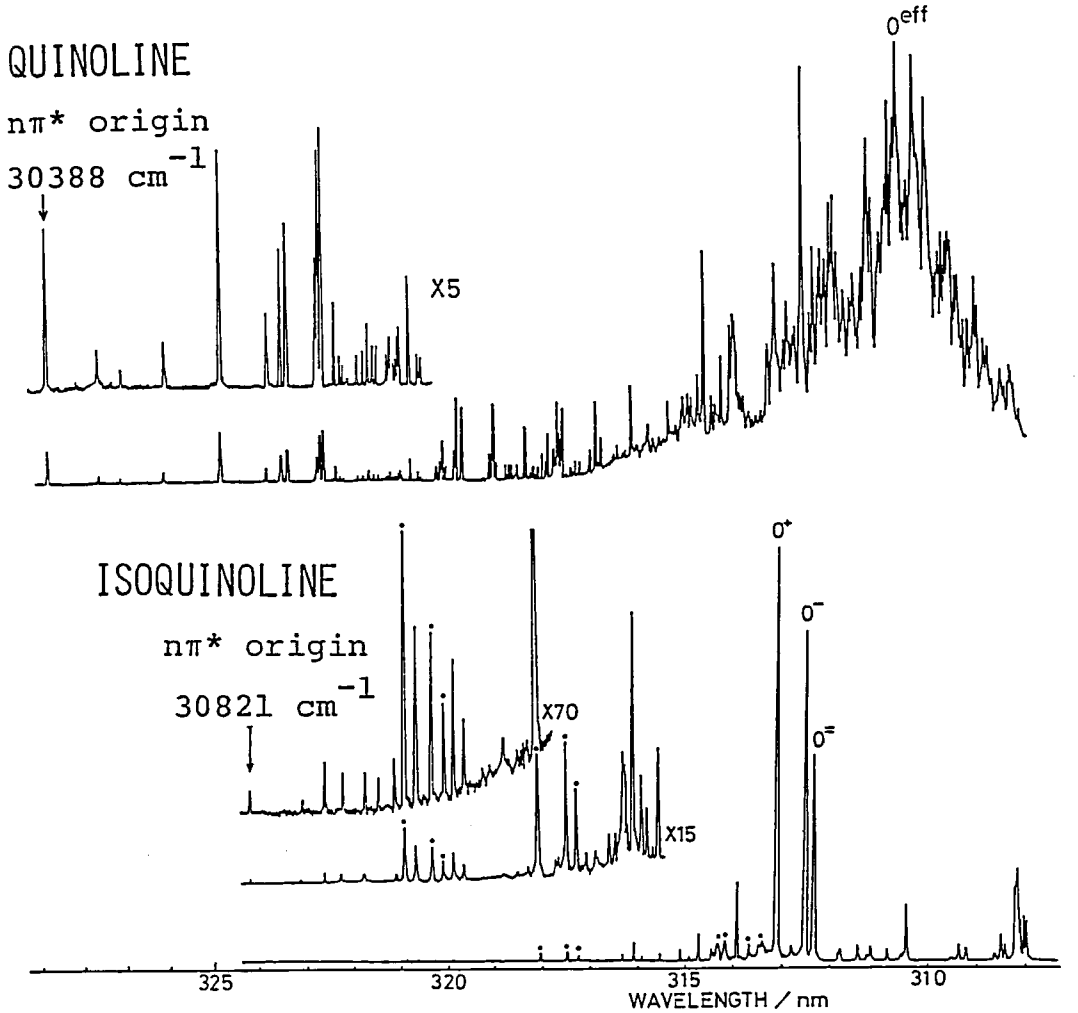

Figure 1. Resonance-enhanced two-color ionization spectra of jet-cooled quinoline (upper) and isoquinoline (lower). Arrows indicate the origin band of the $n \rightarrow \pi^*$ transition of these molecules. The origin band group of the $\pi\pi^*$ state of isoquinoline are labeled as 0^+, 0^-, and $0^=$. The bands marked with dots are hot bands belonging to the $\pi \rightarrow \pi^*$ transition. The most intense feature in the spectrum of quinoline at about 310.6 nm was taken as the effective origin (0^{eff}) of the $\pi\pi^*$ state. The sample was seeded in a He free-jet through a pulsed nozzle at 500 Torr stagnation pressure. ArF (193 nm) excimer laser was used to ionize excited molecules produced by a tunable UV pump laser.

IV-K-8 Vibrationally Resolved Photoelectron Spectra of Jet-Cooled Naphthalene: Intramolecular Relaxation Processes in S_1 and S_2 States

Atsunari HIRAYA *(Tohoku Univ. and IMS)*, **Yohji ACHIBA, Naohiko MIKAMI** *(Tohoku Univ. and IMS)*, **and Katsumi KIMURA**

Combining a photoelectron spectroscopic technique with a (1 + 1) resonant ionization method, we have investigated photoelectron spectra by ionizing naphthalene through single vibronic levels of the S_1 state up to an internal energy (E_{vib}) of about 2500 cm^{-1} as well as through some vibronic levels of the S_2 origin region. The photoelectron spectra thus obtained, presented in Figure 1, have been found to show many bands which are interpreted as the vibrational structure of the

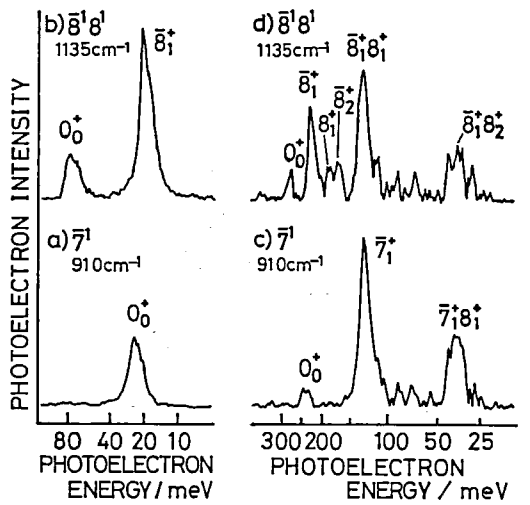

Figure 1. Photoelectron spectra of jet-cooled naphthalene obtained by (1 + 1) resonant ionization through the $\bar{7}^1$ and $\bar{8}^1 8^1$ vibronic levels of the S_1 state in one- and two-color experiments. Vibrational excess energies above the S_1 origin are indicated in wavenumbers. One-color experiments: (a) $\bar{7}^1$, (b) $\bar{8}^1 8^1$. Two-color experiments: (c) $\bar{7}^1$, (d) $\bar{8}^1 8^1$ (Wavelength of the ionizing laser is 288.1 nm).

naphthalene cation. The present photoelectron results also support the available spectroscopic evidence that intramolecular vibrational redistribution occurs at the energy levels higher than 2200 cm^{-1} above the S_1 origin.

Intramolecular electronic relaxation from the S_2 to the S_1 state has been found to be faster than ionization under the present laser irradiation conditions, suggesting that the relaxation rate is larger than the order of 10^{11} sec^{-1}.

IV-K-9 Multiphoton Ionization of Photoelectron Spectroscopic Study on Multiphoton Dissociation of Fe Complexes

Yatsuhisa NAGANO *(Osaka Univ., IMS)*, **Yohji ACHIBA and Katsumi KIMURA**

In the multiphoton ionization study on $Fe(CO)_5$, it has been found that by changing the laser wavelength from 480 to 360 nm, the resulting MPI ion current spectra become to accompany broad band structures (composing of many sharp lines) as well as laser-wavelength independent ionization signals in addition to very sharp MPI lines. The sharp lines reflect the resonance character of atomic Fe with relatively low-lying excited states. In the present work, we have investigated to clarify the origin of each type of the MPI bands mentioned above, using a photoelectron spectroscopic technique.

The photoelectron spectra measured by fixing the laser wavelength at the sharp and broad as well as the background band indicate that the MPI bands are described by two- or three-photon ionization from various excited states of Fe atoms, forming mainly the ground state and/or the second excited Fe^+.

The most interesting points deduced from the present photoelectron spectroscopic work are the followings: 1) the multiphoton dessociation of $Fe(CO)_5$ proceeds almost non-selectively, producing many electronic states of Fe atoms, and 2) although the decomposition itself takes place via complicated multiphoton processes, the energy of the highest excited state of Fe* produced in the process is always coincident with only a one-photon energy of the laser wavelength used. Applying this technique to various other Fe complexes (iron acetylacetonate, $Fe_3(CO)_{12}$, $FeCl_3$, ferrocene, and 1,1'-benzoyl ferrocene), it has been concluded that the distribution of the excited states for the decomposed atomic Fe is much dependent on the size of ligands, *i.e.*, the vibrational degrees of freedom of ligand molecules.

IV—L Production, Characterization, and Spectroscopic Studies of Molecular Complexes and Clusters

There are several techniques to investigate the physics and chemistry of molecular complexes and clusters. One of the most powerful techniques for production of such weakly bound complexes is the supersonic expansion of a high pressure gas through a small nozzle hole, by which one can produce a very large number of exotic complexes. However, the characterization of these complexes is hard because of its weak bonding character.

In this project we adopt a couple of different approaches to determine the interaction potential between atoms and molecules. One approach is to apply a crossed molecular beams technique to the measurement of differential scattering cross sections. Another approach is to study the spectroscopy of van der Waals complexes and clusters. We plan to use both the Molecular Beam Chemistry Apparatus (MBC-1) and a color center infrared laser to investigate predissociation dynamics of vibrationally excited van der Waals molecules.

Furthermore a molecular beam apparatus to study photochemistry of electronically excited van der Waals complexes irradiated by the vacuum ultraviolet photons from our UVSOR facility is being constructed. This apparatus applies mainly dispersed and time-resolved fluorescence spectroscopy.

IV—M Molecular Beam Studies of Reaction Dynamics Involving Chemically Reactive Atoms and Free Radicals

In this project we investigate the dynamics of chemical reactions involving reactive species such as N, B, C, CH, etc. using a crossed molecular beams technique. For the production of supersonic nozzle beams of these reactive species, especially for active nitrogen atoms, an arc-heated nozzle beam source has been used. Two molecular beam machines, MBC-I which applies the rotatable mass spectrometer detector and MBC-II with optical spectroscopic detection, are operational.

IV-M-1 Collision Energy Dependence of Integral Cross Section for the Chemiluminescent Reaction: $N(^2D, ^2P) + HI \rightarrow NH(A^3\Pi) + I(^2P_{3/2})$.

Kiyohiko TABAYASHI, Shigeru OHSHIMA, and Kosuke SHOBATAKE

In the previous chemiluminescence study of the molecular beam reactions of $N^*(^2D$ and $^2P)$ with HI and HBr, we have reported (1) the rotational and vibrational distribution of the nascent NH $(A^3\Pi)$ product at the average collision energy $\bar{E}$ = 1.12 eV and (2) the dependence of the NH $(A^3\Pi - X^3\Sigma)$ fluorescence intensity upon the average collision energy varied between 0.5 and 1.6 eV by controlling the stagnation temperature.[1] In the present study, we have applied the crossed molecular beam TOF energy selection technique to more accurate determination of the collision energy dependence of the integral cross section for the reactions:

$$N(^2P) + HI \rightarrow NH(A^3\Pi) + I\ (^2P_{3/2}) \qquad \Delta H = -0.20\ \text{eV} \qquad (1a)$$

$$N(^2D) + HI \rightarrow NH(A^3\Pi) + I\ (^2P_{3/2}) \qquad \Delta H = 0.99\ \text{eV} \qquad (1b)$$

The relative cross section as a function of collision energy E, Sr(E), obtained for the mixed $N^*(^2D$ and $^2P)$ beam, is plotted in Figure 1. A break in the Sr(E) profile is evident, which corresponds to the onset of $NH(A^3\Pi)$ formation by process (1b). Below this threshold the $NH(A^3\Pi)$ product is formed only by process (1a) and the cross section is nearly constant with E.

The present Sr(E) profile enables us to evaluate the relative contribution of both reactants $N(^2D)$ and $N(^2P)$ to the observed chemiluminescence intensity. Hence, for example, at $\bar{E}$ = 1.12 eV, comparable amounts of $NH(A^3\Pi)$ products are

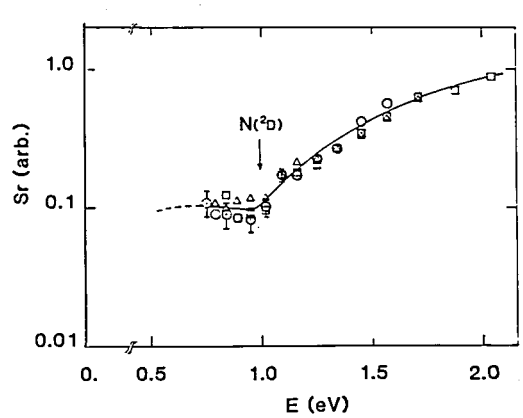

Figure 1. Relative integral cross section Sr(E) vs collision energy E for the reaction: $N(^2D, ^2P) + HI \rightarrow NH(A^3\Pi) + I(^2P_{3/2})$. Each symbol corresponds to the data obtained under the same beam stagnation condition. The arrow indicates the threshold energy for the reaction (1b).

produced from both reactants, that is, the N(^{2}D) reaction (1b) contributes more than we assumed in the previous study.[1] Therefore, one can conclude that these reactions proceed via a direct reaction mechanism rather than the statistical one.

Reference

1) K. Tabayashi, S. Ohshima, and K. Shobatake, *J. Chem. Phys.*, **80**, 5335 (1984).

IV-M-2 Electronic Excitation Transfer Reaction. I. Collision Energy Dependence of the Cross Section for Ar*(^{3}P$_{0,2}$) + N$_2$ → Ar + N$_2$(C$^3\Pi_u$, v' = 0)

Kiyohiko TABAYASHI, Shigeru OHSHIMA, and Kosuke SHOBATAKE

An application of our arc-heated atomic beam to reactive scattering experiments has proved to be fruitful in extending the range of collision energy to the above-thermal region. The title reaction is known to be one of the prototype reactions of the electronic excitation transfer reactions involving metastable rare gas atoms. In the present study, the collision energy dependence of the cross sections for the title reaction has been determined for the collision energies between 0.3 and 2.5 eV by applying the crossed molecular beam TOF energy selection technique.

The experimental procedure is briefly explained in the following. 1) Using a TOF technique we determine the energy flux distribution $I_x(E)$ of the reactant Ar* as shown in Figure 1a (Note that the translational energy of Ar* beam is converted to the collision energy). 2) Then one measures the time evolution of the fluorescence intensity of N$_2$ (C−B) emission produced by the collision of Ar* beam with the N$_2$ free jet at the interaction region 72 cm downstream from the chopper disc. The TOF distribution is also converted to the energy distribution $I_f(E)$. The relative cross section $Sr(E)$ is then calculated by $Sr(E) = I_f(E)/I_x(E)$. In order to determine the absolute cross section for these process, our relative value was calibrated to the ones obtained by Parr and Martin[1] for the collision energies below 0.8 eV. The resulting cross sections are plotted in Figure 1b.

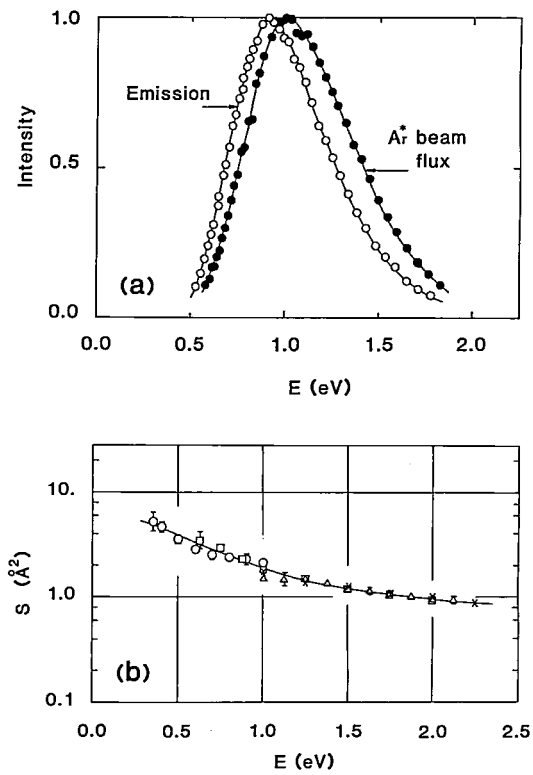

Figure 1. a) Collision energy dependences of the reactant Ar* (●) and the fluorescence intensity (○). b) Cross sections for the excitation transfer reaction Ar*(^{3}P$_{0,2}$) + N$_2$ → Ar + N$_2$(C$^3\Pi_u$, v' = 0) against the collision energy E.

Reference

1) T. P. Parr and R. M. Martin, *J. Chem. Phys.* **69**, 1613 (1978).

IV-M-3 Electronic Excitation Transfer Reaction. II. Collision Energy Dependence of the Integral Cross Section for Kr*(^{3}P$_{0,2}$) + N$_2$ → Kr + N$_2$ (C$^3\Pi_u$, v' = 0).

Kiyohiko TABAYASHI, Shigeru OHSHIMA, and Kosuke SHOBATAKE

The relative integral cross sections for the endoergic processes

$$\mathrm{Kr}^*(^3\mathrm{P}_0) + \mathrm{N}_2 \rightarrow \mathrm{Kr} + \mathrm{N}_2\ (\mathrm{C}^3\Pi_u,\ v' = 0) \qquad \Delta H = 0.47\ \mathrm{eV} \qquad (1a)$$

$$\mathrm{Kr}^*(^3\mathrm{P}_2) + \mathrm{N}_2 \rightarrow \mathrm{Kr} + \mathrm{N}_2\ (\mathrm{C}^3\Pi_u,\ v' = 0) \qquad \Delta H = 1.12\ \mathrm{eV} \qquad (1b)$$

have been determined for the collision energies between 0.6 and 1.8 eV by applying an arc-heated

Kr* beam to the crossed molecular beam-TOF energy selection experiment. The results are summarized in Figure 1. From this one finds that the cross section for each channel increases steeply above the threshold energy and then levels off. Since, in the present experiment, two spin-orbit metastable Kr* atoms contribute to the $N_2(C^3\Pi - B^3\Sigma)$ emission, the total cross section $Sr(E)$ can be expressed as the sum of both contributions

$$Sr(E) = C_0\sigma_0(E) + C_2\sigma_2(E) \quad (2)$$

where C_J is a fractional population of spin-orbit $Kr(^3P_J)$ atoms in the beam and $\sigma_J(E)$ is the collision energy dependent cross section for $Kr(^3P_J)$ atoms. By comparison of the fluorescence intensity for the present experiment with those of Ar* + N_2 reaction (see IV-M-2), one obtains $Sr(E)$ = 0.02 Å^2 at collision energy E = 1.0 eV. Adoption of a near statistical population $C_2/C_0 = 5$[1] enables us to estimate the cross section for the process (1a) at σ_2 = 0.12 Å^2 for collision energy E = 1.0 eV.

The present study shows that the collision energy plays a very important role in promoting the endoergic excitation energy transfer processes. Furthermore the fact that the estimated maximum cross sections for these processes, $\sigma_J(E)$'s, are smaller than that for N_2 + Ar* process by a factor of about 10 indicates that these processes can be explained by a surface crossing mechanism.

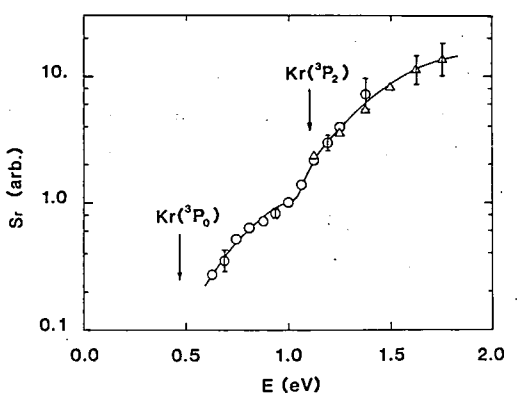

Figure 1. Relative cross section Sr(E) vs collision energy E for the production of $N_2(C^3\Pi_u, v' = 0)$ by collision of $Kr^*(^3P_{0,2})$ upon N_2. The arrows indicate the threshold energies for the processes (1a) and (1b). Each symbol corresponds to the data obtained under the same beam stagnation condition.

Reference

1) For example, V. E. Bondybey and T. A. Miller, *J. Chem. Phys.* **66**, 3337 (1977).

IV-M-4 Dissociation Dynamics of BrCN in Collision with Energetic $Ar(^3P_{0,2})$.

Yoshio FUKUDA,* Tamotsu KONDOW,* Kozo KUCHITSU,* *(*Univ. of Tokyo)*, Kiyohiko TABAYASHI, Shigeru OHSHIMA, and Kosuke SHOBATAKE

Metastable $Ar^*(^3P_{0,2})$ atoms produced from the arc-heated source were allowed to collide with BrCN at the average collision energies, 1.3 and 2.9

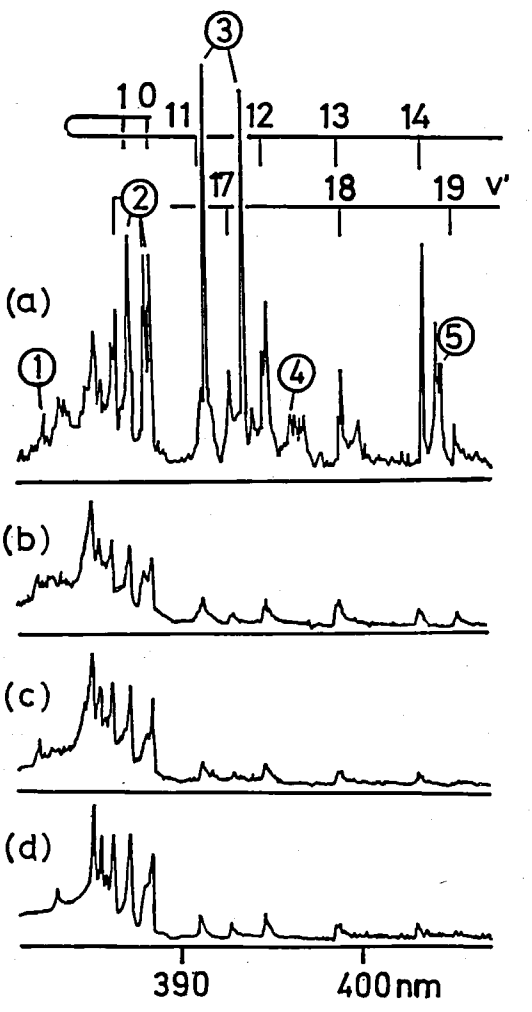

Figure 1. $CN(B^2\Sigma^+ - X^2\Sigma^+)$ emission spectra produced in the collision of $Ar(^3P_{0,2})$ with BrCN for thermal (a), 1.3 eV (b) and 2.9 eV (c) collisions. Trace (d) is a theoretical spectrum which reproduces the observed spectrum (c). Perturbed lines are indicated by 1–5.

eV. The resulting fragment emission $CN(B^2\Sigma^+-X^2\Sigma^+)$, was analyzed to determine vibrational and rotational distributions of the nascent $CN(B^2\Sigma^+)$ fragment. As shown in Figure 1 the dispersed CN(B-X) emission spectra obtained from the present molecular beam experiment are very different from that (Figure 1a) for thermal collision obtained from a flowing afterglow experiment.[1] That is, the anormalous enhancement of the vibrational distributions for $v' = 0, 4, 11, 12, 14, 17$ and 18 levels in the $B^2\Sigma^+$ state observed for thermal collision, which were assigned to perturbations between the $B^2\Sigma^+$ state and other electronic states, is completely disappeared in the spectra for higher collision energies. The ratios of the electronic branching of the CN fragments were estimated from the intensities of the perturbed lines. These results were successfully explained by a scheme that the reaction proceeds via two competing Rydberg manifolds 3π and 5σ of Br-CN molecule with the aid of a semiclassical collision theory and the molecular orbital correlation in the Br-CN system.

Reference

1) a) T. Urisu and K. Kuchitsu. *J. Photochem.* **2**, 409 (1973/74);
b) A. J. Yencha, Y. Ozaki, T. Kondow, and K. Kuchitsu, *Chem. Phys.* **51**, 343 (1980).

IV—N Physics and Chemistry of Various Types of Molecular Aggregates

IV-N-1 Optical Properties of Amorphous Molecular Aggregates

Hisayo SASAKI *(Ochanomizu Univ.)*, **Rumiko HORIGUCHI** *(Ochanomizu Univ. and IMS)*, **Noriko IWASAKI** *(ISSP, Univ. of Tokyo)* **and Yusei MARUYAMA**

Amorphous structures of evaporated thin tetracene films, *o*-terphenyl solids and anthracene liquids have been studied by the time-resolved fluorescence spectroscopy.

Intermolecular excimer spectra of the amorphous tetracene films were strongly dependent on annealing temperature. This means that the excimer formation in these films is intrinsic process. This fact was also demonstrated by the time-resolved spectroscopy.

Intermolecular excimer spectra were observed for the *o*-terphenyl crystalline and glassy solids. Temperature and excitation energy dependence of the excimer spectra and time characteristics were examined. The significant difference in the excimer characters between crystalline and glassy solids could not be detected within the observed temperature (4.2-300 K) and excitation energy ranges (4-5 eV).

Absorption and fluorescence spectra of anthracene liquids were observed for the first time. These spectra definitely demonstrate the expected existence of dimeric structure units in the liquid. A further verification is under way using the time-resolved spectroscopy.

IV-N-2 Intercalation Compounds of Black Phosphorus

Kyoko NAGASATO *(Ochanomizu Univ.)*, **Sumiko SAKAI** *(Ochanomizu Univ.)*, **Ichimin SHIROTANI** *(Muroran Inst. of Tech.)*, **Toshifumi NISHII** *(Mitsubishi Yuka Co. Ltd. and IMS)* **and Yusei MARUYAMA**

Alkali metal intercalation into black phosphorus single crystals was carried out for the first time. Cesium metal vapor was adsorbed into black phosphorus crystals and the intercalation was assured by the x-ray diffractometry. The conductivity increased up to several times of the value of the parent crystal after the completion of the intercalation. Lithium ion intercation was tried by the electrolysis of $LiClO_4$ solution. The conductivity seemed to be reduced with proceeding of intercalation. Iodine seemed to be a candidate for an electron accepting intercalant for black phosphorus.

The electronic structure of black phosphorus single crystals prepared by a high pressure technique is being studied by the analysis of the tunneling spectra at various temperatures.

IV-N-3 Synthesis of a Novel Organic Conductor

Hatsumi URAYAMA *(Ochanomizu Univ. and IMS)*, **Gunji SAITO** *(ISSP, Univ. of Tokyo)*, **Tamotsu INABE and Yusei MARUYAMA**

The molecular design and synthesis of a new type of organic conductor were undertaken by the stimulation of the recent advance in this field.

The points are the followings:

(1) In order to get the enforced or built-in segregated arrangement of donors and acceptors, we proposed to employ intramolecular charge transfer compounds.

(2) The success in TMTSF or BEDT-TTF complexes clearly demonstrates that the intermolecular interaction and its dimensionality in these crystals are enough to afford a superconducting phase. Thus, we proposed to use TMTTF or BEDT-TTF for the donor part of the compound.

(3) For the acceptor part, we selected Aza-TCNQ type structure. This moiety will be directly or indirectly (via-$(CH_2)_n$-) linked to donor part at the N-site of the pyridine skelton. Thus, the high electronic polarizability of the acceptor part and the proximity of two parts may presumably introduce large attractive interaction between conduction electrons in the donor part coloum or plane. This might lead us to high T_c organic superconductor (Little's excitonic mechanism). The synthesis of this type of compounds is now under way.

IV-N-4 Ultra-Thin Organic Multi-Layers Film Prepared by Molecular Beam Epitaxy Technique

Yusei MARUYAMA

The apparatus for the preparation of ultra-thin organic multi-layers films is now under construction. Highly regulated deposition of various organic substances will be carried out under ultra-high vacuum and the layer structure are to be monitored *in situ* with RHEED and/or SEM. Various combination of layers could produce artificial super lattices and quite novel substances. Electrical and optical properties will be measured *in situ*.

IV—O Two-color Resonant Multiphoton Spectroscopic studies of Rydberg States of Jet Cooled Molecules

Multiphoton spectroscopy by using visible or near UV laser sources has been well demonstrated to be a powerful method for a study of highly lying excited states, such as Rydberg series. The high sensitivity and the better resolution of this method are the principal advantages over the conventional spectroscopy. In this project we have developed advanced techniques of the multiphoton spectroscopy by using two different light sources; the two color multiphoton ionization method and the fluorescence dip spectroscopy. By these methods we have observed a number of series of Rydberg transitions converging to the first ionization continuum for a small molecule (NO) and a large molecule (DABCO). Combinning this method with the super sonic free jet, we have obtained the selective excitation of the Rydberg states without a spectral congestion which is often seen in conventional spectroscopic methods. We have studied on 1) selection rules and/or propensity rules of the autoionization processes from the rotationally or vibrationally excited Rydberg states, 2) identification of the Rydberg states from the precisely determined quantum defects, and 3) cross sections of the relevant transitions.

IV-O-1 High Rydberg States of NO Studied by Two-Color Multiphoton Spectroscopy

T. EBATA *(Tohoku Univ.)*, **Y. ANEZAKI** *(Tohoku Univ.)*, **M. FUJII** *(Tohoku Univ.)*, **N. MIKAMI** *(Tohoku Univ. and IMS)*, **and M. ITO** *(Tohoku Univ.)*

[*J. Phys. Chem.* **87**, 4773 (1983)]

The high Rydberg states of NO close to the ionization limit and the sharp ionization threshold

have been measured for the gas at room temperature and for the isolated molecule in a supersonic jet by using the two-color multi-photon spectroscopy in which the various rovibronic levels of the $A^2\Sigma^+(3s\sigma)$ state were used as an intermediate state. The ionization limit obtained from the Rydberg series and that from the ionization threshold were found to be in good agreement. It was also found that the rotational selection rule $\Delta(N,R) = 0$ and the vibrational propensity rule $\Delta v = 0$ are operative for the transitions to the high Rydberg states.

IV-O-2 Two-Color Excitation of NO in a Supersonic Free Jet—Autoionization of High Rydberg States

Y. ANEAKI *(Tohoku Univ.)*, **T. EBATA** *(Tohoku Univ.)*, **N. MIKAMI** *(Tohoku Univ. and IMS)*, **and M. ITO** *(Tohoku Univ.)*

[*Chem. Phys.*, in press]

High Rydberg states of NO above the ionization limit have been measured for the isolated molecule in a supersonic free jet by means of the two-color multiphoton spectroscopy. Figure 1 shows the two-color MPI and the fluorescence dip spectra obtained by pumping the $J = 1/2$ ($N = 0$) level of the $A^2\Sigma^+(v = 1)$ state. The sharp peaks can be analyzed by the well-known formula,

$$E = I.P. - R/(n-\delta)^2.$$

Three Rydberg series (ns, np and nf) were identified, which appeared by the rotational and the vibrational auto-ionization. The rotational structures of the 13s ($v = 1$), 13p ($v = 1$) and 12f ($v = 1$) states have been analyzed in detail. The absorption cross sections for the transitions to the Rydberg states from the A state were obtained to be 1.5×10^{-19}, 3.3×10^{-19} and 9.4×10^{-19} cm^2 for the 13s, 12f and 13p, respectively.

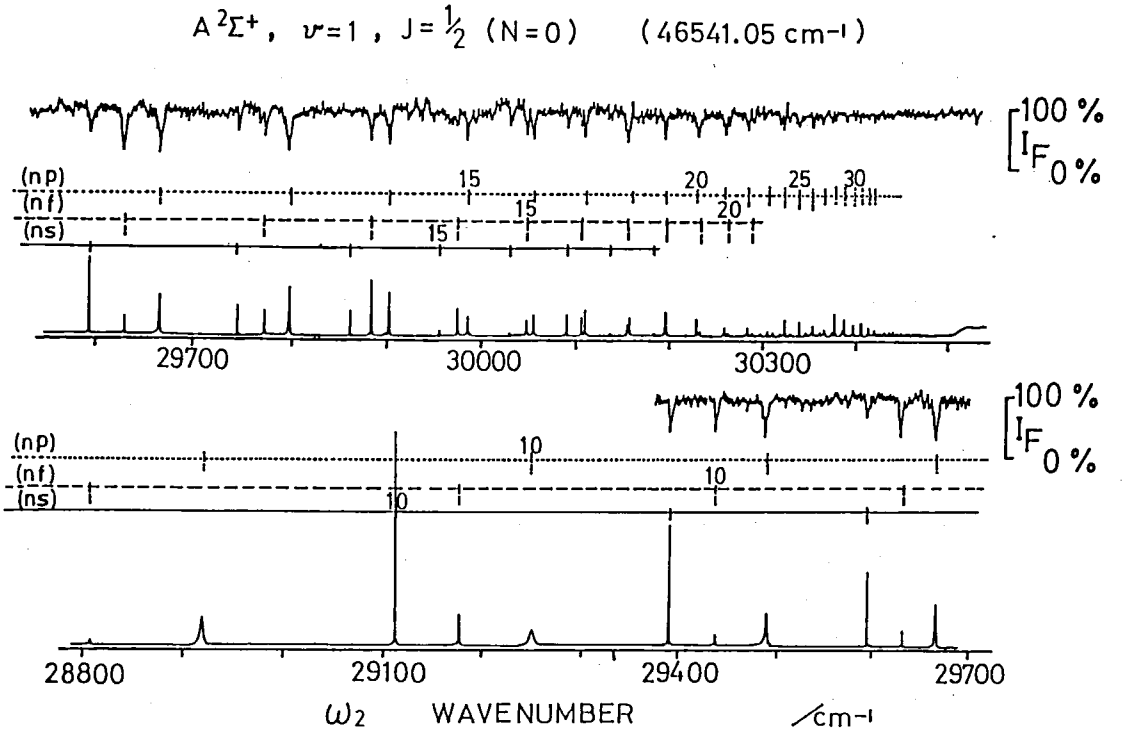

Figure 1. Two-color double resonance enhanced MPI and fluorescence dip spectra of ns(v = 1), np(v = 1) and nf(v = 1) ← $A^2\Sigma^+$(v = 0, J = 1/2, N = 0) transition.

IV-O-3 Two-Color Multiphoton Ionization of Diabicyclooctane in a Supersonic Free Jet

M. FUJII *(Tohoku Univ.)*, **T. EBATA** *(Tohoku Univ.)*, **N. MIKAMI** *(Tohoku Univ. and IMS)*, **and M. ITO** *(Tohoku Univ.)*

[*Chem. Phys. Lett.*, **101**, 578 (1983)]

Two-color multiphoton ionization (MPI) spectroscopy has been applied for diazabicyclooctane (DABCO) in a supersonic free jet. The MPI spectra due to transitions from the various vibronic levels of the S_1 (3s Rydberg) state which were excited by the first laser revealed the high Rydberg states above the adiabatic ionization potential. The ionization process and the vibrational potential of the ion are discussed.

IV-O-4 Two-Color Multiphoton Ionization and Fluorescence Dip Spectra of Diazabicyclo [2.2.2] octane in a Supersonic Free Jet. Rydberg States (n = 5 − 39) and Autoionization

M. FUJII *(Tohoku Univ.)*, **T. EBATA** *(Tohoku Univ.)*, **N. MIKAMI** *(Tohoku Univ. and IMS)*, **and M. ITO** *(Tohoku Univ.)*

[*J. Phys. Chem.*, **88**, in press]

Two-color multiphoton ionization (MPI) and fluorescence dip spectra have been observed for diazabicyclo [2.2.2] octane (DABCO) in a supersonic free jet. Figure 1 represents a typical spectrum showing the Rydberg states from n = 10 to n = 39 and the ionization threshold. By this method we have observed all the series from n = 5. From the MPI spectrum due to the transition from a vibronic level involving a combination vibration in the S_1 state to the high Rydberg state, definite evidence was obtained that the autoionization is vibrationally induced and the $\Delta v = -1$ propensity rule holds. It has been demonstrated that the two-color fluorescence dip spectroscopy has a great advantage in observation of the highly excited states ranging over a wide spectral region. One photon absorption cross sections for the transitions

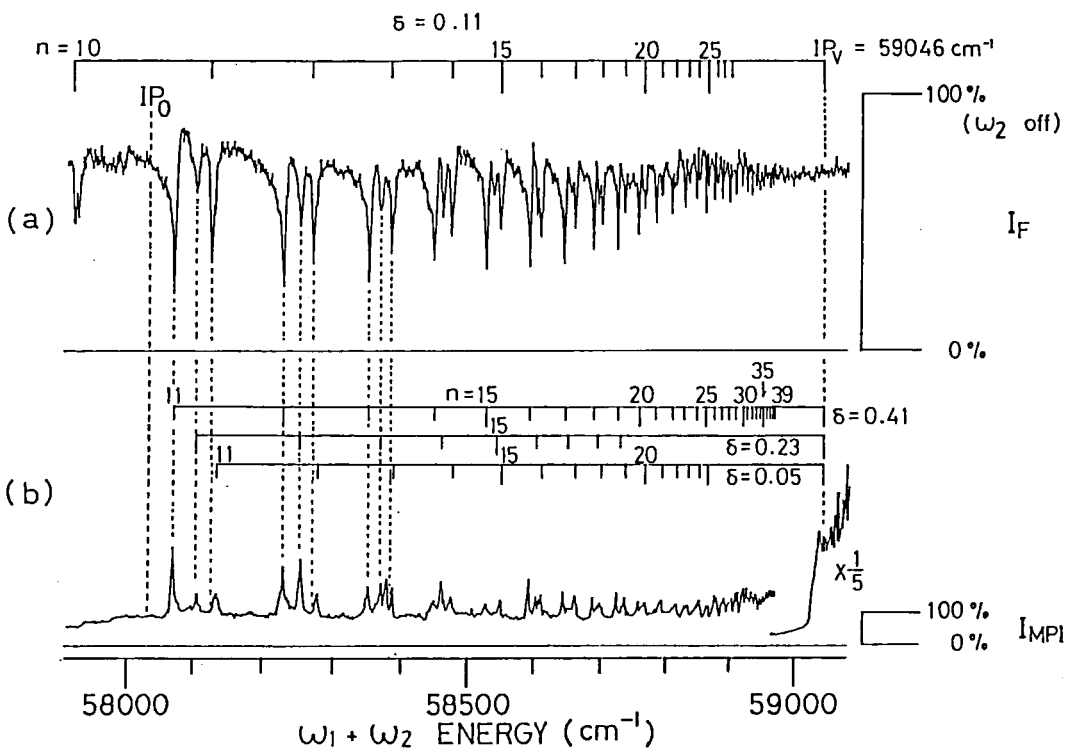

Figure 1. Two-color fluorescence dip(a) and MPI(b) spectra of DABCO due to the transition from the 20^1 vibronic level. The best fit of the principal quantum numbers n and the quantum defects δ are shown.

from the S_1 state to various Rydberg states have been determined from the dip spectra. The band shape of the fluorescence dip was discussed in relation to the Rydberg-continuum interaction. The vibrational structures of the S_1 state, the Rydberg states and the ion were also discussed.

RESEARCH ACTIVITIES V
Department of Applied Molecular Science

V—A High-Spin Organic Molecules

We have been engaged in molecular design, generation and exploration of physicochemical properties, of high-spin organic molecules. The magnetic susceptibility measurements of the nonet tetracarbene was carried out with a Faraday-type magnetometer. A perturbational method has been applied with success to solve the K-band ESR fine structures taken on unoriented samples of the septet and nonet species. In order to develop magnetic organic materials of interest, there remain several difficulties to overcome. The increase of the spin multiplicity and the thermal stability of the polycarbenes is one of a number of important factors. As a part of these efforts, we have scrutinized a couple of new carbenes to be used as a unit. Studies of triplet nitrenes continued to produce intriguing stereochemical effects and reaction products.

V-A-1 Magnetic Behavior of Nonet Tetracarbene, *m*-Phenylenebis((diphenylmethylen-3-yl)methylene)

Tadashi SUGAWARA, Shunji BANDOW,[1] Keisaku KIMURA,[1] Hiizu IWAMURA, and Koichi ITOH *(Osaka City Univ.)*

[*J. Am. Chem. Soc.*, **106**, 6449 (1984)]

Magnetic properties of **1** as a model for organic ferromagnets[2] have been investigated by magnetic susceptibility measurements. The temperature dependence of paramagnetic susceptibility (χ_p) of **1** in a glassy matrix of 2-methyltetrahydrofuran or in

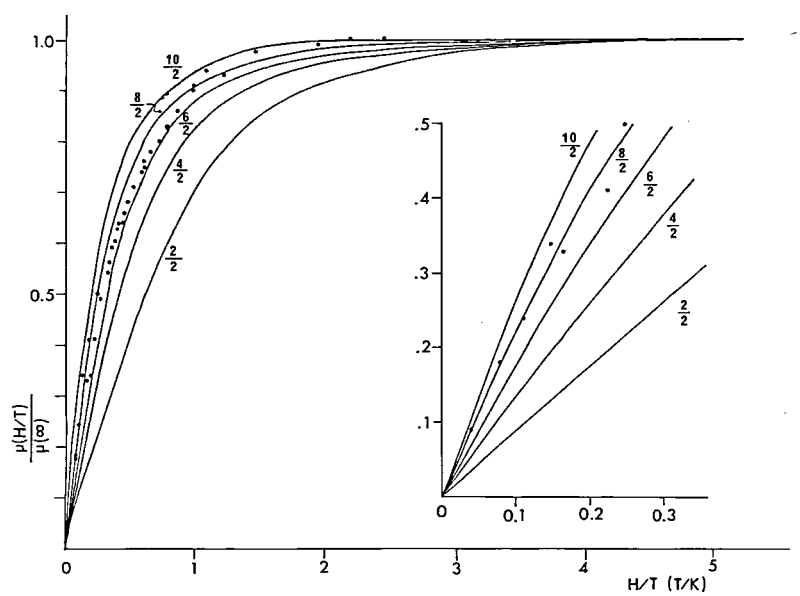

Figure 1. Plots of magnetization of **1** in 2-methyltetrahydrofuran vs temperature-normalized field strength (H/T). The theoretical magnetization curves are given by the Brillouin function in which $J = S = 2/2$, $4/2$, $6/2$, $8/2$ and $10/2$, the saturated values being normalized to 1.0.

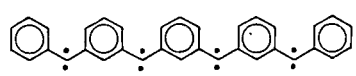

1

a mixed single crystal of benzophenone gave the effective magnetic moment and the number of spins for the nonet spin multiplicity of **1** in the ground state. An anti-ferromagnetic interaction was observed for **1** in the matrix at temperatures lower than 65K and reasoned in terms of the formation of an aggregate of the precursor diazo compound under these conditions. The field dependence of magnetization of **1** was measured at several temperatures. The data were analyzed in reference to the Brillouin function for magnetization (Figure 1) to show independently that **1** was in the ground nonet state. The results suggest that **1** may be regarded as a "micro" domain in ferromagnets.

References

1) Instrument Center.
2) Y. Teki, T. Takui, K. Itoh, H. Iwamura, and K. Kobayashi, *J. Am. Chem. Soc.*, **105**, 3722 (1983); *IMS Ann. Rev.*, 112 (1983).

V-A-2 Electron Spin Resonance Line Shapes of Randomly Oriented Molecules in Septet and Nonet States by Perturbation Approach

Yoshio TEKI *(Osaka City Univ.)*, **Takeji TAKUI** *(Osaka City Univ.)*, **Hirofumi YAGI** *(Osaka City Univ.)*, **Koichi ITOH** *(Osaka City Univ.)*, **and Hiizu IWAMURA**

The electron spin resonance line shapes of randomly oriented molecules in the septet and nonet states are analyzed in terms of the formulas derived by the perturbation treatment to third order in the fine-structure energy. The method is applied to a ground-state septet and nonet hydrocarbons **1** and **2**,[1] randomly oriented in mixed polycrystalline powders of benzophenone. It is shown that the g factor and the fine-structure parameters are determined from the line shape of a K-band spectrum with nearly the same accuracy as in a single crystal experiment. The extra lines have been observed in addition to the canonical lines corresponding to the external magnetic field along the principal axes of

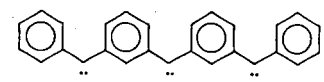

1

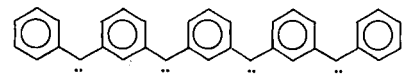

2

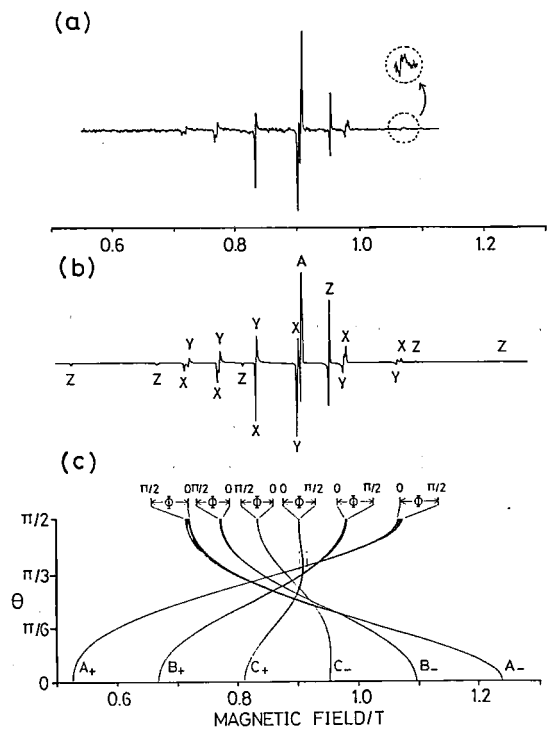

Figure 1. The ESR spectra of the nonet molecule **2** in the polycrystalline powder. (a) The observed spectrum at 77 K. (b) The simulated spectrum. (c) The calculated angular dependence of the resonance field, where A±, B±, C±, and D± refer to the transitions with $M_S = \pm 4 \leftrightarrow \pm 3$, $\pm 3 \leftrightarrow \pm 2$, $\pm 2 \leftrightarrow \pm 1$, and $\pm 1 \leftrightarrow 0$, respectively. The parameters are ν = 24711.0 MHz, g = 2.002 (isotropic), $|D|$ = 0.0332 cm^{-1}, $|E|$ = 0.0043 cm^{-1}, and ΔH_{msl} = 1.6 mT. The assignment was made for $D>0$ and $E<0$.

the fine-structure tensor. The feature of the extra lines due to the septet and nonet molecules is discussed by the third order perturbation theory.

Reference

1) Y. Teki, T. Takui, K. Itoh, H. Iwamura, and K. Kobayashi, *J. Am. Chem. Soc.*, **105**, 3722 (1983).

V-A-3 Photolysis of 1,12-Bis(diazo)-1,12-dihydroindeno[2,3-*a*]fluorene. ESR and Optical Detection of a σ-Type 1,4-Biradical

Tadashi SUGAWARA, Donald BETHELL,[1] and Hiizu IWAMURA

[*Tetrahedron Lett.*, **25**, 2375 (1984)]

When the title bis(diazo) compound (**1**) in 2-methyltetrahydrofuran was photolyzed in an ESR cavity at cryogenic temperature, signals due to triplet monocarbene (3^T) (D = 0.391, E = 0.0258 cm^{-1}) were obtained. Whereas the signal intensities followed the Curie-Weiss plot at 15-50K, they started to disappear with $t_{1/2}$ = 22 min at 55K. In the presence of benzophenone (0.12M), another set of signals due to 5^T (D = 0.0739, E = 0.003 cm^{-1}) were observed during irradiation of a glass in which 3^T had disappeared. The results indicated that the diazo group remaining in **3** is removed thermally to give dicarbene **4** which exists as the singlet 1,4-σ-biradical as a result of conjugation of the p-type electrons on the two carbenic centers; the second triplet species is then generated by benzophenone-sensitized excitation of **5**.

When monitored by uv spectroscopy at 77K, absorptions due to cyclic azine **6** and 5^S were obtained. The branching ratio of **6** to others is estimated to be 1/4. The results are summarized in Scheme 1.

Reference

1) IMS Invited Foreign Scholar 1982.

Scheme 1

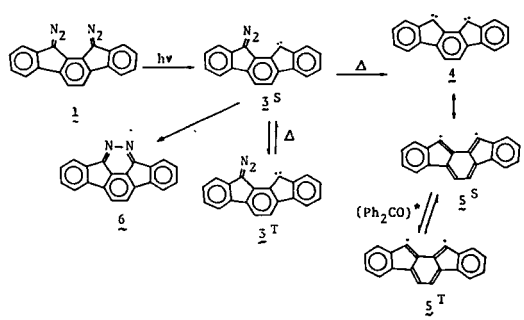

V-A-4 Preparation of 7-Diazo-7*H*-benz[*de*]anthracene

Akira IZUOKA, Shigeru MURATA, and Hiizu IWAMURA

[*Bull. Chem. Soc. Jpn.*, **57**, 3526 (1984)]

The reaction of 7*H*-benz[*de*]anthracen-7-one with hydrazine hydrate in ethylene glycol in the presence of zinc chloride for 12hr gave 7*H*-benz[*de*]anthracen-7-one hydrazone as yellow microcrystalline needles; mp 126-127°C. Oxidation of the hydrazone with yellow mercury(II) oxide in the presence of sodium sulfate and a trace of potassium hydroxide in THF gave in quantitative yield 7-diazo-7*H*-benz[*de*]anthracene; yellow-green prisms, mp 98-100°C (decomp). A characteristic IR band was observed at 2030 cm^{-1}. UV absorptions due to the π-π* and n-π* transitions were observed at 407 ($\log\epsilon$ = 4.14), 425 (4.10) and 600 nm (2.42), respectively. The 400 MHz ^{1}H NMR spectrum exhibited first-order multiplets (Figure 1) which were analyzed by the standard decoupling technique. The upfield shifts of the hydrogens peri to the diazo group are noted. The corresponding hydrogens of the precursor ketone appear in the lowest field.

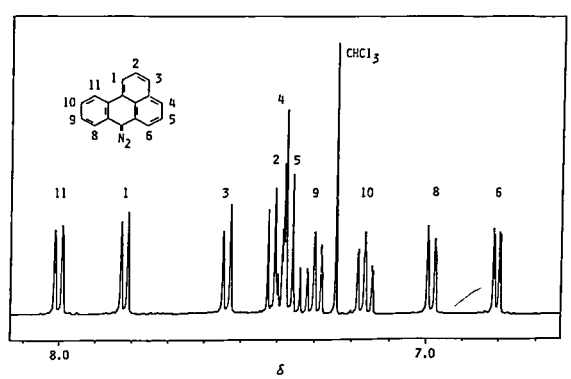

Figure 1. ^{1}H NMR spectrum (400 MHz) of 7-diazo-7*H*-benz-[*de*]anthracene.

V-A-5 7*H*-Benz[*de*]anthracen-7-ylidene

Akira IZUOKA, Shigeru MURATA, and Hiizu IWAMURA

[*Bull. Chem. Soc. Jpn.*, in press]

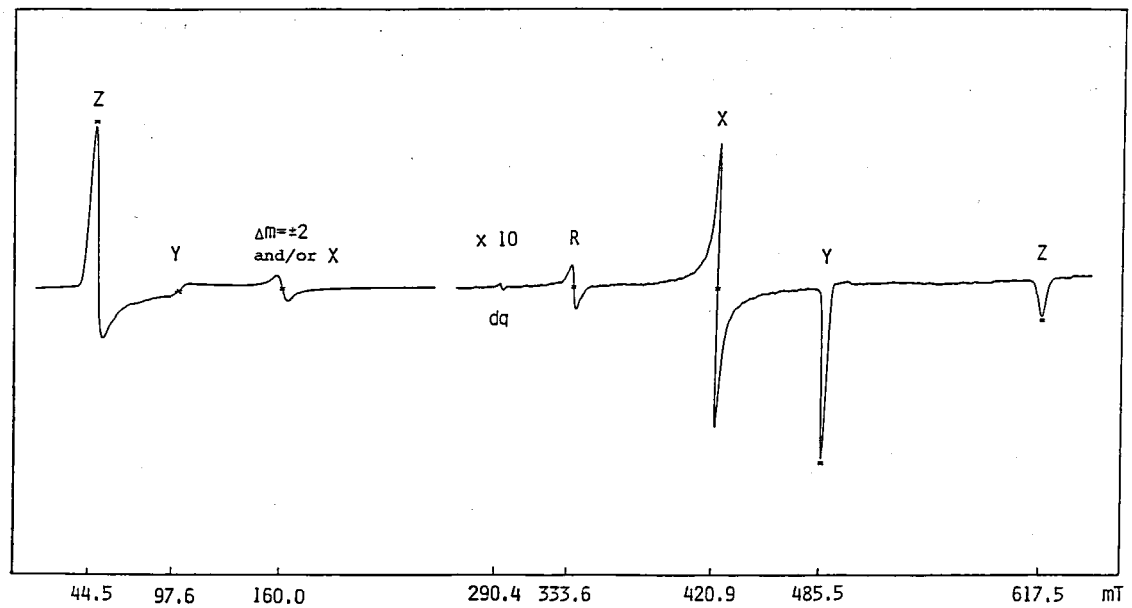

Figure 1. ESR spectrum (9.332 GHz) obtained by photolysis of 7-diazo-7*H*-benz[*de*]anthracene in 2-methyltetrahydrofuran glass at 14 K.

7-Diazo-7*H*-Benz[*de*]anthracene[1] in a 2-methyltetrahydrofuran matrix (1.5×10^{-2}M) was irradiated with a high-pressure mercury lamp in an ESR cavity at 14K. The resulting ESR spectrum obtained at 9.332 GHz is reproduced in Figure 1. The signals are typical fine structure patterns for unoriented triplet species. Those at 420.9, 485.5 and 617.5 mT were assigned to a set of the high-field X, Y and Z transitions from which the zero-field splitting parameters were obtained as $|D| = 0.2662$ and $|E| = 0.0175$ cm^{-1}. A temperature dependence experiment showed linear signal intensities vs. $1/T$ plots, indicating that the carbene is in the ground triplet state.

The D values of typical diarylcarbenes are in the range 0.41~0.37. With the exception of di(9-anthryl)methylene ($D = 0.113$ cm^{-1} at 4K),[2] the D parameter of 7*H*-benz[*de*]anthracen-7-ylidene obtained in this study is the smallest ever reported, showing extensive delocalization of the unpaired electron in the π-framework of the molecule. The zero-field splitting parameters have been reproduced by a theoretical calculation assuming the dipolar interaction of the electron spins one on the n-orbital at the 7-position and the other delocalized on the Hückel π-framework.

References

1) See V-A-4.
2) E. Wasserman, V.J. Kuck, W.A. Yager, R.S. Hutton, F.D. Greene, V.P. Abegg, and W.M. Weinshenker, *J. Am. Chem. Soc.*, **93**, 6335 (1971).

V-A-6 Time-Resolved Spectroscopic Studies on the Reaction of Conformationally Fixed *o*-(9-Fluorenyl)phenylnitrenes

Shigeru MURATA, Tadashi SUGAWARA, Nobuaki NAKASHIMA,[1] Keitaro YOSHIHARA,[1] and Hiizu IWAMURA

[*Tetrahedron Lett.*, **25**, 1933 (1984)]

Previously we were able to demonstrate the contrasting chemical and spectroscopic behaviors of two rotameric *ap*- and *sp*-9-(2-azido-4,6-dimethylphenyl)fluorenes (**3ap** and **3sp**) at cryogenic temperature.[2] Laser-flash photolysis studies (an excimer laser, 248nm, 12ns, <50mJ) have now been carried out on a solution of **3ap** and **3sp** in methanol-ether at 25°C. The rates of formation of azanorcaradiene (**5**) from *ap*-nitrene (**4ap**) and of 9-methoxyfluorene (**7**) from *o*-quinoid intermediate (**6**) were determined. The results are contained in Scheme I. The deuterium isotope effect in the

Scheme 1

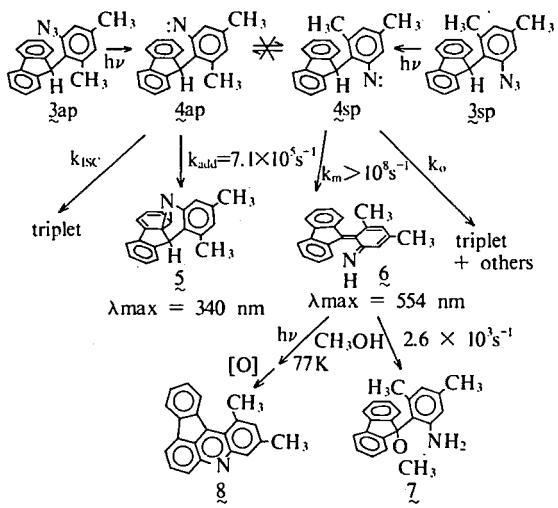

hydrogen migration reaction **4sp** → **6** was estimated to be 1.84. The remarkably higher ratio obtained previously at cryogenic temperature is now understood in terms of a tunneling mechanism.

References

1) Department of Electronic Structure.
2) S. Murata, T. Sugawara, and H. Iwamura, *J. Am. Chem. Soc.*, **105**, 3723 (1983); *IMS Ann. Rev.*, 111 (1983).

V-A-7 An Unusual Photoproduct of *o*-Azidobiphenyl with Tetracyanoethylene. Trapped 2-Azacycloheptatrienylidene

Shigeru MURATA, Tadashi SUGAWARA, and Hiizu IWAMURA

[*J. Chem. Soc., Chem. Commun.*, 1198 (1984)]

When *o*-azidobiphenyl was photolyzed in acetonitrile in the presence of TCNE, a 1:1 adduct of *o*-nitrenobiphenyl with TCNE was obtained in 35% yield. An X-ray crystal structure analysis revealed the adduct ($C_{18}H_9N_5$, monoclinic, $P2_1/a$, $Z = 4$, $a = 19.964(2)$, $b = 8.421(1)$, $c = 9.126(1)$ Å; $\beta = 92.35(1)°$; $V = 1533.0(3)$ Å^3; $D_c = 1.29$ g/cm^3) to be 4-aza-1,1,2,2-tetracyano-9-phenylspiro-[2.6]nona-4,6,8-triene as shown in Figure 1. The unusual 2*H*-azepine ring assumes nearly a boat form. The inversion of the ring in solution is slow in an NMR time scale since all the four cyano carbons are inequivalent in ^{13}C NMR. Just as cycloheptatrienylidene is trapped by electrophilic olefins to

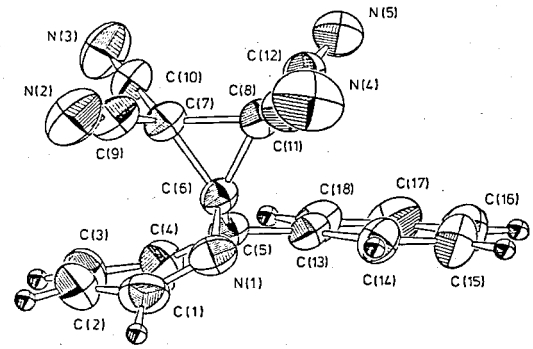

Figure 1. Molecular structure of the title compound. Carbon and nitrogen atoms are shown as 50% probability surfaces and hydrogens are displayed as arbitrary spheres.

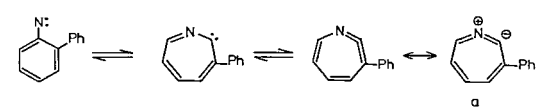

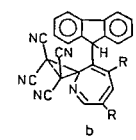

give spiro[2.6]nona-4,6,8-trienes,[1] the present adduct is considered formally to be formed via 2-aza-7-phenylcycloheptatrienylidene trapped by TCNE. Alternatively, the formation of the adduct could be reasoned by way of an electrophilic reaction of TCNE with azacycloheptatetraene which has a canonical structure a. A similar TCNE adduct obtained from 2-(9-fluorenyl)phenyl azide is now thought to have structure b.[2]

References

1) W.M. Jones and C.L. Ennis, *J. Am. Chem. Soc.*, **91**, 6391 (1969); E.E. Waali and W.M. Jones, *ibid.*, **95**, 8114 (1973).
2) S. Murata, T. Sugawara, and H. Iwamura, to be published elsewhere.

V-A-8 π-Electron Density Distribution in Benz[*a*]indeno[1,2,3-*cd*]azulene and the Corresponding Azepinium Ion

Shigeru MURATA and Hiizu IWAMURA

[*Bull. Chem. Soc., Jpn.* **57**, 1697 (1984)]

Recently we found a facile access to the dibenzo derivative (**1**) of cyclopent[*cd*]azulene via the photorearrangement of 1-alkoxytriptycenes.[1] The corresponding azepinium salt (**2**) was also obtained by the hydride abstraction of the similar photoproduct of 1-azatriptycene.[2] Since **1** and **2** proved to be interesting donor molecules, their π-electron density distributions have been calculated by the PPP MO method. The results are collected in Table 1. We note that the charge density at the positive nitrogen center (position 3) is effectively neutralized by carbon atoms 2, 4 and 12. Dibenzo annellation has the effects of reducing the dipolar character and increasing the bond alternation in the 7-membered ring. An operational test for the validity of the calculated charge distributions is provided by the ^{1}H NMR data for **1** and **2**. Plots of the chemical shifts of the nonbenzenoid hydrogens 4~7 vs. the calculated π-electron densities gave a line with the slope of ca. 10 ppm/π-electron.

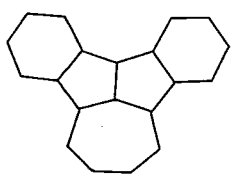

1

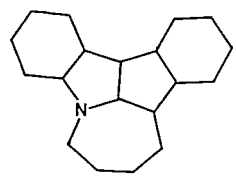

2

References

1) Y. Kawada, H. Tukada, and H. Iwamura, *Tetrahedron Lett.*, **21**, 181 (1980).
2) T. Sugawara and H. Iwamura, *J. Am. Chem. Soc.*, **102**, 7134 (1980).

Table I. π-Electron densities and bond orders of dibenzocyclopent[*cd*]azulenes

carbon atom	π-electron densities 1	2	bond	π-bond orders 1	2
1	0.971	0.977	1- 2	0.568	0.550
2	1.057	1.018	1-11	0.413	0.424
3	0.933	1.151	2- 3	0.406	0.453
4	0.956	0.840	3-12	0.408	0.441
5	0.968	0.991	3- 4	0.686	0.675
6	0.968	0.930	4- 5	0.591	0.546
7	0.956	0.969	5- 6	0.704	0.729
8	0.933	0.898	6- 7	0.591	0.568
9	1.057	1.063	7- 8	0.686	0.705
10	0.971	0.958	8- 9	0.406	0.401
11	1.118	1.120	8-12	0.408	0.376
12	1.069	1.032	9-10	0.568	0.565
13	0.993	0.998	10-11	0.413	0.403
14	1.025	1.026	11-12	0.687	0.684
15	0.993	1.000	2-13	0.594	0.570
16	1.013	1.015	13-14	0.701	0.709
17	0.993	0.998	14-15	0.624	0.618
18	1.025	1.026	15-16	0.702	0.704
19	0.993	0.986	1-16	0.595	0.593
20	1.013	1.013	9-17	0.594	0.599
			17-18	0.701	0.696
			18-19	0.624	0.628
			19-20	0.702	0.696
			10-20	0.595	0.601

V—B Stereochemical Consequences of the Non-bonded Interactions in Overcrowded Molecules

Disrotatory coupling of the internal rotational degrees of freedom in double rotor molecules has been designed and achieved in bis(9-triptycyl)methanes (Tp_2CH_2) and bis(9-triptycyl) ethers (Tp_2O). These molecules undergo rapid internal rotation in a strictly gear-meshed fashion, giving rise to new stereoisomerism in the tooth-labeled compounds. The racemic and meso isomers due to different phase relationship between the substituted benzene rings were separated by HPLC. The high energy barrier to the gear-slipping process was obtained as 33 and 43 kcal mol^{-1} for Tp_2CH_2 and Tp_2O, respectively, by the isomerization study. One last remaining question is how fast the gear-meshing process takes place and how high is the barrier to that torsional motion. Since the barrier height appeared to be too low to determine by the NMR line-shape analysis, we prepared a Tp_2O derivative carrying the naphthalene chromophore on one Tp unit and the *tert*-amino group on the other. Analyses of the exciplex fluorescence dynamics of this molecule disclosed the rate and activation energy of the geared rotation.

V-B-1 Preparation of a Bis(9-triptycyl) Ether Derivative Exhibiting Intramolecular Exciplex Fluorescence

Noboru KOGA and Hiizu IWAMURA

In order to disclose the rate of geared rotation in bis(9-triptycyl) ether (Tp_2O) in fluid solution by

Scheme 1

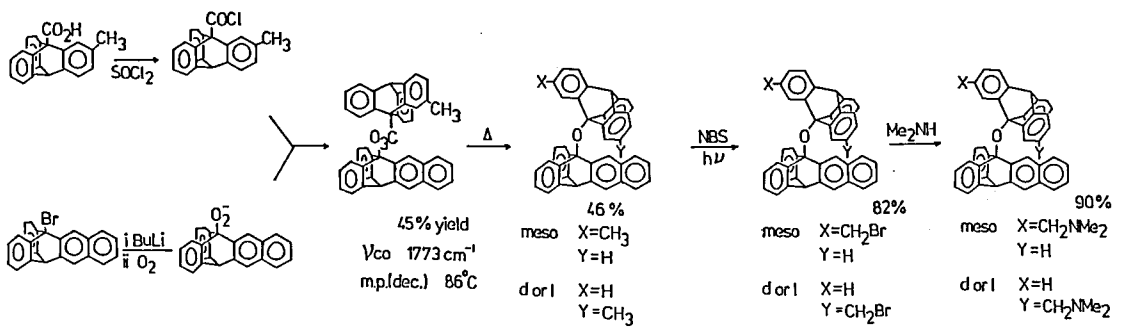

means of exciplex fluorescence dynamics, a Tp_2O derivative carrying an aliphatic *tert*-amino group (D) on one Tp unit and the naphtho chromophore (A) on the other has been prepared by a series of reactions as summarized in Scheme 1. When excited at 290 nm, the meso isomer showed typical fluorescence due to A* in the 320-360 nm region, showing there is no conformation available for this isomer in which D and A come next to each other. The racemic isomer showed characteristic exciplex fluorescence (EX) at longer wavelength (max at 412 nm in *n*-butyl ether) in addition to the weakened fluorescence (LE) due to A*. Since there is no D/A interaction in the ground state as shown by the normal absorption spectra, the exciplex formation in the racemic compound indicates that, when A* is formed by light absorption, internal rotation takes place during the lifetime of A* to bring D to the proximity and generate D·A* complex. Plots of $\log(\Phi_{EX}/\Phi_{LE})$ vs $1/T$ gave the activation energy of 3.8 kcal mol^{-1} and the enthalpy of the D·A* formation of −6.1 kcal mol^{-1} from the slopes of the low and high temperature limits, respectively. The former value is considered to be a good measure of the barrier height to the gear-meshing process of Tp_2O.

V-B-2 Kinetics of Intramolecular Exciplex Formation in 9-(2-(*N*,*N*-Dimethylaminomethyl)-9-triptycyloxy)-2,3-benzotriptycene

Noboru KOGA and Hiizu IWAMURA

The Tp_2O derivative exhibiting intramolecular exciplex fluorescence (see V-B-1) has been studied with the single-photon counting technique. The kinetics of the intramolecular exciplex formation can be described as shown in Scheme 1. In the case of δ excitation with the pulsed light, the time dependence of the emission of the locally excited state $I_{LE}(t)$ and the exciplex $I_{EX}(t)$ are given by

$$I_{LE}(t) = C_1(e^{-\lambda_1 t} + Ae^{-\lambda_2 t})$$
$$I_{EX}(t) = C_2(e^{-\lambda_1 t} - e^{-\lambda_2 t})$$

where λ_1 and λ_2 are observable decay constants and functions of k_3, k_4, k_7 and k_8. By assuming that the k_7 value should be equal to that of the meso isomer, the k_3, k_4 and k_8 values of the racemic compound was obtained from the observed λ_1 and λ_2. In *n*-butyl ether at 10°C, $k_3 = 9.0 \times 10^8 s^{-1}$. From the Arrhenius plots, we obtained $E_3^a = 4.2$, $E_4^a = 8.5$, $E_8^a = 1.0$, $\Delta H° = -4.2$ kcal mol^{-1} and $\Delta S° = -13$ e.u. The E_3^a value is thought to be the activation energy which is closely related to the height of the barrier to geared rotation in the Tp_2O double rotor.

Scheme 1

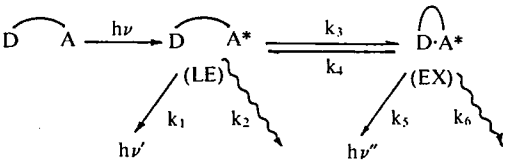

$$k_7 = k_1 + k_2$$
$$k_8 = k_5 + k_6$$

V—C Structural and Mechanistic Studies Aided with NMR

A stereoelectronic effect has been studied for the hydrogen abstraction reaction at the anomeric center of pyranose model compounds. The results were in parallel with the ^{13}C-H spin-spin coupling data. The pyramidal structure of the intermediate radical was confirmed by the α-^{13}C hyperfine coupling constants on the enriched samples. An extremely high quantum efficiency has been found for the photoisomerization of a *cis*-stilbazole salt in anionic micellar solutions. Ion pairing of the stilbazole cations with the SDS anions in the micelles has been demonstrated by measuring the ^{23}Na NMR relaxation rates.

V-C-1 The Anomeric Effect in Hydrogen-Abstraction Reactions of Conformationally Fixed 2-Alkoxytetrahydropyrans

Ronald D. MCKELVEY[1] and Hiizu IWAMURA

The relative reactivities of axial and equatorial hydrogens in 2-alkoxytetrahydropyrans toward abstraction by benzophenone triplet were determined. Thus cis-trans mixtures of 2-methoxy-*cis*-4,6-dimethyltetrahydropyran (**3**), 2-ethoxy-*cis*-4,6-dimethyltetrahydropyran (**4**), 6-*t*-butyl-2-methoxytetrahydropyran (**5**), and 2-isobutoxy-6-*t*-butyltetrahydropyran (**6**) were irradiated with benzophenone in benzene. The relative rates of disappearance of the starting materials were used to obtain the cis/trans reactivity ratios according to Eq. 1.

$$k_{cis}/k_{trans} = \ln([cis]/[cis]_0)/\ln([trans]/[trans]_0) \quad (1)$$

The results are summarized in Table I. The ratios 10-16 are considered to be representative of the anomeric effect in undistorted 2-alkoxytetrahydrofurans. The higher ratios are due to stereochemical effects from distortions caused by the *t*-butyl group on the ring. The lower value for 2-methoxy-4-methyltetrahydrofuran (**1**) in the literature[2] may not be representing the rate ratio, since a single methyl group cannot be enough to keep the compound in a single conformation. Thus the cis isomer might spend some of its time in the less reactive diaxial conformation, while the trans isomer might derive some of its reactivity from the minor alternative chair conformation.

Table I. Relative Rates of Hydrogen Abstraction

	R	R_4	R_6	k_{cis}/k_{trans}
1	CH_3	CH_3	H	8.0[2]
2	CH_3	H	CH_3	10.0[2]
3	CH_3	CH_3	CH_3	16.0
4	C_2H_5	CH_3	CH_3	10.6
5	CH_3	H	*t*-Bu	49
6	*i*-Bu	H	*t*-Bu	36

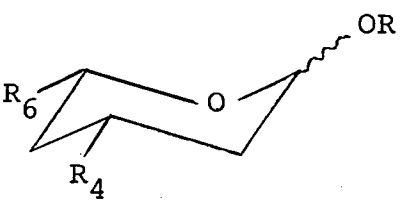

References

1) JSPS Invited Foreign Scholar 1983 from the University of Wisconsin–La Crosse.
2) K. Hayday and R.D. McKelvey, *J. Org. Chem.*, **41**, 2222 (1976); B.W. Babcock, D.R. Dimmel, D.P. Graves, Jr., and R.D. McKelvey, *ibid.*, **46**, 736 (1981)

V-C-2 The Structure at the Anomeric Center in 2-Alkoxytetrahydropyrans and Their Radicals, Studied by ^{13}C Coupling in NMR and ESR Spectra

Ronald D. MCKELVEY,[1] Tadashi SUGAWARA, and Hiizu IWAMURA

[*Org. Magn. Reson.*, in press]

Several 2-alkoxytetrahydropyrans labeled with ^{13}C in the 2-position were prepared by hydroboration-carbonylation (with ^{13}CO) of the protected 3-buten-1-ol derivatives (see Scheme 1). The ESR spectra were measured for the corresponding 2-alkoxy-

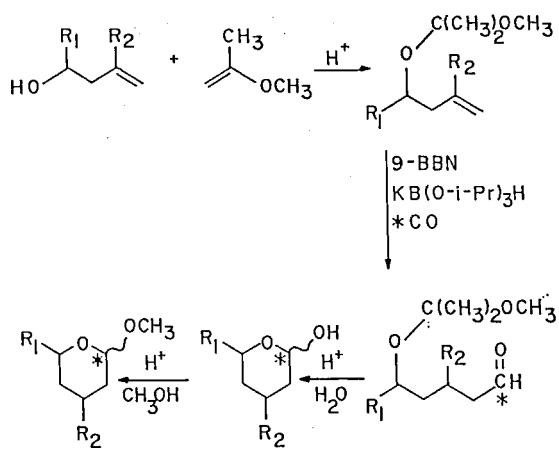

Scheme 1. Synthesis of ^{13}C-labelled 2-Methoxytetrahydropyrans.

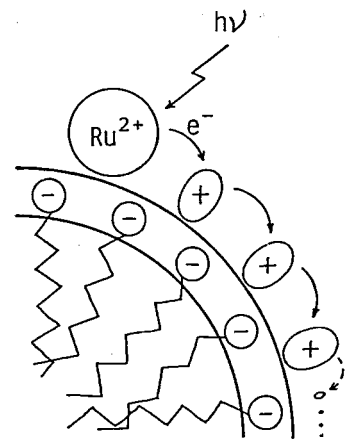

Figure 1. A schematic picture for electron-relay chain reaction. Ru^{2+} and + represent $Ru(bpy)_3^{2+}$ complex and *cis*-4-MSPI molecules on a SDS micelle, respectively.

tetrahydropyran-2-yl radicals produced by the reaction with the *t*-butoxyl radical. The hyperfine coupling constant to carbon was 99 ± 0.5 gauss. The deviation from planarity for these radicals was estimated to be approximately 11°, with sigma bond angles of 116°. The s-character of the singly occupied orbital was approximately 8.1%.

Anomeric, one bond ^{13}C-H NMR coupling constants were also determined. Axial hydrogens had coupling constants of approximately 155 Hz, while equatorial hydrogen coupling constants were ca. 164 Hz. These values were interpreted in terms of greater s-character in the equatorial C-H bonds. This could be caused by greater ring C-O double bond character when alkoxy is axial, through no-bond resonance to the exocyclic alkoxy group.

Reference

1) JSPS Invited Foreign Scholar 1983 from the University of Wisconsin–La Crosse.

V-C-3 Electron-Relay Chain Mechanism in the Sensitized Photoisomerization of Stibazole Salts in Aqueous Anionic Micelles

Katsuhiko TAKAGI *(Nagoya Univ.)*, **Keitaro AOSHIMA** *(Nagoya Univ.)*, **Yasuhiko SAWAKI** *(Nagoya Univ.)*, **and Hiizu IWAMURA**

[*J. Am. Chem. Soc.*, in press]

Cis to trans isomerization of *N*-methyl-4-(β-styryl)pyridinum halide(4-MSPX, X = I or Cl) via electron-transfer sensitization with $Ru(bpy)_3^{2+}$ has been studied for some micellar systems under irradiation at 468 ± 5 nm. Efficiencies for the isomerization($\Phi_{c\to t}$) were markedly enhanced by addition of anionic surfactants; e.g., the quantum yields in the presence of sodium dodecylsulfate (SDS) reached to a maximum value of 64 ± 2, which was about 100-fold as much as that without SDS. The value is comparable to the aggregation number, N_A, of the SDS micelle, involving the pyridinium ions equal to SDS molecules. Similar agreements between N_A and $\Phi_{c\to t}$ values were observed with micelles of other anionic surfactants $CH_3(CH_2)_nOSO_3Na$ (n = 9 and 13). It is postulated that an electron-relay chain mechanism is operative on the anionic micellar surface for sensitized isomerization of pyridinium ions attached electrostatically (Figure 1). The line width of ^{23}Na nmr for aqueous SDS solution decreased from 16 Hz to 7 Hz by the addition of 0.01 M *cis*-4-MSPI, indiating that 4-MSP ion effectively substitutes the Na^+ ion adsorbed on SDS micelles. An overwhelming high adsorptivity of 4-MSP ion on anionic micelles over Na^+ ion was also evidenced by the effects of various added salts in the reaction mixture.

V—D CO_2 Uptake by Tetraazacycloalkane Complexes

Coordination of CO_2 to a transition metal complex and reactions of the resulting complex have been of interest in connection with the utilization of CO_2. Besides direct coordination of CO_2 to transition metals with its intact form, many insertion reactions of CO_2 into an M-X bond (X = H, C, O, N) have been reported. We have found new systems of divalent metal complexes containing tetraazacycloalkanes (L) shown below, which take up CO_2 as $ROCO_2^-$, $RR'NCO_2^-$, or $HOCO_2^-$. The CO_2 up-take reactions described herein are of the type that tetraaza macrocyclic complexes (ML^{2+}) take up $ROCO_2^-$, $R_2NCO_2^-$, or $HOCO_2^-$, which have been produced from CO_2 in solution in the presence of base (B). The reaction involves the increase in coordination number of metal ion from four to five or six and is described as follows.

$$ML^{2+} + CO_2 + XH \xrightarrow[B]{} M(O_2CX)(L)^+ + BH^+ \qquad (1)$$

where XH = ROH, R_2NH, or H_2O. The starting complex ML^{2+} is of the square-planar type, while the coordination geometry of the resulting complex is octahedral or trigonal bipyramidal. Unsaturated coordination of the starting ML^{2+} makes this type of reactions possible. We have studied complexes of Ni^{2+}, Zn^{2+}, and Cd^{2+} which often show the required coordination behavior. From the CO_2 uptake reactions, X-ray structures of the products, and solution behaviors by means of NMR, roles of metal ion and macrocyclic ligand have been studied in connection with coordination stereochemistry.

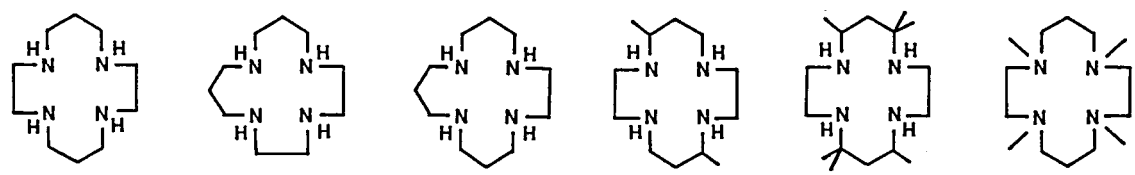

[14]aneN$_4$ iso-[14]aneN$_4$ [15]aneN$_4$ Me$_2$[14]aneN$_4$ Me$_6$[14]aneN$_4$ Me$_4$[14]aneN$_4$

V-D-1 Monoalkylcarbonato(tetraazacycloalkane)zinc(II) Complexes

Masako KATO and Tasuku ITO

Zn(II)-tetraazacycloalkane complexes take up CO_2 in alcohol very easily and reversibly at room temperature to fix it into resulting complexes as monoalkyl carbonate. A series of Zn(II)-monoalkylcarbonato complexes, Zn(L)(O_2COR)(ClO_4) (L = [14]aneN$_4$, [15]aneN$_4$, Me$_2$[14]aneN$_4$, Me$_4$-[14]aneN$_4$; R = CH_3, Et) and {Zn(L)}$_3$(O_2COR)$_2$(ClO_4)$_4$ (L = [15]aneN$_4$; R = n–Bu), have been obtained from the reactions with CO_2 and characterized by IR and NMR spectroscopies. Generally, addition of base such as NaOR or NEt_3 facilitates the uptake reaction of CO_2. In systems of methanol solution of the [14]aneN$_4$ or [15]aneN$_4$ complex, the reaction proceeds spontaneously in a neutral solution below *ca.* 10°C, CO_2 being taken up from the air. The monoalkylcarbonato complex (Zn-O_2COR) existes in organic solvent such as chloroform and dichloromethane in equilibrium with its decarboxylated Zn-OR complex (Figure 1).

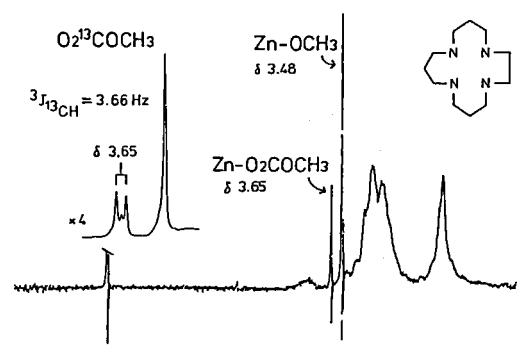

Figure 1. ^{1}H NMR spectrum of Zn([15]aneN$_4$)(O_2COCH$_3$)(ClO_4) in $CDCl_3$.

The equilibrium involves reversible desorption and absorption of CO_2. A decrease in temperature makes the equilibrium shift toward the increase in the amount of the Zn-O_2COR complex. For the [15]aneN$_4$ system, the equilibrium constant (K = [Zn([15]aneN$_4$)O_2COCH$_3$] / [Zn([15]aneN$_4$)OCH$_3$] [CO_2]) is found to be $K_{20.2°C}$ = 5.8 M^{-1}. The monoalkylcarbonato ligand has been converted into dialkyl carbonate by treating with FSO_3R (R = CH_3 or Et).

V-D-2 N,N-Dialkylcarbamato Complexes of Nickel(II), Zinc(II), and Cadmium(II)-tetraazacycloalkanes Derived from Reaction with CO_2 and N,N-Dialkylamines

Haruko ITO *(Aichi Kyoiku Univ.)* **and Tasuku ITO**

Nickel(II), Zinc(II), and Cadmium(II) complexes of certain tetraazacycloalkanes(L), [ML]$(ClO_4)_2$: M = Ni^{2+}, L = Me$_4$[14]aneN$_4$ and *rac*-Me$_6$[14]aneN$_4$; M = Zn^{2+} and Cd^{2+}, L = Me$_4$[14]aneN$_4$, take up CO_2 as $R_2NCO_2^-$, to give carbamato complexes $M(L)(O_2CNR_2)^+$. The carbamato complexes are obtained *via* either route (A) or (B),

$$\text{(A)}\quad ML^{2+} + CO_2 + 2R_2NH \longrightarrow M(O_2CNR_2)L^+ + NH_2R_2$$

$$\text{(B)}\quad M(O_2CX)L^+ + R_2NH \longrightarrow M(O_2CNR_2)L^+ + HX$$

where X = CH_3O^- or OH^- (see preceding section for X = CH_3O^-). The carbamato complexes thus obtained are listed in Table I, along with monoalkylcarbonato complexes obtained in the series of study (cf. V-D-1). The reaction through route (B) proceeded much easily and cleanly. Carbamato complexes were obtained with Me$_4$[14]aneN$_4$ and *rac*-Me$_6$[14]aneN$_4$ in the α-form, while macrocyclic ligands which hardly fold did not work at all.

X-ray analysis of [Ni(O_2CNEt$_2$)(*rac*-Me$_6$[14]-aneN$_4$)]ClO_4 shows that it is a discrete six-coordinate complex with *cis*-NiO_2N_4 geometry.

These results indicate that use of tetraazacycloalkane which folds readily is essential for CO_2 uptake as $R_2NCO_2^-$.

Table I List of $M(L)(O_2CX)^+$ Prepared and Characterized†

ROCO$_2^-$ Complexes

Zn(L)(O_2COR)(ClO_4)
- L = [14]aneN$_4$: R = Me*, Et
- L = [15]aneN$_4$: R = Me, Et
- L = Me$_2$[14]aneN$_4$: R = Me
- L = TMC : R = Me*, Et
- L = iso-[14]aneN$_4$: R = Me

{Zn(L)}$_3$(O_2COR)$_2$(ClO_4)$_4$
- L = [15]aneN$_4$: R = Me*, n-Bu

Cd(L)(O_2COR)(ClO_4)
- L = TMC : R = H*, Me

Ni(L)(O_2COR)(ClO_4)
- L = [14]aneN$_4$: R = Me
- L = [15]aneN$_4$: R = Me
- L = TMC : R = Me*
- L = iso-[14]aneN$_4$: R = Me

Ni(L)(H_2O)(O_2COR)(ClO_4)
- L = CTH : R = Me, Et

Ni(L)(O_2COR)$_2$
- L = TMC : R = Me*

$R_2NCO_2^-$ Complexes

Zn(L)(O_2CNR$_2$)(ClO_4)
- L = TMC : R = Me, Et

Cd(L)(O_2CNR$_2$)(ClO_4)
- L = TMC : R = Me, Et

Ni(L)(O_2CNR$_2$)(ClO_4)
- L = TMC : R = Me, Et
- L = CTH : R = Me*, Et, n-Pr, n-Bu

† TMC and CTH stand for Me$_4$[14]aneN$_4$ and *rac*-Me$_6$[14]aneN$_4$, respectively.
* X-ray structure available.

V-D-3 Structural Aspects of the CO_2 Uptake by Tetraazacycloalkane Complexes

Tasuku ITO, Masako KATO, and Haruko ITO
(Aichi Kyoiku Univ.)

In order to determine the coordination stereochemistries of the $M(L)(O_2CX)$ complexes formed upon CO_2 uptake and to investigate therefrom structural factors upon the efficient CO_2 uptake, single crystal X-ray analyses have been carried out on seven such compounds: $Zn([14]aneN_4)(O_2COCH_3)ClO_4$, $\{Zn([15]aneN_4)\}_3(O_2COCH_3)_2(ClO_4)_4$, $Zn(Me_4[14]aneN_4)(O_2COCH_3)ClO_4$, $Ni(Me_4[14]aneN_4)(O_2COCH_3)ClO_4$, $Ni(Me_4[14]aneN_4)(O_2COCH_3)_2$, $Cd(Me_4[14]aneN_4)(O_2COH)ClO_4$, Ni (*rac*-$Me_6$[14]aneN$_4$)$(O_2CNEt_2)ClO_4$. It turned out, complemented with IR and NMR spectral studies, that the $M(L)(O_2CX)$ complexes are structurally calssified into four groups, A-D. Figure 1 shows examples of each structural type.

Efficiency of the uptake reaction of XCO_2^- by ML^{2+} depends on choice of metal ion and/or macrocyclic ligand as well as coordination geometry of $M(L)(O_2CX)^+$. They are deeply related to one another. In the case of Zn(II), which is superior as to the efficiency among the metal ions studied, its driving force results from "*square-planar*" geometry of the starting $Zn(L)^{2+}$. Such the coordination environment is very rare for Zn(II) and is built up successfully by the use of tetraazacycloalkane with an appropriate cavity size.

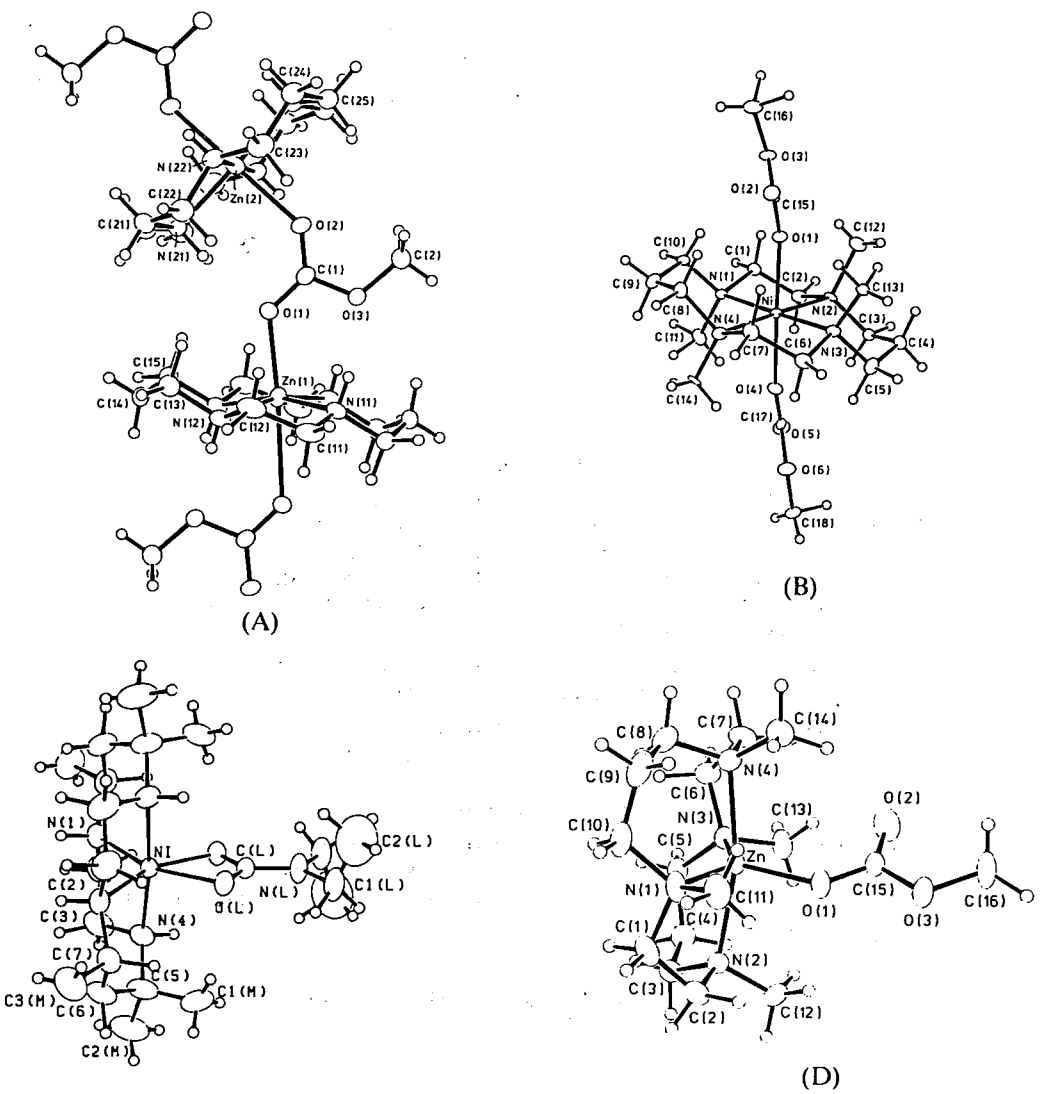

Figure 1. Examples of four structural types of the $M(L)(O_2CX)$ complexes: (A), $Zn([14]aneN_4)(O_2COCH_3)^+$; (B), $Ni(Me_4[14]aneN_4)(O_2COCH_3)_2$; (C), $Ni(rac\text{-}Me_6[14]aneN_4)(O_2CNEt_2)^+$; (D), $Zn(Me_4[14]aneN_4)(O_2COCH_3)^+$.

V—E One-Dimensional Halogen Bridged Ni(II)-Ni(IV) Mixed Valence Complexes

One-dimensional M(II)-M(IV) mixed valence compounds (M = Pt, Pd, Ni) having a linear chain structure shown below, have attracted much interest in the field of solid state physics and chemistry, since one-dimensional structures of this type can be a good model for the Peierls-Hubbard theory in which an electron-phonon interaction is taken into account.

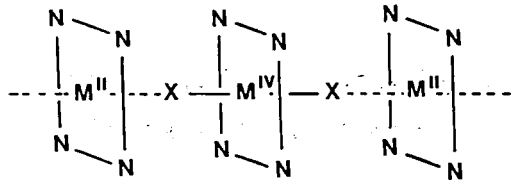

Previously, we prepared a new series of Pd and Ni analogs belonging to this class of compound and characterized them by means of X-ray analyses, XPS, electrical conductivities, and so on (see *IMS Ann. Rev.*, 119 (1983)). Syntheses and characterization of such compounds are the subject of our continued interest. Our studies along this line have now been extended to structural characterization of the Ni analog by means of EXAFS, since the Ni compounds do not afford single crystals suitable for X-ray work. Preliminary study by means of in-laboratory EXAFS was presented in *IMS Ann. Rev.*, (1983). In the present study, SOR-EXAFS was used so that informations of the one-dimensional structure can be obtained from both Ni-*K* edge and Br-*K* edge spectra.

V-E-1 Structural Study by Means of EXAFS

Koshiro TORIUMI, Toshiaki KANAO *(Kumamoto Univ.)*,[1] **Masahiro YAMASHITA, Yuji UMETSU** *(Kumamoto Univ.)*,[2] **Masako KATO, Akira OHYOSHI** *(Kumamoto Univ.)*, **and Tasuku ITO**

Detailed analyses of both Ni-*K* and Br-*K* edge EXAFS spectra measured with synchrotron radiation were carried out for Br-bridged Ni(II)-Ni(IV) mixed valence compounds: $[Ni([14]aneN_4)][NiBr_2([14]aneN_4)](ClO_4)_4$, $[Ni([15]aneN_4)][NiBr_2([15]aneN_4)](ClO_4)_4$, and $[Ni(chxn)_2][NiBr_2(chxn)_2](BF_4)_4$. Reference EXAFS were also observed for structurally known Ni(II) and Ni(III) complexes with similar coordination geometry: $[NiBr_2([14]aneN_4)]$ and $[NiBr_2([14]aneN_4)]ClO_4$. Figure 1 shows Fourier transform of Br-*K* edge EXAFS spectra measured at 80 K. All the spectra show a similar feature and contain four major peaks. They were assigned to Br-Ni, Br···N, Br···C, and Br-Ni-Br separations. The spectral pattern of the mixed valence compounds is consistent with the linear chain structure, though Ni(II)···Br separation has

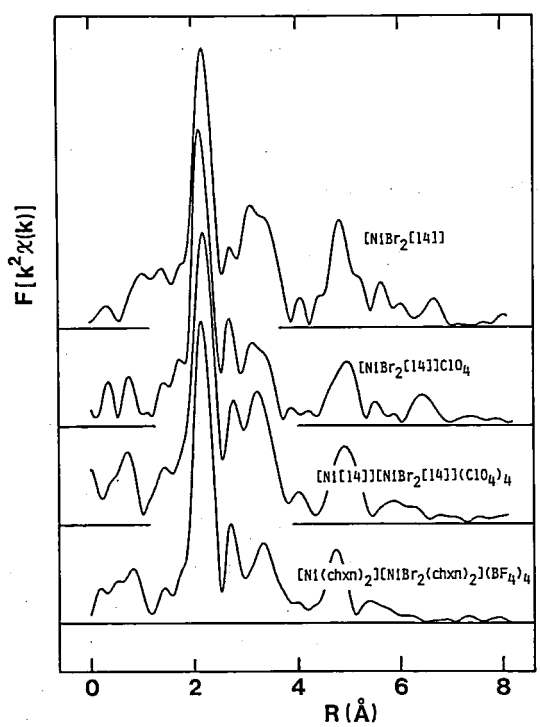

Figure 1. Fourier transform of Br-*K* edge EXAFS spectra.

not been observed clearly. Coordination bond distances of Ni-N and Ni-Br obtained by FABM analyses[3] vary in an expected way depending on the oxidation and/or spin states of Ni. Mean Ni-Br length of 2.64Å in the mixed valence compounds are distinctly shorter than corresponding value of Ni(II) complexes, but are comparable to that of Ni(III) complexes. This is due to electronic interaction along the chain. Contribution of Ni(II)···X in the mixed valence compounds to EXAFS would be small if any, because of essentially weak bonding nature of Ni(II)···X bond.

References

1) IMS graduate Student from Kumamoto University for 1983.
2) IMS graduate Student form Kumamoto University for 1984.
3) B.K. Teo, M.R. Antonio, and B.A. Averill, *J.Am. Chem. Soc.*, **105**, 3751 (1983).

V—F Organo-Aluminum Complexes of Tetra-aza Macrocyclic Ligands

The coordination chemistry of Al^{3+} with nitrogen containing ligands has not been extensively investigated because of their ease of hydrolysis and general lack of kinetic and thermodynamic stability relative to their transition metal counterparts. However, the radii of trivalent Al in a variety of systems is generally midway between that of high-spin and low-spin first-row transition metal complexes. According to the fundamental properties of macrocyclic ligands as first outlined by Busch, Al^{3+} macrocyclic complexes should be stable once obtained. It therefore appears that the lack of published results in this area relates to the anticipated difficulty in inserting Al^{3+} into the appropriate macrocyclic ligand. This perceived difficulty has been overcome by using trialkyl aluminum complexes as the source of Al^{3+} and macrocyclic ligands with two ionizable N-H protons in a non-reactive solvent. The resultant acid-base reaction generates two equivalents of ethane and concommitant insertion of Al into the macrocycle, forming an organo-aluminum complex. These organo-aluminum macrocyclic complexes provide a new entry into the field of aluminum macrocyclic chemistry. Areas which are of particular interest are the stability of the Al-C bond in constrained environments, the characterization of the Al-C bond rupture under thermal and photolytic conditions, and the electronic and molecular structure of the organo-aluminum complexes and their derivatives.

V-F-1 Synthesis and Reactivity of $Al(C_{22}H_{22}N_4)(C_2H_5)$

Virgil L. GOEDKEN *(Florida State Univ. and IMS)* **and Tasuku ITO**

[*J. Chem. Soc., Chem. Commun.*, in press]

Reaction of Al_2Et_6 in hexane solution with the dibenzotetraaza[14]annulene macrocycle, $C_{22}H_{24}N_4$, **I**, results in a two step insertion reaction first yielding the half-inserted species, $Al(C_{22}H_{23}N_4)Et_2$, **II**. Heating **II** in the solid state to 100° yields $Al(C_{22}H_{22}N_4)Et$ and ethane quantitatively. This complex is remarkably stable to Al-Et dissociation and also is resistant to demetallation. Heating the solid to 300° under inert atmosphere or recrystallization from hydroxylic or water containing solvents results in no decomposition. Cleavage of the Al-C bond does occur in acidic media, but the course of the reaction is acid dependent. Reaction with HCl produces the de-ethylated and protonated macrocyclic complex $[Al(C_{22}H_{24}N_4)Cl(H_2O)]Cl_2$ on mixing. However, perchloric acid protonates the methine carbons of the macrocycle first while protonation of the ethyl groups occurs relatively slowly and the loss of the ethyl group is easily followed by NMR spectroscopy. Dealkylation appears to be facilitated by protonation of the macrocycle, producing cationic $[Al(C_{22}H_{24}N_4)Et]^{2+}$ and coordination of nucleophiles such as Cl^- to the sixth position.

The Al-Et bond of **III** is photosensitive to visible light and undergoes homolytic bond cleavage as determined from the ESR signal of the trapped ethyl radical, when irradiated in the presence of spin trapping agents. Irradiation of **III** in $CHCl_3$ produces the chloro complex, $Al(C_{22}H_{22}N_4)Cl$, **VIII** and ethane. Hydrolysis of **VIII** yields the hydroxo

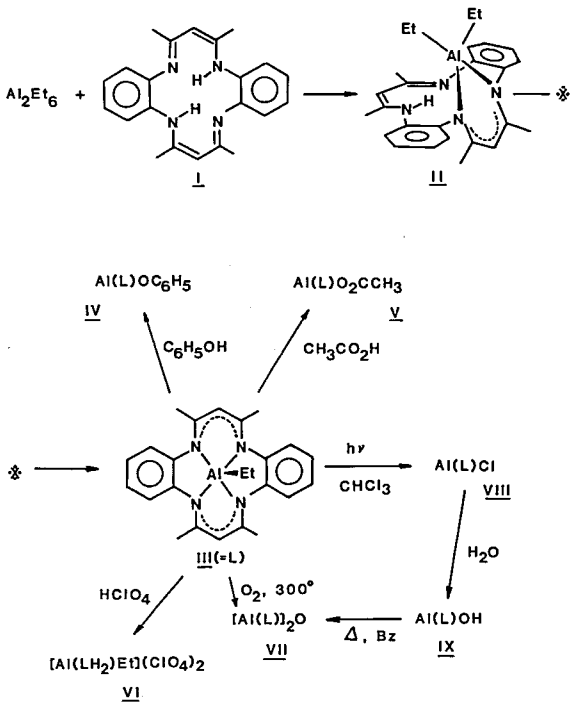

complex, **IX**. The μ-oxo complex **VII**, is obtained either from heating **III** to 300° in the presence of O_2 or from refluxing **IX** in benzene or toluene.

V-F-2 Crystal and Molecular Structure of $Al(C_{22}H_{22}N_4)(C_2H_5)\cdot 1/2C_6H_6$

Haruko ITO, Virgil L. GOEDKEN *(Florida State Univ. and IMS)*, **and Tasuku ITO**

[*J. Chem. Soc., Chem. Commun.*, in press]

The remarkable stability of the $Al(C_{22}H_{22}N_4)C_2H_5$ to thermal and acid degradation, together with the paucity of structural data for aluminum macrocyclic complexes, warrants a detailed study of its structure. Crystals of $Al(C_{22}H_{22}N_4)C_2H_5\cdot 1/2C_6H_6$ are orange and monoclinic, $P2_1/n$ with $a = 8.114(1)$, $b = 22.159(3)$, $c = 13.599(2)$ Å, $\beta = 92.90(2)$, $Z = 4$, $U = 2442.1(4)$ Å^3. Refinement with 2764 independent reflections ($2\theta<55°$) converged to conventional R values of $R = 0.048$ and $R_w = 0.054$. The crystal structure (Figure 1) reveals a five-coordinate square pyramidal coordination geometry and the usual saddle shape observed for this ligand. The average Al-N distance, 1.967Å, is close to that predicted from additivity of normal covalent radii and the Al-C distance, 1.976(3) Å is close to that of the terminal Al-C

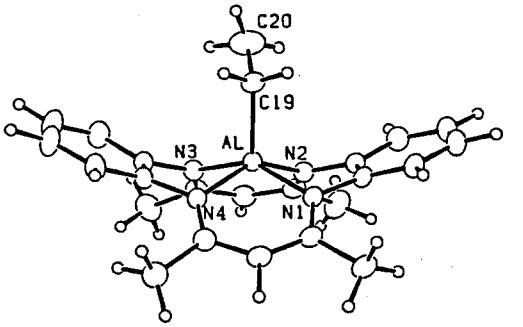

Figure 1. Structure of $Al(C_{22}H_{22}N_4)(C_2H_5)$.

distance, 1.970 Å observed for $Al_2(Me)_6$. The Al is displaced 0.57 Å from the N_4 plane and the N-Ct distance is 1.88 Å. These bond parameters are comparable to those observed for transition metal complexes of this ligand.[1] The M-N distances are shorter than found for high-spin five-coordinate Mn(II) and Fe(III) complexes (2.118 and 2.002 Å respectively) and longer than observed for a five-coordinate Co(III) complex, 1.901 Å. The stability of the Al-C bond of the title compound is attributed to kinetic factors. There are no accessible metal orbitals to facilitate β-elimination. Simple dissociation is prohibitive energetically and the complex shows no tendency to coordinate a sixth axial ligand which would weaken the Al-C bond.

Reference

1) M.C. Weiss, B. Bursten, S.M. Peng, and V.L. Goedken, *J. Am. Chem. Soc.*, **98**, 8021 (1976), and references cited therein.

V-F-3 ^{27}Al NMR Studies of Organo-Aluminum Complexes of Macrocyclic Ligands

Masako KATO, Virgil L. GOEDKEN *(Florida State Univ. and IMS)*, **and Tasuku ITO**

^{27}Al NMR is a potentially useful probe to study the chemical environment of the Al nucleus. Although the resonances are broad in nonsymmetrical environments, the large chemical shift dependence provides useful information for observed signals. The advent of high-field, sensitive spectrometers enables ^{27}Al NMR spectra to be taken quickly with solutions of moderate concentration.

We have recently prepared a series of organo-

aluminum macrocyclic complexes and their derivatives. The ligands differ in the extent of their conjugation and charge and range from the fully conjugated aromatic tetraphenylporphyrin to the fully saturated 14-membered tetraazacyclotetradecane (cyclam). ^{27}Al NMR spectra of these complexes have been measured to examine the following effects on the ^{27}Al chemical shift: 1) nature of the macrocycle, 2) coordination number, 3) nature of the axial ligand. Table I lists the metal complexes studied, the observed chemical shift, the halt-width of the resonance, and also the coordination number. Very large shifts are observed on going from four to five coordination, but significant chemical shifts are also with changes in the axial ligand. For these complexes, ^{27}Al NMR is a more sensitive probe of compound purity than ^{1}H NMR, and has also been a useful tool to follow the course of substitution reactions.

Table I. ^{27}Al NMR data

Compd.	Chem. Shift/ppm[a]	$\Delta\nu$/Hz	Coord. No.
Al_2Et_6	156	1.96×10^3	4
Al(TPP)Et	46	1.65×10^3	5
$Al(C_{22}H_{23}N_4)Et_2$	156	2.85×10^3	4
$Al(C_{22}H_{22}N_4)Et$	79	1.65×10^3	5
$Al(C_{22}H_{22}N_4)Cl$	58	849	5
$Al(C_{22}H_{22}N_4)OH$	58	208	5
$Al(cyclam)Et^{2+}$	52	369	5

[a] from $Al(NO_3)_3 \cdot 9H_2O$ in D_2O.

V-F-4 Detection of Ethyl Radicals and Aluminum Radicals Produced During the Homolytic Photochemical Cleavage of Al(TPP)Et and $Al(C_{22}H_{22}N_4)Et$

Shozo TERO, Masako KATO, Virgil GOEDKEN *(Florida State Univ. and IMS)*, **and Tasuku ITO**

The aluminum-carbon bonds of Al(TPP)Et and $Al(C_{22}H_{22}N_4)Et$ are sensitive to visible light and are believed to undergo homolytic Al-C bond rupture.[1,2] The radical species generated from this reaction, $^{\bullet}$Et and $^{\bullet}$Al(TPP) normally have a very short life in solution. We have applied the technique of spin trapping, using 2,4,6-tri-*tert*-butylnitrosobenzene (TBN), to characterize the identity of the ethyl radical and the here-to-fore unknown $^{\bullet}$Al(TPP) radical.

Photolysis of Al(TPP)Et with light (λ>420 nm) in the presence of TBN gave the ESR spectrum, in benzene, as shown in Figure la. Hyperfine splitting constants (hfs) of a^N = 1.34, a^H(2H) = 1.79 and a^H(2H) = 0.08 mT and g-value of 2.0061, obtained from this spectrum, are essentially the same as those of the previously reported TBN-Et adduct.[3] Irradiation with light in the range 300<λ<400 nm produced a new signal which consisted of a triplet of sextets with equal intensity (Figure lb). It is obvious that these splittings were caused by ^{14}N (I = 1) and ^{27}Al (I = 5/2) nuclei. Then a^N = 1.20, a^{Al} = 0.19 mT and g = 2.0049 are derived. These values are consistent with those expected for the aminyl radical rather than the normal nitroxide radical.

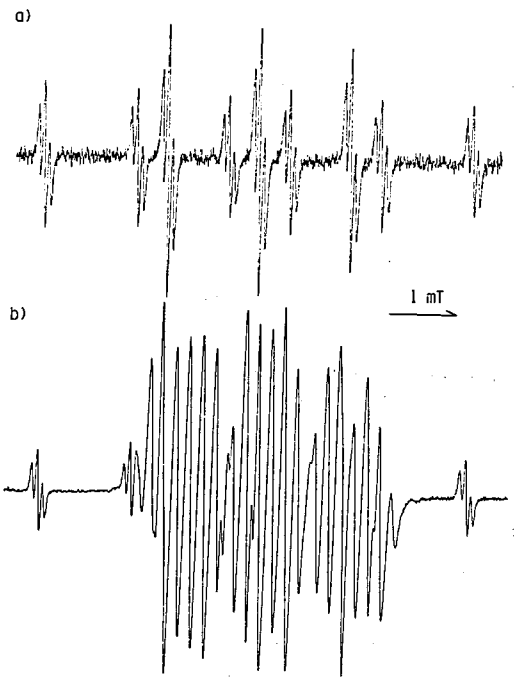

Figure 1. ESR spectra obtained from the photolysis of Al(TPP)Et with 2,4,6-tri-*tert*-butylnitrosobenzene(TBN). (a) TBN-Et adduct generated by the irradiation with light $\lambda > 420$ nm. (b) TBN-Al(TPP) adduct produced by the photolysis with light $300 < \lambda < 400$ nm.

References

1) H. Murayama, S. Inoue, and Y. Ohkatsu, *Chem. Lett.* **1983**, 381.
2) V. Goedken, H. Ito, and T. Ito, *J. Chem. Soc., Chem. Commun.*, in press.
3) S. Terabe, and R. Konaka, *J. Chem. Soc. Perkin II*, **1973**, 369.

V—G Syntheses and Mechanistic Studies of New Organometallic Compounds

Syntheses and mechanistic studies of new organometallic compounds with catalytic activities are the subject of continuing interest. Double carbonylation reactions promoted by palladium have been explored intensively.

V-G-1 Palladium-Promoted Double Carbonylation Reactions. Reactions of Organopalladium Compounds with Carbon Monoxide and Amines to Give α-Keto Amides

Fumiyuki OZAWA, Takeshi SUGIMOTO, Yasuhiro YUASA, Manoranjan SANTRA, Takakazu YAMAMOTO *(Tokyo Inst. of Tech.)*, **and Akio YAMAMOTO** *(Tokyo Inst. of Tech. and IMS)*

[*Organometallics*, **3**, 683 (1984)]

A variety of mono- and diorganopalladium complexes, *trans*-$PdR(X)L_2$ (R = Me, Et, and Ph; X = Cl, Br, I, and aryloxo; L = tertiary phosphine ligand) and *cis*-$PdMe_2L_2$, react with carbon monoxide and secondary amines under mild conditions to give α-keto amides as double carbonylation products. A series of acylpalladium complexes, *trans*-$Pd(COR)X(PMePh_2)_2$(R = Ph, X = Cl, Br, and I; R = Me, X = Cl), the presumed reaction intermediates, were prepared and their reactions with carbon monoxide and amines were investigated.

On the basis of these results, an ionic, CO-coordinated acylpalladium complex $[PhCOPd(CO)L_2]^+X^-$ (X = Br, I) was inferred as an active species in catalytic double carbonylation of phenyl bromide and iodide to undergo the nucleophilic attack of amines on the coordinated CO ligand liberating α-keto amides (Scheme 1).

Scheme 1

$$PhCOPd(X)L_2 \overset{CO}{\rightleftharpoons} [PhCOPd(CO)L_2]^+X^-$$

$$\overset{+2R_2NH}{\rightleftharpoons} PhCOPd(CONR_2)L_2$$

$$\overset{CO}{\longrightarrow} PhCOCONR_2 + PdL_n(CO)_m$$

V—H Nucleophilic Aromatic Photosubstitution

Exploratory and mechanistic studies have been carried out on the rearrangements, additions and substitutions of organic compounds initiated by electron transfer in the photo-excited state. A theory on the apparently erratic regioselectivity in the nucleophilic photosubstitutions of nitroanisoles has been proposed.

V-H-1 A Rationalization of Orientation in Nucleophilic Aromatic Photosubstitution[1)]

Kiyoshi MUTAI *(Univ. of Tokyo and IMS)* **and Ryoichi NAKAGAKI**[2)]

[*Chem. Lett.*, **1984**, 1537]

A mechanistic interpretation, consisting of two rules based upon frontier molecular orbital theory, has been presented for sometimes apparently conflicting regioselective behavior exhibited by nitroanisoles and thier analogs in nucleophilic aromatic photosubstitutions. The first rule is concerned with photoreactions accompanying direct addition of a nucleophile to an excited substrate whose HOMO and LUMO are both singly occupied. Interaction of these MO's with a nucleophile is more stabilizing for the HOMO, and regioselectivity is HOMO-controlled (eq 1).

$$ArH + :Nu \rightarrow ArH^* + :Nu \rightarrow \sigma\text{-complex} \quad (1)$$

The second rule is for the reactions involving photoinduced electron transfer from a nucleophile to the LUMO of a substrate, followed by recombination of a resultant radical ion pair (eq 2).

$$ArH + :Nu \xrightarrow{h\nu} ArH^* + :Nu \rightarrow ArH^{\cdot-} + Nu^{\cdot+} \rightarrow \sigma\text{-complex} \quad (2)$$

Thus the regioselectivity is LUMO-controlled. Application of these rules to photoreactions of nitroanisoles, nitroveratroles, and the photo-Smiles rearrangement of their analogs[1] has been discussed on the basis of mechanistic aspects. Validity of the rules has also been shown in newly designed naphthalene systems.

Reference

1) K. Mutai, *IMS Ann. Rev.*, 124, (1983).
2) Department of Electronic Structure.

V—I Thionitrosobenzene and Related Compounds

Kinetic stabilization of unstable functional groups is often effected by means of introduction of bulky substituents around the functional group. The strategy has now been applied to characterize the elusive thionitrosobenzene and related compounds.

V-I-1 Photoreaction of 2,4-Di-*t*-butyl-6-methyl-*N*-thiosulfinylaniline

Renji OKAZAKI *(Univ. of Tokyo and IMS)* **and Tadashi SUGAWARA**

The photoreaction of 2,4-di-*t*-butyl-6-methyl-*N*-thiosulfinylaniline (**1**) was studied by variable temperature electronic spectroscopy. The reactions carried out in EPA matrices at various tempertatures (77-300K) and concentrations in the presence or absence of oxygen suggested the following reaction mechanism involving thionitrosobenzene intermediate (**2**).

$$(Z)\text{-}1 \underset{\Delta}{\overset{h\nu}{\rightleftharpoons}} (E)\text{-}1$$

Ar = 2, 4-di-*t*-butyl-6-methylphenyl

$$(Z)\text{-}1 \text{ or } (E)\text{-}1 \xrightarrow{h\nu} Ar\text{-}N\begin{matrix}\diagup S \\ | \\ \diagdown S\end{matrix} \text{ or } Ar\text{-}N^+\begin{matrix}\diagup S^- \\ \diagdown\!\!\diagdown S\end{matrix}$$

$$\rightarrow Ar\text{-}N = S \begin{matrix}\diagup \\ \diagdown\end{matrix} \begin{matrix} Ar\text{-}N = S = O \\ Ar\text{-}N = S = N\text{-}Ar + ArNH_2 \end{matrix}$$

(2)

The photoisomerization of (Z)-**1** to (E)-**1** and thermal reversion of (E)-**1** to (Z)-**1** even at 140K indicate much greater stability of (Z)-**1** than (E)-**1**.[1] This was confirmed by an *ab initio* molecular orbital calculation (4-31G* RHF) using HNSS (**3**) as a model. Thus, (Z)-**3** was found to be 4.81 kcal mol^{-1} more stable than (E)-**3**.[2]

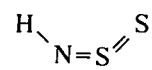

(Z)-3

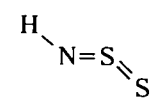

(E)-3

References

1) It has been established by X-ray crystallography that **1** exists as Z-form in the solid state. F. Iwasaki, *Acta Cryst.*, **B35**, 2099 (1979).
2) The calculation was performed by Professor Morokuma of Department of Theoretical Studies.

RESEARCH ACTIVITIES VI

Coordination Chemistry Laboratories

Coordination Chemistry Laboratories were established in April 1984 to facilitate the studies of coordination chemistry in wide sense, particularly in the interdisciplinary region between molecules and a variety of inorganic compounds. Laboratory of Synthetic Coordination Chemistry was transferred for the period of two years from Research Institute for Iron, Steel and Other Metals, Tohoku Univerisity ("Ryudo Bumon") to develop the synthesis of metal cluster complexes with characteristic physical and chemical properties. Laboratory of Complex Catalysis aims fundamental studies of complex catalysis with special reference to the relationship between homogeneous complex catalysis and heterogeneous metal surface catalysis. Present research plans are as follows.

VI-A Synthesis of Ternary Transition Metal Cluster Complexes

Humihiko TAKEI, Shin TSUNEKAWA, and Syoichi HOSOYA

Solid cluster complexes containing transition metal ions and non-metallic atoms or ions are synthesized by use of a newly designed multi-purpose high temperature furnace (up to 2500°C, 100 atm, sample size $\sim 10^1$g). The aimed compounds include modified Chèvrel-type compounds with hexamolybdenum core and calchogenide ions (*e.g.* $Mo_6Se_8^{(4-x)-}$), lanthanoid salts of boride clusters of platinum metals and solid clusters containing phosphide. Relationship among the stoichiometry, structure and characteristic properties will be discussed.

VI-B Synthesis and Characterization of Organometallic Complexes of Low-Valent Early Transition Metals

Akira NAKAMURA, Hajime YASUDA*, and Kazuyuki TATSUMI* *(Osaka Univ.*)*

π-Complexes of low-valent titanium, zirconium, niobium and tantalum are expected to be useful complex catalysis, but they are not well characterized. Synthesis of pure complexes of these elements with diens including cyclopentadiene is attemped under inert gas atmosphere, and their separation by high precision liquid chromatography (HPLC).

VI-C Kinetic Studies of Electron Transfer Reactions Involving Transition Metal Ions and Organic Radicals

Kazuo SAITO, Shozo TERO, Masahiro EBIHARA, and Yoichi SASAKI* *(Tohoku Univ.*)*

Kinetic studies of redox reactions of transition metal complexes are important for elucidating the mechanism of complex catalysis, but the mechanism is often made ambiguous by environmental effect including ion-pair formation and solvation. Organic radicals either stable or short-lived are good reducing agents without electric charge, and their reactions are followed by esr spectroscopy and stopped flow technique. For instance, it was found that the second order rate constant between 2,2,6,6-tetramethyl-l-piperidinyloxy (TMPNO) radical and μ-hyperoxo-μ-amidobis[bis(ethylenediamine)cobalt (III)] is independent of pH at 2.5 to 5.0 (5.2×10^4 $mol^{-1}dm^3s^{-1}$ at 24.8°C) and gives $\Delta H^{\neq} = 45$ kJ mol^{-1}, $\Delta S^{\neq} = -3.7$ J mol^{-1} K^{-1} and $\Delta V^{\neq}$ almost 0. These values are useful for discussing the participation of charge in solvation on encounter complex formation.

VI-D Structure and Lewis Acid-Base Reactions of Transition Metal Complexes with Hard Metal Ions and Soft Ligating Atoms

Kazuo KASHIWABARA, and Kiyohiko NAKAJIMA

When ligands with soft ligating atoms such as sulfur, selenium, phosphorus and arsenic form chelate complexes with transition metal ions with high electric charge, characteristic structure and chemical properties are observed. For instance *cis*-dichloro-bis[1,2-bis(dimethylphosphino)ethane]cobalt (III) undergoes geometrical isomerization under UV light, and the kinetics are followed by the usual method. Such studies provide useful information for discussing the mechanism of complex catalysis.

VI-E Detection of Alkyl Radicals Formed by Photochemical Homolysis of Organometallic Complexes

Shozo TERO, Masako KATO, Virgil GOEDKIN* *(Florida State Univ. USA* and IMS)*, **and Tasuku ITO**

cf. **V-F-4**

RESEARCH ACTIVITIES VII

COMPUTER CENTER

VII—A Theoretical Investigations of Metalloporphyrins by the *Ab Initio* SCF MO Method

Metalloporphyrin complexes are interesting polyatomic systems because of their complicated electronic structure and because of their catalytic function. Heme and chlorophyll are prominently important as an active center of energy conversion processes in biological systems. In this project the electronic structure and the fundamental functions are studied for several complexes by perfoming *ab initio* MO computations.

VII-A-1 *Ab Initio* MO Study on Relationships between the Electronic State and Out-of-Plane Displacement of the Iron Atom in Four-Coordinate Fe-Porphine

Minoru SAITO *(IMS and Nagoya Univ.)* **and Hiroshi KASHIWAGI**

Potential curves for the out-of-plane displacement of the iron atom were calculated on several ferrous and ferric states of four-coordinate Fe-porphine (FeP) by the *ab initio* SCF MO method. The calculated curves are shown in Figure 1. The equilibrium position of the iron atom is the center of the porphine plane for all the calculated states. The out-of-plane displacement of the iron atom in five-coordinate porphyrins is not due to the size of the central ion.

The force constant for the out-of-plane motion is directly proportional to the overlap population between the $d_{x^2-y^2}$ orbital and pyrrole-nitrogen orbitals, and also depends on the occupation number of the $d_{x^2-y^2}$ orbital and oxidation number of the iron atom, as follows, $Fe(II)(d_{x^2-y^2})^1 < Fe(III)(d_{x^2-y^2})^1 < Fe(II)(d_{x^2-y^2})^0 < Fe(III)(d_{x^2-y^2})^0$.

The out-of-plane displacements in Fe(III)(TPP)F^-, Fe(III)(TPP)$(OClO_3)^-$, and Fe(II)(TPP)$(SC_2H_5)^-$ were estimated by using the calculated potential curves of FeP and taking into account of the coulomb repulsion between the fifth ligand and pyrrole nitrogens. The estimated values were close to the experimental values of the three complexes. The origin of the out-of-plane displacement is mainly the repulsion between the fifth ligand and the pyrrole nitrogens.

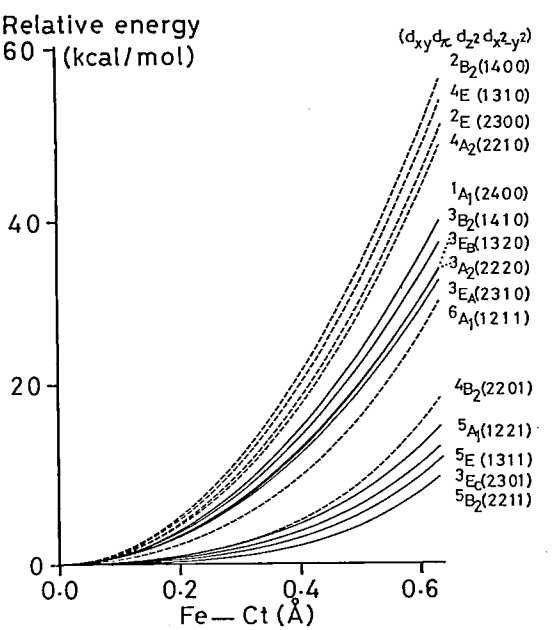

Figure 1. Potential energy curves as a function of the out-of-plane displacement (Fe-Ct) of the iron atom in Fe-porphine. (They are shifted to have zero energy at Fe-Ct = 0.)

VII-A-2 *Ab Initio* SCF-Cl Calculations on the Free Base Porphine and Chlorine

Unpei NAGASHIMA, Toshikazu TAKADA *(NEC)*, **Kiyoshi TANAKA** *(Hokkaido Univ.=*)*, **and Kimio OHNO** *(*)*

Chlorine is the skeletal part of chlorophyll which plays an important role in photosynthesis. The

photoabsorption coefficient of the lowest peak (so called Q_x) of chlorine is about fifty times greater than that of porphine as shown in Figure 1. An investigation on the origin of this difference is a staring point for understanding the mechanism of photosynthesis.

Ab initio SCF MO calculations were carried out on the ground states of porphine and chlorine with minimal basis sets by using JAMOL3 program. Then, configuration interaction (CI) calculations including single and double excitations rerative to several reference configuration state functions (CSFs) were performed by the use of COMICAL2 program. The number of CSFs was of the order of 30,000.

The lowest excitation energies are in good agreement with observed ones, and the second-fourth excitation energies are higher than corresponding observed ones by 1-2 eV. The oscillator strength of the lowest excitation agrees well with experimental data for both porphine and chlorine.

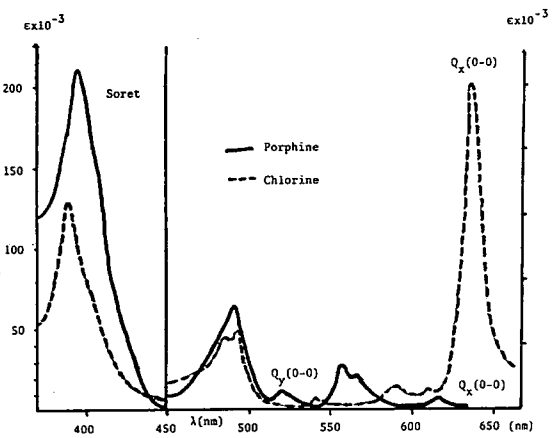

Figure 1. Absorption spectra of porphine and chlorine.

The difference in the absorption coefficient between the two molecules is originated by the reverse order of the two HOMOs and two LUMOs in the orbital energy, and by the distortion of these MOs in chlorine.

CHEMICAL MATERIALS CENTER

VII—B Isolation and Characterization of New Metallacycle Compounds

The preparation and study of metallacycle compounds is directly relevant to an understanding of the reaction mechanisms of many synthetically important catalysis such as olefin oligomerization, cyclocoupling, polymerization, and so on, and may also provide the basis for developments of new effective catalyst systems. In this project, we have been studying synthesis, isolation, and characterization of new metallacycle compounds.

VII-B-1 Synthesis and Reactions of New Titanacyclopentanes

Kazushi MASHIMA, and Hidemasa TAKAYA

Although many metallacycle compounds have been prepared and characterized so far, only a limited number of compounds of the elements of the first transition series have been reported. Titanacyclopentane (**1**) (Cp = cyclopentadienyl) collapses into 1-butene and ethylene in solution even at −30°C. We found that an introduction of cyclopropane ring in **1** results in the much increased

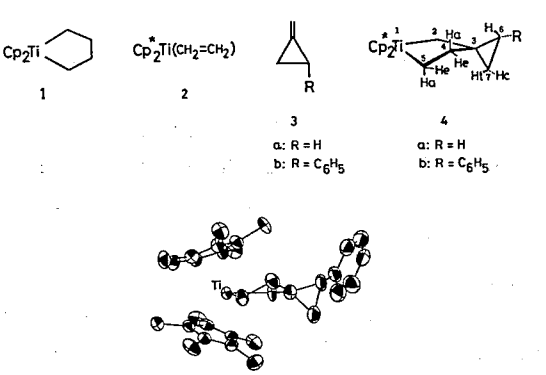

Figure 1. A perspective view of **4b**. The hydrogen atoms are omitted for simplicity.

stability of the titanacyclopentanes. Thus, treatment of a light-green solution of titanocene–ethylene complex **2** (Cp* = pentamethylcyclopentadienyl) in hexane with methylenecyclopropane (**3a**) at −10°C for 48h resulted in a deep red solution, from which new titanacyclopentane **4a** was isolated as orange needles in 65% yield. The solid **4a** is quite stable (mp156–158°C (dec)), but in solution it slowly decomposes at 95°C ($\tau_{1/2}$ 91 min. in toluene). Similarly, the complex **4b** was prepared by the reaction of **2** with **3b** in 83% yield, mp 122–124°C (dec). The molecular structure of **4b** is shown in Figure 1. The unique chemical behaviors of **4a** and **4b** have been elucidated.

VII—C Synthesis of New Chiral Diphosphines and Their Use in Homogeneous Asymmetric Catalysis

The molecular designing and synthesis of new effective chiral ligands are the most important requirements for developing synthetically useful asymmetric catalysis. Our attention has been focussed on the subjects of developments of new effective homogeneous asymmetric catalysts, investigation, and elucidation of the reaction mechanisms and factors controlling the asymmetric induction.

VII-C-1 Synthesis of New Optically Active Diphosphines Bearing 1,1′-Binaphthyl Group

Kinko KOYANO, Hidemasa TAKAYA, and Ryoji NOYORI* *(*: Nagoya University)*

We reported the synthesis of 2,2′-bis(diphenylphosphino)-1,1′-binaphthyl (**1**) (BINAP) which possesses numerous conspicuous structural characteristics and demonstrated that **1** is an efficient ligand for asymmetric hydrogenations of α-acylaminoacrylic acids leading to α-amino acids (eq (1)).[1] Later it was revealed that **1** is the most effective ligand for asymmetric isomerization of allylamines to enamines.[2] This novel reaction has been successfully applied to the industrial production of *l*-menthol according to eq (2). We showed that the most reliable route to optically active (*R*)-**1** or (*S*)-**1** is the synthesis of the racemic diphosphine followed by optical resolution. At an early stage of this study, we used optically active Pd complexes as resolving agents. This time we found that 2,3-*O*-dibenzoyltartaric acid is an effective resolving agent of the dioxide of BINAP (BINAPO). The procedure given in Scheme I now provides a more convenient way to obtain the optically pure BINAP in a large quantity. Similarly, 2,2′-bis(dicyclohexyl)-1,1′-binaphthyl and 2,2′-bis(diisopropyl)-1,1′-binaphthyl were prepared in optically pure forms in good yields.

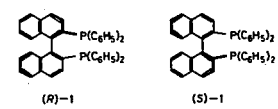

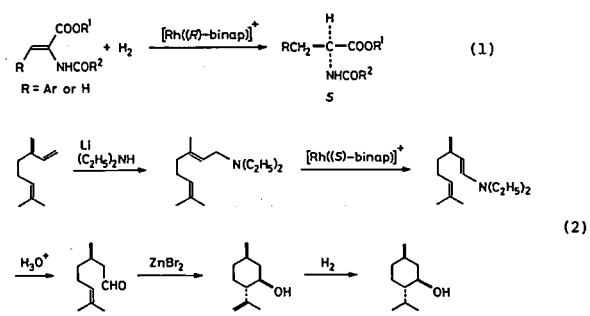

Scheme I.

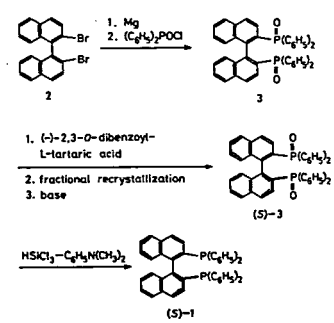

References

1) A. Miyashita, H. Takaya, T. Souchi, and R. Noyori, *Tetrahedron*, **40**, 1245 (1984).
2) K. Tani, T. Yamagata, S. Akutagawa, H. Kumobayashi, T. Taketomi, H. Takaya, A. Miyashita, R. Noyori, and S. Otsuka, *J. Am. Chem. Soc.*, **106**, 5208 (1984).

VII-C-2 The Crystal Structure of a Complex of BINAPO, (-)-Camphorsulfonic Acid, and Acetic Acid

Kazushi MASHIMA, and Hidemasa TAKAYA

The optical resolution of the racemic BINAPO (**1**) has been attained by S. Akutagawa and his coworkers (Takasago Perfumery Co.) by the use of camphorsulfonic acid in the presence of excess acetic acid. We have carried out the *X*-ray crystal structure analysis of the complex of BINAPO, (-)-camphorsulfonic acid, and acetic acid. A stereoview of the molecular structure of the complex was given in Figure 1. It was revealed that the complex is a 1:1:1 mixture of BINAPO, camphorsulfonic acid, and acetic acid, and each component is complexed through hydrogen bonds. It was also confirmed that the levorotatory BINAPO has *S* configuration.

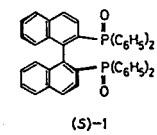

(S)-1

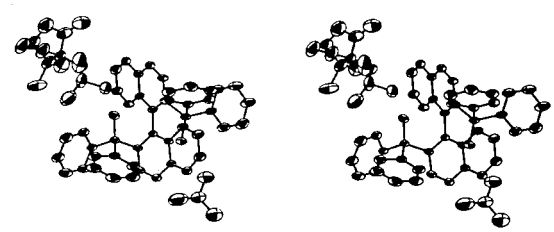

Figure 1. Stereoscopic view of the structure of a 1:1:1 complex of (*S*)-**1**, (1*R*)-(−)-camphorsulfonic acid, and acetic acid.

INSTRUMENT CENTER

VII—D Picosecond Time-Resolved Fluorescence Spectroscopy of Photophysical Processes in Liquid Crystals

Liquid crystals are highly anisotropic molecular systems which exhibit phase transitions in several stages on going from the crystal to the isotropic liquid phases. Mesophases such as smectic A and nematic phases are defined depending on orientational and spatial ordering of molecules. In a typical thermotropic liquid crystal, 4-cyano-4-n-octyloxybiphenyl, the phase transitions take place as follows:

	54.5°C		67°C		80°C	
Crystal	↔	*Smectic A*	↔	*Nematic*	↔	*Liquid*
(K)		(SmA)		(N)		(I)

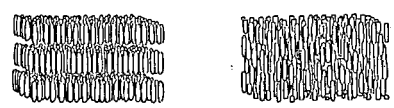

Recently we have found that the liquid crystal forms an excimer, and studied the dynamics of excimer formation by means of a picosecond time-resolved fluorescence spectroscopy. In the present study, we are concerned with effects of molecular anisotropy of the liquid crystal on chemical reactions and photophysical processes.

VII-D-1 Picosecond Dynamics on Excimer Formation in Liquid Crystal

Naoto TAMAI, and Iwao YAMAZAKI

The present study is directed toward dynamics of an intermolecular excimer formation in a thermotropic liquid crystal, 4-cyano-4-n-octyloxybiphenyl (80CB). It was found that dynamical behaviors of the excimer formation in liquid crystal depend strongly on the phase and temperature. Figure 1 shows typical examples of picosecond time-resolved fluorescence spectra in the smectic A (SmA) phase at 329.1K with reference to those in the crystalline (K) phase at 298.9K. In SmA, a monomer-like fluorescence with a peak at 360 nm was observed immediately after excitation. After 100 ps, a new fluorescence band at 380 nm appears. We assigned this band to an excimer fluorescence.[1] From inspection of spectral changes and decay curves, kinetic parameters in the excimer formation were derived on the basis of the following reaction scheme.

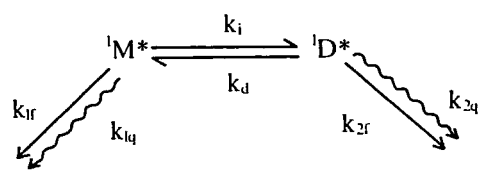

The results are summarized as follows: (1) k_i is on the average constant irrespective of the phase, while k_d varies by a factor of six on going from SmA to I phase. This means that 80CB in the ground state forms a weakly coupled molecular pair. (2) SmA phase is divalent: k_d is significantly lower in the quasi-stable state ($0.7 \times 10^9 s^{-1}$) than in the stable state ($1.5 \times 10^9 s^{-1}$).

Reference

1) N. Tamai, I. Yamazaki, H. Masuhara, and N. Mataga, *Chem. Phys. Lett.*, **104**, 485 (1984).

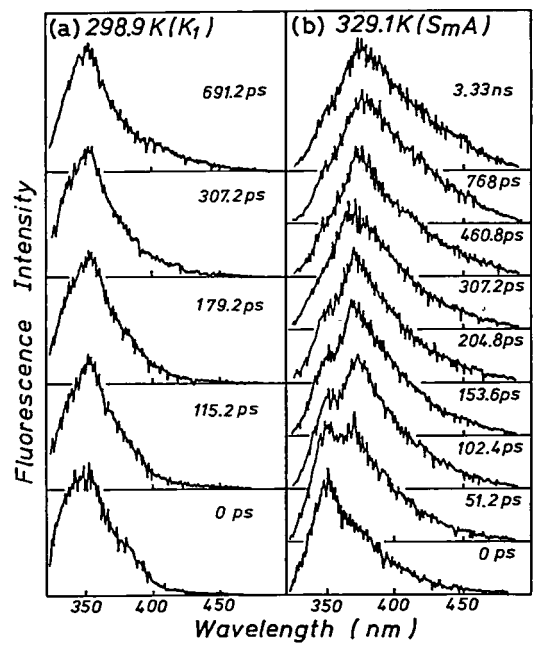

Figure 1. Time-resolved fluorescence spectra of neat 80CB in the crystalline (K_1) and smectic A (SmA) phases, obtained with excitation at 300 nm. Delay times after exciting pulse are indicated in the figure.

VII-D-2 Rotational Relaxation of Liquid Crystal Molecule

Naoto TAMAI, and Iwao YAMAZAKI

Rotational diffusion dynamics of liquid crystalline molecules, 4-cyano-4-n-alkyloxybiphenyl (nOCB), was examined by means of the picosecond time-resolved fluorescence depolarization method. Figure 1 shows typical examples of anisotropy decays of 80CB in 1-butanol and n-hexane. It is seen that, in viscous solvents such as butanol, anisotropy decay is obviously biexponential. Observed anisotropy decays were analyzed in terms of a model of the rotational diffusion of symmetry-top molecule with an electronic transition moment oblique to the symmetry axis. The results were compared with the modified wobbling-in-cone model.[1] It was found that the libration motion in the cone angle θ_c should

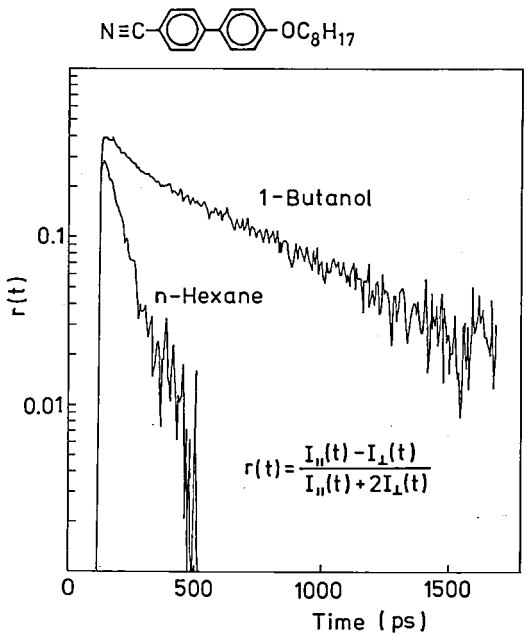

Figure 1. Anisotropy fluorescence decay r(t) of 8OCB in 1-butanol and n-hexane. r(t) was calculated from the intensities of fluorescence polarized parallel and perpendicular to the exciting laser light which is polarized with the electric vector perpendicular to the plane formed by the laser beam and the emission beam.

play a predominant role for the rotational diffusion of liquid crystal molecule with a long methylene chain. Negative deviation from the classical Stokes-Einstein relation was observed in viscous solvents. This may suggest an inclusion of the non-Markovian process for the Brownian motion of methylene chain. The activation energy of the rotational diffusion was estimated to be $\Delta H = 13.8$ kJ/mol in ethanol. This is in good agreement with the solvent activation energy.

Reference

1) K. Kinoshita, S. Kawato, and A. Ikegami, *Biophys. J.*, **20**, 289 (1977).

VII—E Photophysical Dynamics in Multilayer Molecular Assemblies

Multilayers as well as liquid crystals are typical examples of highly-ordered molecular systems or assemblies. In molecular assemblies, photons are absorbed to produce excited species, which then engage in an excitation energy transfer to reaction centers. In the reaction center, photochemical reactions including excimer formation and charge separation take place under the specifically organized molecular arrangement. In this research project, we are concerned with micelles, vesicles and several kinds of multilayers. The focus has been directed to (1) fundamentals of energy migration and collection in multilayer architecture, (2) photochemical reactions under the highly-ordered molecular assemblies and (3) new electrooptic devices capable of spatial control and switching of photonic-energy transport.

VII-E-1 Picosecond Dynamics of Photonic Energy Transport in Multilayer Systems

Tomoko YAMAZAKI, Naoto TAMAI, and Iwao YAMAZAKI

Multilayers such as Langmuir-Blodgett multilayer is a system suitable for investigating photophysics in highly-ordered molecular assemblies, since it could be build up in a desired structure of various kinds of molecular arrangements. Langmuir-Blodgett films are prepared by transferring a monolayer spread on a water surface onto a quartz substrate. By dipping and raising a substrate through the compact monolayer, different kinds of monolayers are deposited successively on each excursion. The present study has been initiated with a view to obtaining dynamical aspect of Förster type of excitation energy transfer in multilayer systems. Figure 1 shows a multilayer system concerned here, which consists of three components of energy donors and acceptors with the distance between the layers being changed. When the carbazole-containing layer is excited at 290 nm with picosecond laser pulses, photonic energy is transferred sequentially among the layers of carbazole, anthracene and cyanine dye. The fluorescence time

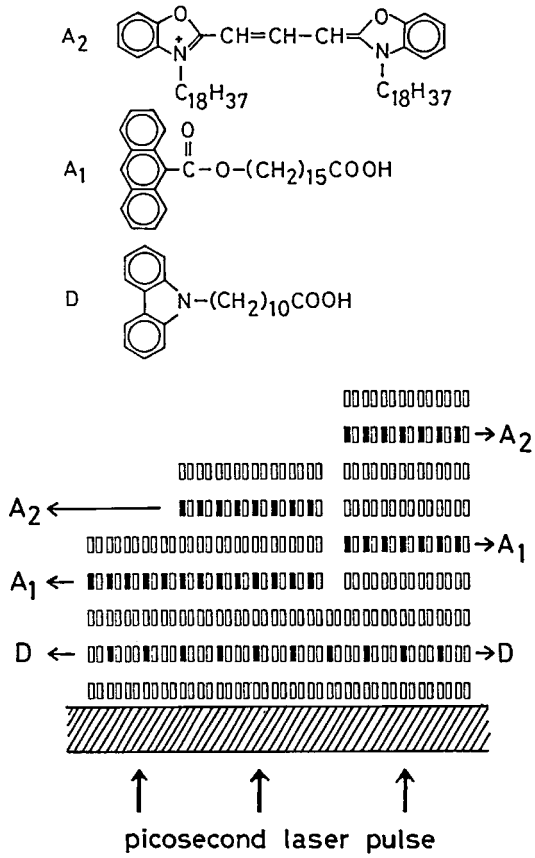

Figure 1. Langmuir-Blodgett multilayer system consisting of layers with chromophores: carbazole (D), anthracene (A_1) and cyanine dye (A_2). The excitation energy transfer takes place sequentially from D to A_2 through A_1. Distances between D, A_1 and A_2 are changed with interposing cadmium arachidate layers as spacers.

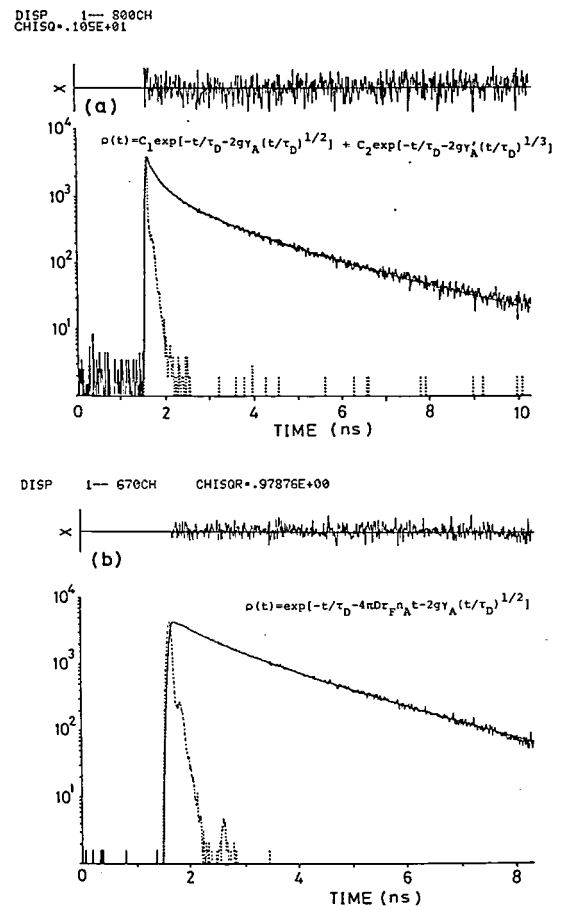

Figure 1. Fluorescence decays of rhodamine 6G (donor) on vesicle surface (a) and in aqueous solution (b) in the presence of malachite green (acceptor). Calculated curve (——) is a best-fit curve convoluted from the instrument response curve for the excitation laser pulse (·····).

behaviors of each layer are measured by means of a picosecond time-resolved spectrophotometer to deduce a kinetics of energy transport as a function of distance between the layers. The goal of the present study is to find new electrooptic devices in molecular scale that control the light energy transport in the two dimentional and in the three dimensional architectures.

VII-E-2 Two-Dimensional Excitation-Energy Transfer on Vesicle Surface

Naoto TAMAI, Tomoko YAMAZAKI, Iwao YAMAZAKI, Akira MIZUMA *(Osaka Univ.)*, **and Noboru MATAGA** *(Osaka Univ.)*

Excitation-energy transfer in a two-dimensional plane has still remain unsolved, although the theoretical formulation has been proposed by several workers.[1] In this study, we are concerned with vesicles on which surface rhodamine 6G (donor) and malachite green (acceptor) are adsorbed in various concentrations. For rhodamine 6G on vesicles, picosecond fluorescence decay kinetics were examined by means of a time-correlated single-photon counting method. Fluorescence decay curves were analyzed by the use of the nonlinear least-square fitting of Maraquat method. Figure 1(a) shows fluorescence decay curve of rhodamine 6G on vesicle surface in the presence of malachite green under the Förster limit condition. Figure 1(b) is a corresponding decay curve taken for aqueous solution. Energy transfer on vesicle surface can be interpreted in terms of superposition of two dimensional and three dimensional decay dynamics,

which is distinct from the systems of micelles and isotropic solution. From an analysis of fluorescence decay curves, the critical distance of energy transfer is estimated to be 62.3 ± 1.7 A, which is in good agreement with that calculated from the spectroscopic data.

Reference

1) M. Hauser, U.K.A. Klein, and U. Gosele, *Z. Physik. Chem. NF*, **101**, 255 (1976).

VII-E-3 Time-Resolved Total Internal Reflection Fluorescene Spectroscopy of Polymer Films

Hiroshi MASUHARA *(Kyoto Inst. Tech.)*, **Noboru MATAGA** *(Osaka Univ.)*, **Shigeo TAZUKE** *(Tokyo Inst. Tech.)*, **Naoto TAMAI, and Iwao YAMAZAKI**

[*Chem. Phys. Lett.*, **100**, 415 (1983)]

Using total internal reflection, the possibility of a subnanosecond fluorescence spectroscopy for elucidating photophysical and photochemical processes of polymer surface is demonstrated. The thickness which can be studied under the present experimental conditions is of the order of 0.01 μm.

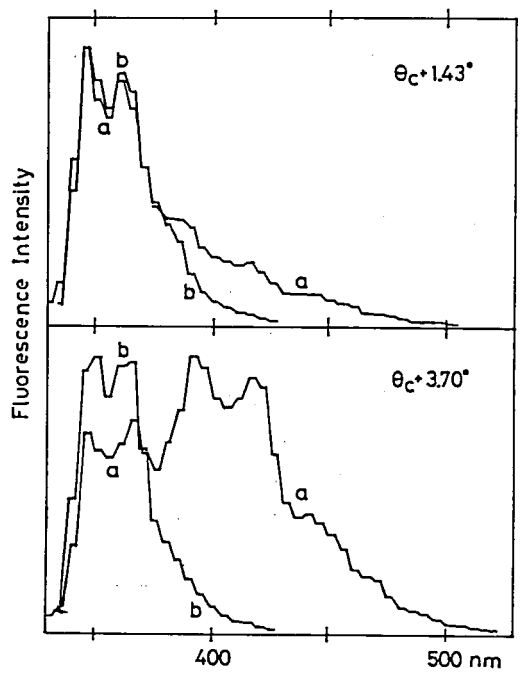

Figure 1. Normalized time-resolved fluorescence spectra of a bilayer system of the 0.01 m A-film doped with POPOP and the thick B-film with N-ethylcarbazole. Gated times are (a) 0.4–1.4 ns and (b) 24.4–44.4 ns. The incident angle is given in the figure.

VII-E-4 Vacuum-Deposited Films of 12-(1-Pyrenyl)dodecanoic Acid Analyzed by Picosecond Time-Resolved Fluorescence Spectroscopy

Munehisa MITSUYA, and Yoshio TANIGUCHI *(Hitachi Central Res. Lab.)*, **Naoto TAMAI, Iwao YAMAZAKI, and Hiroshi MASUHARA** *(Kyoto Inst. Tech.)*

Fluorescence measurements of vacuum-deposited films were demonstrated to be useful in examining deposition conditions and in analysing their structures. Especially, the followings were elucidated for the 12-(1-pyrenyl)dodecanoic acid. (1) Aromatic

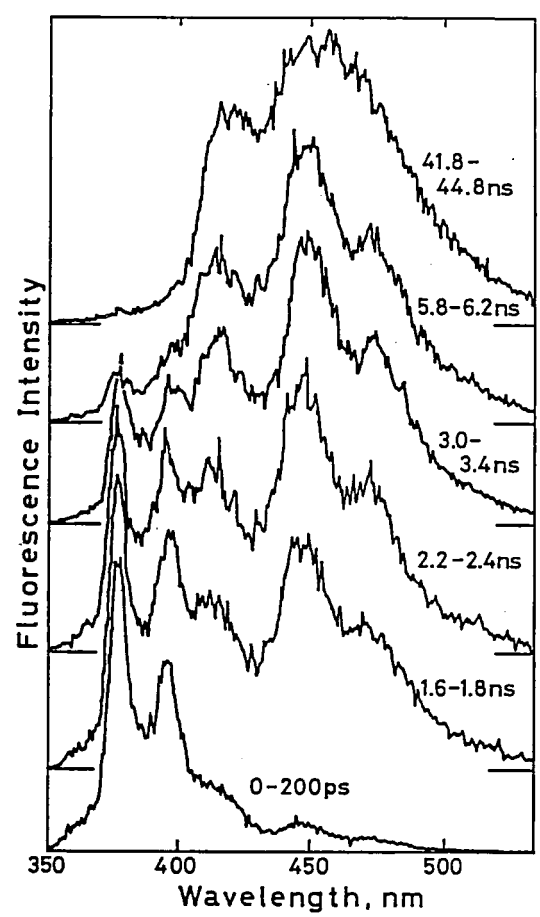

Figure 1. Normalized time-resolved fluorescence spectra of vacuum-deposited film of 12-(1-pyrenyl)dodecanoi acid. Time window is given in the Figure.

hydocarbon having long-chain aliphatic group was easily deposited on the substrate at room temperature, and its formed state was stable. (2) The aggregate structure of the vacuum-deposited film was different from that of the film formed by evaporation of the solvent and did not favor the parallel geometry of pyrenyl groups giving the sandwich excimer. (3) Co-deposition with stearic acid provided a useful tool for decreasing the chromophore concentration in the film. (4) The film structure near the interface to the substrate was not different from that of the bulk structure.

VII—F Excitation Energy Transfer in Photosynthetic Bilepigments

Tomoko YAMAZAKI, Naoto TAMAI, Iwao YAMAZAKI, Mamoru MIMURO *(NIBB)*, **and Yoshihiko FUJITA** *(NIBB)*

Primary processes of the photosynthesis in plants are characterized by highly efficient absorption and subsequent transfer of excitation energy to the reaction centers. In green algae, each of photosystems I and II (PSI and PSII) consists of antenna chlorophyll a (Chl a) proteins and reaction center. In the present study, time-resolved fluorescence spectra emitted from intact cells of green alga *Chlorella pyrenoidosa* have been measured by means of a new detection technique using a microchannel-plate photomultiplier. As is shown in Fig. 1, a new fluorescence band was observed at 690-730 nm in the initial time region (0-180 ps), in addition to the well-known spectrum of PSII-Chl a with a peak at 685 nm: hereafter these two spectra are referred to as F700 an F685, respectively. F700 decays rapidly with lifetime of 104 ps, while F685 decays much more slowly in bi-exponential form with lifetimes of 0.64 and 1.7 ns. Appearance of F700 is independent of closure of the reaction center II (RCII). F700 is thus assigned to the fluorescence from PSI-Chl a, whose decay is governed by a fast energy transfer process form the antenna Chl a of PSI to P700 of RCI.

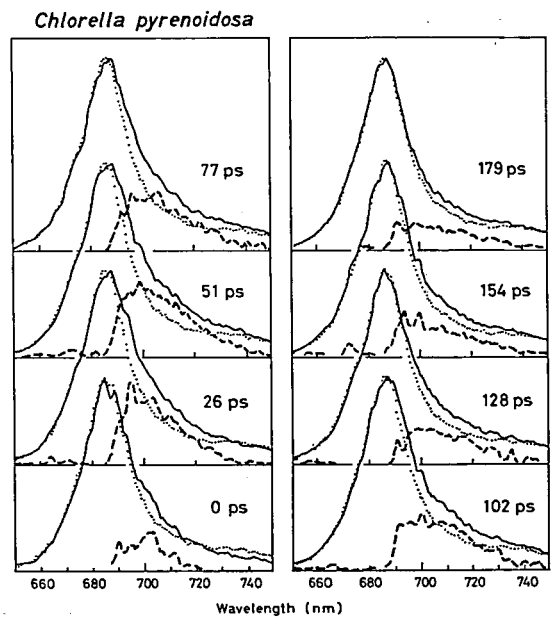

Figure 1. Time-resolved fluorescence spectra of *Chlorella pyrenoidosa* in the 0-180 ps time region (——) and at 1.1 ns (·····), obtained by excitation at 630 nm. The highest intensities are normalized to a common value. Difference spectra (——) between the 1.1-ns spectrum and the respective spectra are shown after two-fold expansion.

VII—G Magnetic Resonance Study of Hydrogenase and Cytochrome c_3

Hydrogenase is an enzyme for hydrogen cleaverage reaction and cytochrome c_3 is a native electron carrier in this reaction. The active center of hydrogenase was reported to be an iron-sulfur cluster like in ferredoxin. However the mechanism of the catalytic reaction of hydrogenase has not yet been clarified. Cytochrome c_3 has four hemes in a single polypeptide chain. This peculiar structure reflects in its physico-chemical properties such as electrochemical reactivity, ionization potential and electric conductivity of thin films.

VII-G-1 Electron Spin Resonance of Hydrogenase

Tatsuhiko YAGI *(Shizuoka Univ.)*, **Keisaku KIMURA, and Hiroo INOKUCHI**

Hydrogenase from a particulate fraction of *D. vulgaris* strain Miyazaki F contains 8 iron and 8 labile sulfide ions in a molecule which is composed of two unequal subunits. EPR spectrum has an isotropic signal at g = 2.017 which is independent of the temperature. The peak to peak width of the signal is about 20 G. The signal intensity is nearly equivalent to 1 unpaired electron per molecule. The power dependence of the EPR spectrum of purified hydrogenase from 0.01 mW to 100 mW at 17K, is shown in Figure 1. The power dependence of the spectrum at 3.7K, 10K and 40K were also measured. The saturation factor was obtained from the EPR absorption intensity as a function of microwave power. It was found that ferricyanide had a little effect on the shape and intensity of the EPR signal.

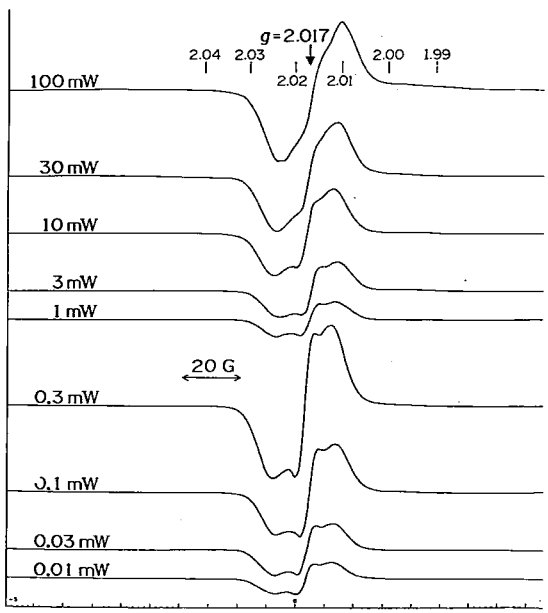

Figure 1. Power dependence of the EPR spectrum of hydrogenase. Receiver gain is 2×10^2 for the spectra taken under the microwave power of 1 mW or over, and 1.6×10^3 for the others. Microwave power is indicated on the left shoulder in the figure. Temperature, 17 K. Modulation frequency, 100 kHz.

VII-G-2 ^{1}H NMR of Multihemoprotein, cytochrome c_3

Keisaku KIMURA, Shinsuke NAKAJIMA *(Yokohama Nat. Univ.)*, **Katsumi NIKI** *(Yokohama Nat. Univ.)*, **and Hiroo INOKUCHI**

Macroscopic redox potentials of tetrahemoprotein cytochrome c_3 from *D. vulgaris* were determined with 400 MHz ^{1}H NMR. These potentials have previously been obtained by simulation of the redox titration curve of pulse polarogram.[1] The redox potential, E, of cytochrome c_3 is defined by

$$E = E^0_{i+1} + RT/F \ln [f_i]/[f_{i+1}]$$

where E^0_{i+1} is the macroscopic formal potential to the $f_i \leftrightarrow f_{i+1}$ equilibrium, where f_i is the i-th oxidation state. In order to determine the first redox potential, E^0_1, we compared the intensity of the optical absorption spectrum of the intermediate oxidation state to that of the MNR spectra at the same time. The degree of the reduction was 9.2% from visible absorption spectra as against 30% determined by ^{1}H NMR of heme methyl of f_0 state. From these values together with the average redox potential, $E_0 = -0.300$V, the redox potential E^0_1, was determined to be $-0.245\text{V} \pm 0.005\text{V}$, in good agreement with that derived from electrochemical method, -0.240V.

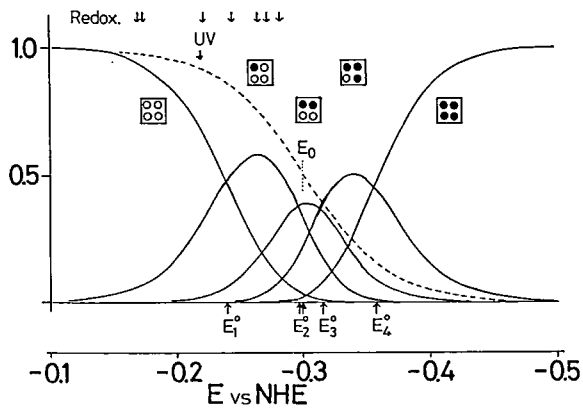

Figure 1. Population of five redox states as a function of electrochemical potential. Solid lines are calculation curves and broken line is the average population of the oxidized heme. Arrows on the top of the figure designate to each redox state in the intermediate oxidation states.

We have also measured the redox titration spectra of the intermediate oxidation species. Comparing the spectral intensities of heme methyl resonance spectra, we have derived the relative concentrations of the five redox states as a function of the electrochemical potential as shown in Figure 1. At the bottom of the figure, the four macroscopic potentials are indicated. The broken line represents the average fraction of oxidized heme which is the one observed by optical absorption spectroscopy and polarography.

Reference

1) W. Sokol, D.H. Evans, K. Niki, and T. Yagi, *J. Electroanal. Chem.*, **108**, 107 (1980).

VII—H The Study of Metal Fine Particles Produced by Means of Gas Evaporation Technique

Fine particles whose sizes are several hundreds angstrom or less, are characterized by the quantum size effect, surface effect on the bulk properties and also a fluctuation of a thermodynamical properties by its low dimensionality. These effects were studied as functions of metal species and solvents.

VII-H-1 Conduction Electron Spin Resonance of Ultrafine Particles of Magnesium

Keisaku KIMURA, and Sanshiro SAKO *(Mie Univ.)*

[*Chem. Lett.*, 973 (1984)]

We have measured the conduction electron spin resonance (CESR) of ultrafine particles of Mg produced by the matrix isolation method.[1] In the low temperature X-band CESR spectra, there were two peaks with different linewidths, 6G and 1.6G. The sharp line was easily saturated even at a microwave power of 0.1 mW at very low temperatures and has a nature of a localized spin. On the other hand, the broad line had a shorter relaxation time than the sharp one. Comparing the X-band spectrum with the Q-band, we have assigned the narrow one coming from the surface impurities and the broad one from volume effect, most probably quantum size effect. We have also measured the solvent effect on the surface state of the fine particles. Figure 1 shows the X-band CESR

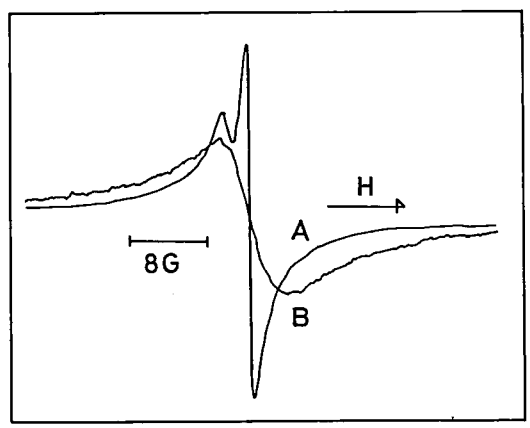

Figure 1. A: in THF. B: in hexane. The linewidth of the broad line is 6 G for both samples and that of narrow line is 1 G. Both at 9 K and 8 mW.

derivative spectra in THF and in hexane at 9K and 8 mW. It is noteworthy that the narrow central line is missing in the spectrum of fine particles in hexane. Since hexane is chemically more inactive than THF, the surface reaction may be suppressed in the Mg/hexane system. Therefore, the narrow

central line observed both at the two frequencies is due to the impurity at the surface. It was also observed that the central narrow line was enhanced even in the sample prepared in hexane when the fine particles were produced under bad vacuum conditions.

Reference

1) K. Kimura, and S. Bandow, *Bull. Chem. Soc. Jpn.*, **56**, 3578 (1983).

VII-H-2 Conduction-Electron Spin Resonance in Fine Particles of Magnesium and Calcium

Sanshiro SAKO *(Mie Univ.)*, **and Keisaku KIMURA**

[*J. Phys. Soc. Jpn.*, **53**, 1495]

The conduction electron spin resonance (CESR) of Mg and Ca fine particles produced by the gas evaporation technique, was observed at 9.1 GHz in the temperature range from 2.7K to room temperature and at 35 GHz at room temperature. In Mg fine particles, a broad and an anomalously narrow resonance lines were observed one over the other as shown in Figure 1. The former showed the Pauli paramagnetic behavior like the bulk metal, and the latter the increase of the absorption intensity with decreasing temperature like the Curie law. In Ca fine particles, only the anomalously narrow line was observed. Those narrow lines were thought to be due to the smallness of size and be composed of numerous spin packets with different g values and linewidths. Their natures are discussed in relation to the quantum size effect.

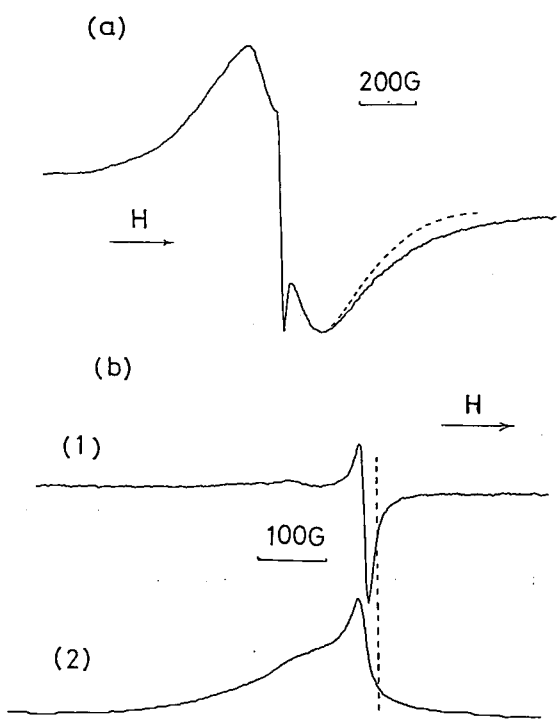

Figure 1. a) A spectrum of the CESR derivative line of Mg fine particles having the average diameter of 1859 A at 4 K. A broad line and a narrow line were observed. The broken line shows the Lorentzian line shape. b) The CESR derivative spectrum of the central part of a). 1) is the derivative spectrum and 2) is the integral of 1).

VII-H-3 Magnetic Susceptibilities of Small Particles of Magnesium and Beryllium

Keisaku KIMURA, Shunji BANDOW, and Sanshiro SAKO *(Mie Univ.)*

The quantum size effect was reported for small particles of magnesium by conduction electron spin resonance (CESR). In the very small particles, however, the contribution of surface to the volume properties becomes very large, because the ratio of the number of surface atoms to that of total atoms in a particle becomes large. Therefore it is very important for the study of the quantum size effect to distinguish the volume effect from the surface effect. The surface condition can be effectively modified in the colloidal system by changing the chemical reactivity of the solvent. We have shown the difference of surface states in two colloidal systems

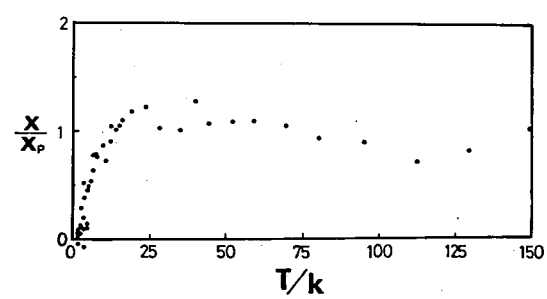

Figure 1. Magnetic susceptibility of very small particles of Mg in hexane as a function of temperature. Magnetic susceptibility is normalized against the bulk metal. Sample weight was 2.96 mg and the average size was 20 A.

where hexane was used as a stable solvent and THF as a reactive solvent.[1] The static magnetic susceptibility of Mg fine particles in hexane was measured in order to clarify the origin of the broad line observed in CESR.

Figure 1 shows the magnetic susceptibility of small particles of Mg in hexane as a function of temperature. The most striking feature in the figure is the rapid decrease of magnetic susceptibility in a very low temperature region. We also notice that the magnetic susceptibility once increases at arround 50K with decreasing temperature. The decrease of the magnetic susceptibility of very small divalent metal particles at low temperature was predicted by Kubo. Therefore our findings are consistent with the quantum size effect, although we have also observed the slight increase during the intermediate region. Another divalent metal particles, Be small particels, have revealed the similar behavior in the temperature dependence of magnetic susceptibilities.

Reference
1) K. Kimura, and S. Sako, *Chem. Lett.*, 973 (1984).

VII—I Development of Experimental Devices and Techniques

The Instrument Center is equipped with various types of instruments for molecular spectroscopy, solid-state chemistry and magnetic spectroscopy.[1] All of them are opened widely for researchers in universities and institutions as well as staffs in IMS. In view of efficient use of these instruments, the Center staffs are concerned with development of new experimental devices and techniques.

Reference
1) List of Instruments, No. 4 IMS Instrument Center (1983)

VII-I-1 Application of Transient Digital Memory to the Single-Photon Counting Spectrofluorimeter

Takaya YAMANAKA, Hisashi YOSHIDA, and Iwao YAMAZAKI

A multichannel transient digital memory (Biomation 6500) with a 2-nsec/channel resolution has been applied to the single-photon counting spectrofluorimeter of nanosecond time resolution. In a combination with a pulsed laser such as an excimer laser which is operated in high output power and in low-repetition rate, this system is capable of receiving multi-fold photoelectron pulses in every laser excitation, so that fluorescence decays and time resolved spectra can be measured with high efficiency in a short time period. Figure 1 shows schematic diagram of the electric circuit. The system consists mainly of comparator, timing controller and memory. Following excitation of a sample with a pulsed laser, a series of single-photoelectron pulses associated with fluorescence signals are recorded in the transient memory. The

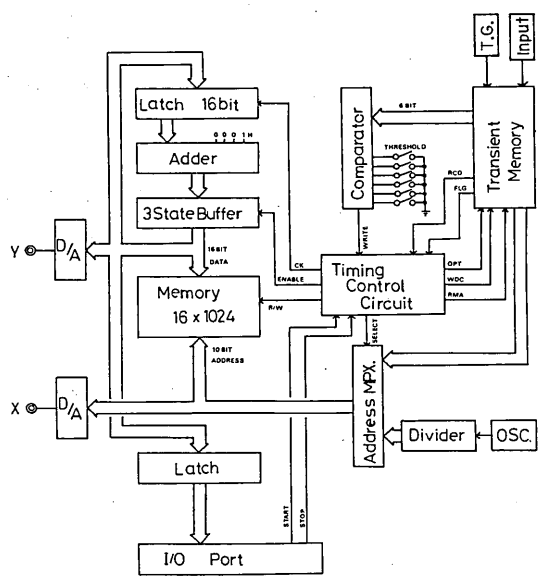

Figure 1. Schematic diagram of electric circuits of the integrator and of the interface between the transient memory and the microcomputer.

records are transferred to the comparator and resultant pulses are added at channels corresponding to delay time. As a consequence, one can obtain fluorescence decay curves with dynamic range up to 10^4 in several minutes.

VII-I-2 Computer aided system of magnetic susceptibility measurement by Faraday method

Shunji BANDOW, and Keisaku KIMURA

We have constructed a laboratory automation system[1] based on a Faraday type magnetic balance, product of Oxford Instrument, installed in this center. This system consists of a magnetic susceptibility measurement sequence and a temperature control loop, these are controlled with the aid of a computer. Temperature is manually controlled between the temperature range from 2.2K to 20K, but above 20K it is set under the computer operation using a PID temperature controller (DTC2) up to 300K. When the temperature stabilizes, magnetic susceptibility is measured, calculated and printed out under the computer control. Figure 1 shows a block-diagram of the system. RS-232C and GP-IB are used for a data communication. The stability of a temperature $\Delta T/T_{set}$, in a computer control mode is the order of 10^{-2}. After a measurement, we can easily correct a cell blank and data are plotted in forms of $\chi - T$, $\chi - 1/T$, etc., using a data processing program. This system can detect a susceptibility of the order of 10^{-6}emu/g with a sample of several mg.

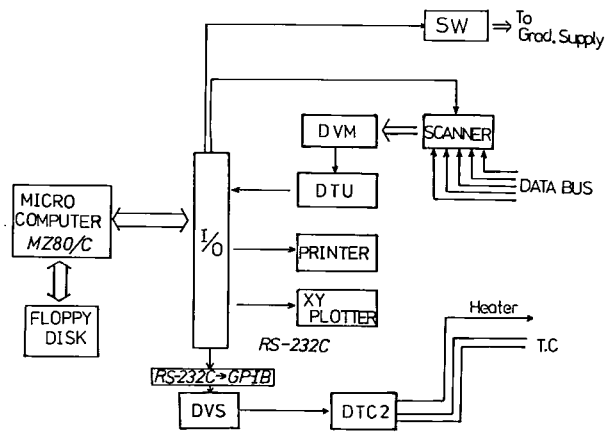

Figure 1. Block-diagram of a computer processing system. DVM; Digital voltmeter, DTU; Data transfer unit, DVS; Digital voltage source.

Reference

1) K. Kimura, and S. Bandow, *Kotaibutsuri* (in Japanese), **19**, 467 (1984).

LOW TEMPERATURE CENTER

VII—J Development of Intermediate Temperature Techniques

VII-J-1 A Temperature Controlled Cryostat for Intermediate Temperatures between 20K and 77K

Keiichi HAYASAKA, Norio OKADA, Nobuo MIZUTANI, Toshio HORIGOME, Kenichi IMAEDA, and Toshiaki ENOKI

The intermediate temperature is defined as the temperature between the boiling points of liquid nitrogen (77K) and liquid hydrogen (20K). In this temperature region there are many interesting photochemical reactions and processes known to occur. Therefore, we have constructed a temperature controlled cryostat convenient for experiments done at the intermediate temperatures and for the production of liquid hydrogen. A schematic drawing of our cryostat is illustrated in Figure 1. The cryostat consists of a liquid helium reservoir, a heat exchanger and an experimental chamber. Liquid helium is introduced through three concentric layers of 5mm o.d. coppertubing wound around and soft soldered to the single layered 5mm o.d. coppertubing for flowing a warm gas such as hydrogen gas. The latter tubing is wound around

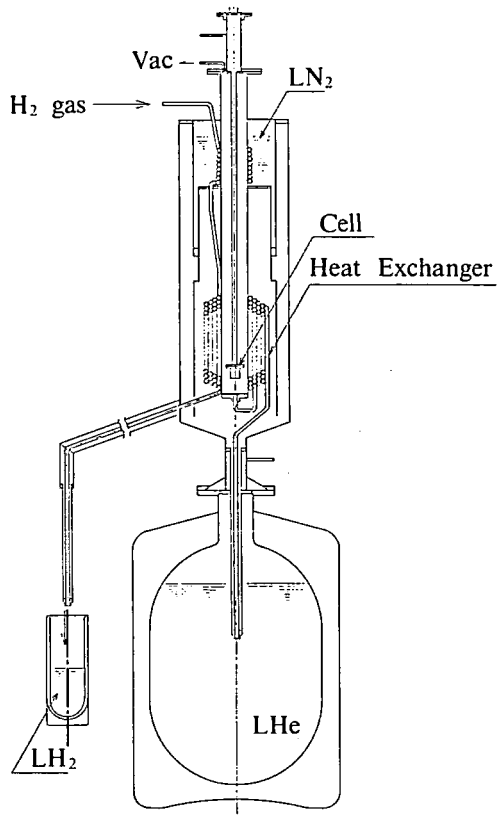

Figure 1. Schematic drawing of a temperature controlled cryostat for intermediate temperatures.

and soldered to a 60mm i.d. and 140mm long stainless steel pipe which serves as an experimental chamber. The helium gas evaporated in the heat exchanger is then introduced into the bottom of the experimental chamber. The cold He gas keeps the sample at a controlled temperature and pumped into a pressure controlled vacuum system.

When the hydrogen gas is run as a warm gas and cooled in the heat exchanger, liquid hydrogen can be obtained.

Any temperatue between 20K and 77K can be attained by controlling the flow rates of liquid helium and the hydrogen gas.

VII—K Polyvalency-Type Charge Transfer Complexes

VII-K-1 Electric and Magnetic Properties of Tetrabenzo[de,hi,op,st]pentacene-Alkali Metal Complexes

Kenichi IMAEDA, Toshiaki ENOKI, Hiroo INOKUCHI, Junji AOKI *(Toho Univ.)*, **Minoru TAKEKAWA** *(Toho Univ.)*, **and Satoshi IWASHIMA** *(Meisei Univ.)*

[*Chem. Lett.*, 331 (1984)]

The electric and magnetic properties of the charge transfer complexes of tetrabenzo[de,hi,op,st]pentacene(TBPA) with various Cs compositions have been investigated. Its nonplanarity of molecule causes the restriction against complex formation. TBPA-Cs complexes are good conductors, which is consistent with their characteristics of a partial charge transfer.

EQUIPMENT DEVELOPMENT CENTER

VII—L Studies of Quasi-One-Dimensional Materials

VII-L-1 Soliton Formation at Neutral-to-Ionic Phase Transition in Mixed-Stack Charge Transfer Crystal TTF-p-Chloranil

Tadaoki MITANI, Yoshinori TOKURA,* Gunji SAITO,* and Takao KODA* *(*Nuniv. of Tokyo)*

[*Phys. Rev. Lett.*, **53**, 842 (1984)]

Intrinsic paramagnetic defects have been detected by ESR measurements in tetrathiafulvalene (TTF)-p-chloranil(CA) single crystals associated with the neutral-to-ionic phase transition at T_c = 84K. From characteristic angular dependence and a remarkable narrowing of the ESR lines, two kinds of paramagnetic species are identified with delocalized spins propagating on either donor or acceptor sites. Total spin density and electric conductivity were found to increase discontinuously as temperature is lowered across T_c. These features are attributed to the formation of mobile soliton (and anti-soliton)-like paramagnetic defects induced in the dimerized lattice of TTF-CA crystal upon the neutral-to-ionic phase transition.

VII-L-2 Polarized Electro-reflectance Measurements on Elongated Cis- and Trans-Polyacetylene films

Yoshiki WADA,* Tadaoki MITANI, Kazuo HAYAKAWA, Takao KODA, and Hideki SHIRAKAWA***** *(*Univ. of Tokyo and IMS, **Univ. of Tokyo, ***Univ. of Tsukuba)*

The polarized electroreflectance measurements have been made on elongated cis- and trans-polyacetylene films. A weak and electric-field-sensitive absorption band was observed for the both isomers slightly below the gap energy. Modulated spectra of this band are found to be well polarized to the elongated polymer axis. The structures contain the set of overtone transitions associated with the single-bond-streching mode. The whole aspect of the fine structures implys a posibility of occurence of direct transitions to the self-trapped exciton. Such a relaxed exciton state is believed to play an essential role in a dynamical process of the photo-generation of soliton states in trans-polyacetylene.

VII-L-3 Optical Study of Linear-Chain Mixed-Valence single crystals of $[MA_2][MA_2X_2](ClO_4)_4$ (M = Pt,Pd, X = Cl,Br,I and A = ethylenediamine)

Yoshiki WADA,* Tadaoki MITANI, Masahiro YAMASHITA, and Takao KODA***** *(*Univ. of Tokyo and IMS, **Kyushu Univ., ***Univ. of Tokyo)*

Polarized reflectivity and luminescence measurements have been made on the $[MA_2][MA_2X_2](ClO_4)_4$, M = Pt,Pd, X = Cl,Br,I, and A = ethylenediamine, single crystals. A giant oscillator strength due to the charge-transfer(CT) transitions has been revealed by the Kramers-Kronig analysis from the reflectivity spectra. The M and X dependences of the energy position and half-width of the transitions, and an observed luminescence with a large Storks-shift can be explained in terms of the one-dimensional CT exciton model. An origin of the giant oscillator strength are found to be attributable to the super-transfer mechanism between adjacent metal ions via a halogen ion.

VII—M Construction of a Vacuum-UV Spectrophotometer

Toshio HORIGOME, Kazuo HAYAKAWA, Mitsukazu SUZUI, Norio OKADA, Hisashi YOSHIDA, Nobuo MIZUTANI, Shinji KATO, Masaaki NAGATA, Kusuo SAKAI, and Tadaoki MITANI

A Seya-Namioka-type vacuum-UV spectrophotometer has been constructed by the members of the Equipment Development Center and has been connected to the UVSOR beam line. A picture of this apparatus is presented in Figure 1. Its ability has satisfied the essential requirements for the spectroscopy of solids as expected as the results of the ray trace calculation. The improvement of the monochromator was made by introducing a new technique utilizing a microcomputer system so as to change three concave gratings, having 600, 1200 and 2400 ruled lines per mm, mounted in an ultra-high vacuum. By an application of a ball-spline mechanics to linear and rotatory driving mechanisms, we achieved high reproducibility of

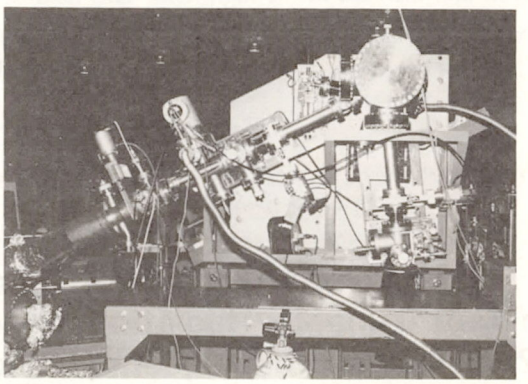

Figure 1. The Seya-Namioka-type vacuum-UV spectrophotometer.

scanning motion of the gratings. This apparatus can be used in various kinds of optical measurements, which require either highly resolved or highly intensive monochromatic light source.

VII—N Impact Optical Spin Orientation in the Excited Triplet State of Aromatic Hydrocarbons at Room Temperature

Yoshihiro TAKAGI

Optically induced magnetization (OIM)[1] has been observed in polycrystals of aromatic carbonyls and azines at room temperature using a simple pickup coil detection. Magnetic field dependence of the induced magnetization proved that direct S → T photoexcitation or S → S excitation followed by fast intersystem crossing gives rise to the spin orientation in the lowest triplet state. Materials in which OIM signal was detected were benzophenone, benzil, benzoin, acetophenone, benzaldehyde, xanthone, anthrone, anthraquinone, pyrazine, phenazine, quinoxaline, phthalazine, etc.. Typical time-derivative signals of the OIM are shown in Figure 1. The signal polarity of benzil and pyrazine was opposite to that of other species in consistent with the opposite sign in zero-field splitting parameter D. Decay time of the OIM signal changed differently in different materials in the range of the order of 1 to 100 ns. Most of the above materials showed increase of the decay time with increasing magnetic field but benzoin and pyrazine exhibited decrease of the

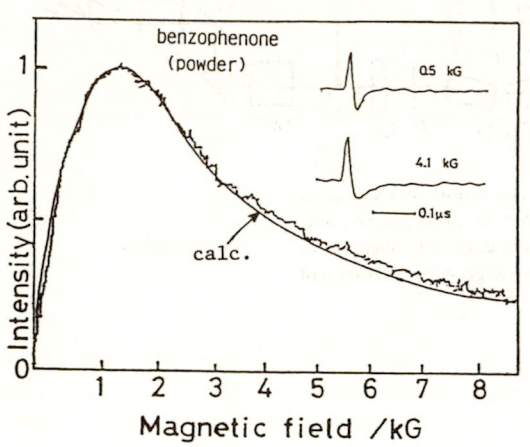

Figure 1. Time derivative signals of optically induced magnetization (accumulated over fifty shots) and its magnetic field dependence in polycrystal of benzophenone.

decay time in the low field region and increase in the high field. This field dependence of the decay time was found to be due to the cross-relaxation by considering the magnetophotoselection and the energy level splitting under the magnetic field. The decay corresponds to the spin relaxation in the triplet exciton.

Reference

1) Y. Takagi, Laser Spectroscopy VI, pp.85-88 (Springer, Berlin, 1983) and references therein.

VII—O Efficient Generation of Picosecond Coherent Tunable Radiation between 190-212 nm by Sum-Frequency Mixing from Raman and Optical Parametric Radiations

Yoshihiro TAKAGI, Minoru SUMITANI, Nobuaki NAKASHIMA, and Keitaro YOSHIHARA

[*IEEE J. Quantum Electron.*, in press]

Tunability range of 214-460 nm in the picosecond laser system previously reported[1] has been extended to 190-212 nm by an efficient sum-frequency mixing using KDP. The optical arrangement for sum-frequency generation is shown in Figure 1. We have added one more optical line to the optical arrangement in ref. 2. An optical parametric radiation tunable between 850 and 1500 nm, which is pumped by the second harmonic of a mode-locked Nd:YAG laser, was frequency-mixed with the fourth harmonic, nitrogen Raman, and hydrogen Raman to generate tunable radiation with energy of 0.1 mJ ranging 214-226, 222-238, and 227-250 nm, respectively. The tunable radiation and a nitrogen Raman radiation (1414 nm) pumped by the fundamental of the YAG laser were frequency-mixed again. Tunig ranges of 190-195, 192-203, and 196-212 nm were obtained corresponding to the above three tuning ranges. The output energy was 20 to 40 μJ. Phase-matching in the near vuv region is thus available for KDP by using incident radiations of short and long wavelengths.

References

1) Y. Takagi, M. Sumitani, N. Nakashima, and K. Yoshihara, *IMS Ann. Rev.*, 135 (1983).
2) Y. Takagi, M. Sumitani, N. Nakashima, and K. Yoshihara, *Appl. Phys. Lett.*, **42**, 489 (1983).

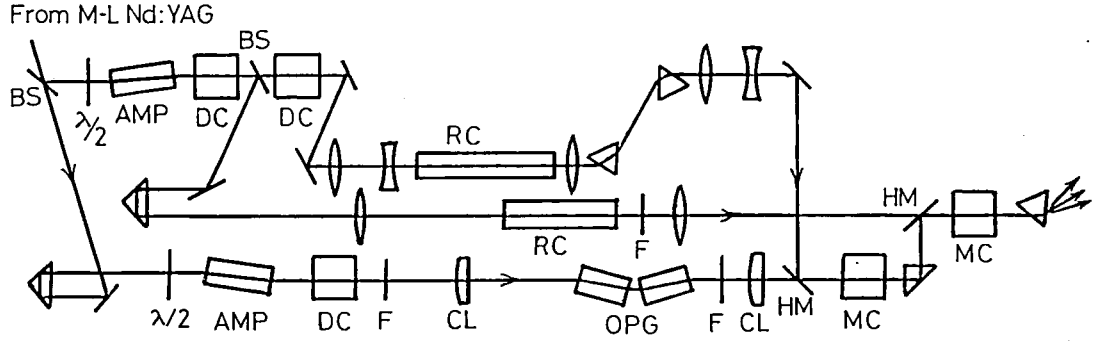

Figure 1. Optical arrangement for generation of picosecond tunable uv radiation. (BS) beam splitter; (λ/2) half-wave plate; (DC) doubling crystal; (RC) Raman cell; (F) filter; (CL) cylindrical lense; (OPG) optical parametric generator; (HM) half mirror; (MC) mixing crystal.

ULTRAVIOLET SYNCHROTRON ORBITAL RADIATION FACILITY

VII—P Construction of UVSOR (Ultraviolet Synchrotoron Orbital Radiation) Light Source

Makoto WATANABE, Toshio KASUGA, Hiroto YONEHARA, Akira UCHIDA, Kusuo SAKAI, Osamu MATSUDO, Toshio KINOSHITA, Masami HASUMOTO, Jun-ichiro YAMAZAKI, Eiken NAKAMURA, Kiyoshi TAKAMI,* Takeshi KATAYAMA, Katsuhide YOSHIDA,** Motohiro KIHARA,*** and Godfrey SAXON****** *(*Kyoto Univ., **Univ. of Tokyo, ***National Lab. High Energy Phys., ****Daresbury Lab. and IMS)*

UVSOR light source is a 600 MeV (max. 750 MeV) electron storage ring dedicated to synchrotron radiation research. In 1981, its construction was started. In November 1983, its commissioning was succeeded. The maximum current so far is 170mA. It will be opened to users in near future. The present status of UVSOR light source is given in "Ultraviolet Synchrotron Orbital Radiation Facility" in this issue and some developments are given in following papers.

VII-P-1 Beam Position Monitor in UVSOR

Toshio KASUGA, Masami HASUMOTO, Toshio KINOSHITA, and Hiroto YONEHARA

Measurements of horizontal and vertical orbit distortions in the UVSOR storage ring are important to detect displacements of radiant points of synchrotron radiation and to correct the orbit distortions. Sixteen position monitors were installed in the ring. Each position monitor consists of four button type electrodes. One of sixty four electrodes is selected by a coaxial switch multiplexer system, and signal from the electrode is detected by a linear detector. Data from the detector are taken by a micro-computer system and the orbit distortion is calculated by the computer. Horizontal and vertical closed orbit distortions were formed artificially and these distortions were measured by the beam position monitor system to test the performance of the system. The results of the test were satisfactory.

VII-P-2 Correction of Closed Orbit in UVSOR

Toshio KASUGA, Hiroto YONEHARA, Masami HASUMOTO, Toshio KINOSHITA, and Osamu MATSUDO

Eight vertical steering magnets and trim coils wound on eight bending magnets are available to correct orbit distortions. We used "least squares method" to find a set of deflection angles to be applied to the correction elements. Vector $\mathbf{x}' = (x'_i)$ denotes beam displacement at beam position monitor points in the ring due to vector $\mathbf{b} = (b_i)$ which is a set of deflection angles, and $\mathbf{x}' = M\mathbf{b}$ where M is a matrix. The optimum $\mathbf{b}$ to correct an orbit distortion $\mathbf{x} = (x_i)$ is $\mathbf{b} = ({}^tMM)^{-1}\,{}^tM\mathbf{x}$. A computer program which calculated $\mathbf{b}$ was written. Matrix elements were determined by measurements of orbit displacements due to the excitation of the correction elements. Correction of closed orbit distortion was tried in July. Maximum horizontal and vertical excursions without the correction were ± 5mm and ± 3.6mm respectively, and the correction reduced them to ± 2mm and ± 1mm.

VII-P-3 Single Bunch Storage in UVSOR

Toshio KASUGA, Toshio KINOSHITA, Masami HASUMOTO, and Hiroto YONEHARA

The period of the pulsed light from the UVSOR is about 11 nsec in case of usual operation. The period can be elongated to 180 nsec by single bunch storage. Two methods to form a single bunch in the

ring were tried. First, nano-second grid pulser method was tested. The grid of the electron gun of the linac is excited by a short pulse which is synchronized to a certain bucket of the synchrotron, and only this bucket can be filled with electrons. Another method is RF knockout method. All bunches except two bunches in the synchrotron are destroyed by a deflector, and one of two survivors is transfered to the storage ring. As the ratio of radii of the storage ring and the synchrotron is 2, two buckets of the storage ring are synchronized to a bucket of the synchrotron. Therefore the transfer timing must be synchronized to either of the two buckets. These two methods were tried successfully. Single bunch purity was better than 99%, and these two methods can be used together to improve the purity.

VII-P-4 Undulator and Wiggler

Hiroto YONEHARA, Toshio KASUGA, Keiichi HAYASAKA, Osamu MATSUDO, Jun-ichiro YAMAZAKI, Masami HASUMOTO, Toshio KINOSHITA, Hideo KITAMURA,* and Tatsuya YAMAKAWA* *(*National Laboratory for High Energy Physics)*

A permanent magnet undulator and a super-conducting wiggler (wave length shifter) were installed in March 1984. The first light from the undulator was observed in September. Though the position of the stored beam was slightly disturbed by the undulator, the lifetime of the beam was not influenced. Maximum magnetic field of the wiggler is 4 Tesla. The magnetic field was measured and the result was satisfactory. Electron beam could be injected and stored on condition that the wiggler was fully excited, but the beam position and the number of the betatron oscillation were somewhat influenced by it. Correction of the influence of the wiggler will be done soon.

VII-P-5 Construction of a Constant Offset Double Crystal Monochromator for BL-7A of UVSOR

Takatoshi MURATA *(Kyoto Univ. of Education and IMS)*, **Tokuo MATSUKAWA** *(Osaka Univ.)*, **Kusuo SAKAI, Toshio HORIGOME, Osamu MATSUDO, and Jun-ichiro YAMAZAKI**

A constant offset double crystal monochromator was constructed for the experiments in the soft x-ray region at UVSOR. The features of the monochromator are as follows.

(a) The basic concept of the mounting is that of Cowan *et al.*[1] A linear guide is used for maintaining the height of the output beam.

(b) The monochromating crystals are manually interchangeable in a reproducible way.

(c) A fine adjustment of the crystal plane is made by piezo-electric devices (Berley Inchworm IW-50 and Physik Instrumente P700.10).

(d) In order to separate the low vacuum of the monocromator chamber (about 10^{-7} mmHg) from the vacuum of the main ring a 10 μm thick light tight Be foil is placed at the upstream of the monochromator. As a result, the longest accessible wavelength is about 15Å. In Figure 1 is shown the monochromating crystals and their accessible energy regions below 2.5 keV.

Reference

1) P.L. Cowan, J.B. Hastings, T. Jach, and J.P. Kirkland, *Nucl. Instrum. Methods* **208**, 349 (1983).

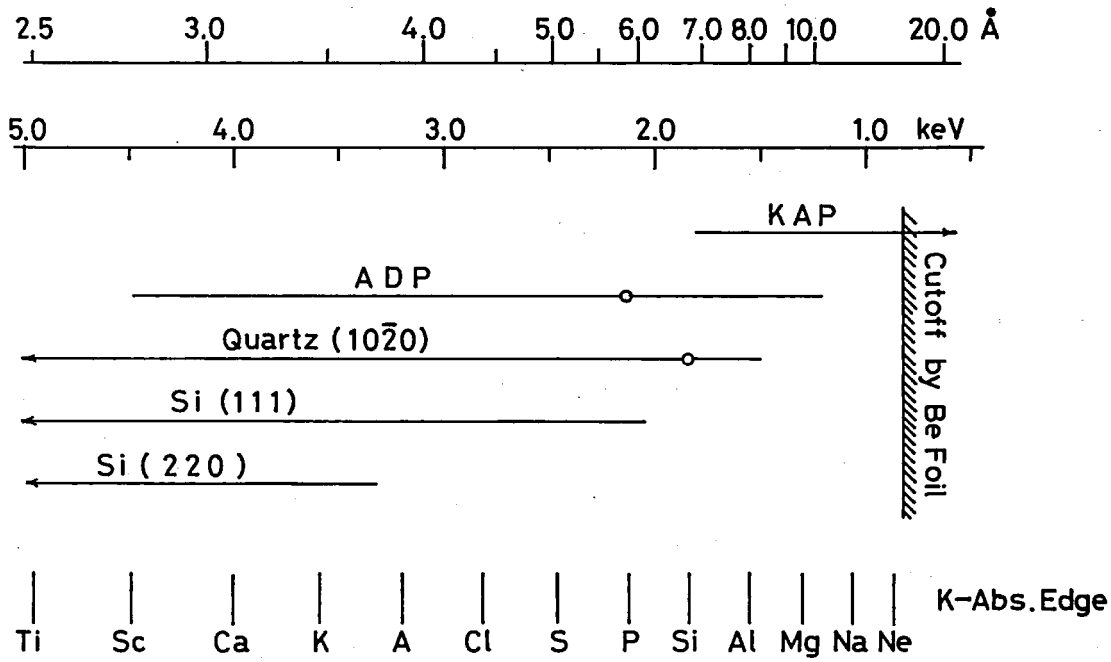

Figure 1. Monochromating crystals and their accessible energy regions below 2.5 keV. Vertical lines at the bottom mean the energies of K absorption edges of various atoms.

RESEARCH FACILITIES

For the sake of brevity of the present issue are included only the newly installed facilities and the acitivities since September 1983. Concerning the activities and facilities before September 1983, please refer to IMS Annual Review (1978~1983)

Computrer Center

The main facilities of the Computer Center are two HITAC M-200H computers, which have a processing capacity of over 10 million instructions per second. They have 32 mega byte main memory and 14 giga byte disk memory. The computers are used not only by the research staff at IMS but also by the staff at nearby National Institute as well as by scientists outside the Institutes in the related fields. As of March 1984, the number of project groups was 213 consisting of 587 users. In the twelve month period ending March 1984, 236519 jobs were processed with 8489 hours of the CPU time.

A program library for molecular science has been established under a unique library management system, with which users can search on their TSS terminal whereabouts and guides of wanted programs. Until March 1984, 109 programs have been registered on the disk memory and are being used frequentry. NUMPAC (Nagoya University Mathematical Package, including 603 programs) has also been registered. All of the QCPE programs has been obtained and will be so on the continued basis. The center is in service of five date bases, QCLDB (Quantum Chemistry Literature Data Base), IRDC (Infra-Red spectral Data Base), CHEMICS (Automated Organic Chemical Structure Elucidation System), STERIC (STEReochemistry by Input of CHEMO) and CMQCA (Carnegie-Mellon Quantum Chemistry Archive).

Chemical Materials Center

The Chemical Materials Center plays an important role in the synthesis and purification of organic and inorganic substances and preparation of single crystals. During 1983, much increased number of people used the Center to carry out the above works. The scientists and technical associates of this facility also carry out their own researches in collaboration with other scientists in IMS. Parts of the scientific activities are presented in the Section VI.

The Center is equipped with many kinds of instruments. In 1983, gas chromatograph–mass spectrometer (JEOL JMS D300) was overhauled and rebuilt for higher performance (rapid magnetic field scan and disk memory). Measurements of GC–milli-mass are much easier than before.

Instrument Center

For the efficient use of instruments, the Center is equipped with various types of instruments for general use.[1] Two instruments have been newly installed in 1984.

1) Excimer Laser and Dye Laser (Lambda Physik EMG50MSC, FL2002)

This excimer laser generates a pulse with pulse energy of 45 mJ/pulse at 308 nm (XeCl) and with repetition rate up to 100 MHz. Coupled with the excimer laser, the dye laser is operated in the tuning ranges of 315-970 nm in fundamentals and 217-360 nm in frequency doubling.

2) UV-Vis absorption spectrophotometer (Varian 2390)

This is a second version of UV-visible spectrophotometer in the Center, having basic specifications similar to the previous one, Cary 17. Wavelength range covers from 185 to 3152 nm. Absorbance range is selectable with 9 modes in full-scale range of 0.01 to 4.0.

Reference

1) *List of Instruments,* No.4, IMS Instrument Center (1983).

Low Temperature Center

The Center introduced a new system for supplying liquid nitrogen in July 1983: the supply of liquid nitrogen into a vessel is controlled and registered automatically.

The liquid helium container with a capacity of 1000/ has been equipped in May 1984 for increasing supply of liquid helium.

Equipment Development Center

A number of research instruments have been designed and constructed by making use of the mechanical, electric and glass-blowing technologies available at this facility. Representative instruments developed during this fiscal year of 1983 are listed below.

Molecular-Beam-Type Liquid-chromatograph-Mass Spectrometer
Molecular Beam Mass Spectrometer for IRMPD
Cryostat for Electrical Conductivity and Thermopower Measurements
Hydrogen liquefying cryostat (VII-J-1)
Atomic Fluorine Beam Source
Pressure Cell for ESR Measurement
Fabry-Perot Type Cavity Cell for MODR Spectroscopy
Penning Ionization Cell (II-A-6)
Digital Image Prossesing Unit for Streak Camera
Controller for Vacuum-UV Spectrophotometer (VII-M)
CAMAC Crate Controller
Spectrofluorimeter with Nanosecond Time Resolution (VII-I-1)
Programable power supply for photomultiplier (VII-L-2)
Multianode MCP Control System (Special Research Project)
Subpicosecond Auto Correlater (Special Research Project)
Glass Cryostat for Raman Spectroscopy
Glass Column with water- and vacuum-jackets

Ultraviolet Synchrotron Orbital Radiation Facility

On 10th Novembr 1983 (at 9 pm), the commissioning of UVSOR light source was succeeded. At that time, 450 MeV electrons with only less than 1 mA current were accumulated. At the end of February 1984, accumulation of 600 MeV electrons with 170 mA current was achieved. Figure 1 is a picture of synchrotron radiation from a bending section. The light source had been shut down since the beginning of March until the middle of June. During this shutdown, a wiggler and an undulator were installed, and RF cavity and vacuum doughnut were improved. At the end of June, electrons were accumulated again. Single bunch operation was

performed successfully.

The connection of monochromators to the synchrotron radiation outlets is under way, as one can see in Figure 2. At the beginning of October, the first monochromatized beam will go out from following monochromators; three 1m Seya-Namioka, one plane grating, one 3 m normal incidence and one double crystal monochromators.

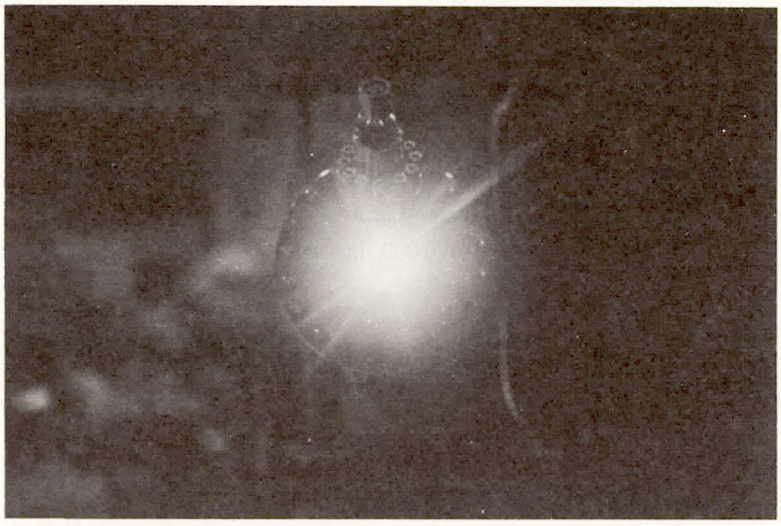

Figure 1. Synchrotron radiation from a bending section.

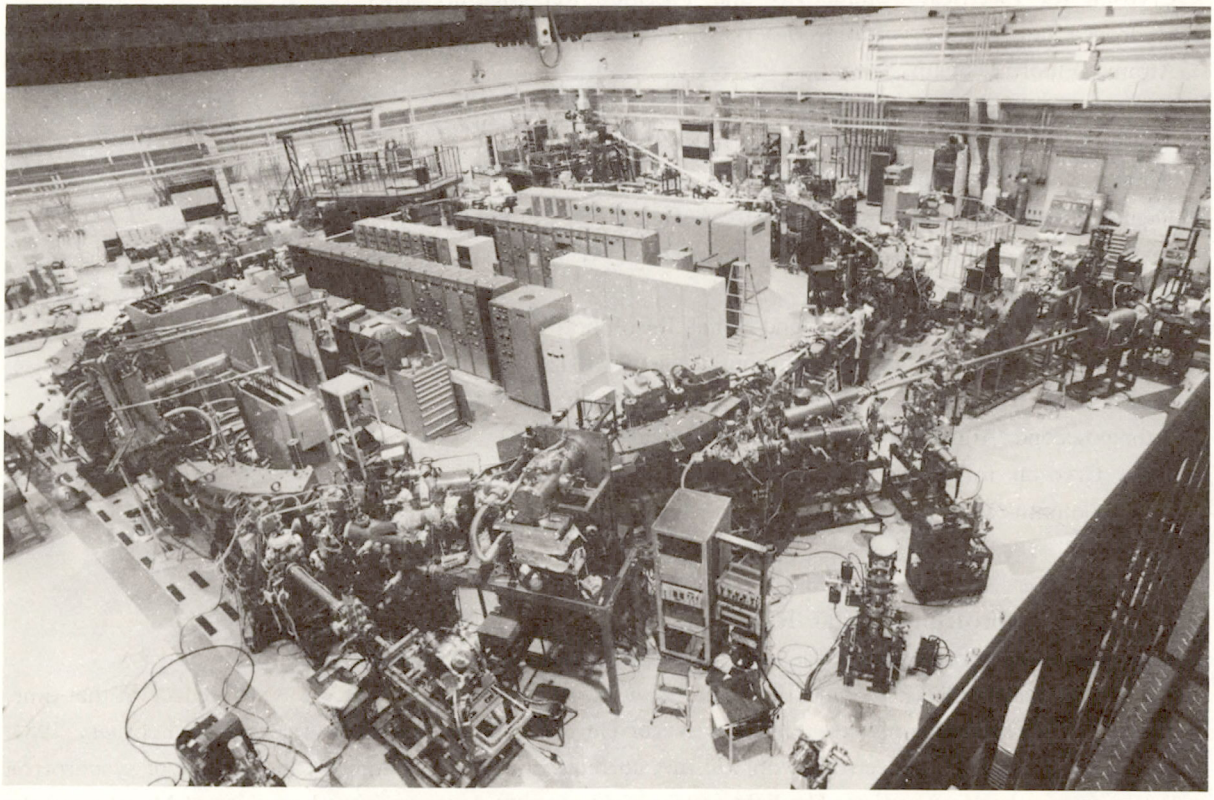

Figure 2. UVSOR storage ring with beam lines and monochromators.

SPECIAL RESEARCH PROJECT

IMS has special research projects supported by national funds. Two projects presently in progress under the second five year plan (1980–1985) are:

(1) The development and control of molecular functions,

(2) Energy transfer and energy conversion through molecular processes.

The third special research project started in the 1982 fiscal year is:

(3) Molecular science of primordial chemical evolution.

These projects are being carried out with close collaboration between research divisions and facilities. Collaborators from outside also make important contributions. Research fellows join these projects. In this report, the results in 1983 are reviewed.

(1) The Development and Control of Molecular Functions

Dynamical Molecular Structure and Control of Reactive Molecules

Eizi HIROTA,* Shuji SAITO,* Chikashi YAMADA, Yasuki ENDO, Kentarou KAWAGUCHI, Tetsuo SUZUKI, Hideto KANAMORI, Tatsuya MINOWA, and J.E. BUTLER *(NRL and IMS)*

Electrical discharge of either DC, 60 Hz, or microwave has proved to be extremely efficient in generating transient molecules; nearly 60 species investigated by the present research group were obtained by this means. However, it also produces a number of by-products in most cases. Furthermore, transient species of more complicated structures will be difficult to prepare by discharges, because they may be easily decomposed by discharge plasma.

Photolysis is much more attractive in this respect, because it is more selective than discharge. One important problem is the intensity of the light source, which has been too low. However, some of excimer lasers deliver nsec light pulses of 100 mJ with the repetition rate of up to 200 Hz. This pulse involves 10^{17} photons, which may be large enough to generate interesting transient species. We have combined this light source with our infrared diode laser system (II-B-1) and have obtained a few interesting results (II-A-11, II-A-12, and II-A-21).

High-Spin Hydrocarbons as a Model for Organic Ferromagnets

Hiizu IWAMURA,* Tadashi SUGAWARA, Hideyuki TUKADA, and Akira IZUOKA

A series of high-spin hydrocarbons have been designed by taking advantage of triplet diphenylcarbene as a building block and connecting the units in a non-Kekule fashion. In order to increase the thermal stability and incorporate the switching function, we have scrutinized several new carbenes to be used as a unit (V-A-3, V-A-4, and V-A-5). Some methoxy-substituted diphenylcarbenes were found to show an interesting singlet-triplet interconversion under UV-irradiation. The magnetic susceptibility measurements of the nonet tetracarbene, m-phenylenebis((diphenylmethylen-3-yl) methylene), were carried out with a Faraday-type magnetometer. The method proved to be useful in determining the high number of parallel spins which was conventionally determined by the ESR fine structure analyses and therefore difficult as the spin multiplicity increased. An anti-ferromagnetic interaction was observed for the tetracarbene molecules in the 2-methyltetrahydrofuran matrix (V-A-1).

Synthesis of Highly Functional Transition Metal Complexes and Their Use in Catalytic Reactions

Hidemasa TAKAYA,* Kazushi MASHIMA, and Tetsuo OHTA

We have been studying the synthesis of new chiral transition metal catalysts and their application to asymmetric organic reactions. We prepared 2,2′-bis(diphenylphosphino)-1,1′-binaphthyl (BINAP) and showed that it is a quite effective ligand for Rh(I)-catalyzed asymmetric hydrogenations of α-acylaminoacrylic acids and asymmetric rearrangements of allylamines to enamines. This time, we have developed new optical resolution techniques to obtain optically pure BINAP in large quantity. We also prepared many differently substituted BINAP ligands and elucidated their structures by *X*-ray analysis. A variety of asymmetric catalytic reactions are in progress by the use of these ligands.

Studies on the chemistry of metallacycle compounds are also the subject of our interests. We have prepared new stable titanacyclopentanes and revealed their interesting chemical behaviors. Parts of these results are presented in the Section VII-B and C.

CO_2 Uptake by Tetraazacycloalkane Complexes, and Syntheses and Structures of Ni(II)-Ni(IV) Mixed Valence Complexes

Tasuku ITO,* Koshiro TORIUMI, Masako KATO, Toshiaki KANAO, Masahiro YAMASHITA, and Haruko ITO *(Aichi Kyoiku Univ.)*

The chemical consequences of ligand macrocyclization in tetraazacycloalkane complexes and their applications are the subject of our continued interest. Our studies along this line have now been extended to the two titled projects. Parts of our results are presented in V-D and V-E.

Construction of a Multi-channel Detector for Inelastic X-ray Scattering

Kazuyuki TOHJI, Kazuo HAYAKAWA, and Yasuo UDAGAWA

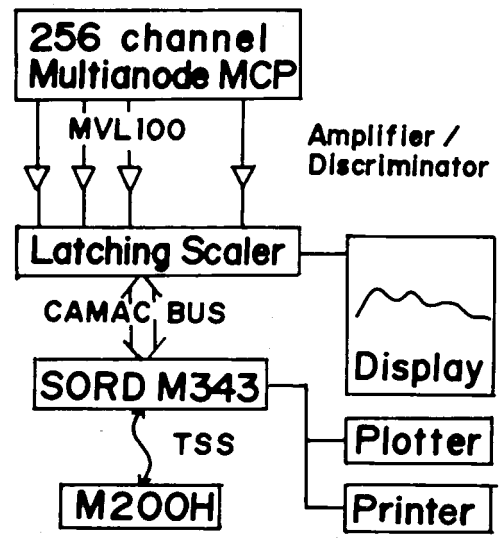

Figure 1. A block diagram of the detection system with multianode MCP.

Existence of inelastic Raman scattering in the x-ray region has been known for over 20 years. The full use of chemical information contained in the scattering, however, has been prevented because of the very low intensity. In order to obtain spectra of high quality from which plenty of structural information can be extracted, a construction of a multichannel x-ray detector has been attempted.

It consists of a microchannel plate (MCP) having 256 anodes with dimension of 0.1 × 10 mm, preamps based on LeCroy MVL100 amplifier/comparator, latching scalers (LeCroy 4434), and data acquisition electronics which is controlled by SORD M343 microcomputer through CAMAC bus. A block diagram of the system is shown in Figure 1. The system is still being developed and the performances will be reported in a near future.

Control of Molecular Function in Charge-Transfer complexes

Tadaoki MITANI, and Gunzi SAITO *(at present, Univ. of Tokyo)*

The physical properties of charge-transfer (CT) complexes are essentially under control of the degree of charge-transfer from donor- to acceptor-molecules. Some CT complexes, e.g. TTF-*p*-chloranil, were found to undergo a phase transition

from nominally neutral phase to nominally ionic (N-I) phase as a function of temperature and pressure. This fact suggests a possibility of control of molecular function of the CT complexes by using critical phenomena near the phase transition region. The experimental results of X-ray, ESR (see VII-L-1) and electrical conductivity measurements on TTF-p-chloranil single crystals indicates that the carrier density is discontinuously enhanced by the N-I phase transition. The mechanism of the carrier generation is attributable to the strong electron-lattice coupling induced by the increase of magnitude of the charge transfer. Furthermore, the conductivity can be varied over six order of magnitude under a pressure up to about 6 kbar and has a nonlinear responce to the magnitude of applied electric field. More detailed investigations of the transport mechanism are undertaken by using the photo-induced optical, ESR and conductivity measurements.

(2) Energy Transfer and Energy Conversion through Molecular Processes

Photocatalytic Effect of Semiconductor and Dyes: Its Application to Hydrogen Production and Organic Reactions

Kazuhito HASHIMOTO, and Tadayoshi SAKATA*

Highly efficient photocatalytic synthesis of amino acids was succeeded in by using organic acids and ammonia with powdered semiconductors or dyes. The quantum yields of these reactions amount to 20-40% with visible light without metal catalyst such as Pt. Moreover the reactions are highly selective and depends strongly on the kind of semiconductors. Among various organic acids, keto-, hydroxy- and unsaturated carboxylic acids were found to produce efficiently the corresponding amino acids.

Dynamics of photoelectrode processes including dye sensitization was investigated by measuring the transient photocurrent with a pulsed laser. For a highly doped TiO_2 single crystal electrode, a slow rise was observed in the time domain of 100-1000 ns. Such a rise due to charge transfer reaction at the interface is expected theoretically. Since this slow rise depends on the kind of redox reagent, it is considered to reflect the charge transfer reaction. In the case of dye sensitization, the life time of excited dyes adsorbed on the electrode surface was also measured. By measurement of the luminescence lifetimes of rose bengal and rhodamine B, which are adsorbed on semiconductor plates or quartz under air, it was found that for some cases fluorescence was quenched by the semiconductor, suggesting electron transfer occurs from the excited singlet states of these dyes. In the case of rose begal electron transfer from triplet state was suggested because of heavy atom effect.

Elucidation of the Activation Mechanism of Molecular Oxygen by Iron-porphyrin

Teizo KITAGAWA, Takashi OGURA, Shinji HASHIMOTO, Junji TERAOKA *(Osaka City Univ.)*, **and Muneteru KOZUKA** *(Tohoku Univ.)*

Activation scheme of molecular oxygen by heme enzymes is specific to a class of proteins such as oxidases, monooxygenases, dioxygenases, and peroxidases. We have characterized the iron coordination environments inherent to each class of hemeproteins. As the next stage of this project, we intends to investigate the reaction intermediates of the enzymes and the oxygen adduct of iron-porphyrin isolated by inert gas matrix at helium temperature. For this purpose a system to measure resonance Raman spectra at 4K was constructed and is coming into routine use. It is well known that electron donation to the oxygen adduct of hemeproteins produces an actual activated state. Therefore, we also try to elucidate the spectral properties of an electron rich porphyrin, that is, Fe(I) porphyrin. Combining the results of two kinds of experiments would allow us to discuss correctly the activation mechanism of molecular

oxygen by heme iron and a role of protein in the catalysis.

Development of the High Power Picosecond and Subpicosecond UV Laser System

Noriaki IKEDA, Nobuaki NAKASHIMA, and Keitaro YOSHIHARA

The laser system of high power picosecond and subpicosecond UV light pulses is constructed. A colliding pulse passive mode-locking ring dye laser is used as a source of subpicosecond light. The light pulses with 0.3-0.5 ps at 616 nm are amplified by a three-stage dye amplifier pumped by the 2ω of a YAG laser, frequency doubled to 308 nm, and then finally amplified by a XeCl excimer laser. Amplification of UV subpicosecond pulses by an excimer laser has been investigated for the first time. High power subpicosecond UV light pulses are expected to be very useful for elucidating photophysical and photochemical problems.

Picosecond Dynamics of Photophysics in Highly-Ordered Molecular Assemblies

Iwao YAMAZAKI, Naoto TAMAI, and Tomoko YAMAZAKI

In this research project, we are concerned with (1) liquid crystals, (2) multilayer systems and (3) biological systems, in which photophysical and photochemical processes of specific functions are expected to occur. In 1984, we have found that an excimer state forms in a liquid crystal. According to a picosecond time-resolved fluorescence spectroscopy, the excimer forms in 100 psec and decays with lifetime of 10 nsec. Also we found that the smectic A phase exhibits a divalent nature; there exist two states at a particular temperature, i.e., stable and quasi-stable states. Thermodynamical and optical characteristics are significantly different between them. The mutual change between the two states is performed with changing temperature. The paper was presented at Topical Meeting on Ultrafast Phenomena, Monterey, California, June, 12–15, 1984.

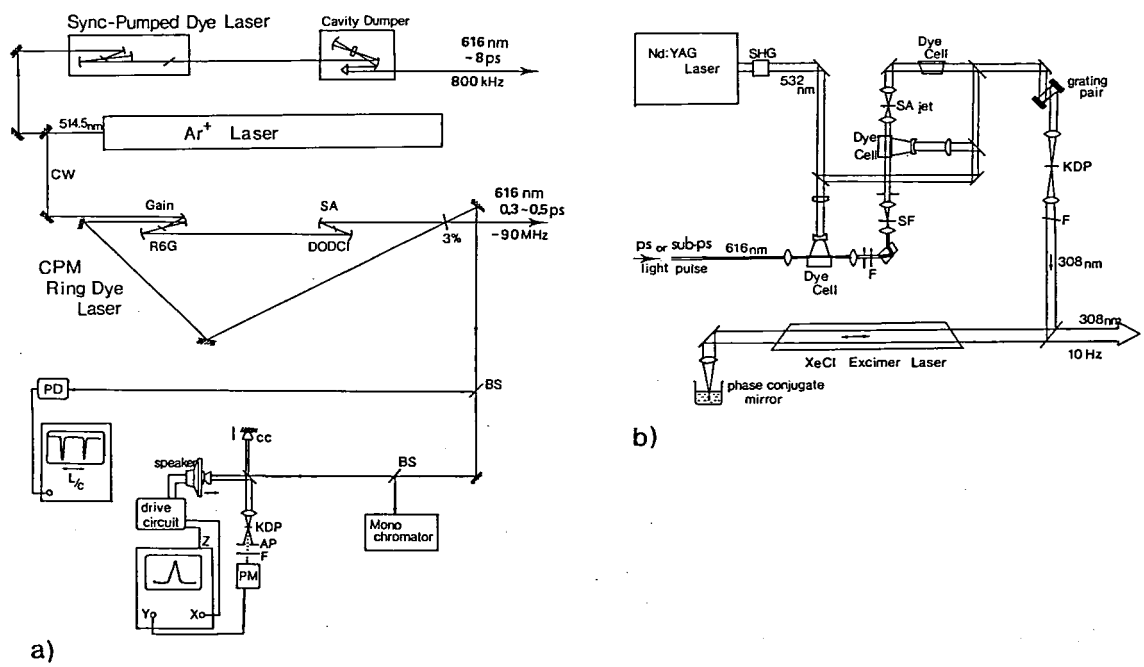

Figure 1. High power picosecond and subpicosecond UV laser system, a) dye lasers as a light source and monitor system, b) light amplification systems.

External Magnetic Field Effects upon Chemical Reactions

Yoshifumi TANIMOTO* *(Kanazawa Univ. and IMS)*, **Ryoichi NAKAGAKI,* Takeshi WATANABE, Mitsuo HIRAMATSU** *(Hamamatsu Photonics K.K. and IMS)*, **and Saburo NAGAKURA**

External magnetic field effects on chemical reactions can be used as an excellent probe for reaction mechanism in the solution phase. In the present project, we have studied photochemical and electrochemical reactions in solution.

(1) Photochemistry: photo-Fries rearrangement of 1-naphtyl acetate was found to occur through homolytic cleavage of the C-O bond in the excited singlet state. Observed results were explained by using a radical pair model.

(2) Electrochemistry: electrolysis of ferricyanide and ferrocyanide was found to be influenced by an external magnetic field. Observed results were interpreted in terms of the mangetohydrodynamic effect.

Photoelectron Spectroscopy of Excited States by Laser Multiphoton Ionization: Its Applications to Molecules and van der Waals Molecules in Supersonic Jet

Katsumi KIMURA,* Yohji ACHIBA, and Kenji SATO

In order to follow excited states of single molecules and van der Waals molecules from a new spectroscopic point of view, we have recently developed a laser photoelectron spectroscopic technique of resonant multiphoton ionization with a supersonic jet. This method makes it possible to study excited states which cannot be detected by other spectroscopic techniques. The aim of this work in the Special Research Project is to apply this technique to study photochemical and photophysical processes such as intramolecular vibrational relaxation, photodissociation, and intermolecular electron transfer, using molecular species in supersonic beams. In order to do this, we have been studying (1) organo-metalic compounds, (2) van der Waals complexes on NO, and (3) aromatic compounds (see IV-K).

Intramolecular Energy Transfer in Vibrationally Excited Molecular Clusters and Molecular Beam Studies of Reaction Dynamics of Chemically Reactive Atoms and Free Radicals

Kosuke SHOBATAKE, Kiyohiko TABAYASHI, and Shigeru OHSHIMA

We have continued the studies of reaction dynamics involving active nitrogen atoms $N^*(^2P, ^2D)$ and metastable rare gas atoms produced from an arc-heated nozzle beam source. In order to determine accurate collision energy dependences of reactive as well as excitation energy transfer reactions, a time-of-flight (TOF) energy selection technique combined with the crossed molecular beam method was newly introduced. We have so far studied (1) chemiluminescent reactions of $N^*(^2P, ^2D)$ + HI and HBr forming $NH(A^3\Pi)$ (see Research Activities IV-M-1), and (2) excitation energy transfer processes $Ar^*(^3P_{0,2})$ + N_2 (see IV-M-2) and $Kr^*(^3P_{0,2})$ + N_2 (see IV-M-3) producing nascent N_2 $(C^3\Pi_u)$.

We have initiated photoassisted surface reactions. To begin with, a 308 nm laser assisted eching reaction of solid Si surface with fluorine molecules has been studied using a crossed molecular beam apparatus (Model MBC-1).

(3) Molecular Science of Primordial Chemical Evolution

Laboratory Microwave Spectroscopy of Interstellar Molecules; the 2_{20} — 2_{21} transition of the H_2D^+ ion

Shuji SAITO,* Kentarou KAWAGUCHI, and Eizi HIROTA

The ion-molecule reaction model is currently believed to explain formation and existence of various and complex interstellar molecules.[1] Identification of several molecular ions and free radicals has given a strong support to the theory. However, many molecular ions fundamentally important in the model have been left to be identified in space. H_3^+ is such an example and the most important molecular ion in the model.

We have observed a microwave spectral line of the monodeuterated species of H_3^+. The experimental details are given in II-A-18. The frequency determined is 155987.185 ± 0.037 MHz. The transition observed is the most suitable spectral line for ground-based radioastronomical search for H_2D^+ in space when the frequency regions and sensitivities of radiotelescope available and excitation of molecules in space are considered. Oka[2] observed the infrared active ν_2 band of H_3^+ by using a difference-frequency laser spectroscopy. However, observations of the corresponding spectrum from space with an infrared telescope seem to be difficult because infrared emission in the 2500 cm^{-1} region requires H_3^+ to be efficiently excited (~3600°K) and infrared absorption may be seen only when a large amount of H_3^+ is present between the earth and an infrared source.[3] Therefore, if the $2_{20} - 2_{21}$ line of H_2D^+ is observed by radiotelescopes, it would be very useful for diagnoses of interstellar molecular clouds.

References

1) E. Herbst, and W. Klemperer, *Astrophys. J.* **185**, 505 (1973).
2) T. Oka, *Phys. Rev. Letters*, **45**, 531 (1980).
3) T. Oka, *Phil. Trans. Roy. Soc. Lond.* **A303**, 543 (1981).

Roles of Internal and Collisional Energies in Ion-Molecule Reactions

Inosuke KOYANO,* Kenichiro TANAKA, and Tatsuhisa KATO

In order to investigate specific roles played by various forms of reactant energy in chemical reactions, studies of state-selected ion-molecule reactions have been performed over the last several years, using a coincidence technique which we have developed recently.[1] The internal states selected include vibrational states of diatomic and polyatomic ions, vibronic states of diatomic ions, and spin-orbit states of rare gas ions. Last year, emphasis has been placed on the reactions in four-atomic systems, such as $(H_2 + O_2)^+$, $(H_2 + NO)^+$, and $(H_2 + N_2)^+$, and the charge transfer reactions in the $Ar^+ + BC \rightleftharpoons Ar + BC^+$ systems, where BC = H_2, O_2 and NO. Comparison of experimental results among various systems, combined with a close examination of the nature and location of relevant potential energy curves of the reactant and product systems (at infinite inter-molecular separation), revealed that the characteristic roles of vibrational and translational energies in chemical and charge transfer reactions are indeed determined by the types of interactions and nonadiabatic transitions among relevant potential energy surfaces caused by reactants' approach. Two typical types of such nonadiabatic transitions have been extracted from these studies.

Reference

1) I. Koyano and K. Tanaka, *J. Chem. Phys.* **72**, 4858 (1980).

C_n Production following IRMPD of Hydrocarbons

Ichiro HANAZAKI and Masaaki BABA

The C_n molecule is important in chemical evolution processes, whose emission has been observed in comets. The C_2 and C_3 molecules can be easily produced by infrared multiphoton dissociation (IRMPD) using a CO_2 laser. The main purpose of this work is to find the optimum condition for the production of larger C_n molecules ($n \geq 4$) and to investigate the chemical reaction of these molecules. Here we report the preliminary results for the C_3 molecule. The C_3 molecule was produced by the IRMPD of allene (C_3H_4) and detected by the use of laser induced fluorescence technique. This measurement has been made first by Lesieckl *et al.*[1] The fluorescence spectrum of $C_3(^1\Pi_u \leftarrow {}^1\Sigma_g^+)$ following the 0-0 band excitation (405nm) is shown in Figure 1. The spectral resolution was much higher than that of Lesieckl *et al.* and we could partially resolve rotational levels.

The infrared irradiation of hydrocarbons is a clean source of C_n. This study will be extended to

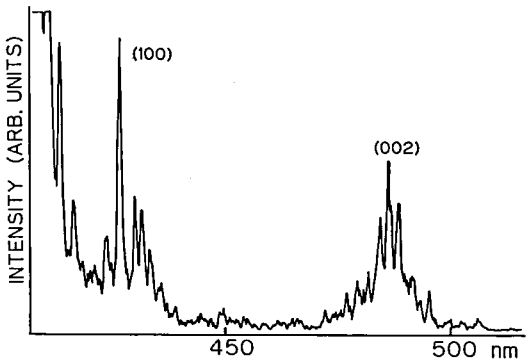

Figure 1. $C_3(^1\Pi_u \leftarrow {}^1\Sigma_g^+)$ fluorescence spectrum following 405 nm excitation of C_3H_4 in $Ar(C_3H_4/Ar = 1{:}35$, total pressure is 15 Torr.).

the chemical reaction with other molecules and we expect to obtain some useful information on the production of large organic molecules in comets or intersteller space.

Reference

1) M.L. Lesieckl, K.W. Hicks, A. Orenstein, and W.A. Guillory, *Chem. Phys. Lett.*, **71**, 72 (1980).

Development of a New-Type Low-Temperature Liquid Chromatograph-Mass Spectrometer for the Analysis of Unstable Molecules Formed by Surface Reactions

Tohru OKUYAMA, Toshio HORIGOME, and Nobuyuki NISHI

In order to investigate dust-surface reactions at low temperature, one needs to isolate and identify the reaction products before their chemical change during an analytical procedure. Photochemical reactions or hot atom reactions of interstellar molecules such as cyanide compounds or acetylene compounds produce many labile molecules which are easily polymerize at room temperature. The reactions at room temperature have different factors which do not exist at low temperature surfaces.

We have designed and constructed a new LC-MS machine with a sophisticated vaporization interface using a coaxial molecular beam technique. The detailes of the interface will be reported somewhere else. The use of this interface made it possible to get constant gas flow of solute and solvent molecules. Solute molecules are concentrated depending on the mass number relative to the mass of solvent molecules. An LC column is situated in an ultra-low temperature freezer with a volume of 180 *l*, which is capable of the operation at $-90 \sim -50°C$ for methanol or liquid dimethyl ether. Signals are stored in a microcomputer disk.

Other advantages of this LC-MS system are; 1) the use of electron impact ionization which can provide structural informations through cracking patterns of isolated molecules, 2) the detection of molecules which have no absorption at visible and UV region (<200 nm), 3) relatively high resolution of the LC system at low temperatures. 1 ng of benzene in methanol has been detected and now further improvement for much higher detection sensitivity is in progress. Application of this machine to the analysis of HCN containing solid systems will be reported in near future.

OKAZAKI CONFERENCES

"Okazaki Conferences" are principal symposia at IMS, which are held on the subjects related to the "Special Research Projects". They are held usually twice a year, with a moderate number of participants around 50, including several invited foreign speakers. The formal language for the conference is English. Outlines of the seventeenth to twentieth conferences are as follows.

The Seventeenth Okazaki Conference

Aromaticity and Aromatics

(September 26—28, 1983)

Organizers: I. Murata *(Osaka Univ.)*, **H. Inokuchi** *(IMS)*
Invited Speakers: W.C. Herndon *(Univ. of Texas)*, **W. Schmidt** *(Biochem Inst., Ahrensburg)*, **F. Vögtle** *(Univ. Bonn)*

At 17th. conference, 50 attendants discussed on recent progress of aromaticity and aromatics.

The conference was divided into three sessions: (1) Theoretical approach of aromaticity, (2) Characterization of aromatic compounds in which nonbenzenoid aromatics were included and (3) Synthesis of novel aromatic compounds.

The conference was started with the opening address by Prof. S. Nagakura, Director-General, and followed by 23 lectures. Prof. W.C. Herndon presented the concept of three-dimensional aromaticity by means of structure-resonance theory and Prof. J. Aihara explained aromaticity and diatropicity with graph − theoretical interpretation. Dr. W. Schmidt talked on structure elucidation of many polycyclic aromatic hydrocarbons by photo-electron spectroscopical method and Prof. H. Iwamura presented a producing ferromagnetic

character in high spin aromatic hydrocarbons. Further, Prof. F. Vögtle discussed the linked system between chromophore and ionophore.

Prof. Murata expressed, in his conclusion address, that the conference has been successful to find a future trend in the research field of "aromatics and aromaticity".

The Eighteenth Okazaki Conference

Theories of Reaction Mechanisms: New Concepts and Prospects

(January 19—21, 1984)

Organizers: K. Nishimoto *(Osaka City Univ.)* **and K. Morokuma** *(IMS)*
Invited Speakers: D.G. Truhlar *(Univ. of Minnesota)*, **J.C. Lorquet** *(Univ. de Liege)*, **M. Yoshimine** *(IBM San Jose)*, **J.T. Hynes** *(Univ. of Colorado)*, **and T.H. Dunning** *(Argonne National Lab.)*

Complete understanding of chemical reaction mechanisms is one of the most important goals of theoretical chemistry. Recent advent of the energy derivative method allows theoreticians to explore efficiently potential energy hypersurfaces that control chemical reactions. Concurrent with such a development, collisional and statistical approaches to reaction rates and mechanisms are providing a new insight into reactions of excited states and reactions in solution as well as reactions of gas phase ground state molecules. The purpose of the present conference was to comprehend new waves of theoretical studies, to reveal new concepts that are cooking and to explore directions of future development. There were about 70 participants, about two thirds theoreticians and the rest experimentalists.

Among the invited speakers D. Truhlar talked about dynamic bottlenecks and tunneling effects in atom-transfer reactions. T. Fueno discussed paths and rates of gas phase elementary reactions. J.C. Lorquet's talk was on rate constants of non-adiabatic unimolecular reactions. H. Nakamura presented semiclassical theories for nonadiabatic transitions and chemical reactions. M. Yoshimine talked about interconversion on the C_3H_4 potential

energy surface. J.T. Hynes' presentation was about the reaction coordinate in solution. T.H. Dunning discussed potential energy surfaces for simple chemical reactions. E.R. Davidson talked about potential energy surfaces for radical rearrangements.

A panel discussion was held in the evening of the first day to create a forum between experimentalists and theoreticians. As a panel experimental groups at IMS presented new techniques and results in which reaction mechanisms and dynamics were being studied. Participants are convinced that collaboration between experimentalists and theoreticians is essential for better understanding of reaction mechanisms and for a further step of controlling chemical reactions.

The Nineteenth Okazaki Conference

Formation and Evolution of Molecules in Space

(March 19—21, 1984)

Organizers: I. Hanazaki, I. Koyano, S. Saito, and N. Nishi *(IMS)*

Invited Speakers: W.M. Irvine *(Univ. Massachusetts)*, **E. Herbst** *(Duke Univ.)*, **D.K. Bohme** *(York Univ.)*, **L.J. Stief** *(NASA Goddard Space Flight Center)*, **and A. Bossard** *(Univ. Paris Val de Marne)*

Radioastronomy, especially that with millimeter wavelength telescopes, has shown the presence of a vast array of molecules in interstellar space. The formation and evolution of interstellar molecules occur under drastically different conditions from those on the earth. For the understanding of this big subjects, it is required to concentrate and develop the knowledges in the fields of astronomy, physics, physical chemistry, and biochemistry. Specialists from these fields joined to discuss the recent progress of this problem. The topics discussed in this conference is classified into four categories.

Session 1: Prof. Hayakawa gave a lecture on "Roles of Molecules in the Evolution of the Universe". The invited speaker, Prof. W.M. Irvine presented the results of recently completed "spectral scan" of the several molecular clouds at the Onsala

Space Observatory. The results of molecular survey at Nobeyama Radio Observatory and Nagoya University were also reported. Prof. Takayanagi gave an after dinner talk on his research history in this field.

Session 2: Gas phase chemistry, especially the role of ion-molecule reactions, was discussed following the lecture by Prof. E. Herbst. Prof. D.K. Bohme reported the laboratory measurements of rate constants for ion-molecule reactions by SIFT technique.

Session 3: The topics on the molecular composition of cometary nuclei and chemical reactions on cometary ices were presented in this session. Dr. L.J. Stief was invited to give a talk on the photochemistry and the connection of interstellar molecules and cometary molecules.

Session 4: The last session was focused on the topics in chemical evolution. Dr. A. Bossard examined the possible syntheses of organics in reduced or oxidized atmosphere. In the last talk, Prof. Harada introduced us the chemical reactions of organic compounds in aqueous solution as possible pathways for the formation of bio-organic compounds on the primitive earth.

The Twentieth Okazaki Conference

Photochemical Electron Transfer Assisted by Functionalized Interface

(August 18—20, 1984)

Organizers: I. Tabushi *(Kyoto Univ.)*, **K. Yoshihara, and T. Sakata** *(IMS)*
Invited Speakers: M. Grätzel *(EPF, Lausanne)*, **M.A. Fox** *(Univ. Texas at Austin)*, **A. Heller** *(Bell Laboratories)*, **A. Mackor** *(Institute of Applied Chemistry TNO)*, **and T.J. Meyer** *(Univ. North Carolina)*

The conference was held for the purpose of discussing recent progress in photochemical electron transfer at the functionalized interface as related to photo-conversion of solar energy. Before the conference, an informal meeting was held in the evening of the 17th, chaired by Prof. A. Fujishima. Lively discussions about the future of photochemical energy conversion were held. Lectures at

the conference can be classified into the following three subjects; (1) Electron transfer and water cleavage by excited dye molecules. (2) Mechanism of charge separation at the functionalized semiconductors (including organic solids)/liquid (or gas) interface. (3) Photocatalysis on the functionalized interface and its application to reduction of CO_2 and other organic reactions.

Active discussions were held on the physical and chemical properties of the functionalized interface and the possibility of controlling the photochemical electron transfer at the interface. Several efficient systems for hydrogen evolution, CO_2 reduction and organic synthesis were shown.

Besides the plenary lectures, many foreign scientists, Drs. F. Willig (Max Planck Inst.), A.J. Nozik (SERI), G. Hodes (Weizman Inst. Sci.), A. Frank (SERI), M.G. Kinnaird (Univ. North Carolina and Kyoto Univ.) and J.L. Sessler (Stanford Univ. and Kyoto Univ.) were invited in this conference.

JOINT STUDIES PROGRAMS

As one of the important functions of an inter-university research institution, IMS undertakes joint studies programs for which funds are available to cover research expenses as well as travel and living expenses of individuals. The proposals from domestic scientists are reviewed and controlled by the inter-university committee. The programs are carried out under one of four categories:

1) Joint Studies on special projects (a special project of significant relevance to the advancement of molecular science can be carried out by a team of several groups of scientists).
2) Research Symposia (on timely topics in collaboration with both outside and IMS scientists).
3) Cooperative Research (carried out in collaboration with both outside and IMS scientists).
4) Use of Facility (the Computer Center, Instrument Center and other research facilities at IMS are open to all researchers throughout the country).

In the fiscal year 1983, numbers of joint studies programs accepted amounted to 3, 8, 215, and 186 for categories 1) – 4), respectively.

1) Joint Studies

Cytochrome c_3 as Molecular Device Material

Coordinators: **Hiroo INOKUCHI** *(Department of Molecular Assemblies)*
Tatsuhiko YAGI *(Shizuoka University)*

In many characteristics of cytochrome c_3 that make this molecule unique organometallic compounds, we observed AC conductivity of cytochrome c_3 film at reduced state and magnetic resonance of this hemoprotein. Further, theoretical approach for electron transfer in the crystal is being studied.

Molecular Design and Construction of New Organic Reactive Intermediates

Coordinator: **Hiizu IWAMURA** *(Department of Applied Molecular Science)*

The joint study was started in 1983 with the aim of preparing and characterizing new organic reactive intermediates such as carbonium ions, carbanions, carbenes and nitrenes of molecular scientific interest. We have since been concentrating ourselves on three projects. In close collaboration with the scientists of Osaka City University, we generated polycarbenes that had ground multiplet states and therefore the potentiality of organic magnetic materials. Pentakis(diazo) compound was prepared. The magnetic susceptibility of the nonet tetracarbene was measured (see V-A-1). A perturbational method has been applied with success to solve the K-band ESR fine structures taken on unoriented samples of the septet and nonet species (see V-A-2). In a second project with the University of Tokyo group, we designed a series of ortho-ester anhydrides in which the rates of ionic dissociation and ion-pair return were determined independently by the ^{1}H and ^{17}O DNMR technique. The method proved to be useful in analyzing the solvolytic reaction mechanism. New reactions via carbonyl oxides and dioxiranes were studied in collaboration with the Nagoya University group. Importance of these reactions in oxidation processes was disclosed.

Spectroscopy of Organic Semiconducting Crystals under Hydrostatic Pressure

Coordinators: **Tadaoki MITANI** *(Equipment Development Center)*
Takao KODA *(Univ. of Tokyo)*

Studies of pressure-induced effect upon electronic properties of organic crystals are becoming increasingly important in molecular crystal physics and chemistry, since the pressure-induced changes in the intermolecular interactions in organic crystals often bring about many novel features which are

not expected to be observable at ambient pressure. In the first stage of the present program, efforts have been made to design and construct an assembly of high-pressure system for the accurate measurements of various optical spectra including reflectivity, absorption, luminescence, Raman scattering, photoconductivity etc. over a wide photon energy region (1~5 eV). In the second stage of the program, attempts were successfully made to observe pressure-induced changes of the reflectivity of some organic semiconductors, such as TTF-*p*-chloranil crystals. As a further extension of this study, the following plan is being made; development of high-pressure optical cell for lower temperature measurement down to liquid Helium temperature, establishment of magnetic resonance (ESR, NMR) measurement technique under high-pressure.

The members of the program are T. Koda, Y. Tokura, Y. Kaneko, Y. Wada, S. Tanuma *(Univ. of Tokyo),* T. Takahashi, Y. Maniwa *(Gakushuin Univ.),* A. Matsui *(Konan Univ.),* H. Nishimura *(Osaka City Univ.),* H. Yoshioka, S. Kazama *(Sizuoka College of Pharmacy)* and T. Mitani *(Equipment Development Center).*

2) Research Symposia

1. Photoionization Spectroscopy of Molecules and Molecular Clusters.
   (June 18th, 1983)
   Organizer: K. Kimura (IMS)
2. Solar Energy Conversion Utilizing Dye Staffs
   (April 26th, 1983)
   Organizer: K. Yoshihara (IMS)
3. Applications of Methodology of Molecular Science to Coordination Chemistry.
   (January 8th — 9th, 1984)
   Organizer: H. Ohtaki (Tokyo Inst. Tech.)
4. EXAFS — Present Status of Experiments and Data Analysis.
   (January 13th — 14th, 1984)
   Organizer: Y. Udagawa (IMS)
5. Properties of Lipid Membrane Double Layers.
   (November 10th — 11th, 1983)
   Organizer: T. Izuyama (Univ. Tokyo)
6. Experiments and Theories on the Rate of Chemical Reaction —Transition States—.
   (October 28th — 29th, 1983)
   Organizer: S. Tsuchiya (Univ. Tokyo and IMS)
7. Vibrational Relaxation and Nonradiative Transition of Optical Excitation.
   (January 28th, 1984)
   Organizer: K. Nasu (IMS)
8. Role and Possible Applications of Computer Calculations in Molecular Science.
   (March 28th — 30th, 1984)
   Organizer: K. Nakanishi (Kyoto Univ.)

3) Cooperative Reseach

This is one of the most important programs IMS undertakes for conducting its own research of the common interest to both outside and IMS scientists by using the facilities at IMS. During the first half of fiscal year of 1983 ending on September 30, 91 outside scientists including 6 invited collaborated with IMS scientists; and during the second half of the fiscal year, 76 outside scientists including 7 invited worked in collaboration with IMS scientists. the names and the affiliations of these collaborators are found in the Research Activities.

4) Use of Facility

The number of projects accepted for the Use of Facility Program of the Computer Center during the fiscal year of 1983 amounted to 139 (383 users), and the computer time spent for these projects is 4669 hours (58% of the total annual CPU time).

Forty seven projects (71 users) were accepted for the Use fo Facility Program of the Instrument Center during the fiscal year of 1983.

FOREIGN SCHOLARS

Visitors from abroad play an important role in research activities and are always welcomed at IMS. The following is the list of foreign scientists who visited IMS in the past year (Aug. 1983 – Jul. 1984). The sign *1 indicates a scientist invited to attend an Okazaki Conference, *2 a scientist invited on the Invited Foreign Scholars Program, *3 a councillor of IMS, *4 an IMS visiting scientist and *5 an adjunct professor from abroad.

Dr. M. Yoshimine*[4]	IBM	(USA)	Aug. 1983
Prof. H. Tributsch	Hahn Meitner Inst.	(W. Germany)	Aug. 1983
Prof. T. Ree	Seoul Natl. Univ.	(Korea)	Aug. 1983
Prof. F.K. Tittel*[4]	Rice Univ.	(USA)	Aug. 1983
Prof. J.R. McNesby*[2]	Univ. of Maryland	(USA)	Sep. – Dec. 1983
Prof. S.H. Bauer*[5]	Cornell Univ.	(USA)	Sep. – Dec. 1983
Dr. L. Woeste	Ec. Polytech. Lausanne	(Switzerland)	Sep. 1983
Dr. H. Seki	IBM	(USA)	Sep. 1983
Dr. E. Kay	IBM	(USA)	Sep. 1983
Prof. W.C. Herndon*[1]	Univ. of Texas at El Paso	(USA)	Sep. 1983
Prof. W. Schmidt*[1]	Biochemisches Inst.	(W. Germany)	Sep. 1983
Prof. F. Vogtle*[1]	Rhein Friedrich-Wilhelm Univ.	(W. Germany)	Sep. 1983
Prof. B.K. Cheng*[4]	Natl. Taiwan Univ.	(Taiwan)	Sep. 1983
Dr. G. Saxon*[5]	Daresbury Lab.	(UK)	Oct. 1983 – Mar. 1984
Dr. J. Los	FOM	(Netherland)	Oct. 1983
Prof. W. Fosong	Acad. of Sci. of China	(China)	Oct. 1983
Mr. B. Wang	Mongolian Educational Univ.	(China)	Oct. 1983
Prof. P. Olum	Univ. of Oregon	(USA)	Oct. 1983
Prof. M. Kasha*[3]	Florida State Univ.	(USA)	Oct. – Nov. 1983
Prof. H. Zollinger	Eidgerossische Technische Hochschule Zurich	(Switzerland)	Nov. 1983
Dr. L.C.L. Yuan*[4]	Brookhaven Natl. Lab.	(USA)	Nov. 1983
Dr. L. Vo Ky*[-]	Observatoire de Paris	(France)	Nov. – Dec. 1983
Prof. T. Theophanides	Univ. of Montreal	(Canada)	Nov. 1983
Prof. K. Nakamoto*[4]	Marquette Univ.	(USA)	Nov. 1983
Prof. W.M. Jackson, Jr*[4]	Howard Univ.	(USA)	Nov. 1983
Prof. W. Lester*[4]	Univ. of California, Berkeley	(USA)	Nov. 1983
Dr. Z.M. Bao*[4]	Univ. of Sci. and Tech. of China	(China)	Nov. 1983
Dr. F.H. Wang*[4]	Univ. of Sci. and Tech. of China	(China)	Nov. 1983
Dr. X.B. Wang*[4]	Univ. of Sci. and Tech. of China	(China)	Nov. 1983
Dr. I. Munro*[4]	Daresbury Lab.	(UK)	Dec. 1983
Prof. E.R. Davidson*[5]	Univ. of Washington	(USA)	Dec. 1983 – Jun. 1984
Prof. M.D. Morris	Univ. of Michigan	(USA)	Dec. 1983
Dr. L. Radom*[2]	Australian Natl. Univ.	(Australia)	Dec. 1983 – Jan. 1984
Prof. E.C. Lim*[2]	Wayne State Univ.	(USA)	Jan. – May 1984
Prof. C.D. Lin	Kansas Univ.	(USA)	Jan. 1984
Prof. R.K. Helmut	Univ. Dortmund	(W. Germany)	Jan. 1984
Prof. K.H. Reich*[4]	Univ. Dortmund	(W. Germany)	Jan. 1984
Dr. P.J. Wu*[2]	Acad. of Sci. of China	(China)	Jan. 1984 –

Prof. Z.G. Soos	Princeton Univ.	(USA)	Jan. 1984
Prof. K.H. Peich	Univ. Dortmund	(W. Germany)	Jan. 1984
Dr. T.H. Dunning*[1]	Argonne Natl. Lab.	(USA)	Jan. 1984
Dr. M. Yoshimine*[1]	IBM	(USA)	Jan. 1984
Prof. J.C. Lorquet*[1]	Univ. of Liège	(Belgium)	Jan. 1984
Dr. A.J. Lorquet	Univ. of Liège	(Belgium)	Jan. 1984
Prof. D.G. Truhlar*[1]	Univ. of Minnesota	(USA)	Jan. 1984
Prof. J.T. Hynes*[1]	Univ. of Colorado	(USA)	Jan. 1984
Prof. R.Z. Sagdeev*[4]	Inst. of Chemical Kinetics and Combustion	(USSR)	Jan. 1984
Prof. J. Belloni	Univ. Paris-Sud	(France)	Feb. 1984
Prof. R.M. Metzger*[4]	Univ. of Mississippi	(USA)	Feb. 1984
Prof. B. Horovitz	Weizmann Inst. of Sci.	(Israel)	Feb. 1984
Dr. T.B. Tang*[2]	Univ. of Cambridge	(UK)	Mar. 1984 –
Dr. Z. Latajka*[2]	Univ. of Wrocław	(Poland)	Mar. 1984 –
Dr. M. Bouréne	Sci. Attache, French Embassy	(France)	Mar. 1984
Prof. J.H. Fendler	Clarkson College of Tech.	(USA)	Mar. 1984
Prof. M. Calvin	Univ. of California, Berkeley	(USA)	Mar. 1984
Dr. J. Katz	Argonne Natl. Lab.	(USA)	Mar. 1984
Prof. J. Kozak	Univ. of Notre Dame	(USA)	Mar. 1984
Dr. J. Miller	Argonne Natl. Lab.	(USA)	Mar. 1984
Dr. S. Feldberg	Brookhaven Natl. Lab.	(USA)	Mar. 1984
Prof. G. McLendon	Univ. of Rochester	(USA)	Mar. 1984
Dr. N. Sutin	Brookhaven Natl. Lab.	(USA)	Mar. 1984
Dr. J. Connolly	SERI	(USA)	Mar. 1984
Prof. S.G. Boxer	Stanford Univ.	(USA)	Mar. 1984
Prof. J.K. Thomas	Univ. of Notre Dame	(USA)	Mar. 1984
Mr. C.T. Owenes	NSF	(USA)	Mar. 1984
Dr. C.W. Wallace	NSF	(USA)	Mar. 1984
Prof. D.G. Whitten	Univ. of Rochester	(USA)	Mar. 1984
Dr. E. Greenbaum	Oak Ridge Natl. Lab.	(USA)	Mar. 1984
Dr. J. Norris	Argonne Natl. Lab.	(USA)	Mar. 1984
Prof. D.K. Bohme*[1]	York Univ.	(Canada)	Mar. 1984
Prof. A. Bossard*[1]	Univ. Paris Val De Marne	(France)	Mar. 1984
Prof. W.M. Irvine*[1]	Univ. of Massachusetts	(USA)	Mar. 1984
Dr. L.J. Stief*[1]	NASA	(USA)	Mar. 1984
Prof. E. Herbst*[1]	Duke Univ.	(USA)	Mar. 1984
Prof. D. Phillips*[2]	The Royal Institution	(UK)	Mar. – Jul. 1984
Mr. J. Moore*[4]	The Royal Institution	(UK)	Mar. – Jul. 1984
Dr. S. Mahjan*[2]	Indian Inst. of Tech.	(India)	Mar. 1984
Dr. B.T. Lim*[4]	Wayne State Univ.	(USA)	Mar. – Apr. 1984
Prof. M.L. Ginter	Univ. of Maryland	(USA)	Apr. 1984
Prof. R. Rigler	Karolinska Inst.	(Sweden)	Apr. 1984
Prof. A. Ehrenberg	Stockholm Univ.	(Sweden)	Apr. 1984
Prof. A. Padwa	Emory Univ.	(USA)	Apr. 1984
Dr. M. Key	Rutherford Lab.	(UK)	Apr. 1984
Dr. W.X. Zheng	Univ. of Sci. and Tech. of China	(China)	Apr. 1984
Dr. Y.X. He	Acad. of Sci. of China	(China)	Apr. 1984
Dr. Z.Z. Li	Acad. of Sci. of China	(China)	Apr. 1984

Dr. P.J. Yao	Acad. of Sci. of China	(China)	Apr. 1984
Dr. W.Z. Jin	Acad. of Sci. of China	(China)	Apr. 1984
Dr. D.F. Hu	Univ. of Sci. and Tech. of China	(China)	Apr. 1984
Dr. Z.Y. Zhao	Acad. of Sci. of China	(China)	Apr. 1984
Dr. Y.S. Zhan	Acad. of Sci. of China	(China)	Apr. 1984
Dr. M.L. Xu	Acad. of Sci. of China	(China)	Apr. 1984
Prof. A.B.P. Lever*[4]	York Univ.	(Canada)	Apr. 1984
Prof. R.L. Carrie	Univ. de Rennes 1	(France)	Apr. 1984
Prof. R.A. Stradling*[4]	Univ. of St. Andrews	(UK)	Apr. 1984
Prof. A.J. Leadbetter*[4]	Rutherford Lab.	(UK)	Apr. 1984
Dr. J. Richards*[4]	British Council	(UK)	Apr. 1984
Prof. Y.L. Chow*[2]	Simon Fraser Univ.	(Canada)	May 1984
Prof. V.L. Goedken*[2]	Florida State Univ.	(USA)	May – Aug. 1984
Prof. A. Carrington*[2]	Oxford Univ.	(UK)	May 1984
Prof. P.O. Lowdin*[3]	Univ. of Florida	(USA)	May 1984
Dr. N.W. Broten	Herzberg Inst. of Astrophys.	(Canada)	May 1984
Dr. I.R. Peterson	GEC Res. Lab.	(England)	May 1984
Dr. D.R.J. Milverton	GEC Res. Lab.	(England)	May 1984
Prof. X. Chen	Acad. of Sci. of China	(China)	May 1984
Prof. C. Cuei	Acad. of Sci. of China	(China)	May 1984
Prof. T.E. Tsai	Natl. Taiwan Univ.	(Taiwan)	May 1984
Prof. Y.C. Liu	Natl. Tsing Hua Univ.	(Taiwan)	May 1984
Prof. C.N. Chang	Natl. Normal Univ.	(Taiwan)	May 1984
Mr. H.S. Tzeng	Natl. Tsing Hua Univ.	(Taiwan)	May 1984
Prof. S.C. Kim	Han Yang Univ.	(Korea)	May 1984
Prof. H.S. Pak	Seoul Natl. Univ.	(Korea)	May 1984
Prof. B.K. Park	Yeungnam Univ.	(Korea)	May 1984
Prof. I. Lee	Inha Univ.	(Korea)	May 1984
Prof. M.S. Jhon	Korea Advanced Inst. of Sci. and Tech.	(Korea)	May 1984
Prof. Y.S. Lee	Korea Advanced Inst. of Sci. and Tech.	(Korea)	May 1984
Prof. K.T. Noh	Sung Jun Univ.	(Korea)	May 1984
Prof. B.S. Lee	Inha Univ.	(Korea)	May 1984
Prof. U.R. Kim	Keimyung Univ.	(Korea)	May 1984
Prof. S. Ahn	Jeonbug Natl. Univ.	(Korea)	May 1984
Prof. J.W. Lee	Seoul Natl. Univ.	(Korea)	May 1984
Prof. D.J. Lee	Jeonbug Natl. Univ.	(Korea)	May 1984
Prof. J.J. Kim	Korea Advanced Inst. of Sci. and Tech.	(Korea)	May 1984
Prof. Y.K. Kang	Changbuk Natl. Univ.	(Korea)	May 1984
Prof. T. Toribara	Univ. of Rochester	(Korea)	May 1984
Dr. F. Galsbøl	Univ. of Copenhagen	(Denmark)	Jun. 1984
Prof. K.H. Chae	Chonnam Natl. Univ.	(Korea)	Jun. – Aug. 1984
Prof. Y. Ouyang	Univ. of Hainan Island	(China)	Jun. 1984
Prof. M.K. DeArmond	North Carolina State Univ.	(USA)	Jun. 1984
Prof. B.J. Yoon*[2]	Kangreung Natl. Univ.	(Korea)	Jun. – Sep. 1984
Prof. S.H. Suck Salk	Univ. of Missouri-Rolla	(USA)	Jun. 1984
Prof. D.M. Silver	Johns Hopkins Univ.	(USA)	Jun. 1984

Dr. J.T. Hougen*[5]	N.B.S.	(USA)	Jul. 1984 –
Prof. W.R. Gentry	Univ. of Minnesota	(USA)	Jul. 1984
Dr. H.C.W. Beijerinck	Eindhoven Univ. of Tech.	(Netherland)	Jul. 1984
Prof. U.R. Kim*[2]	Keimyung Univ.	(Korea)	Jul. – Aug. 1984
Dr. I. Sasaki	Univ. Paris-Sud	(France)	Jul. 1984
Prof. M.K. Doh	Yeung Nam Univ.	(Korea)	Jul. 1984
Prof. R. Poirier*[2]	Univ. of Toronto	(Canada)	Jul. 1984
Prof. F.C. Hurlbut	Univ. of California, Berkeley	(USA)	Jul. 1984

AWARD

Prof. Tadayoshi Sakata received the Divisional (Interdisciplinary Chemistry) Award of the Chemical Society of Japan in 1984 for his contribution to "Photocatalytic Effect of Dyes and Semiconductors – Its Application to Photochemical Conversion,"

Prof. Sakata's Scientific Achievement

Since 1976 Prof. Sakata has devoted himself to the construction of a new laboratory in IMS. He and his coworkers have made several important contributions in the research field of photochemical conversion of solar energy. These are divided into the following three.

(1) The Mechanism of Photogalvanic Cell and the Photovoltaic Effect of Metal-Porphyrin Thin Film Electrode

He contributed to the elucidation of the molecular mechanism of photogalvanic effect and succeeded in hydrogen evolution in 1978 by using porpyrin thin film electrode under irradiation.

(2) The Reaction of Organic Compounds with Water—Hydrogen Evolution by Photocatalysis of Dyes and Semiconductors

In collaboration with Dr. T. Kawai, he succeeded for the first time in photoinduced water gas reaction. He exploited various photocatalysts and succeeded in highly efficient hydrogen production from alcohols and carbohydrates. He extended this method to hydrogen production from various kinds of organic compounds including biomasses. These reactions are new and unique in that various organic compounds react with water to produce hydrogen and reactions proceed quantitatively.

(3) Dynamics of Semiconductor Photoelectrode and Photocatalysis

He showed the validity of transient photocurrent and luminescence measurements to investigate fast processes at photoelectrode and photocatalysts. He also exploited a pulsed-laser dynamic mass technique for the study of photocatalysis at semiconductor/gas interface.

Dr. Yasuki Endo received a Chemical Society of Japan Award for Young Chemists in 1984 for his contribution to the "Development of High-Sensitive Microwave Spectroscopy and Application to Structure Determination of Transient Molecules".

Dr. Endo's Scientific Achievemnts:

Dr. Endo has designed and set up a high-sensitivity microwave spectrometer covering the frequency region up to 200 GHz, by introducing a minicomputer for controlling the scanning, accumulating the signal, smoothing noises, correcting for background distortions, and reading-out the absorption frequency and also by improving the cell design so as to increase the pumping speed.

He has employed this spectrometer to investigate a number of short-lived free radicals, exploiting the high-resolution advantage of microwave spectroscopy to resolve fine and hyperfine structures. (1) He has shown that the CF_3, CH_2F, and CH_2Cl radicals are pyramidal, almost planar, and planar, respectively. (2) He has unraveled the effect of Jahn-Teller interaction in the methoxy radical in the $\tilde{X}^2E$ state, by paying special attention to the hyperfine structure. (3) He has succeeded in detecting microwave spectra of astronomically interesting free radicals such as PH_2, CCl, and FeO in addition to CH_3O. (4) He has shown that the magnetic hyperfine coupling constants observed for CCl, NCl, and OCl allow us to interpret the eQq coupling constants on a more sound basis that is possible with the usual Townes-Dailey's theory treatment.

LIST OF PUBLICATIONS

N. TANAKA, Y. HAMADA, Y. SUGAWARA, M. TSUBOI, S. KATO, and K. MOROKUMA, "Force Field in the Hydrazine Molecule from Ab Initio MO Calculation", *J. Mol. Spectr.*, **99**, 245 (1983).

M.J. WOJCIK, A.Y. HIRAKAWA, M. TSUBOI, S. KATO, and K. MOROKUMA, "Ab Initio MO Calculation of Force Constants and Dipole Derivatives for the Formamide Dimer. An Estimation of Hidrogen-bond Force Constants", *Chem. Phys. Lett.*, **100**, 523 (1983).

K. OHTA, K. KITAURA, Y. YOSHIOKA, and K. MOROKUMA, "The Effective Fragment Potential Method — An approximate Ab Initio MO Method for Large Molecules", *Chem. Phys. Lett.*, **101**, 12 (1983).

L.L. LOHR, JR., M. HANAMURA, and K. MOROKUMA, "The 1, 2 Hydrogen Shift as an Accompaniment to Ring Closure and Opening: Ab Initio MO Study of Thermal Rearrangements on the C_2H_3N Potential Energy Hypersurface", *J. Am. Chem. Soc.*, **105**, 5541 (1983).

Y. HAMADA, K. HASHIGUCHI, A.Y. HIRAKAWA, M. TSUBOI, M. NAKATA, M. TASUMI, S. KATO, and K. MOROKUMA, "Vibrational Analysis of Ethylamines: Trans and Gauche Forms", *J. Mol. Spectr.*, **102**, 123 (1983).

H. YAMATAKA, T. ANDO, S. NAGASE, M. HANAMURA, and K. MOROKUMA, "Ab Initio MO Calculations of Isotope Effects in Model Processes of Neopentyl Ester Solvolysis", *J. Org. Chem.*, **49**, 631 (1984).

S. HAYASHI, J. UMEMURA, S. KATO, and K. MOROKUMA, "Ab Initio Molecular Orbital Study on the Formic Acid Dimer", *J. Phys. Chem.*, **88**, 1330 (1984).

Y. OSAMURA, S. KATO, K. MOROKUMA, D. FELLER, E.R. DAVIDSON, and W.T. BORDEN, "Ab Initio Calculation of the Transition State for the Cope Rearrangement", *J. Am. Chem. Soc.*, **106**, 3362 (1984).

N. KOGA, S. OBARA, and K. MOROKUMA, "Intramolecular CH···M Interaction: A Theoretical Study of the Structure of Six-coordinate $Ti(C_2H_5)(PH_3)_2(X)_2(Y)$", *J. Am. Chem. Soc.*, **106**, 4625 (1984).

C. SATOKO, "Force and Virial Formula in the Linear Combination of Atomic Orbitals Xα Method and Its Application to Oxygen Chemisorption on the AL(111) and Mg(0001) Surfaces", *Phys. Rev.*, **B30**, 1754 (1984).

C. SATOKO, and M. TSUKADA, "The Role of d-orbitals in Dissociative Chemisorpiton of Hydrogen Molecules on Metal Surfaces", *Surf. Sci.*, **134**, 1 (1983).

R. SUZUKI, H. NAKAMURA, and E. ISHIGURO, "Semiclassical Scattering Theory Based on the Dynamical-state Representation: Application to the Li^+ + Na and Li + Na^+ collisions", *Phys. Rev.*, **A29**, 3060 (1984).

H. NAKAMURA, "Unified Treatment of Nonadiabatic Transitions in the Rotating Frame of the Complex" in Electronic and Atomic Collisions edited by J. Eichler, I.V. Hertel, and N. Stolterfoht, Elsevier Science Publishers, 1984, p.661.

H. TAKAGI, H. NAKAMURA, Y. ITIKAWA, and H. SATO, "Theoretical Analysis of Elastic Scattering of Electrons from H_2^+" in Electron-Molecule Collisions and Photoionization Processes edited by V. McKoy, H. Suzuki, K. Takayanagi, and S. Trajmar, Verlag Chemie International Inc., 1983, p.27.

T. SHIRAI, Y. NAKAI, and H. NAKAMURA, "Ionization Collisions between Excited Atoms: Application of the Glauber Amplitude in the Framework of the Impulse Approximation", *Phys. Rev.*, **A30**, 1672 (1984).

H. NAKAMURA, "Electronic Transitions in Atomic and Molecular Dynamic Processes", *J. Phys. Chem.* **88**, 4812 (1984).

K. NASU, "Extended Peierls-Hubbard Model for One-Dimensional N-Sites N-Electrons System. II.—Effect of Fluctuation, Optical and Magnetic Excitations", *J. Phys. Soc. Jpn.*, **53**, 302 (1984).

K. NASU, "Extended Peierls-Hubbard Model for One-Dimensional N-Sites N-Electrons System. III.—Lattice Relaxation after Optical Excitation in CDW", *J. Phys. Soc. Jpn.,* **53**, 427 (1984).

N. SHIDA, K. TANAKA, and K. OHNO, "An ab initio Calculation of Symmetric Bending and Stretching Vibrational States of the H_3O^+ and D_3O^+ Ions", *Chem. Phys. Lett.,* **104**, 575 (1984).

I. SHIMAMURA, "Rotational Excitation of Molecules by Slow Electrons" in "Electron-Molecule Collisions", I. Shimamura, and K. Takayanagi, Eds., Plenum Press, p.89 (1984).

I. SHIMAMURA, "Line-Shape Analysis of Energy-Loss Spectra and Photoelectron Spectra" in "Wavefunctions and Mechanisms from Electron Scattering Processes", F.A. Gianturco and G. Stefani, Eds., Springer-Verlag, p.210 (1984).

Y. ENDO, and M. MIZUSHIMA, "Microwave Absorption Lines of $^{18}O_2$ in its Electronic Ground State ($X^3\Sigma_g^-$).", *Jpn. J. Appl. Phys.,* **22**, L534 (1983).

K. HAKUTA, H. UEHARA, K. KAWAGUCHI, T. SUZUKI, and T. KASUYA, "Laser-Induced Fluorescence Spectrum of the CCN Radical. II. Excitation of $A^2\Delta_i$: (010)Π-$X^2\Pi_r$: (010)Σ^- Vibronic Band.", *J. Chem. Phys.,* **79**, 1094 (1983).

A.R.W. McKELLAR, C. YAMADA, and E. HIROTA, "Detection of the ν_2 Bands of CD_2 and CH_2 by Infrared Diode Laser Spectroscopy.", *J. Chem. Phys.,* **79**, 1220 (1983).

M. TANIMOTO, S. SAITO, Y. ENDO, and E. HIROTA, "Microwave Spectroscopic Study of the SiF Radical.", *J. Mol. Spectrosc.,* **100**, 205 (1983).

Y. ENDO, C. YAMADA, S. SAITO, and E. HIROTA, "The Microwave Spectrum of the Fluoromethyl Radical, CH_2F.", *J. Chem. Phys.,* **79**, 1605 (1983).

T. SUZUKI, S. SAITO, and E. HIROTA, "Laser Excitation Spectrum and Microwave Optical Double Resonance Spectrum of the 3_0^1 Band in the $\tilde{a}^3A_2$-$\tilde{X}^1A_1$ System of H_2CS: The Hyperfine Structure of the $\tilde{a}^3A_2$ State." *J. Chem. Phys.,* **79**, 1641 (1983).,

Y. ENDO, S. SAITO, and E. HIROTA, "Microwave Spectroscopy of Boron Chloride (BCl). The Chlorine Nuclear Quadrupole Coupling Constant.", *Bull. Chem. Soc. Jpn.,* **56**, 3410 (1983).

K. KAWAGUCHI, N. OHASHI, S. SAITO, J.E. BUTLER, and E. HIROTA, "High Resolution Spectroscopy of a Few Phosphorus-Containing Molecules.", *Bull. Soc. Chim. Belg.,* **92**, 504 (1983).

J.E. BUTLER, K. KAWAGUCHI, and E. HIROTA, "Infrared Diode Laser Spectroscopy of the PO Radical.", *J. Mol. Spectrosc.,* **101**, 161 (1983).

C. YAMADA, Y. ENDO, and E. HIROTA, "The Microwave Spectrum of the $N^{35}Cl$ Radical in the $X^3\Sigma^-$ State.", *J. Chem. Phys.,* **79**, 4159 (1983).

N. TANAKA, Y. HAMADA, M. TSUBOI, S. SAITO, Y. ENDO, and E. HIROTA, "Microwave Spectrum of $^{15}N^{16}O_2$ in the Ground State.", *J. Mol. Spectrosc.,* **103**, 87 (1984).

S. SAITO, Y. ENDO, and E. HIROTA, "The Microwave Spectrum of a Triplet Carbene: HCCN in the $X^3\Sigma^-$ State.", *J. Chem. Phys.,* **80**, 1427 (1984).

Y. ENDO, S. SAITO , and E. HIROTA, "Laboratory Millimeter-Wave Spectrum of Iron Monoxide, FeO.", *Astrophys. J.,* **278**, L131 (1984).

M. TANIMOTO, S. SAITO, Y. ENDO, and E. HOROTA, "The Microwave Spectrum of the SiCl Radical.", *J. Mol. Spectrosc.,* **103**, 330 (1984).

N. OHASHI, K. KAWAGUCHI, and E. HIROTA, "Far-Infrared Laser Magnetic Resonance Spectra of the PH and PD Radicals in $X^3\Sigma^-$.", *J. Mol. Spectrosc.,* **103**, 337 (1984).

J.E. BUTLER, K. KAWAGUCHI, and E. HIROTA, "Infrared Diode Laser Spectroscopy of the BrO Radical.", *J. Mol. Spectrosc.,* **104**, 372 (1984).

R.J. BUTCHER, S. SAITO, and E. HIROTA, "Magnetic Properties of the $\tilde{A}^1A''$ State of HCF.", *J. Chem. Phys.,* **80**, 4000 (1984).

C. YAMADA and E. HIROTA, "The Infrared Diode Laser Spectrum of the ν_2 Band of the FO_2 Radical.", *J. Chem. Phys.,* **80**, 4694 (1984).

T.A. MILLER, T. SUZUKI, and E. HIROTA, "High Resolution, cw Laser Induced Fluorescence Study of the $A^2\Pi_u$-$X^2\Sigma_g^+$ System of N_2^+.", *J. Chem. Phys.,* **80**, 4671 (1984).

J. NAKAGAWA, M. HAYASHI, Y. ENDO, S. SAITO, and E. HIROTA, "Microwave Spectrum and Internal Rotation of 2-Butyne-1,1,1-d_3(Dimethylacetylene), $CH_3C \equiv CCD_3$.", *J. Chem. Phys.*, **80**, 5922 (1984).

Y. ENDO, S. SAITO, and E. HIROTA, "The Microwave Spectrum of the Methoxy Radical CH_3O.", *J. Chem. Phys.*, **81**, 122 (1984).

J. TERAOKA, D. JOB, Y. MORITA, and T. KITAGAWA, "Resonance Raman Study of Plant Tissue Peroxidases: Common Characteristics in Iron Coordination Environments", *Biochem. Biophys. Acta,* **747**, 10 (1983).

T. OGURA, K. HON-NAMI, T. OSHIMA, S. YOSHIKAWA, and T. KITAGAWA, "Iron-Histidine Stretching Raman Lines of the aa_3-Type Cytochrome Oxidases", *J. Am. Chem. Soc.*, **105**, 7781 (1983).

T. KITAGAWA, S. CHIHARA, K. FUSHITANI, and H. MORIMOTO, "Resonance Raman Study of Subunit Assemby Dependent Photoreduction of Heme of Extracellular Giant Hemoglobin", *J. Am. Chem. Soc.*, **106**, 1860 (1984).

K. KAMOGAWA, K. TAJIMA, K. HAYAKAWA, and T. KITAGAWA, "Raman Spectroscopic Studies of Submillimolar Surfactant Solutions; Concentration Dependence of the C-H Stretching Raman Lines", *J. Phys. Chem.*, **88**, 2494 (1984).

T. OGURA, N. SONE, K. TAGAWA, and T. KITAGAWA, "Resonance Raman Study of an aa_3-Type Cytochrome Oxidase of Thermophilic Bacterium", *Biochemistry,* **23**, 2826 (1984).

S. YOSHIKAWA, H. MOCHIZUKI, S. CHIHARA, B. HAGIHARA, and T. KITAGAWA, "Determination of the Effects of the Mg^{2+} Ion on the O_2 Affinity of Chlorocruorin by Resonance Raman Spectroscopy", *Biochim. Biophys. Acta,* **786**, 267 (1984).

K. TOHJI, Y. UDAGAWA, T. KAWASAKI, and K. MASUDA, "Laboratory EXAFS Spectrometer with a Bent Crystal, a Solid State Detector, and a Fast Detection System", *Rev. Sci. Instrum.*, **54**, 1482 (1983).

K. TOHJI, Y. UDAGAWA, S. TANABE, and A. UENO, "Catalyst Preparation Procedure Probed by EXAFS Spectroscopy I. Nickel on Silica", *J. Am. Chem. Soc.*, **106**, 612 (1984).

S. TANABE, T. IDA, H. TSUIKI, A. UENO, Y. KOTERA, K. TOHJI, and Y. UDAGAWA, "Formation of Co_3O_4 Clusters in TiO_2 Support Observed by EXAFS", *Chem. Lett.*, 1271 (1984).

N. ITO, and T. KATO, "Orientational Pair Correlation of Pyridine and 2,4-Dimethylpyridine in Water by Depolarized Rayleigh Scattering and Nuclear Magnetic Resonance Spectra", *J. Phys. Chem.*, **88**, 801 (1984).

T. KATO, "Kirkwood-Buff Parameters and Correlation Length in Aqueous Solutions of n-Alkoxyethanols", *J. Phys. Chem.*, **88**, 1284 (1984).

K. KOJIMA, T. KATO, and H. NOMURA, "Estimation of the Parameters in the Kirkwood-Buff Theory of Solution using Percus-Yevick Fluid Mixtures", *J. Solution Chem.*, **13**, 151 (1984).

D.V. O'CONNOR, M. SUMITANI, Y. TAKAGI, N. NAKASHIMA, K. KAMOGAWA, Y. UDAGAWA, and K. YOSHIHARA, "Fluorescence Spectra from Highly Excited Vibrational Levels in Benzene", *J. Phys. Chem.*, **87**, 4848 (1983).

K. KEMNITZ, T. MURAO, I. YAMAZAKI, N. NAKASHIMA, and K. YOSHHARA, "Picosecond Fluorescence Measurement of Submono- and Monolayer of Adsorbed Rhodamine B on a Single Crystal of Naphthalene and on Glass", *Chem. Phys. Lett.*, **101**, 337 (1983).

H. SATO, M. KAWASAKI, K. KASATANI, N. NAKASHIMA, and K. YOSHIHARA, "Interaction of Cationic Dye and Anionic Detergent above and below the Critical Micelle Concentration as Revealed by Fluorescence Characteristics", *Bull. Chem. Soc. Jpn.*, **56**, 3588 (1983).

S. NAGAOKA, N. HIROTA, M. SUMITANI, and K. YOSHIHARA, "Investigation of the Dynamic Processes of the Excited States of *o*-Hydroxybenzaldehyde and *o*-Hydroxyacetophenone by Emission and Picosecond Spectroscopy", *J. Am. Chem. Soc,*. **105**, 4220 (1983).

T. ICHIMURA, Y. MORI, M. SUMITANI, and K. YOSHIHARA, "Decomposition Rate of Benzyl Chloride Excited at 266 nm in the Vapor Phase", *J. Chem. Phys.*, **80**, 962 (1984).

S. TAGAWA, N. NAKASHIMA, and K. YOSHIHARA, "Absorption Spectrum of the Triplet State and the Dynamics of Intramolecular Motion of Polystyrene", *Macromolec.*, **17**, 1167 (1984).

S. NAKAMURA, N. KANAMARU, S. NOHARA, H. NAKAMURA, Y. SAITO, J. TANAKA, M. SUMINATI, N. NAKASHIMA, and K. YOSHIHARA, "The Photoionization Mechanism of *N,N,N',N'*-Tetramethyl-*p*-phenylenediamine in Acetonitrile", *Bull. Chem. Soc. Jpn.,* **57**, 145 (1984).

T. ICHIMURA, Y. MORI, N. NAKASHIMA, and K. YOSHIHARA, "Formation of Hot Hexafluorobenzene in the 193 nm Photolysis", *Chem. Phys. Lett.,* **104**, 533 (1984).

M. SUMITANI, D.V. O'CONNOR, Y. TAKAGI, and K. YOSHIHARA, "The Importance of the ν_7 Vibration in the Study of Channel Three Decay in S_1 Benzene" *Chem. Phys. Lett.,* **108**, 11 (1984).

K. YOSHIHARA, D.V. O'CONNOR, M. SUMITANI, Y. TAKAGI, and N. NAKASHIMA, "Single Vibrational Level Dependence of Picosecond Fluorescence in the Channel 3 Region of Benzene", *Application of Picosecond Spectroscopy to Chemistry,* K.B. Eisenthal, Ed. NATO ASI Series, D. Reidel Publ. Co., Dordrecht, 261 (1984).

K. MIYASHITA, T. SAKATA, K. NAKAMURA, T. KAWAI, and T. SAKATA, "Photoinduced Catalytic Decomposition of Pyruvic Acid", *Photochem. Photobiol.,* **39**, 151 (1983).

T. KAWAI, T. SAKATA, K. HASHIMOTO, and M. KAWAI, "Structure and Reactivity of Particulate Semiconductor Photocatalysts", *Nippon Kagaku Kaishi* (in Japanese), 277 (1983).

S. YANAGIDA, H. KAWAKAMI, K. HASHIMOTO, T. SAKATA, C. PAC, and H. SAKURAI, "Photocatalysis of Zinc Sulfide Microcrystals in Reductive Hydrogen Evolution in Water/Metanol Systems", *Chem. Lett.,* 1449 (1984).

T. SAKATA, T. KAWAI, and K. HASHIMOTO, "Heterogeneous Photocatalytic Reactions of Organic Acids and Water—New Reaction Paths besides the Photo-Kolbe Reaction", *J. Phy. Chem.,* **88**, 2344 (1984).

K. HASHIMOTO, T. KAWAI, and T. SAKATA, "Photocatalytic Reactions of Hydrocarbons and Fossil Fuels with Water: Hydrogen Production and Oxidation", *J. Phys. Chem.,* **88**, 4083 (1984).

M. BABA, and I. HANAZAKI, "The S_1, $^1A_2(n, \pi^*)$ state of Acetone in a Supersonic Nozzle Beam. Methyl Internal Rotation", *Chem. Phys. Lett.,* **103**, 93 (1983).

B.R. HENRY, M. ALI MOHAMMADI, I. HANAZAKI, and R. NAKAGAKI, "Overtone Spectra and Spectral Bandwidths in Liquid- and Vapor-Phase Tetramethylsilicon, -Germanium, and -Tin", *J. Phys. Chem.,* **87**, 4827 (1983).

T. OHNO, S. KATO, S. KAIZAKI, and I. HANAZAKI, "Enhanced S-T Transitions of Aromatic Compounds Coordinating to Paramagnetic Chromium (III)", *Chem. Phys. Lett.,* **102**, 471 (1983).

S. KUWABARA, K. KUWATA, I. NISHIYAMA, and I. HANAZAKI, "Acoustically Oscillating Emission from NO_2^* Produced by Infrared Photosensitized Reaction in $SF_6 + NO_2$", *Chem. Phys. Lett.,* **106**, 540 (1984).

H. KATO, M. BABA, and I. HANAZAKI, "Effects of an External Magnetic Field on Laser-induced Fluorescence and Photodissociation of NaK", *J. Chem. Phys.,* **80**, 3936 (1984).

N. NISHI, H. SHINOHARA, and T. OKUYAMA, "Photodetachment, Photodissociation, and Photochemistry of Surface Molecules of Icy Solids Containing NH_3 and Pure H_2O Ices", *J. Chem. Phys.,* **80**, 3898 (1984).

M. BABA, H. SHINOHARA, N. NISHI, and N. HIROTA, "Multiphoton Ionization and Fragmentations of Acetone and Cyclic Ketones: Effects of One-photon Dissociation", *Chem. Phys.,* **83**, 221 (1984).

M. KAWASAKI, K KASATANI, H. SATO, H. SHINOHARA, and N. NISHI, "Photodissociation of Molecular Beams of Halogenated Hydrocarbons at 193 nm", *Chem. Phys.,* **88**, 135 (1984).

H. SHINOHARA, N. NISHI, and N. WASHIDA, "Photoionization of Ammonia Clusters in a Pulsed Supersonic Nozzle Beam by Vacuum-UV Rare-Gas Resonance Lines", *Chem. Phys. Lett.,* **106**, 302 (1984).

Y. TANIMOTO, H. UDAGAWA, Y. KATSUDA, and M. ITOH, "Magnetic Field Effects on the Photolysis of *p*-Benzoquinone Derivatives in Sodium Dodecyl Sulfate Micelles.", *J. Phys. Chem.,* **87**, 3976 (1983).

Y. TANIMOTO, K. SHIMIZU, and M. ITOH, "Magnetic Field Effect on the Hydrogen Abstraction of Anthraquinones in SDS Micellar Solutions.", *Photochem. Photobiol.,* **39**, 511 (1984).

S. NAGAKURA and H. HAYASHI, "External Magnetic Field Effects upon Photochemical Reactions in Solutions.", *Radiat. Phys. Chem.,* **21**, 91 (1983).

H. HAYASHI and S. NAGAKURA, "Theoretical Study of Relaxation Mechanism in Magnetic Field Effects on

Chemical Reactions.", *Bull. Chem. Soc. Jpn.*, **57**, 322 (1984).

M. SCHMID, N. SATO, and H. INOKUCHI, "Elimination of Sample Charging in UV Photoemission from Single Crystals of Several Polycyclic Hydrocarbons", *Chem. Lett.*, 1897 (1983).

J. TANAKA, M. TANAKA, H. FUJIMOTO, M. SHIMIZU, N. SATO, and H. INOKUCHI, "Spectral Studies on the Electronic Structure of Polyacethylene", *J. de Phys.*, **44**, 279 (1983).

S.X. CHEN, K. SEKI, H. INOKUCHI, N. UENO, and K. SUGITA, "Ultraviolet Photoelectron Spectroscopy of Fluoro-Substituted Polyethylenes", *Polymer J.*, **15**, 763 (1983).

K. SEKI, U. KARLSSON, R. ENGELHARDT, and E.E. KOCH, "Intramolecular Energy Band Dispersion of n-$C_{36}H_{74}$ Observed by Angle-Resolved Photoemission with Synchrotron Radiation", *Chem. Phys. Lett.*, **103**, 343 (1984).

J.M. NICHOLLS, G.V. HANSSON, U.O. KARLSSON, R.I.G. UHRBERG, R. ENGELHARDT, K. SEKI, S.A. FLODSTRÖM, and E.E. KOCH, "Confirmation of a Highly Dispersive Dangling Bond Band on Ge (111)-2x1", *Phys. Rev. Lett.*, **52**, 1555 (1984).

H. KOBAYASHI, A. KOBAYASHI, Y. SASAKI, G. SAITO, and H. INOKUCHI, "The Crystal Structure of $(TMTTF)_2ReO_4$", *Bull. Chem. Soc. Jpn.*, **57**, 2025 (1984).

T. ENOKI, M. SANO, and H. INOKUCHI, "Hydrogen Adsorption of Alkali Metal Complexes of Polycyclic Aromatic Hydrocarbon and Graphite and Their Solid State Properties", *Mol. Cryst. Liq. Cryst.*, **96**, 21 (1983).

G. SAITO, T. ENOKI, H. INOKUCHI, and H. KOBAYASHI, "Suppression of Peierls Transition by Chemical Modification", *J. de Phys.*, **44**, 1215 (1983).

H. KOBAYASHI, R. KATO, T. MORI, A. KOBAYASHI, Y. SASAKI, G. SAITO, T. ENOKI, and H. INOKUCHI, "The Crystal Structures and Electrical Resistivities of $(BEDT\text{-}TTF)_3(ClO_4)_2$ and $(BEDT\text{-}TTF)_2ClO_4(C_4H_4O_2)$", *Chem. Lett.*, 179 (1984).

H. KOBAYASHI, A. KOBAYASHI, Y. SASAKI, G. SAITO, and H. INOKUCHI, "The Crystal Structures of $(BEDT\text{-}TTF)ReO_4(THF)_{0.5}$ and $(BEDT\text{-}TTF)ClO_4(THF)_{0.5}$", *Chem. Lett.*, 183 (1984).

H. TAJIMA, K. YAKUSHI, H. KURODA, G. SAITO, and H. INOKUCHI, "The Polarized Reflectance Spectrum of a Novel Organic Conductor $(BEDT\text{-}TTF)_2ClO_4(C_2H_3Cl_3)_{0.5}$, *Solid State Commun.*, **49**, 769 (1984).

T. MORI, A. KOBAYASHI, Y. SASAKI, H. KOBAYASHI, G. SAITO, and H. INOKUCHI, "The Intermolecular Interaction of Tetrathiafulvalene and Bis(ethylenedithio)-tetrathiafulvalene in Organic Metals. Calculation of Orbital Overlaps and Models of Energy-band Structures", *Bull. Chem. Soc. Jpn.*, **57**, 627 (1984).

T. MORI, A. KOBAYASHI, Y. SASAKI, H. KOBAYASHI, G. SAITO, and H. INOKUCHI, "Band Structures of Two Types of $(BEDT\text{-}TTF)_2I_3$", *Chem. Lett.*, 957 (1984).

H. KOBAYASHI, R. KATO, T. MORI, A. KOBAYASHI, T. SASAKI, G. SAITO, T. ENOKI, and H. INOKUCHI, "Crystal Structures and Electrical Properties of BEDT-TTF", *Mol. Cryst. Liq. Cryst.*, **107**, 33 (1984).

T. KATO, K. TANAKA, and I. KOYANO, "State Selected Ion-Molecule Reactions by a TESICO Technique. VIII. Vibronic-State Dependence of the Cross Sections in the Reactions $NO^+(a^3\Sigma^+,v;\ b^3\Pi,v) + Ar \rightarrow NO + Ar^+$", *J. Chem. Phys.*, **79**, 5969 (1983).

T. KATO, "State Selected Charge Transfer Reactions in the $BC^+ + Ar \rightleftharpoons Ar^+ + BC$ Systems: Comparison among $BC = H_2$, O_2 and NO", *J. Chem. Phys.*, **80**, 6105 (1984).

E. NISHITANI, I. TANAKA, K. TANAKA, T. KATO, and I. KOYANO, "New Vibrational Assignments for the Autoionization Bands of O_2 Based on Isotope Shifts" , *J. Chem. Phys.*, **81**, 3429 (1984).

Y. ACHIBA, K. SATO, K. SHOBATAKE, and K. KIMURA, "Resonant Multiphoton Ionization Photoelectron Spectroscopic Study of Benzene. Evidence for Fast Intramolecular vibrational Relaxation within the $^1E_{1U}$ state", *J. Chem. Phys.*, **79**, 5213 (1983).

K. SATO, Y. ACHIBA, and K. KIMURA, "A Photoelectron Spectroscopic Study of Ionization Selectivity in Resonantly Enhanced Multiphoton Ionization of Xe and Kr.", *J. Chem. Phys.*, **80**, 57 (1984).

K. SATO, Y. ACHIBA, and K. KIMURA, "The Ar-NO van der Waals Complex Studied by Resonant Multiphoton Ionization Spectroscopy Involving Photoion and Photoelectron Measurements.", *J. Chem. Phys.*, **81**, 57 (1984).

Y. ACHIBA, A. HIRAYA, and K. KIMURA, "New Aspects of "Channel Three" Problem in Benzene, as Revealed by Multiphoton Ionization Photoelectron Spectroscopy.", *J. Chem. Phys.*, **80**, 6047 (1984).

K. FUKE, H. YOSHIUCHI, K. KAYA, Y. ACHIBA, K. SATO, and K. KIMURA, "Multiphoton Ionization Photoelectron Spectroscopy and 2-Color Multiphoton Ionization Threshold Spectroscopy on the Hydrogen Bonded Phenol and 7-Aza-Indole in a Supersonic Jet.", *Chem. Phys. Lett.*, **108**, 179 (1984).

S. TOMODA, and K. KIMURA, "Proton Transfer Potential Energy Surfaces of the Water Dimer Cation $(H_2O)_2^+$ in the 1^2A States.", *Chem. Phys.*, **82**, 215 (1983).

S. TOMODA, and K. KIMURA, "Ionization Energies and Hydrogen-Bond Strength of the Water Clusters.", *Chem. Phys. Lett.*, **102**, 560 (1983).

K. TABAYASHI, S. OHSHIMA, and K. SHOBATAKE, "Chemiluminescence Produced in the Reaction between $N(^2D, ^2P)$ Atoms and HI and HBr, in Crossed Molecular Beam", *J. Chem. Phys.*, **80**, 5335 (1984).

T. ONAKA-ITO, and Y. MARUYAMA, "Fluorescence Spectra and Energy Migration Behavior of o-Terphenyl Single Crystal and Glassy Solid.", *Mol. Cryst. Liq. Cryst.*, **91**, 187 (1983).

H. ASASHINA, Y. MARUYAMA, and A. MORITA, "Optical Reflectivity and Band Structure of Black Phosphorus.", *Physica*, **117B**, 419 (1983).

T. ISHIGURO, K. MURATA, K. KAJIMURA, N. KINOSHITA, H. TOKUMOTO, M. TOKUMOTO, T. UKACHI, H. ANZAI, and G. SAITO, "Superconductivity and Metal-Nonmetal Transitions in $(TMTSF)_2ClO_4$, *J. Phys. (Paris)*, **44**, 831 (1983).

N. KINOSHITA, T. UKACHI, M. TOKUMOTO, H. ANZAI, T. ISHIGURO, G. SAITO, T. YAMABE, and H. TERAMAE, "ESR Anisotropy of $(TMTSF)_2ClO_4$", *J. Phys. (Paris)*, **44**, 1029 (1983).

K. KAJIMURA, H. TOKUMOTO, M. TOKUMOTO, K. MURATA, T. UKACHI, H. ANZAI, T. ISHIGURO, and G. SAITO, "Magnetoresistance of $(TMTSF)_2ClO_4$", *J. Phys. (Paris)*, **44**, 1059 (1983).

T. ISHIGURO, T. UKACHI, M. TOKUMOTO, K. MURATA, K. KAJIMURA, H. ANZAI, K. KATO, and G. SAITO, "Mechanical Twinning of $(TMTSF)_2ClO_4$ Single Crystal", *J. Phys. (Paris)*, **44**, 1062 (1983).

H. ANZAI, T. MORIYA, K. NOZAKI, T. UKACHI, and G. SAITO, "Effects of Solvents and Cell Design for Crystal Growth of Organic Metals", *J. Phys. (Paris)*, **44**, 1195 (1983).

N. KINOSHITA, M. TOKUMOTO, H. ANZAI, T. ISHIGURO, G. SAITO, T. YAMABE, and H. TERAMAE, "ESR *g* Factors of Isolated $(TMTSF)^+$ and $(TMTSF)_2ClO_4$ Single Crystals: Comparison with Molecular Orbital Calculation", *J. Phys. Soc. Jpn.*, **53**, 1504 (1984).

Y. TEKI, T. TAKUI, K. ITOH, H. IWAMURA, and K. KOBAYASHI, "Design, Preparation, and ESR Detection of a Ground-State Nonet Hydrocarbon as a Model for One-Dimensional Organic Ferromagnets", *J. Am. Chem. Soc.*, **105**, 3722 (1983).

T. SUGAWARA, H. IWAMURA, N. NAKASHIMA, K. YOSHIHARA, and H. HAYASHI, "Transient Absorption Spectra of the Excited States of Triptycene and 3-Acetyltriptycene", *Chem. Phys. Lett.*, **101**, 303 (1983).

W. NAKANISHI, Y. KUSUYAMA, Y. IKEDA, and H. IWAMURA, "The Sulfuranyl Radical Structure and Reactions of *o*-(Thio)-benzoyloxyl Radicals Formed by the Decomposition of *t*-Butyl *o*-(Thio) perbenzoates Studies by ^1H and ^{13}C CIDNP and ^{17}O NMR", *Bull. Chem. Soc. Jpn.*, **56**, 3123 (1983).

Y. KAWADA, Y. OKAMOTO, and H. IWAMURA, "Correlated Internal Rotation in Bis(2,6-dichloro-9-triptycyl)methane. To What Extent Can Phase Isomers be Separated and Identified?", *Tetrahedron Lett.*, **24**, 5359 (1983)

E. LIPCZYNSKA-KOCHANY, H. IWAMURA, K. TAKAHASHI, A. HAKURA, and Y. KAWAZOE, "Mutagenicity of Pyridine- and Quinoline-carbohydroxamic Acid Derivatives", *Mutation Res.*, **135**, 139 (1984).

S. MURATA and H. IWAMURA, "π-Electron Distribution in Benz[*a*]indeno[1,2,3-*cd*]azulene and the

Corresponding Azepinium Ion", *Bull. Chem. Soc. Jpn.*, **57**, 1697 (1984).

S. MURATA, T. SUGAWARA, N. NAKASHIMA, K. YOSHIHARA, and H. IWAMURA, "Time-Resolved Absorption Spectroscopic Studies on the Reaction of Conformationally Fixed *o*-(9-Fluorenyl)phenylnitrenes", *Tetrahedron Lett.*, **25**, 1933 (1984).

T. SUGAWARA, D. BETHELL, and H. IWAMURA, "Photolysis of 1,12-Bis(diazo)-1,12-dihydroindeno [2,3-*a*]fluorene. ESR and Optical Detection of a σ-Type 1,4-Diradical", *Tetrahedron Lett.*, **25**, 2375 (1984).

H. IWAMURA, T. ITO, H. ITO, K. TORIUMI, Y. KAWADA, E. ŌSAWA, T. FUJIYOSHI, and C. JAIME, "Crystal and Molecular Structure of Bis (9-triptycyl) Ether", *J. Am. Chem. Soc.*, **106**, 4712 (1984).

S. MURATA, T. SUGAWARA, and H. IWAMURA, "An Unusual Photoproduct of o-Azidobiphenyl with Tetracyanoethylene: Trapped 2-Azacycloheptatrienylidene", *J. Chem. Soc., Chem. Commun.*, 1198 (1984).

T. TSUBOMURA, S. YANO, S. YOSHIKAWA, K. TORIUMI, and T. ITO, "Reactions of Metal Complexes with Carbohydrates. 3. The Crystal Structure of (Ethylenediamine)(2-[(2-aminoethyl)amino]2-deoxy-L-sorbose)nickel(II) Dichloride Hemi Methanol—[Ni(en)(L-sor-en)]Cl_2·1/2CH_3OH." *Polyhedron*, **2**, 123 (1983).

K. MOCHIZUKI, K. TORIUMI, and T. ITO, "Efficient Synthesis and Structure of Bis[acetonitrile (11,13-dimethyl-1,4,7,10-tetraaza-10,13-cyclotridecadiene-12-ylidene)nickel(II)] Perchlorate.", *Bull. Chem. Soc. Jpn.*, **57**, 881 (1984).

T. ITO, M. KATO, and H. ITO, "Correlation between Axial and In-Plane Coordination Bond Lengths in Tetragonal Six-coordinate Complexes of the *trans*-MX_2N_4 Type (M = Co^{3+}, Ni^{2+}, and Zn^{2+}). X-Ray Structural and *ab initio* Molecular Orbital Studies.", *Bull. Chem. Soc. Jpn.*, **57**, 1556 (1984).

T. TSUBOMURA, S. YANO, K. TORIUMI, T. ITO, and S. YOSHIKAWA, "Reactions of Metal Complexes with Carbohydrates. Synthesis and Structure of (2-[(2-Aminoethyl)amino]-2-deoxy-L-sorbose)(ethylenediamine)nickel(II) Dichloride Hemi Methanol Solvate: [Ni(en)(L-sor-en)]Cl_2·1/2CH_3OH (en = ethylenediamine and sor = sorbose).", *Bull. Chem. Soc. Jpn.*, **57**, 1833 (1984).

T. ITO, M. KATO, and H. ITO, "X-Ray Structural Study on Molecular Stereochemistries of Six-coordinate Zn(II) Complexes of *trans*-ZnX_2N_4 Type. Outof plane Displacement of Zn(II) from a Plane Formed by In-plane Four Nitrogens.", *Bull. Chem. Soc. Jpn.*, **57**, 2634 (1984).

T. ITO, M. KATO, and H. ITO, "The Structures of *trans*-Dichloro- and *trans*-Bis(isothiocyanato)—nickel(II) Complexes with 1, 4, 8, 11-Tetraazacyclotetradecane, 1, 4, 8, 12-Tetraazacyclopentadecane, and 1, 5, 9, 13-Tetraazacyclohexadecane. The Negative Correlation between the Axial and In-plane Coordination Bond Lengths in Tetragonal Ni(II) Complexes or the trans-NiX_2N_4 Type.", *Bull. Chem. Soc. Jpn.*, **57**, 2641 (1984).

M. YAMASHITA, and T. ITO, "Direct Evidence for the Formation of One-Dimensional Ni(II)-Ni(IV) Mixed-Valence Complexes by the X-Ray Photoelectron Spectra", *Inorg. Chim. Acta*, **87**, L5 (1984).

K. OHNO, K. MOROKUMA, F. HIROTA, H. HOSOYA, S. IWATA, Y. OSAMURA, H. KASHIWAGI, S. YAMAMOTO, N. KOSUGI, H. NAKATSUJI, K. NISHIMOTO, S. OBARA, K. TANAKA, M. TOGASHI, and S. YAMABE, "Quantum Chemistry Literature Data Base—Bibliography of *Ab Initio* Calculations for 1982", *J. Mole Struct. (Theochem)*, **106**, 1-252 (1983).

H. TAKAYA, M. YAMAKAWA, and K. MASHIMA, "Synthesis and Characterization of 2-[Di(cyclopentadienyl)-zircona]-1-oxacyclopentanes. X-Ray Crystal Structure of [(η-C_5H_5)$_2$ZrOCH$_2$CH$_2$CHMe]$_2$.", *J. Chem. Soc., Chem. Commun.*, 1283 (1983).

A. MIYASHITA, H. TAKAYA, T. SOUCHI, and R. NOYORI, "Synthesis and Its Use in the Rh(I)-Catalyzed Asymmetric Hydrogenation of α-(Acylamino)acrylic Acids.", *Tetrahedron*, **40**, 1245 (1984).

K. TANI, T. YAMAGATA, S. AKUTAGAWA, H. KUMOBAYASHI, T. TAKETOMI, H. TAKAYA, A. MIYASHITA, R. NOYORI, and S. OTSUKA, "Highly Enantioselective Isomerization of Prochiral Allylamines Catalyzed by Chiral Diphosphine Rhodium(I) Complexes. Preparation of Optically Active Enamines", *J. Am. Chem. Soc.*, **106**, 5208 (1984).

I. YAMAZAKI, M. MIMURO, T. MURAO, T. YAMAZAKI, K. YOSHIHARA, and Y. FUJITA, "Picosecond Time-Resolved Fluorescence Spectroscopy of Excitation Energy Transfer—Photoexcitation

Transport in Light-Harvesting Antenna System in Algae", *Nippon Kagaku Kaishi,* 75 (1984).

N. TAMAI, I. YAMAZAKI, H. MASUHARA, and N. MATAGA, "Picosecond Time-Resolved Fluorescence Spectra of a Liquid Crystal: Fluorescence Behavior Related to Phase Transitions in Cyanooctyloxybiphenyl", *Chem. Phys. Lett.,* **104,** 485 (1984).

M. MIMURO, I. YAMAZAKI, T. MURAO, T. YAMAZAKI, K. YOSHIHARA, and Y. FUJITA, "Excitation Energy Transfer in Phycobilin-Chlorophyll a System in Blue-Green and Red Algae", *Advance in Photosynthesis Research* (ed. C. Sybesma), Vol.1, 21 (1984).

H. MASUHARA, N. TAMAI, N. MATAGA, F.C. DE SCHRYVER, N. MATAGA, and J. VAN DEN DRIESSCHE, "Absorption Spectra and Dynamics of Some Excited and Ionic Dicarbazolyl Compounds with Specific Geometrical Structures," *J. Am. Chem. Soc.,* **105,** 7256 (1983).

H. MASUHARA, K. INOUE, N. TAMAI, and N. MATAGA, "Intrapolymer S_1–S_1 Annihilation and the Triplet State of Polymers Having Carbazolyl Groups in Solution", *Nippon Kagaku Kaishi,* 14 (1984).

K. KIMURA, and S. BANDOW, "The Study of Metal Colloids Produced by Means of Gas Evaporation Technique. I. Preparation Method and Optical Properties in Ethanol", *Bull. Chem. Soc. Jpn.,* **56,** 3578 (1983).

K. KIMURA, "The Study of Metal Colloids Produced by Means of Gas Evaporation Technique. II. Reaction of Metal Sols in Organic Solvents", *Bull. Chem. Soc. Jpn.,* **57,** 1683 (1984).

K. KIMURA, and S. SAKO, "Conduction Electron Spin Resonance of Ultrafine Particles of Magnesium", *Chem. Lett.,* 973 (1984).

S. SAKO, and K. KIMURA, "Conduction-Electron Spin Resonance in Fine Particles of Magnesium and Calcium", *J. Phys. Soc. Jpn.,* **53,** 1495 (1984).

K. KIMURA, and S. BANDOW, "Surface State and Magnetic Properties of Magnesium Ultrafine Particles", *Nippon Kagaku Kaishi* (in Japanese), 916 (1984).

K. IMAEDA, T. ENOKI, H. INOKUCHI, J. AOKI, M. TAKEKAWA, and S. IWASHIMA, "Electric and Magnetic Properties of Tetrabenzo [de, hi, op, st] pentacene-Alkali Metal Complexes", *Chem. Lett.,* 331 (1984).

T. MITANI, G. SAITO, Y. TOKURA, and T. KODA, "Soliton Formation at the Neutral-to-Ionic Phase Transition in the Mixed-Stack Charge-Transfer Crystal Tetrathiafulvalene-*p*-Chloranil.". *Phys. Rev. Lett.,* **53,** 842 (1984).

Y. TAKAGI, "Fast Transient Digitizer System Using a TV Camera for the Measurement of Optically Induced Spin Polarization", *Rev. Sci. Instrum.,* **53,** 1677 (1982).

Y. TAKAGI, "Optically-Induced Spin Polarization in Transition Metal Complexes and Aromatic Hydrocarbons at Room Temperature", in "Laser Spectroscopy", Vol.VI, H.P. Weber, and W. Luthy Ed., Springer, pp.85—88 (1983).

Y. TAKAGI, K. YAMADA, Y. FUKUDA. and T. HASHI, "Optically Induced Transverse Magnetization in Ruby near Zero Magnetic Field; Magnetically Detected Transient Hanle Effect", *Phys. Lett.,* **98A,** 306 (1983).

Review Articles and Textbooks

E. HIROTA, "Free Radicals. High-Resolution Spectroscopy and Molecualr Structure.", *J. Phys. Chem.,* **87**, 3375 (1983).

S. SAITO, "Chemistry in Ultrahigh Vacuum—Formation and Reaction of Interstellar Molecules.", Kagaku to Kogyo (in Japanese), **36**, 772 (1983).

S. SAITO, "Searches of Interstellar Molecules in Laboratory.", Science (in Japanese), **13**, No.10, 48 (1983).

E. HIROTA, "Structure of Molecular Ions by High Resolution Infrared Spectroscopy.", *Kagaku* (in Japanese), **39**, 568 (1984).

E. HIROTA, and S. SAITO, "Introduction to Spectroscopy. III. Rotation Vibration Spectrum of Molecules.", *Bunko Kenkyu* (in Japanese), **33**, 199 (1984).

S. SAITO, and E. HIROTA, "Introduction to Spectroscopy. IV. Electronic Sepctrum of Molecules: Free Radicals.", *Bunko Kenkyu* (in Japanese), **33**, 280 (1984).

T. KITAGAWA, "The Iron-Histidine Stretching Raman Line as a Probe of the Strain in the Low Affinity Hemoglobin", in "Hemoglobins: Structure and Function" G.A. Schnek ed. Brussels University Press (1984). pp.235—251.

K. YOSHIHARA, "The Ultimate Light Source and Their Application to Photochemistry", *Chemistry* (in Japanese), **38**, 759 (1983).

M. SUMITANI, Y. TAKAGI, N. NAKASHIMA, and K. YOSHIHARA, "Application of Picosecond and Nanosecond Spectroscopy to Photochemistry", *Appl. Phys.* (in Japanese), **52**, 941 (1983).

N. NISHI, "Formation of Molecules in Space: Interstellar Molecules-Comets-Earth", *Kagaku* (in Japanese), **54**, 419 (1984).

N. NISHI, H SHINOHARA, and I. NISHIYAMA, "Neutral Clusters" in "Materiral Synthesis and Processing by Plasma Reaction", Ionics Co. Ltd., 1984, pp.81—90.

H. INOKUCHI, "Structure of Low-Dimensional Materials", in "Chemistry of Low-Dimensional Materials", S.Tanaka Ed., *Gakkai Shuppan* (in Japanese), (1983), p.27.

I. KOYANO, and K. TANAKA, "Energy Dependence of Ion-Molecule Reactions" in "Synthesis and Treatment of Materials by Plasma Reactions", Inst. Phys. Chem. Res. Ed., Ionics, (in Japanese) 1984, pp.46—60.

K. KIMURA, "Photoelectron Spectroscopy of Excited States by Laser Multiphoton Ionization", *Photochemistry* (in Japanese), **8**, 14 (1984).

K. SHOBATAKE, "How Do Gas-Phase Chemical Reactions Proceed?—Crossed Molecular Beams Investigation.", *Kagaku no Ryoiki* (in Japanese), **37**, 940 (1983).

Y. MARUYAMA, "Black Phosphorus", in "Chemistry of Low-Dimensional Materials", S. Tanaka Ed., Gakkai Shuppan (in Japanese) (1983), p.212.

Y. MARUYAMA, "Electrical Properties of Layered Materials", *KAGAKUKOGYO* (in Japanese), **35**, 765 (1984).

Y. MARUYAMA, "Properties of Phosphorus-Black Phosphorus", *Kagaku to kogyo (in Japanese),* **37**, 214 (1983).

G. SAITO, and K. YAMAJI, "TTF TCNQ and Its related Compounds", in "Chemistry of Low-Dimensional Materials", S. Tanaka Ed., Gakkai Shuppan (in Japanese) (1984), p.59.

H. IWAMURA, and H. TUKADA, "Nuclear Magnetic Resonance of Other Nuclei", *Kagaku no Ryoiki Zokan* (in Japanese), **141**, 33 (1983).

K. TORIUMI, and Y. SAITO, "Electron Density Distribution in Inorganic Compounds", *Adv. Inorg. Chem. Radiochem.,* **27**, 27 (1983).

H. KASHIWAGI, "Features of the Program JAMOL 3 for Molecular Orbital Calculations and Large-Scale Calculations in the Supercomputer Period" (in Japanese), Nagoya University Computer Center News. Vol.14, No.3, 250—259 (1983).

H. KASHIWAGI, "Present and Future Status of Electronic Theory on Body—Possibility of the ab initio MO

Method—" (in Japanese), Seibutsubutsuri, **24**, 105—109 (1984).

H. KASHIWAGI, "Dreams and Expectation of Scientists—Molecular Science—" (in Japanese), Computer Today, **2**, 21 (1984).

K. KIMURA, and S. BANDOW, "Laboratory Automation of Magnetic Susceptibility Measurment by Faraday Method", *Kotai Buturi* (in Japanese), **19**, 467 (1984).

K. KIMURA, and H. INOKUCHI, "Electrical Conductivity of Cytochrome c_3", *Kotai Buturi (in Japanese),* **19**, 474 (1984).

Institute for Molecular Science, Myodaiji, Okazaki 444, Japan